THE UNIVERSITY
of EDINBURGH

The metabolic and vascular effects of thiosulfate sulfurtransferase deletion.

Matthew Gibbins

Thesis for the Degree of Doctor of Philosophy (PhD)

The University of Edinburgh

2018

Declaration

This thesis has been composed by myself and contains work to which I made a significant contribution. Any work within the thesis which was not performed entirely by myself is clearly indicated in the text. This work has not been submitted for any other degree or professional qualification.

Abstract

Hydrogen sulfide (H_2S), is a gasotransmitter with several key roles in metabolism and vascular function. The effects of H_2S are dependent on concentration and target organ. For example, increased H_2S concentrations impair liver metabolic function but protect against vascular dysfunction and atherosclerosis. Thiosulfate sulfurtransferase (TST), a nuclear encoded mitochondrial matrix enzyme, is proposed to be a component of the sulfide oxidising unit (SOU) which metabolises H_2S. Preliminary data has shown that *Tst* deletion in mice (*Tst$^{-/-}$*) increases circulating H_2S levels measured in whole blood. Therefore, it was hypothesised that *Tst$^{-/-}$* mice would exhibit worsened metabolic function in the liver but also protection of vascular function under conditions of vascular stress e.g. atherosclerosis. Liver metabolism was assessed by extensive metabolic phenotyping of *Tst$^{-/-}$* mice fed control diet and in conditions of metabolic dysfunction induced by a high fat diet (HFD). *Tst* deletion altered glucose metabolism in mice; gluconeogenesis was increased in liver from *Tst$^{-/-}$* mice fed control diet. Glucose intolerance in HFD-fed *Tst$^{-/-}$* mice was also more severe than HFD-fed C57BL/6 controls. In vitro metabolic investigations in primary hepatocytes isolated from *Tst$^{-/-}$* mice demonstrated that mitochondrial ATP-linked and leak respiration were increased compared to controls. The effect of *Tst* deletion on vascular function was investigated in *Tst$^{-/-}$* mice fed control or HFD using myography. *Tst* deletion did not alter vessel function when mice were maintained on a normal diet. HFD feeding (20 weeks) reduced maximal vessel constriction in the presence of endothelial nitric oxide synthase and cyclooxygenase inhibitors in C57BL/6 aorta. However, in *Tst$^{-/-}$* mice fed HFD there was no reduction in maximal constriction suggesting a protective action of *Tst* deletion. The effects of *Tst* deletion on atherosclerotic lesions was investigated by generating double knock-out (DKO) mice by deletion of the *Tst* gene in *ApoE$^{-/-}$* mice and (*ApoE$^{-/-}$Tst$^{-/-}$*). Atherosclerotic lesion formation was accelerated by feeding mice a western diet. Within the brachiocephalic branch lesion volume and total vessel volume were reduced in DKO mice fed western diet for 12 weeks, indicating that *Tst* deletion reduced lesion formation. Plasma cholesterol was reduced in DKO mice compared to *ApoE$^{-/-}$* controls and a trend towards reduced systolic blood pressure was also noted. Overall this work supported the hypothesis that *Tst* deletion engenders metabolic dysfunction but vascular protection. The findings are consistent with the reported effects of increased H_2S signalling. Overall inhibition of TST represents a novel target for treatment of atherosclerosis, with the caveat that glycaemia may be worsened due to hepatic metabolic dysfunction.

Lay Abstract

Hydrogen sulfide (H_2S) is a toxic gas with a characteristic smell of rotten eggs. It has recently been discovered that H_2S is produced within the cells of mammals. High levels of H_2S can impair the liver's ability to regulate glucose, leading to diabetes. However, in blood vessels high H_2S can be beneficial and has been found to protect vessels from developing the fatty plaques (atherosclerosis) that cause heart disease. Cells have mechanisms to eliminate H_2S and prevent it rising to toxic levels. Thiosulfate sulfurtransferase (TST) is a protein thought to be involved in elimination of H_2S. In mice genetically altered to remove TST (*Tst* knockout mice) increased levels of H_2S were found in the blood. Therefore, it was hypothesised that *Tst* knockout mice would have impaired liver function (resulting in diabetes) but be protected from atherosclerosis in the blood vessels. The liver function of *Tst* knockout mice was evaluated extensively. It was found that loss of the TST enzyme led to higher blood glucose levels in mice fed a normal diet (ND). It was also found that feeding mice a high fat diet (HFD) led to more severe diabetes in mice lacking TST. The blood vessels of *Tst* knockout mice were investigated by measuring the response of the aortic artery to drugs which cause vessels to contract or relax. On ND, there were no differences in arterial function between *Tst* knockout and control mice. In control mice fed HFD arteries were less able to contract in response to compounds that blocked natural relaxation processes. In *Tst* knockout mice fed HFD however, this reduction in contraction was not seen. These results suggest that the absence of TST from the artery protected mice from the effects of the HFD. The effect of TST removal on atherosclerosis was investigated by removing the TST protein from a mouse which is at risk of developing atherosclerosis (*ApoE* knockout mice) resulting in a 'double knock-out' (DKO) mouse (*ApoE* & *Tst* knockout). In these mice, atherosclerosis was accelerated by feeding with a high fat, high cholesterol western diet for 12 weeks. Following this, the size of atherosclerotic growths was measured in a susceptible artery. Plaque size was reduced in DKO mice indicating that the removal of TST led to protection from atherosclerosis. This may have been the result of reduced blood cholesterol which was seen in DKO mice or a reduction in blood pressure which was suggested by the data. Overall this work has confirmed the hypothesis. The effects that have been observed are consistent with the reported effect of increased H_2S in these organs. In the future, the inhibition of the TST enzyme may be useful in preventing atherosclerosis, with the caveat that this may lead to diabetes due to impairment of liver function.

Poster presentations

4th International conference on the biology of hydrogen sulfide – Naples, July 2016

'Thiosulfate sulfur-transferase deficiency engenders a diabetogenic metabolic profile in hepatocytes'

Thiosulfate sulfur-transferase gene deficiency activates aortic nitric oxide signalling and ameliorates vascular function after a diabetogenic challenge

Scottish cardiovascular forum – Belfast, January 2016

'Thiosulfate sulfur-transferase gene deficiency activates aortic nitric oxide signalling and ameliorates vascular function after a diabetogenic challenge'

BHF 4-Year PhD Cardiovascular Science Annual Meeting – Cambridge, March 2015

'Targeting sulfide breakdown as a novel treatment for atherosclerosis'

Scottish cardiovascular forum – Edinburgh, February 2015

'Targeting sulfide breakdown as a novel treatment for atherosclerosis'

Acknowledgements

Table of Contents

List of figures

List of tables

1.0 Introduction

1.1 Metabolic syndrome

Metabolic reactions include the full range of biochemical processes occurring in cells which, in concert, act to maintain cellular and organism homeostasis and function despite extreme fluctuations in the external environment. Many metabolic diseases arise from defects in a key enzyme in a certain pathway, often called inborn errors of metabolism. These diseases are usually monogenic and manifest early in life as life-threatening disorders if treatment is not begun immediately. However, more complex disorders of metabolic function exist that impact upon multiple enzymatic pathways and nutrient homeostasis, the most prominent of which has now been termed the metabolic syndrome (MetS, historically known as 'syndrome x') (1–3).

1.1.1 History and definition

Contrary to rare monogenic metabolic diseases (which are driven by clear defects in a specific enzyme and metabolic pathway,), metabolic syndrome is not clearly defined. The concept of an identifiable syndrome was first identified as early as 1920 when a Swedish physician noted the association linking hypertension, hyperglycaemia and gout (1). Over the following generations associations between metabolic disorders (such as hyperglycaemia, hypertriglyceridaemia, hypertension and obesity) in type II diabetes and cardiovascular disease were frequently noted (4). In 1988 Reaven described hyperglycaemia, hypertriglyceridaemia and hypertension as 'a cluster of risk factors for diabetes and cardiovascular disease' which he termed 'Syndrome X' (5). A year later the addition of obesity, or more specifically upper body 'visceral' obesity, by Kaplan to this 'cluster of risk factors' led to his definition of 'The deadly quartet' (6).

Further efforts to establish a clear definition of the syndrome for clinical diagnosis were undertaken by the World Health Organisation (WHO) (7), the European Group for the study of Insulin Resistance (EGIR) (8), the National Cholesterol Education Program Adult Treatment Panel (NCEP/ATP) (9), the American Association of Clinical Endocrinologists (AACE) (10) and the International Diabetes Federation (IDF) (11). The definitions provided by each organisation are summarised in Table 1.1 Despite the range of definitions, it is now generally agreed that MetS represents a clustering of related metabolic conditions including visceral obesity, insulin resistance, atherogenic dyslipidaemia, hypertension, glucose intolerance, and a pro-inflammatory state.

Clinical measures	WHO (1998)	EGIR (1999)	ATPIII (2001)	AACE (2003)	IDF (2005)
Insulin resistance	IGT, IFG, T2DM, or lowered insulin sensitivity[a] plus, any 2 of the following	Plasma insulin >75th percentile plus, any 2 of the following	None, but any 3 of the following 5 features	IGT or IFG plus, any of the following based on the clinical judgment	None
Body weight	Men: waist-to-hip ratio >0.90; women: waist-to-hip ratio >0.85 and/or BMI > 30 kg/m^2	WC ≥94 cm in men or ≥80 cm in women	WC ≥102 cm in men or ≥88 cm in women	BMI ≥ 25 kg/m^2	Increased WC (population specific) plus, any 2 of the following
Lipids	TGs ≥150 mg/dL and/or HDL-C <35 mg/dL in men or <39 mg/dL in women	TGs ≥150 mg/dL and/or HDL-C <39 mg/dL in men or women	TGs ≥150 mg/dL HDL-C <40 mg/dL in men or <50 mg/dL in women	TGs ≥150 mg/dL and HDL-C <40 mg/dL in men or <50 mg/dL in women	TGs ≥150 mg/dL or on TGs Rx. HDL-C <40 mg/dL in men or <50 mg/dL in women or on HDL-C Rx
Blood pressure	≥140/90 mm Hg	≥140/90 mm Hg or on hypertension Rx	≥130/85 mm Hg	≥130/85 mm Hg	≥130 mm Hg systolic or ≥85 mm Hg diastolic or on hypertension Rx
Glucose	IGT, IFG, or T2DM	IGT or IFG (but not diabetes)	>110 mg/dL (includes diabetes)	IGT or IFG (but not diabetes)	≥100 mg/dL (includes diabetes)[b]
Other	Microalbuminuria: Urinary excretion rate of >20 mg/min or albumin: creatinine ratio of >30 mg/g.			Other features of insulin resistance[c]	

Table 1.1 Diagnostic criteria proposed for the clinical diagnosis of metabolic syndrome. Subscript notes: **a)** Insulin sensitivity measured under hyperinsulinemic, euglycemic conditions, glucose uptake below lowest quartile for background population under investigation. **b)** In 2003, the American Diabetes Association (ADA) changed the criteria for IFG tolerance from >110 mg/dl to >100 mg/dl. **c)** Includes family history of type 2 diabetes mellitus, polycystic ovary syndrome, sedentary lifestyle, advancing age, and ethnic groups susceptible to type 2 diabetes mellitus. BMI: body mass index; HDL-C: high density lipoprotein cholesterol; IFG: impaired fasting glucose; IGT: impaired glucose tolerance; Rx: receiving treatment; TGs: triglycerides; T2DM: type 2 diabetes mellitus; WC: waist circumference. Table reproduced from Kaur (2014) (1). Study Abbreviations: WHO 1998: Definition, diagnosis and classification of diabetes mellitus and its complications. Part 1… (7); EGIR: Comment on the provisional report from the WHO consultation (8); ATPIII: Executive Summary of The Third Report of The National Cholesterol Education Program… (9), AACE: American College of Endocrinology Position Statement on the Insulin Resistance Syndrome (10), IDF: Metabolic syndrome-a new world-wide definition. A Consensus Statement from the International Diabetes Federation (11).

1.1.2 Epidemiology

Strikingly, recent IDF estimates predict that around 25% of the world adult population could currently be diagnosed with MetS (1). The proportion of people affected is highly variable between populations. Depending on the region, whether it is an urban or rural environment, and the composition of the population (sex, age and ethnicity), the rate of MetS can vary from <10% to ~84% of individuals affected (12–14). Higher incidence of MetS was associated with increased body mass index (BMI), with over 60% of obese individuals found to have MetS compared with 5% in normal weight individuals (15). The prevalence of MetS also increases with age in both men and women, with post-menopausal women being particularly affected (16,17).

Epidemiological evidence also indicates that the individual conditions that comprise MetS (visceral obesity, insulin resistance, atherogenic dyslipidaemia, hypertension, glucose intolerance, systemic inflammation) share a common aetiology. The metabolic alterations were found to occur simultaneously more frequently than would be expected by chance, suggesting that they share a pathology (18). In terms of increased future disease risk, the number of simultaneous symptoms associated with MetS increases CVD risk is increased to a greater extent than the risk associated with each individual condition (19).

1.1.3 Pathophysiology

1.1.3.1 Visceral obesity

Visceral obesity defines an excess of adipose accumulation in the abdominal cavity. This is mainly due to fat accumulation in the mesenteric, omental, epididymal (or gonadal) and perirenal white adipose depots (20). This type of fat distribution is more commonly associated with the male gender and is, therefore, sometimes referred to as an android pattern of fat distribution as opposed to gynoid (female gender-associated) wherein fat is deposited predominantly on the thighs and buttocks (21). Compared to gynoid or subcutaneous fat distribution, an excess of visceral fat (measured using waist circumference or, more accurately, using computed tomography (CT), dual energy X-ray absorptiometry (DEXA) or magnetic resonance imaging (MRI) scanning), has a strong correlation with CVD risk and insulin resistance (22). The reason for the correlation of excess visceral fat with CVD risk and insulin resistance is not clear. Two key features of visceral adipose tissue depots compared to subcutaneous fat storage are; a direct connection to the portal vein for release of metabolic products such as free fatty acids, and that the depot plays an active role as an endocrine organ. One hypothesis (the portal hypothesis) suggests that an increased release of metabolites and adipokines from visceral adipose depots affects hepatic function and leads to

a loss of metabolic control (23). This may occur particularly in conditions of localised adipose hypoxia which can result when angiogenesis fails to compensate for hypertrophy of the adipose depots (1,24). Localised inflammation resulting from adipose hypoxia has been linked to increased free fatty acid release in addition to the release of many adipocytokines, which can act systemically to impair insulin sensitivity and precipitate diabetes. The release of adipocytokines by the adipose tissue has been linked to many of the features of MetS, including insulin resistance and systemic inflammation (1,25).

The exact cause of increased android fat accumulation is also unknown although, as mentioned, it is most prevalent in males and in post-menopausal females, giving a clear indication of the impact of sex steroids on the risk of visceral adiposity. Other genetic factors have been identified which appear to predispose patients to visceral fat accumulation over other depots (26,27). Some studies have even suggested that visceral obesity is the sole cause of MetS with the other diseases being secondary to its accumulation (28).

1.1.3.2 Insulin resistance

Insulin is a key regulatory hormone of metabolic function and it is unsurprising that resistance to its actions leads to metabolic dysfunction (29). Insulin is the most potent anabolic hormone known and its actions promote synthesis and storage of carbohydrates (mainly liver glycogen), lipids and proteins and suppresses their degradation (Figure 1.1, 30). These actions are stimulated through activation of the insulin receptor which is an auto-phosphorylating tyrosine kinase. Within the liver insulin receptor activation then leads to binding and phosphorylation of many insulin receptor substrates (IRS) proteins as well as other Src-homology-2 (SH2) domain containing proteins. These proteins then activate downstream signalling protein kinases including phosphoinositide 3-kinase (PI3K) and mitogen activated protein kinase (MAPK). Through these pathways insulin signalling is able to cause widespread changes in protein activation and gene transcription which overall lead to suppression of carbohydrate, lipid and protein degradation, suppression of gluconeogenesis and enhancement of glycogen and lipid synthesis (30).
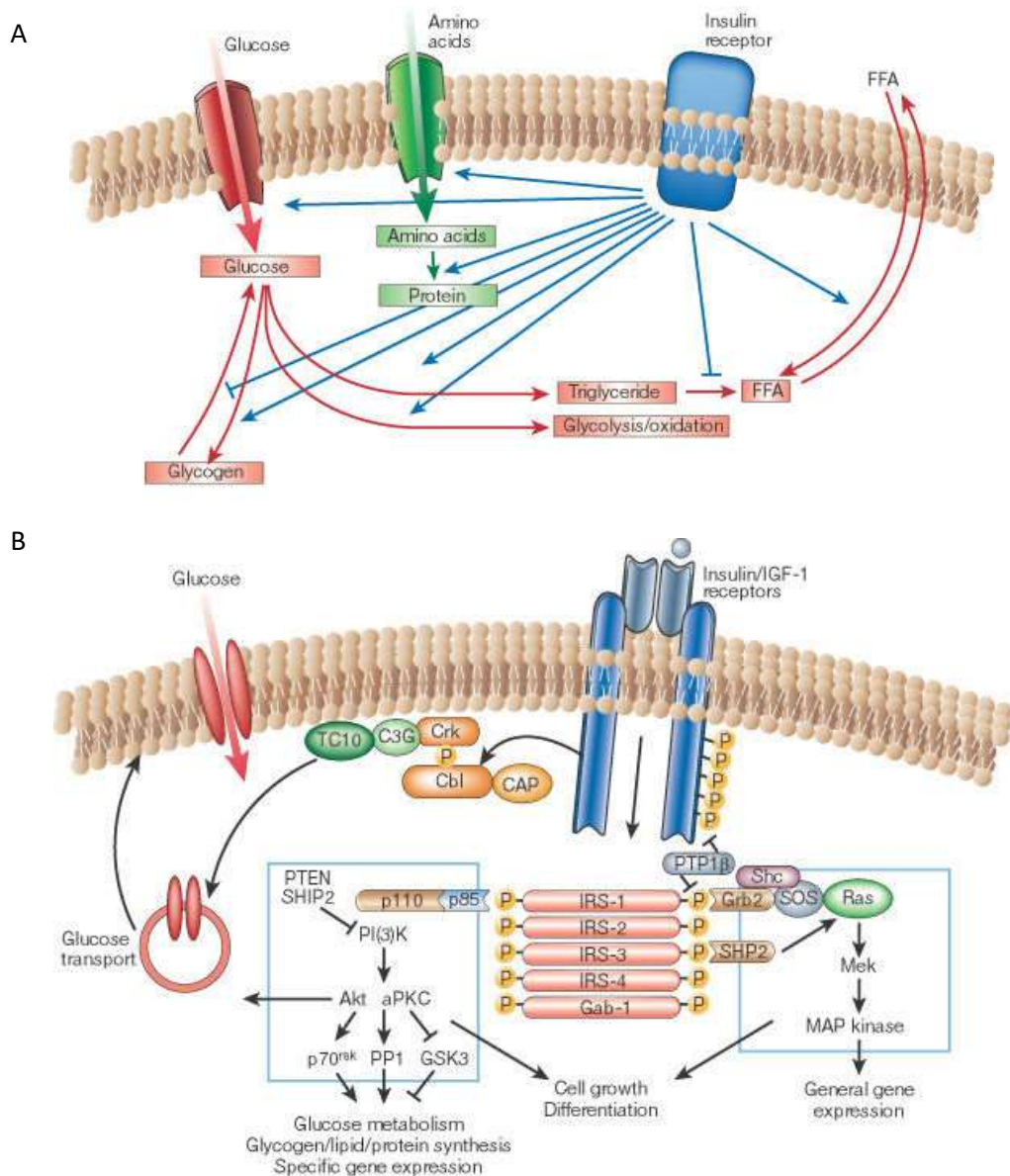
Figure 1.1 Insulin signalling general actions and cellular cascade. a) Insulin is a potent anabolic hormone. Its actions promote the uptake of glucose, amino acids and free fatty acids from the circulation and the synthesis of glycogen, proteins and triglycerides from them. In addition, downstream mediators suppress degradation of these molecules. **b)** The cellular processes by which insulin mediates its anabolic actions. Following receptor binding to insulin autophosphorylation occurs at the insulin receptor. This facilitates binding and activation of numerous proteins which contain 'SH2' domains including the insulin receptor substrate family. Activation of downstream protein kinases such as phosphoinositide-3-kinase and mitogen activated protein kinase then further propagates insulins actions leading to specific protein activation/inhibition and regulation of gene transcription.

Abbreviations: Akt; Protein kinase B, aPKC; atypical protein kinase C, C3G; Cyanidin 3-glucoside, CAP; Cbl associated protein, Cbl; E3 ubiquitin protein ligase, Crk; adaptor molecule Crk, Gab-1; Grb-associated binder-1, Grb2; growth factor receptor-bound protein-2, GSK3; glycogen synthase kinase-3, IGF-1; insulin-like growth factor-1, IRS; insulin receptor substrate, MAP; mitogen activated protein, Mek; mitogen activated protein kinase kinase, p70^{rsk}; 70 KDa S6 kinase, PI(3)K; phosphoinositide-3 kinase, PP1; protein phosphatase-1, PTEN; phosphatase and tension homolog, PTP1β; protein tyrosine phosphatase-1β, Ras; small guanosine

triphosphatases, Shc; SHC-transforming protein 1, SHP2; protein tyrosine phosphatase-1D, SHIP2; SH2 domain containing inositol phosphatase-2, SOS; Son of sevenless protein, TC10; Ras homolog family member Q. Reproduced from Saltiel and Kahn (2001) (30).

Insulin is produced by β-cells within the islets of Langerhans of the pancreas and released in response to increasing blood glucose concentrations (31,32). Destruction of the pancreatic β-cells is well known as a cause of type I diabetes mellitus (T1DM) in which patients suffer from a total lack of insulin action resulting in extreme hyperglycaemia and eventual death if insulin is not replaced through exogenous administration (29).

Insulin resistance represents the converse where insulin is still produced by the pancreas but the target peripheral tissues are resistant to its signalling actions (33). As expected this often, but not always, results in hyperglycaemia and glucose intolerance due to a lack of glucose uptake by the peripheral tissues and a failure to suppress gluconeogenesis within the liver (5,34). This can progress to full type II diabetes mellitus (T2DM) if symptoms worsen. In many insulin-resistant patients who exhibit hyperglycaemia, insulin levels may be unchanged or increased confirming that a lack of sensitivity to insulin is the underlying problem (35).

The exact cause of insulin resistance is not yet established, although it is most simply explained by desensitisation of the insulin signalling cascade in cells because of constant insulin over production and exposure (36,37). Due to the complex nature of insulin signalling desensitisation can occur at many points throughout the pathway and can include a reduction in the number and autophosphorylation activity of insulin cell membrane receptors, decreased IRS concentrations and activities and a decrease in PI(3)K or other intracellular proteins activity (30,38). This effect may especially be stimulated in patients who have a diet which is high in sugars (39,40). Ingestion of these foods requires increased insulin production to compensate for their high glycaemic index and this increase in production can lead to eventual desensitisation of organs due to a decrease in function of the insulin signalling cascade. However, it is likely that beyond this simple mechanism more complex regulation of insulin sensitivity exists as there is evidence that adipokines, such as adiponectin and leptin, can also regulate insulin sensitivity within tissues (41,42).

1.1.3.3 Dyslipidaemia

Dyslipidaemia results from altered, usually increased, levels of triglyceride and/or cholesterol concentrations within the circulation (1,43). When triglyceride or cholesterol content is outside set limits (>2.3 mmol/L for total fasting triglyceride, >5.2 mmol/L total cholesterol, set by the National Cholesterol Education Program (9)) this is considered a

6

disease because increased triglyceride concentrations, increased cholesterol in low density lipoproteins (LDL, >2.6 mmol/L) and decreased cholesterol in high density lipoproteins (<1 mmol/L) can contribute to increased atherosclerotic lesion formation in the blood vessels (9,44,45). Increased plasma triglyceride concentrations are also linked with non-alcoholic fatty liver disease (NAFLD) and non-alcoholic steatohepatitis (NASH) two related conditions which are frequently observed in MetS patients (46,47).

Paradoxically, lipid synthesis is normally stimulated by insulin as a response to excess glucose. The synthesised lipid can then be stored for use in fasting conditions (48). This suggests that post-receptor insulin signalling may be differentially affected during the development of insulin-resistance and depends upon the distinct cellular signalling pathways downstream. As described (section 1.1.2) MetS patients are usually considered to be insulin-resistant and often have hyperglycaemia as a result of this defect. However, increased plasma and liver triglyceride is a common observation in MetS and T2DM patients (1,48). This may be because lipid synthesis is stimulated by an unaffected, insulin-sensitive pathway or is simply due to high levels of excess substrates for lipid synthesis present in patients who have a high sugar and fat diet (1,34,49).

1.1.3.4 Hypertension

Hypertension or high blood pressure is an increase in blood pressure (>140 mmHg systolic and >90 mmHg diastolic in patients <60 years old (50)) which is reproducibly observed in patients (29). It is primarily a concern as increased blood pressure is a risk factor for serious cardiovascular events such as stroke and myocardial infarction (51,52).

The cause of hypertension in MetS is unclear. It has been suggested that hyperinsulinemia and hyperglycaemia, which can occur in MetS due to insulin-resistance, can stimulate the renin-angiotensin system (RAS) (by stimulating expression of angiotensinogen, angiotensin II (AT II), and the AT1 receptor) which can act to increase blood pressure (53,54). Leptin, which is often increased in MetS and obesity, has also been linked to the central control of blood pressure (55,56). Increased leptin can lead to activation of the sympathetic nervous system (SNS) through activation of receptors in the arcuate nucleus (57) resulting in alterations to kidney function, including increased reabsorption of sodium leading to hypervolemia and increased blood pressure (55,56).

Finally, MetS is also frequently associated with vascular endothelial cell dysfunction (58). This is thought to be the result of increased circulating metabolites, such as glucose and oxidised LDL particles, which can damage the endothelium due to increased reactive oxygen

species (ROS) production within the cells (59–61). Endothelial dysfunction can result in the endothelium being unable to correctly modulate vascular function due to reduced production of vasodilator molecules such as nitric oxide (NO) (62). Through this mechanism endothelial dysfunction may also contribute to the pathogenesis of hypertension (63).

1.1.3.5 Proinflammatory state

In recent years MetS has been linked to the development of a systemic 'proinflammatory state' (1). Also known as chronic low-grade inflammation, this type of inflammation relates to the activation state of the immune cells (i.e. whether they are 'primed' for inflammatory activity) systemically rather than in one focal region, as well as to the concentrations of cytokines such as tissue necrosis factor α (TNFα) and interleukin-6 (IL-6) within the circulation (64). Systemic inflammation is linked to a patient's future risk of CVD events (65). One possible mechanism for this is interaction with atherosclerotic lesion formation. Immune cell infiltration is a key component of lesion formation (45) (section 1.3.2) and, therefore, systemic inflammation could increase immune cell infiltration (due to increased activity) and worsen lesion formation. This would naturally increase the risk of CVD events (64).

The exact cause of the proinflammatory state is currently unknown. Increased adiposity, which is typically observed in MetS patients, leads to an overproduction of certain cytokines by the adipose tissue. Examples include IL-6 which can systemically affect the immune system (1,64). One suggestion is that the generation of a pro-inflammatory state by overproduction of these cytokines may be the fundamental defect in MetS. Evidence for this includes the fact that many cytokines which are altered in the pro-inflammatory state can decrease insulin sensitivity and increase triglyceride levels (1). However, it is unlikely that the emergence of systemic low-grade inflammation precedes the other changes in MetS in all human patients (66).

1.1.3.6 Genetics

The cause of MetS is heavily debated and, as referenced, many suspected causes (such as obesity) do not always induce MetS in all patients. Therefore, it has become increasingly accepted that an individual's genetic background can greatly influence their susceptibility to development of MetS (67). Moreover, adiposity is highly heritable, clearly linking genetic factors to an individual's susceptibility to fat mass accumulation, including its anatomical distribution (68,69). The metabolic effects of excess fat accumulation are also genetically influenced. One example is ethnicity; people of South Asian ethnicity, for example, are far more likely to develop T2DM at smaller waist circumference measurements than European

or American populations (1,70). This has necessitated the development of individual diagnosis criteria for certain populations (11).

As well as these examples, variation exists within similar populations in almost all the symptoms associated with MetS. For example, many studies have shown that patients fed identical calorie controlled diets exhibit different levels of weight gain and propensity to obesity (71,72). As discussed (section 1.1.3) the deposition of adipose within the visceral or other depots is also influenced by genetic background. Several polymorphisms within genes which control lipoprotein metabolism have also been identified and these can contribute to a worsening of lipid profile in affected obese patients (73). Glucose intolerance and T2DM have also been linked to genetic factors. Genome wide associated studies (GWAS) of T2DM identified a predominance of genes that predispose patients to worsened insulin secretion. This led to the hypothesis that insulin resistance, accompanied by a defect in insulin secretion, is the reason some insulin resistant patients go on to develop T2DM whereas others increase insulin secretion to compensate for resistance and experience milder glucose intolerance (1,74).

Further to variation within the genome, hypotheses have emerged which suggest that epigenetic mechanisms associated with *in utero* nutrient and stress hormone exposure may explain an individual's susceptibility to MetS development. Barker *et al.* proposed that malnutrition of foetuses during development (for example due to famine as in the Dutch Famine Cohort) meant they were metabolically primed through epigenetic modification to store energy by reducing energy expenditure and optimising absorption and storage (75). This phenotype would be useful in conditions of low food availability but could lead to excessive energy storage and increased risk of MetS development when plentiful high calorie food became readily available in the modern environment. Support for the role of epigenetic mechanisms in the control of MetS susceptibility comes from a number of studies which demonstrate the correlation between low-birth weight (often due to malnutrition during key gestational phases) and later in life risk of insulin resistance and T2DM (1,76).

1.2 Diabetes Mellitus

As discussed in the previous section, one of the main concerns for patients with MetS is the increased risk of developing T2DM. Development of T2DM can often be considered a worsening of the insulin-resistance and hyperglycaemia commonly observed in people with MetS and, therefore, it is a frequent complication of MetS. In addition to the complications of T2DM which can include blindness, poor wound healing, nerve damage, and renal damage (77), T2DM is a major risk factor for development other diseases, including CVD (78).

1.2.1 Epidemiology

The World Health Organisation estimated that 422 million adults were living with diabetes in 2014. Compared to 1980 when 108 million adults suffered from diabetes the percentage of the world population affected by this condition has nearly doubled from 4.7% in 1980 to 8.5% in 2014. Due to the relative complexity of determining whether diabetes is T2DM or type I diabetes mellitus (T1DM) an exact figure for T2DM cannot be generated. However, based on the evidence available, it is highly likely that the increase is mainly due to new cases of T2DM rather than T1DM. General estimates of prevalence suggest that 90% of diabetes cases are T2DM (79).

The increase in the prevalence of T2DM is believed to be mainly due to an increase in risk factors associated with T2DM. Obesity rates in adult men and women have risen from 3% and 6%, respectively, in 1975 to 11% and 13% in 2014 (79,80). Over the same period the percentage of overweight adult men and women has risen from 21% and 23%, respectively, to 39% and 40% (79,80). This increase is seen as the primary driver behind increasing rates of T2DM. Consistent with this belief, rates of both diabetes and obesity have risen to a greater extent in middle and low-income countries and both diseases can now truly be considered a global concern.

T2DM was estimated to be independently responsible for 1.5 million deaths in 2012. As T2DM is a major risk factor for CVD it was also estimated the sub-optimal blood glucose concentrations contributed to a further 2.2 million deaths (79). By 2030 the WHO predicts that diabetes will be the 7th leading cause of death worldwide (79,81). Diabetes was estimated to cost the global economy $825 billion dollars in 2014 in the cost of treatment for T2DM and its associated complications. This calculation does not, however, include the cost of lost work days; with these included the cost is likely to be even higher (79).

1.2.2 Pathophysiology

T2DM can be considered a failure of the pancreas to compensate for insulin resistance (section 1.1.3) (77). While insulin resistance is a major feature of T2DM, the pancreas is able in many patients to increase (at least temporarily) insulin secretion to compensate for this resistance. Consequently, glucose levels are maintained at normal, or only mildly elevated, levels (35,43,77). Hyperglycaemia is often associated with inappropriately increased glucose production by the liver (gluconeogenesis) which can be up to 2-fold higher in fasted T2DM patients compared to those with normal insulin function (1,82). Insulin is a suppressor of key gluconeogenic enzymes, including phosphoenolpyruvate carboxykinase (PEPCK) (83,84). Therefore, liver insulin-resistance is also the cause of increased gluconeogenesis (85). In addition to alterations of glucose metabolism, T2DM is often linked with increased triglyceride synthesis and increased VLDL triglyceride concentrations (48). This is paradoxical as triglyceride synthesis and packaging into VLDL is stimulated by insulin action (48). Suggested causes for this include that the insulin signalling pathway has two signalling arms and some evidence indicates that while resistance in one leads to the effects on glucose metabolism the second, which controls triglyceride synthesis amongst other processes, remains active leading to VLDL triglyceride production (48,49,86).

Why some patients can compensate for insulin-resistance and do not go on to develop the symptoms of T2DM is unclear. However, certain genetic polymorphisms can contribute to this and predispose certain individuals to diabetes development whereas others can maintain glucose homeostasis (87). These polymorphisms primarily appear to affect genes involved in the function of pancreatic β-cells; for example, cyclin-dependent kinase inhibitor 2A which has a role in pancreatic islet regeneration (88). However, as diabetes is a complex disease it is not surprising that polymorphisms in genes affecting the other major metabolic tissues such as glucokinase regulatory protein in the liver (87) and adiponectin within the adipose tissue may also predispose patients to diabetes (89).

The pathologies of T2DM that a patient may experience are associated with the hyperglycaemia which results from the loss of metabolic control by insulin. Hyperglycaemia is well known to cause vascular damage through increased ROS production in endothelial cells (90) and this explains a number of symptoms experienced by people with T2DM,including microvascular damage in retinal vessels for example (91). Damage of the vessels within the retina followed by compensatory angiogenesis to repair this can lead to micro haemorrhages within the retina leading to eventual blindness. The microvasculature of

the kidney is also frequently affected by chronically hyperglycaemia resulting in destruction of nephrons and eventual kidney failure (92).

Micro- and macro-vascular damage also contributes to poor wound healing responses in diabetic patients and an increased risk of peripheral vascular disease where blood supply to the periphery (mainly the lower limbs) is inadequate leading to ischaemia of the tissue (93). These symptoms can be especially troublesome as an additional defect is diabetic neuropathy, which is the result of damage to the peripheral nervous system caused by hyperglycaemia (94). Due to the loss of sensation a common occurrence in T2DM patients is severe ulcer formation on the extremities (93). This can happen when patients fail to realise that they have a wound (due to neuropathy) and, combined with the poor wound healing response, leads to a delay in treatment until the ulcer is serious. In these cases, amputation is often the only remaining treatment available and complications associated with amputation of limbs is a common cause of death in T2DM patients (93).

1.2.3 Treatment

During initial stages of the disease T2DM may be successfully managed through changes in diet and increased exercise. Both of these have been shown to reduce the hyperglycaemia experienced by patients and improve insulin sensitivity (95,96). However, in cases where there is poor compliance with these methods or a continued worsening of symptoms pharmacological treatments are available. These include compounds in the biguanide, sulfonylurea and thiazolidinedione classes. In addition to these compounds insulin analogues may be added to further control blood glucose concentrations (97).

1.2.3.1 Biguanides

The prototypical biguanide compound and first line treatment for T2DM is metformin (98). metformin is listed on the WHO list of essential medicines underlining its usefulness in treating T2DM (99). metformin acts to reduce blood glucose and improve insulin sensitivity in tissues (98). The reduction in blood glucose is thought to be partly caused by a suppression of hepatic gluconeogenesis which is often increased in T2DM patients due to a lack of suppression by insulin. The exact mechanism behind these effects is unknown although activation of AMP kinase (AMPK) by metformin is thought to be involved (100).

AMPK, in addition to other roles, is a downstream mediator of insulin signalling and, therefore, activation of AMPK by metformin may be able to partially restore insulin signalling, resulting in suppression of hepatic gluconeogenesis and increased glucose uptake through the insulin responsive GLUT-4 glucose uptake channel in peripheral tissues such as

muscle (100,101). In addition to its actions on AMPK metformin also has actions which are AMPK-independent, demonstrated by mouse models in which AMPK function is eliminated but metformin remains active (102). These actions may include improved binding of insulin to its receptor, an effect for which the mechanism is not understood (103).

1.2.3.2 Sulfonylureas

If metformin treatment alone is not sufficient to control a patient's hyperglycaemia then a second compound or insulin analogue may also be used in treatment (97). An example of a second line therapy such as this is the sulfonylurea class of compounds, such as glibencamide. These compounds act to increase insulin secretion from the pancreatic β-cells, essentially sensitising the cells to increases in blood glucose (104). They have a relatively simple mechanism of action to explain these effects. Sulfonylureas inhibit the function of ATP-sensitive potassium channels (K_{ATP} channels) (104). Within pancreatic β-cells these channels maintain the polarisation of the cells and prevent action potentials (32). During normal function of pancreatic β-cells as glucose concentrations increase there is an increase in the production of ATP which inhibits the K_{ATP} channels and allows the cells to depolarise. Depolarisation of the cell results in voltage gated calcium channel activation. The influx of calcium permitted by these channels is coupled to the binding of insulin secretary vesicles within the plasma membrane and the release of insulin to the circulation (32). By inhibiting these channels independently of ATP concentrations sulfonylureas can cause depolarisation of the β-cells or sensitise them (due to a partial inhibition for example) to increasing glucose concentrations (104).

1.2.3.3 Thiazolidinediones

Thiazolidinediones or glitazones are another second line therapy which can be considered if metformin fails to control blood glucose concentrations alone. An example of these compounds is the commonly used rosiglitazone (105). Glitazones decrease the plasma concentrations of free fatty acids (FFA) and blood glucose. The proposed mechanism for these effects is complex but mainly relies on the activation of peroxisome proliferator-activated receptors (PPAR), particularly PPARγ (105,106). The endogenous ligands for these receptors are FFA and eicosanoids. PPAR activation results in a wide variety of transcriptional changes, including increased lipoprotein lipase and fatty acyl CoA synthase within adipose cells (106). These transcriptional changes lead to increased storage of FFA in adipocytes. This is suggested to increase the body's reliance on carbohydrate metabolism for energy production and, hence, also results in decreased blood glucose. In addition, a variety of endocrine signals released from the adipose tissue may have beneficial effects on insulin

sensitivity within muscle and liver tissues (105,106). While glitazones are still currently in use, recent evidence has suggested that their use may contribute to increased risk of CVD events such as myocardial infarction and lead to heart failure (107). These findings have led to decreased clinical use of glitazones.

1.2.3.4 Insulin analogues

Insulin can be used as an individual therapy or in combination with one or more of the above compounds when good glycaemic control is not attained with them alone (87,108). As covered in section 1.2.2, the emergence of full T2DM as opposed to milder glucose intolerance has been linked to a reduced ability of pancreatic β-cells to secrete insulin (77). In addition to this the sulfonylurea compounds are also primarily designed to increase insulin secretion and this is shown to be effective in T2DM (104). Therefore, increasing insulin concentrations in T2DM using exogenously administered insulins is an obvious approach to therapy. Most commonly long acting analogues of human insulin are administered once daily to provide increased concentrations over the course of a day. Doses can be increased until blood glucose concentrations are within acceptable ranges or an additional dose of insulin may be added (108).

1.3 Atherosclerosis

In addition to development of T2DM, MetS also leads to increased risk of CVD defined by increased rates of coronary artery disease, MI, and stroke (1). This increased risk is associated with an increased prevalence of atherosclerotic lesion formation. These fatty plaques form within the vessel walls over time and can be either relatively stable and asymptomatic or unstable and vulnerable to rupture. Formation of complex, vulnerable atherosclerotic plaques inherently predisposes a patient to possible cardiovascular events such as MI and stroke because rupture of an atherosclerotic plaque followed by thrombosis and vascular occlusion is the most common cause of these events (45). The increased development of atherosclerotic lesions in MetS patients can be linked to a number of risk factors, including atherogenic dyslipidaemia, hypertension, hyperglycaemia, and the proinflammatory state (1,45).

1.3.1 Epidemiology of CVD and atherosclerosis

Cardiovascular disease (CVD) is a catch-all term for diseases of the heart and blood vessels. CVD is the leading cause of non-communicable disease (NCD) death worldwide. It was responsible for 17.5 million deaths in 2012(109); 31% of all global deaths. Refuting the idea that it is a 'Western' disease 80% of CVD deaths occur in low and middle-income countries. The World Health Organisation (WHO) also suggests that NCDs including CVD 'are major barriers to poverty alleviation and sustainable development (109).

Atherosclerosis is recognised as the cause of several important CVDs including MI and stroke, two of the most acute manifestations of CVD. Atherosclerotic lesions are highly prevalent throughout the population. Fatty streaks which are a first step in their formation have previously been found in childhood autopsies, suggesting very rapid development (110). Autopsies of 300 US soldiers killed in the Korean conflict revealed that 77.3% had gross evidence of coronary atherosclerosis. Again, this study reflects a high degree of prevalence amongst the population as well as early formation as the mean age of the men in the study was only 22.1 years (111). However, despite the extremely high prevalence of coronary atherosclerosis, the observed rate of acute event caused by lesion rupture is not as high. Therefore, these studies also suggest that processes which control the stability of lesions are more important when considering the risk of CVD events than the presence of lesions alone.

1.3.2 Pathophysiology

Atherosclerosis represents a precursor to CVD. Atherosclerotic lesion development is a complex and chronic process involving numerous cell types and pathological processes. A general scheme has been proposed (Figure 1.2) and is widely accepted (112,113). This process begins with accumulation of lipid-containing lipoprotein particles within the vessel wall primarily in the form of low density lipoprotein (LDL). This can be exacerbated in certain areas of the vasculature due to actions of haemodynamic forces on the endothelium leading to altered cell function such as decreased nitric oxide (NO) synthesis, increased permeability and increased adhesiveness for immune cells of the endothelium (113,114). Worsening of endothelial function in areas of high haemodynamic stress due to can occur in hypertension and may explain why it is a risk factor for atherosclerosis development (115). Continuing development of the lesion is caused by recruitment of monocytes (which then become macrophages) in the cell wall due to increased adhesion molecule expression on the endothelial cells. These macrophages uptake and accrue free oxidised LDL via cell surface LDL receptors becoming "foam cells". Uptake of large amounts of lipid eventually leads to cell death by apoptosis and/or necrosis. Consequently, lipids and cellular debris are released back into the lesion, aggravating the immune response further (113).

In complex lesions, smooth muscle cells from the medial vessel wall infiltrate the lesion area forming a cap of cells above a 'necrotic core' of extracellular lipid and cellular debris released from dying foam cells. These cells deposit fibrous tissue, such as collagen, leading to a 'fibrous cap'. In some cases, the 'cap' of lesions may also be actively calcified by smooth muscle cells or vascular pericytes which have taken on osteoblast characteristics (116). This can lead to a brittle, unstable cap structure. In an unstable plaque undergoing these remodelling processes tissue proteinases can degrade the fibrous cap structure leading to rupture of the plaque and exposure of the underlying thrombogenic tissues (113). This can lead to thrombus formation, which, if not effectively cleared, leads to vessel occlusion and ischaemia of the supplied tissue.
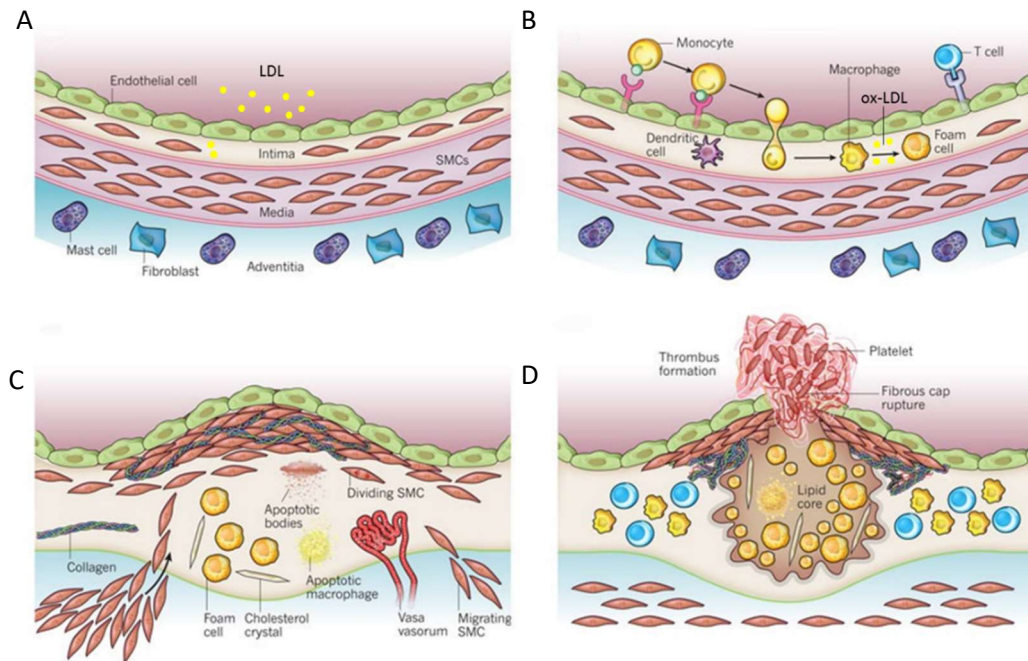
Figure 1.2 A basic scheme of atherosclerotic lesion development. a) In early stages of atherosclerotic disease there is internalisation of low density lipoprotein (LDL) lipid particles into the intimal space. Alterations in endothelial cell function, sometimes caused by altered haemodynamic forces, allow LDL lipoproteins to be taken up into the vessel wall leading to lipid deposition and 'fatty streak' type lesions. **b)** Oxidisation of the LDL particles can lead to adhesion molecule expression on endothelial cells and recruitment of immune cells to the lesion including monocytes which can transmigrate into the intimal layer and become macrophages. These macrophages take-up ox-LDL particles producing 'foam cells' **c)** Uptake of ox-LDL can lead to cell death, releasing lipid and cellular debris into the extracellular environment further aggravating the immune response. This, along with the presence of other risk factors such as high circulating homocysteine, can cause smooth muscle cell proliferation and migration into the intimal layer forming a 'fibrotic cap' above a necrotic core of extracellular lipid and cell debris. **d)** Complex remodelling processes including calcification and proteinase function can cause plaques to become unstable and rupture exposing thrombogenic material to the vessel lumen and leading to thrombus formation and vessel occlusion. Without removal of the thrombus, tissue supplied by the vessel will become ischaemic. Abbreviations: ox-LDL; oxidised low-density lipoprotein, LDL; low density lipoprotein, SMC; smooth muscle cell. Reproduced from Libby *et al.* 2011 (112).

1.3.2.1 Plasma lipoproteins and cholesterol

As described, atherosclerosis is initially driven through accumulation of lipoprotein particles, in the form of LDL, in the vessel wall (45,112). Lipoproteins consist of a core of lipid and cholesterol surrounded by a phospholipid monolayer membrane allowing the hydrophobic fats to be emulsified for transport in the aqueous plasma (117,118). Lipoproteins contain transmembrane proteins, called apolipoproteins, which act to target the lipoprotein to specific tissues. Lipoproteins are classified by density and usually divided into very low density lipoprotein (VLDL), low density (LDL) and high density lipoproteins (HDL) and sometimes intermediate density lipoprotein (IDL) and ultra-low density lipoproteins (ULDL)

(also known as chylomicrons) particles (119,120). The density of the particles is broadly reflective of triglyceride content with lower densities containing the most triglyceride and HDL the least (119). However, the different classes of lipoprotein also contain different types and ratios of the transmembrane proteins which act to direct the particles to certain tissues (120).

The lipid transport process begins with the 'exogenous pathway' in the intestine (Figure 1.3, 121). Following absorption, dietary lipids and cholesterol are packaged into nascent chylomicrons for transport to the liver and, to a lesser extent, to other tissues such as muscle and fat. These particles contain high levels of ApoB48 which permits their release into the lymphatic system (120,121). Through interaction with HDL particles present in the bloodstream chylomicrons receive ApoC-II and E proteins. ApoC-II can interact with the endothelial cell membrane-bound lipoprotein lipase (LPL) which hydrolyses the triglycerides and transfers lipid, in the form of free fatty acids and glycerol, into tissues such as muscle or adipose. ApoE allows interaction of the particle with the remnant reuptake receptor at the liver resulting in absorption of the lipoprotein and intracellular hydrolysis in lysosomes (120,121).

The liver forms the main regulator of what is termed the 'endogenous pathway' for lipoproteins (48,117,118,120,122). It hydrolyses triglycerides from absorbed chylomicron particles and can either use them for energy generation or store them for later use (117). It is also able to synthesise triglycerides and cholesterol *de novo* from excess nutrients. These nutrients are then packaged into VLDL particles for transport to peripheral tissues, such as muscle or adipose, for storage or energy generation. Nascent VLDL synthesised in liver contains ApoB100 which controls export into the bloodstream (117). Similar to chylomicrons, interaction of these nascent particles with HDL allows the donation of ApoC-II and ApoE to the VLDL particles (120). Depletion of the lipid content of VLDL particles through interaction of ApoC-II with LPL in target tissues results in the formation of IDL (also termed VLDL remnants). IDL particles are either reabsorbed by the liver through interaction of ApoE with the remnant receptor or further hydrolysed by hepatic lipase. Hydrolysis by hepatic lipase results in LDL particles which are increasingly cholesterol rich due to removal of triglycerides (122,123). LDL particles are absorbed by the liver, or some peripheral tissues, through an interaction of the LDL receptor and ApoB100 protein on the LDL membrane transferring their cholesterol contents to the tissue. LDL can also be scavenged by macrophages through interaction with low affinity scavenger receptors (120,122).

The final pathway associated with lipid homeostasis is the 'reverse transport pathway' mediated through HDL (118,120). HDL particles are synthesised by the liver and usually contain apolipoproteins from the 'A' family e.g. ApoA-I or II. However, they also contain some ApoC-II and ApoE to allow them to perform their role in maturation of chylomicron and VLDL particles (118,120). The other role of HDL is to transport cholesterol (and some other lipids) from peripheral tissues either back to the liver or to tissues requiring cholesterol for steroid synthesis e.g. the adrenal glands. HDL particles acquire cholesterol and lipids from tissues through interaction with membrane bound proteins such as ABCG1 and PLTP. This content can then be transferred to tissues either directly through uptake of HDL by scavenger receptors or indirectly through interactions with VLDL. The indirect process predominates in mammals and is mediated by cholesterol ester transfer protein (CETP). This protein exchanges triglycerides from VLDL particles for the cholesterol contained in HDL. This forms a cholesterol rich LDL particle and a triglyceride rich HDL particle. While LDL can then be absorbed by tissues, releasing its cholesterol content (discussed above), the HDL is unstable in this form and is hydrolysed by hepatic lipase removing the triglycerides and recycling the HDL particle for reuse (49,118,120).

Given that the accumulation of cholesterol rich LDL within the vessel wall is the initiating step in atherosclerosis, blood lipoprotein levels have long been considered a risk factor for this disease (45). Indeed, increased plasma cholesterol in both human and animal models has been shown to independently cause lesion development in the absence of other known risk factors (124). The atherosclerotic risk of increased cholesterol is also demonstrated by a number of genetic models of elevated circulating cholesterol in mice such as $ApoE^{-/-}$ and $Ldlr^{-/-}$ which develop lesions in aortic vessels unlike wild type animals (125). Similar effects have also been found in human patients with familial hypercholestaemia in whom development of severe atherosclerotic lesions can occur in childhood leading to mortality from cardiovascular events (126).
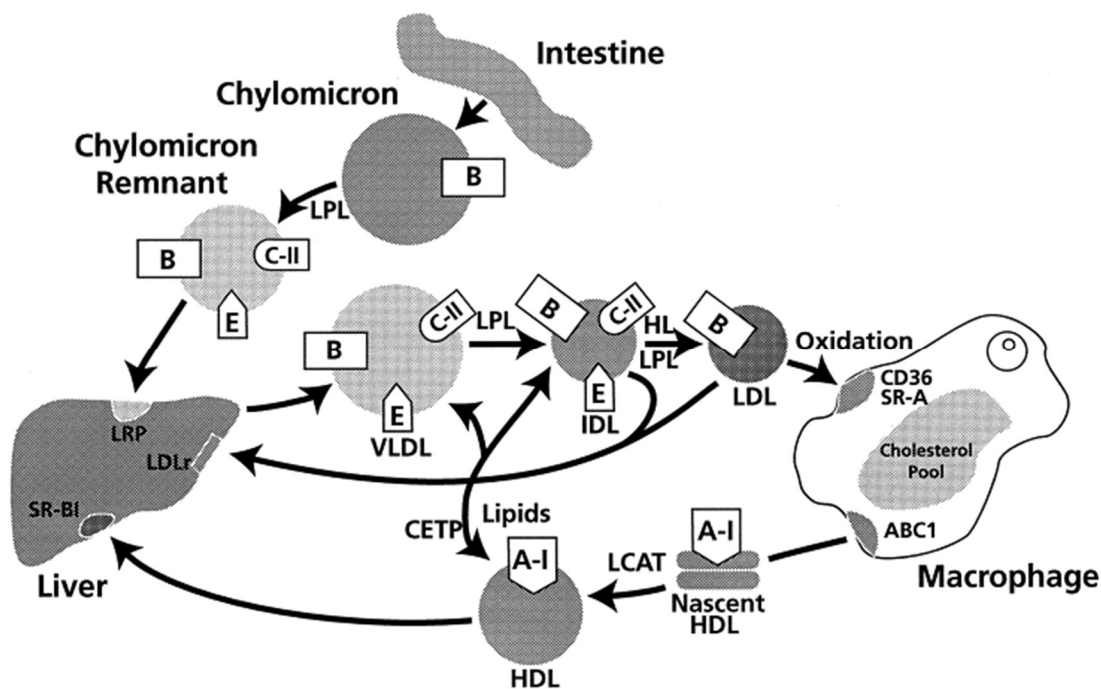
Figure 1.3 Mammalian exogenous and endogenous lipoprotein metabolism. Lipoprotein metabolism begins with lipid absorption from the intestine and transfer to the liver in chylomicron particles (exogenous pathway). The liver regulates secretion of VLDL particles containing cholesterol and triglyceride for transport to peripheral tissues. When VLDL interacts with LPL triglyceride is progressively removed resulting in the generation of cholesterol rich IDL and LDL particles. These can be reabsorbed by the liver or can transfer their contents to other tissues (such as the adrenal glands). The cholesterol can also be absorbed by circulating macrophages. Nascent HDL particles synthesised by the liver or intestine can then interact with cholesterol containing macrophages or tissues to take up cholesterol. These HDL particles can then transport the cholesterol back to the liver or to cholesterol-requiring tissues. A-I; ApoA-I, ABC1; ATP-binding cassette transporter 1, B; ApoB, C-II; ApoC-II, CETP; cholesterylester binding protein, E; ApoE, HDL; high-density lipoprotein, HL; hepatic lipase, IDL; intermediate-density lipoprotein, LCAT; lecithin-cholesterol acyl transferase, LDL; low-density lipoprotein, LDLr; low-density lipoprotein receptor, LPL; lipoprotein lipase, LRP; lipoprotein receptor related proteins; SR-A; scavenger receptor A, SR-BI; scavenger receptor B-I, VLDL; very low-density lipoprotein. Reproduced from Kwiterovich (2000) (120).

1.3.2.2 Hypertension

Hypertension increases the risk of atherosclerosis in patients who already have the additional high risk factor of increased cholesterol (115). The exact mechanisms of this increased risk have not been well elucidated. However, the effects of hypertension on the vascular endothelium may play a key role. A number of groups have hypothesised that atherosclerosis is primarily an unresolved inflammatory response within the vascular wall. The immune response may be triggered by either damage to the endothelium or endothelial cell dysfunction induced through other mechanisms such as hyperglycaemia (61,114). Endothelial dysfunction has classically been defined as a reduction in nitric oxide production by the endothelium in response to acetylcholine stimulation and occurs in areas prone to

formation of atherosclerotic lesions (114,115,127). However, in addition to a reduction in NO formation endothelial cell dysfunction is associated with increased expression of immune cell adhesion molecules, such as vascular cell adhesion molecule 1 (VCAM-1). Increased expression of these molecules leads to greater immune cell attachment and infiltration into the vascular wall, an initiating process in atherosclerosis formation (45,128).

The cause of endothelial cell dysfunction is unclear. However, increased reactive oxygen species (ROS) production in endothelial cells is linked to dysfunction (127,129). Increased ROS production in endothelial cells has been demonstrated with both increased circulating cholesterol concentrations and hypertension (129). The increase in vascular shear stress resulting in increased turbulent blood flow experienced in patients with hypertension can result in altered endothelial cell function and increased ROS production (130). Under normal conditions vascular shear stress (caused by laminar flow of blood through the vessels) initiates signalling processes in endothelial cells through mechanotransduction mechanisms at the cell membrane (131). This can include the stimulated release of vasodilator molecules including NO. In conditions of hypertension not only is shear stress generally increased but more complex changes also occur in certain complex areas of the vascular system such as bifurcations (131). This results in turbulent flow in these regions and alterations to the local shear stress forces experienced by the endothelium in these regions including reversal of flow, oscillatory stress and turbulent flow (131). The altered shear stress experienced by these cells induces transcriptional changes which make them susceptible to focal development of atherosclerosis including downregulation of NO producing eNOS protein (131). This further supports the idea that dysfunction or damage to the endothelium by hypertension is the reason for its effect on atherosclerosis, as these areas are also the most vulnerable to lesion formation (130).

1.3.2.3 Hyperglycaemia

T2DM is recognised as an important risk factor for CVD and atherosclerosis. This is linked to the effect of hyperglycaemia on the vasculature. As discussed in section 1.2.2, hyperglycaemia can lead to vessel damage in both the micro- and macro-vasculature (90). In a similar fashion to hypercholesterolaemia and hypertension this most likely occurs due to stimulation of ROS production in endothelial and other vascular cells by high glucose concentrations. Increased ROS production due to hyperglycaemia has again been linked to endothelial cell dysfunction which is commonly observed in diabetic patients (132). As previously mentioned, endothelial cell dysfunction leading to increased immune cell infiltration has been linked to atherosclerosis and, therefore, this mechanism explains how

hyperglycaemia may contribute to increased atherosclerotic risk (45,114). Insulin-resistance associated with T2DM may be involved in this process as insulin can also stimulate NO production (133). Resistance of the endothelium to insulin has been linked to an early state of endothelial cell dysfunction in T2DM patients that may precede hyperglycaemia. Therefore, endothelial cell resistance to insulin may also be partly responsible for the endothelial dysfunction observed in diabetic patients which contributes to increased atherosclerosis risk (133,134).

1.3.2.4 Pro-inflammatory state

A low-grade systemic inflammation, similar to that observed in MetS, can worsen a person's risk of atherosclerosis (112,135). This is logical as atherogenesis involves an inflammatory response within the blood vessel wall. Increased inflammatory, as opposed to resolution activity of the immune system leads to a worsening of this process as more immune cells are recruited to the lesion and pro-inflammatory cytokines are released (135). Immune cells induce the increased remodelling of lesions through release of a vast array of pro-inflammatory cytokines and proteases (136). Not only can this increase lesion formation but increased inflammatory activity within a lesion is linked to plaque vulnerability and risk of rupture (135,136). Therefore, systemic inflammation which leads to pro-inflammatory priming of the immune system is an inherent risk factor for atherosclerosis.

1.3.3 Treatment of Atherosclerosis

Treatments for atherosclerosis mainly rely on a prophylactic approach: i.e. reducing risk factors associated with lesion development before substantial disease progression has taken place or reducing the risk of plaque rupture leading to a serious cardiovascular event (52,109). These can initially include encouraging lifestyle alterations such as smoking cessation, dietary changes and increasing exercise (109). Therapeutically, using medications to lower blood cholesterol and blood pressure has been shown to be effective in reducing risk of serious cardiovascular events (137). Treatment for hyperglycaemia or T2DM can also reduce risk as covered in section 1.2.3. Finally anti-thrombogenic therapies can be used in conjunction with other therapies to reduce the risk of thrombus formation in the event of plaque rupture (138).

Unfortunately, while current therapies can decrease risk of a serious cardiovascular event they do not lead to lesion resolution and repair as desired, especially for patients with substantial lesion formation prior to initiation of therapy. There is some evidence that chronic (139) or intensive (45) statin therapy can reduce lipid content of lesions and stabilise them, reducing the risk of rupture. These studies require further validation. New therapies

that can complement the current approach are still a high priority for the scientific and clinical community. Suggested avenues for development of new treatments include directly combatting the two key processes which lead to lesion formation; endothelial cell dysfunction (113,114) and the unfavourable immune/inflammatory response which fails to resolve within the vessel wall (45).

1.3.3.1 Statins

Cholesterol for packaging into VLDL lipoproteins is synthesised by the liver from acetyl CoA (29). This synthetic pathway has many steps. The rate-limiting step is catalysed by the enzyme 3-hydroxy-3-methylglutaryl (HMG) reductase which converts a molecule of 3-hydroxy-3-methylglutaryl CoA (HMG-CoA) to mevalonate (45,140). This enzymatic step can be inhibited by statin compounds resulting in a decrease in cholesterol concentrations within the circulation. In addition to this action the inhibition of cholesterol synthesis also results in increased concentration of the LDL receptor (LDLR) in the cell membranes of peripheral tissues increasing their uptake of LDL from the circulation. The mechanism of action for all statins is the inhibition of HMG-CoA reductase. However, they differ in how well individual patients can tolerate the drugs without the occurrence of side effects. Statin therapy has been shown in a number of studies to reduce the occurrence of cardiovascular events and this reduction in risk is positively correlated to the drop in plasma cholesterol cause by statin administration (140,141). Statins are typically well tolerated by patients and are enormously important in reducing the rate of CVD events such as MI on a population level (141,142).

1.3.3.2 Anti-hypertensives

Several classes of anti-hypertensive agents exist. The main classes of drugs used in most patients are diuretics, compounds which reduce the effect of the renin-angiotensin system (RAS) and Ca^{2+} channel blockers (143). The exact regimen of compound administration will depend on an individual's unique circumstances accounting for their tolerance of certain compounds and comorbidities. Diuretic compounds reduce blood volume by increasing urine excretion. Subclasses of diuretic differ in how this is achieved and with regard to where in the nephron they exert their action. Diuretics are recommended as first line therapies for hypertension (144). Diuretics are often combined with compounds that affect the RAS and reduce the stimulation of vascular tone by angiotensin which leads to increased blood pressure (145,146). The two main classes of drugs acting on the RAS are angiotensin converting enzyme (ACE) inhibitors (147), which prevent the production of the hypertensive angiotensin II, and angiotensin II AT_1 receptor antagonists (148). The mechanism of action

for both of these classes is to reduce the hypertensive effect of angiotensin II on blood pressure.

Finally, Ca^{2+} channel blockers, such as nifedipine and verapamil, are also intended to reduce the tone of the vasculature and hence reduce pressure (143,149). These compounds are often used in combination with diuretics and ACE or angiotensin II inhibitors. As expected, Ca^{2+} channel blockers exert their effects by inhibiting the function of Ca^{2+} channels within vascular smooth muscle cells. By blocking Ca^{2+} entry into the cells they reduce the constriction of the muscle and therefore reduce vascular tone and overall blood pressure (149). While the individual mechanisms of action for the first line anti-hypertensives differ the end goal of therapy using these compounds is a reduction in a patient's blood pressure, ideally to normotensive levels, in order to reduce the risk of serious cardiovascular events. Evidence indicates that a reduction in blood pressure of 5 mmHg diastolic reduces the risk of stroke by 34% and MI by 21%, regardless of the starting value (150). Therefore, control of blood pressure using these agents is an important and useful treatment to mediate the effects of atherosclerosis.

1.3.3.3 Anti-thrombotic agents

Used in addition to agents which reduce plasma cholesterol and blood pressure, anti-thrombotic drugs have been shown to reduce the occurrence of serious cardiovascular events such as stroke and MI (151). Plaque rupture and thrombosis are two key events which cause MI and stroke. Therefore, agents which can prevent clot formation or allow for more rapid thrombolysis before occlusion of a vessel takes place can be useful in preventing MI and stroke. For patients with atherosclerotic disease long term anti-thrombotics, such as aspirin and warfarin, can be useful either individually or in combination (152,153). These treatments can reduce the risk of serious cardiovascular events especially in high risk patients who have previously experienced thrombotic events such as MI or ischaemic stroke (153). Aspirin and warfarin have independent mechanisms of action. Aspirin inhibits platelet aggregation, an early stage of clot formation. This is achieved by inhibition of cyclooxygenase (COX). Inhibition of COX prevents thromboxane A2 production which is a key stimulator of platelet aggregation. Daily low dose aspirin therapy can prevent most thromboxane A2 production while avoiding the gastrointestinal side effects of conventional aspirin therapy (154).

Warfarin inhibits the production of a number of active clotting factors used in the coagulation cascade (155). This endogenous cascade leads to activated fibrin formation which is required alongside activated platelets for thrombus formation. Warfarin reduces the availability of vitamin K which is required for carboxylation of clotting factors at certain key

residues. This affects clotting factors II, VII, IX and X and removes their ability to bind to the vessel wall, preventing them from acting in the clotting cascade. Therefore, warfarin reduces clotting and, hence, cardiovascular events in patients with atherosclerosis. However, its administration must be carefully controlled and monitored as it is an irreversible inhibitor and increased accumulation of inactive clotting factors can lead to excessive bleeding (155). Therefore warfarin, especially in combination with aspirin, is often used only in high risk patients (153).

1.4 Hydrogen sulfide

Hydrogen sulfide (H_2S) is an endogenously produced gasotransmitter that may reduce atherosclerotic lesion development (156). H_2S is known for its potent toxicity at high concentrations, which can result from exposure to exogenous sources such as oil/gas production and sewerage. At high concentrations H_2S inhibits ATP generation by the mitochondria by binding with the iron in the mitochondrial cytochrome enzymes resulting in inhibition of the electron transport chain (157). Despite this toxicity, H_2S has recently been found to be produced in physiological quantities by mammalian cells and, therefore, joins nitric oxide (NO) and carbon monoxide (CO) in the family of 'gasotransmitters' (158,159). Recent evidence has shown that H_2S signalling can have effects both on metabolic function and diabetes and on cardiovascular disease, including atherosclerosis, making it a highly interesting target for investigation.

1.4.1 Production of H_2S

H_2S is actively produced by the enzymes cystathionine γ lyase (CSE) and cystathionine β synthase (CBS) from the amino acid cysteine and there is evidence that a third enzyme, 3-mercaptopyruvate sulfurtransferase (MPST) may be able to catalyse H_2S production from 3-mercaptopyruvate (160). Measurement of H_2S concentrations within tissues is technically challenging and is complicated by compounds such as polysulfides which may be formed from H_2S and detected by a number of the methods used for H_2S measurement, thus giving artificially high values (161). Current best estimates of the maximum endogenous H_2S concentration are <500 nM (162) consistent with the signalling range hypothesised for NO. *Cbs* or *Cse* knockout has been demonstrated to reduce tissue and plasma H_2S levels in comparison to wild type mice (162).

1.4.2 H_2S signalling

The biology of H_2S is typically investigated by measuring secondary responses to reduced endogenous (as in the case of $Cse^{-/-}$ and $Cbs^{-/-}$ mice) H_2S production or following exogenous administration of an H_2S donor compound. Increased concentrations could be considered as >500 nM however, donor compounds are often used at much higher concentrations experimentally. While several effects of altered H_2S concentrations have been found (detailed below) the mechanisms which cause them are typically less well defined. However, a general principle adopted within the community is that H_2S signals by reacting with cysteine residues of proteins resulting in -SSH persulfide 'tag' formation on proteins (163–165). Direct persulfidation by H_2S on unreacted cysteines is unlikely to occur as it is an unfavourable reaction (165) however, a number of possible reactions have been identified

either between H_2S and cysteine residues which have already been modified or through the formation of polysulfides which can donate sulfur atoms for persulfidation (165). The formation of persulfide tags on proteins is then thought to cause either direct changes to the active site or changes in protein folding altering activity (figure 1.4) (163,164). Mustafa *et al.* (163) demonstrated that increasing or decreasing the concentration of H_2S (either through H_2S donors or modifying endogenous levels) increases or decreases the number of persulfidated proteins, respectively thereby increasing or decreasing H_2S signalling.
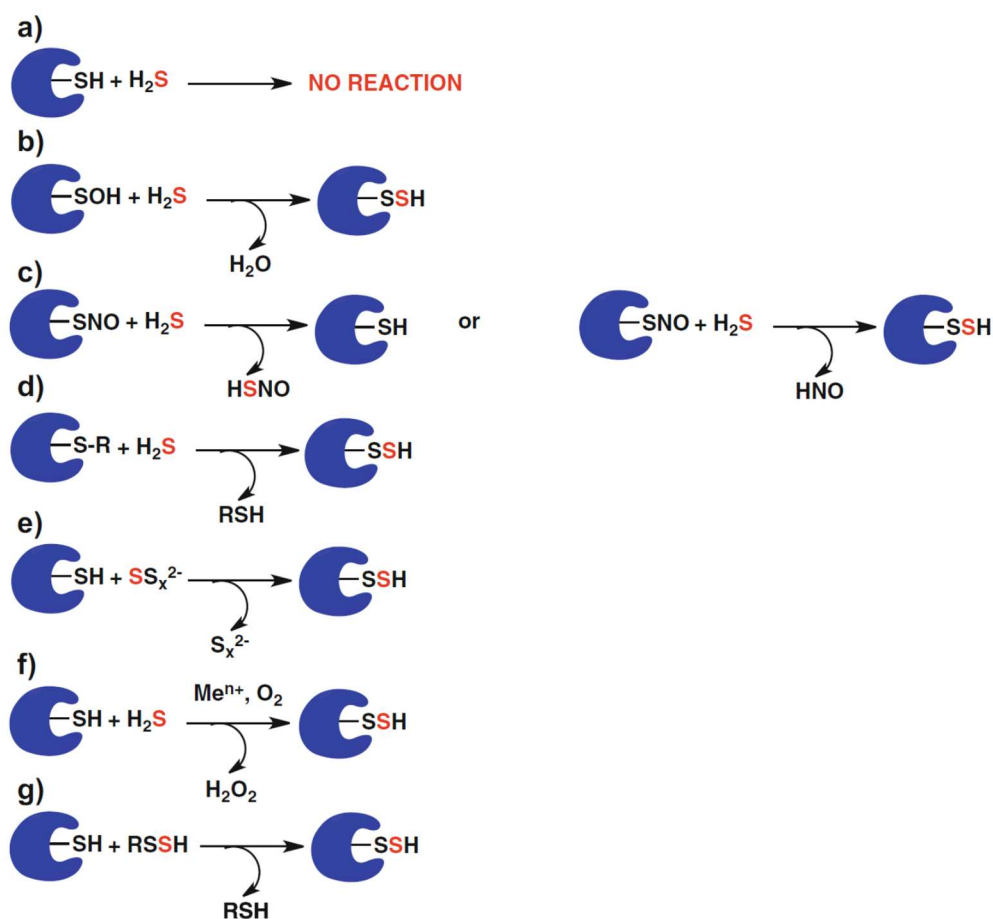
Figure 1.4 Proposed mechanisms for persulfide formation. A number of reaction mechanisms have been proposed by which H_2S, or reaction products of H_2S, may mediate persulfidation of protein cysteine residues. a) No reaction will occur with H_2S and unreacted cysteine as this is thermodynamically unfavourable. b) H_2S can react with sulfenic acids formed on cysteine residues. c) Reaction of H_2S with nitrosylated cysteines can result in HSNO formation or, depending on the protein environment, HNO and persulfidated protein. d) H_2S reaction with existing intra or inter protein disulfide bridges. e) Polysulfides can react with unmodified cysteine residues resulting in persulfide formation. f) Metal ions (e.g. contained within protein active sites) could act as oxidants for formation of persulfides in combination with H_2S. g) Existing persulfides could react in 'transulfuration' reactions transferring persulfides to other cysteine residues. Reproduced with permission from Filipovic (2015) (165).

This mechanism is similar to that of NO which nitrosylates proteins leading to altered activity (163). Compared to nitrosylation persulfidation appears to be even more prevalent within the cell and usually acts to increase a proteins activity (164). In a particularly elegant example Mustafa et al. identified that persulfidation of cys150 within glyceraldehyde-3-phosphate dehydrogenase (GAPDH) led to increased activity whereas nitrosylation of the same residue abolished activity (163). Persulfidation of key proteins is thought to be the mechanism by which H_2S signals and produces the physiological changes observed in vitro and in vivo. As techniques for investigating persulfidation of proteins have developed some mechanisms have now been identified involving persulfidation of specific proteins (sections 1.4-6) lending support to this hypothesis (163,166,167).

1.4.3 Breakdown of H_2S

A working hypothesis for the intracellular breakdown of H_2S was recently proposed by Libiad *et al.* (Figure 1.5, 166) iterating on previous work (169) by altering the suggested chemical reactions occurring at each step. However, both pathways involved the same 3 key mitochondrial enzymes; sulfide:quinone oxidoreductase (SQR), sulfur dioxygenase (SDO) also known as ethylmalonic encephalopathy protein 1 (ETHE1) and thiosulfate sulfurtransferase (TST) (168,169). The coordinated actions of these enzymes result in a final product of thiosulfate which is excreted in the urine. Additionally, conversion of thiosulfate to sulfate can be metabolised by sulfite oxidase (SO) and this occurs in some tissues resulting in a mixture of sulfate and thiosulfate in the urine (168,169).

The pathway established by Libiad *et al.* begins with the oxidation of H_2S to sulfur, which is transferred to an acceptor molecule, such as glutathione (GSH), forming glutathione persulfide (GSSH). This molecule can then donate its persulfide (-SH) to ETHE1 which uses oxygen to form sulfite (SO_3^{2-}) and water. Sulfite is then processed by TST which combines sulfite with persulfide to form thiosulfate ($S_2O_3^{2-}$). Alternatively, SO can use sulfite to generate sulfate (SO_4^{2-}) which is excreted along with thiosulfate. The production ratio of these molecules varies between tissues and potentially reflects differences in expression of the key pathway enzymes (168).
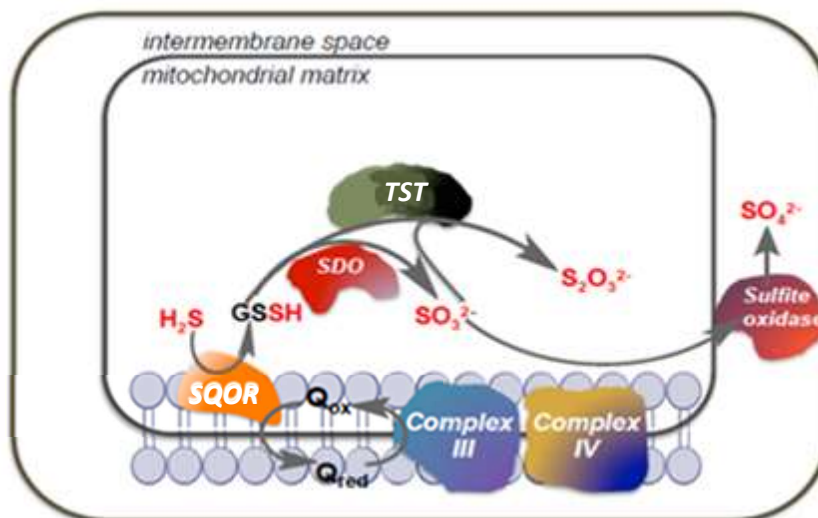
Figure 1.5 A working model of intracellular H$_2$S breakdown in the mitochondria. Oxidation of H$_2$S begins with the transfer of sulfur at the sulfide:quinone oxidoreductase (SQOR) to the acceptor molecule glutathione (GSH) which becomes glutathione persulfide (GSSH). Sulfur dioxygenase (SDO) can then generate sulfite (SO$_3^{2-}$) by combining this persulfide with O$_2$. Sulfite can be further processed either by thiosulfate (S$_2$O$_3^{2-}$) sulfur transferase (TST) to thiosulfate or by sulfite oxidase to sulfate (SO$_4^{2-}$). Both of these compounds represent excretion products. Reproduced from Libiad *et al.* (2014) (the 'rhodanese' label in the original figure has been replaced with 'TST' and the 'SQR' label with SQOR) (168).

During investigations of the disease ethylmalonic encephalopathy by Tiranti *et al.* it was demonstrated that loss of function of the SDO enzyme led to increased H$_2$S concentrations (170). H$_2$S was measured by taking a gas sample for analysis following tissue homogenisation in a sealed vessel. Compared to control mice SDO knockout mice had approximately 10-fold higher H$_2$S concentrations in liver and muscle tissue with a smaller increase (approximately 4-5 times) also observed in brain tissue. Tiranti *et al.* showed that the increase in H$_2$S in this case eventually resulted in toxicity due to inhibition of COX and short-chain acyl-CoA dehydrogenase (SCAD) leading to a range of tissue damage predominately in brain and muscle tissue. Whilst SDO knockout led to growth arrest and eventual death it also provided the first evidence that inhibition of the H$_2$S breakdown pathway is sufficient to increase endogenous H$_2$S concentrations (170).

1.4.4 Metabolic actions of hydrogen sulfide

Many of the physiological actions of H$_2$S have either been inferred from *Cse*$^{-/-}$ and *Cbs*$^{-/-}$ mice (which lack the enzymes associated with production of H$_2$S and, hence, have decreased H$_2$S concentrations) or investigated using exogenously-administrated H$_2$S made from either NaHS or Na$_2$S salts. The concentrations of H$_2$S administered in vitro or in vivo are often considerably higher (in the µM range) than the predicted endogenous levels (<500 nM) and

therefore the physiological relevance of the findings must be questioned. However, from a number of studies have shown that hepatic carbohydrate and lipid metabolism are altered in response to changes in H_2S levels either directly through H_2S mediated signalling or as a result of changes to insulin signalling.

1.4.4.1 Glucose metabolism

H_2S has been linked to diabetic-like phenotypes in the liver [171] and pancreas [172] resulting in increased plasma glucose concentrations. *Cse* overexpression or exogenous administration of NaHS in mouse primary hepatocytes increased glucose production via gluconeogenesis [171,173]. Initially this was linked to increased PEPCK activity which catalyses the first committed step towards gluconeogenesis. However, recent evidence has suggested that it may in fact be the result of increased pyruvate carboxylase (PC) activity [166] which catalyses the preceding step in gluconeogenesis and has been suggested to exert some control over the flux through the gluconeogenic pathway [174,175]. Exogenous NaHS increased PC activity through the formation of a persulfide protein modification at an active cystine residue [166]. Therefore, this represents a direct mechanism by which H_2S is able to increase gluconeogenesis.

Glycogen production was also decreased by *Cse* over-expression or exogenous NaHS administration [173]. Both increased gluconeogenesis and decreased glycogen production occur physiologically during fasting conditions when insulin concentrations are low [29]. Further to this, increased gluconeogenesis and decreased glycogen storage persisted in primary hepatocytes despite insulin stimulation. A dose-dependent inhibition of Akt phosphorylation (a key signalling reaction of the insulin signalling pathway) was also observed in NaHS-treated HepG2 cells (a hepatic cell line) [173]. Taken together these findings suggest that H_2S can drive hepatic insulin resistance, a common feature of diabetes. Finally, increases in CBS or CSE expression have also been found in the livers of streptozocin-induced diabetic rats [176] and insulin resistant HepG2 cells [173], respectively. Along with this suggestive evidence, changes in CBS or CSE expression have also been demonstrated in people with T2DM [177] lending support to the involvement of these enzymes in the pathogenesis of this condition.

In addition to the changes observed in hepatic metabolism, NaHS and the amino acid cysteine (which is a precursor for H_2S generation by CSE or CBS) inhibit the release of insulin from pancreatic β-cell lines [172,178,179]. The most obvious cause of this is the known interaction of H_2S with K_{ATP} channels [180,181]. In contrast to sulfonylurea compounds (section 1.2.3.2) which inhibit the function of K_{ATP} channels, H_2S can

persulfidate K_{ATP} channels leading to increased activity (181). Increased activity of these channels within pancreatic β-cells leads to a suppression of the action potentials required for insulin release (32). In addition to this effect, H_2S has also been linked to inhibition of L-type Ca^{2+} channels within pancreatic β-cells (178). These channels are required for Ca^{2+} influx which is coupled to insulin release (32). Therefore, inhibition of the channels can suppress insulin release.

Finally, H_2S has also been linked to death of pancreatic β-cells. Exogenous NaHS caused apoptosis of an insulin-secreting INS-1E cell line, suggesting that it may inhibit insulin release through destruction of the β-cells (182). However, it should be noted that, as in many tissues, this appears to be dependent on the concentration and environment as several groups have linked to the protection of β-cells in toxic conditions (183,184). Overall these findings suggest that H_2S signalling acts to decrease insulin release; an effect which will naturally result in diabetic-like function. Therefore, H_2S appears to exhibit negative effects on glucose metabolism resulting in hyperglycaemia.

1.4.4.2 Lipid metabolism

The proposed effects of H_2S on lipid metabolism have not been as clearly defined as those on glucose metabolism. Clinical studies have identified a positive correlation between plasma H_2S levels and HDL cholesterol, and a negative correlation with LDL/HDL cholesterol ratio (185). In $Cbs^{-/-}$ mice, which are suggested to have decreased endogenous H_2S concentrations, this relationship was mainly supported as serum triglycerides, non-esterified cholesterol and non-esterified fatty acids were increased in concentration. This finding was associated with a decrease in liver VLDL secretion (186). However, it should be noted that a decrease in H_2S concentrations within the liver was not confirmed in these mice and so these effects may reflect changes elsewhere (171). In $Cse^{-/-}$ mice similar changes in lipid profile were noted; including an increase in total, LDL and HDL cholesterol when mice were fed an atherogenic diet (187). However, in contrast to the effects in $Cbs^{-/-}$ mice, a decrease in total triglyceride content was observed on both control and high fat diets compared to C57BL/6 controls (187). Treatment of $Cse^{-/-}$ mice with the H_2S donor NaHS abolished these changes, suggesting that the lack of H_2S in these mice could be responsible for the changes in lipid profile (187).

Given the importance of the liver in controlling lipid synthesis and release of lipoproteins it is not surprising that changes in lipid metabolism can lead to diseases of the liver, including steatosis (the accumulation of triglyceride within the tissue) (46). Consistent with this in, $Cbs^{-/-}$ mice (in which plasma cholesterol and triglyceride were increased) steatosis of the

liver has been identified even when mice were fed a control chow diet (186). This has led to the suggestion that H_2S signalling prevents hepatic steatosis although this has not yet been tested through exogenous H_2S administration or endogenous enzyme overexpression (171,186). It is also worth noting that $Cse^{-/-}$ mice also suffer from hyperhomocysteinaemia due to decreased function of the trans sulfuration pathway (171). Increased homocysteine has itself been linked to hepatic steatosis and, therefore, this effect may be independent of decreased H_2S signalling (188). Hepatic steatosis has not been thoroughly investigated in $Cse^{-/-}$ mice. However, Mani *et al.* report that no obvious steatosis was evident in these animals (171). $Cse^{-/-}$ mice also exhibit hyperhomocysteinaemia showing that the influence of H_2S on hepatic steatosis is not clear cut. However, overall the evidence suggests that H_2S signalling engenders protective changes with regard to lipid metabolism and that decreased endogenous H_2S signalling results in increased plasma cholesterol and hepatic steatosis but with unknown effects on plasma triglycerides.

1.4.5 Cardiovascular actions of hydrogen sulfide

H_2S was initially investigated primarily as an endogenous vasodilator similar to NO. Therefore, it is of obvious interest in CVD in which impaired activity of vasodilators, such as NO, has been linked to vascular pathologies (129,189). H_2S has been found to influence vascular function, myocardial ischaemia/reperfusion injury and atherosclerogenesis.

1.4.5.1 H₂S and vascular function

H_2S signalling has been linked to activation of potassium channels, including K_{ATP}, intermediate conductance and small conductance potassium channels (159,180,181). The coordinated action of these K^+ channels within the smooth muscle of the vasculature results in hyperpolarisation of smooth muscle cells resulting in fewer action potentials and relaxation of the vessel (190,191). Therefore, H_2S has now been defined as an endothelium-derived hyperpolarising factor (EDHF) (181). H_2S, given exogenously as NaHS, induces vasodilation (measured using myography) in isolated aortic and mesenteric vessels (192). It should be noted that, as seen in metabolic investigations, vasodilator responses have typically been recorded following administration of H_2S concentrations far above the normal physiological concentrations (<500 nM) in the µM or mM range. This evidence questions the direct effect of H_2S on vasodilation physiologically however, it does not rule out that it may modulate the response of the vessels to other vasodilators and hence indirectly stimulate vasodilation. Indeed, as has been extensively reported in the ischaemia field (section 1.4.5.2) H_2S signalling has been demonstrated to increase production and decrease breakdown of NO, a well-known vasodilator (167). Mustafa *et al.* have also reported that ACh-mediated

vasodilation in mesenteric arteries is impaired in $Cse^{-/-}$ mice and this is supported by intermediate effects observed in $Cse^{+/-}$ mice compared to C57BL/6 controls (192). Consistent with this evidence, it has also been reported that $Cse^{-/-}$ mice exhibit hypertension on both control and high fat diet (187). There are few reported data on the effects of increased or decreased H_2S signalling on other aspects of vascular function, such as vasoconstriction.

1.4.5.2 H₂S and ischaemia/reperfusion injury

Elrod *et al.* showed that in C57BL/6 mice with induced myocardial ischaemia and reperfusion (I/R) exogenous Na_2S administration directly into the left ventricle during reperfusion results in decreased injury exemplified by a 72% reduction in infarct size (193). They also demonstrated that mice with myocardial (α-myosin heavy chain driven expression)-specific overexpression of *Cse* had decreased infarct size following myocardial I/R injury. Data from this study suggested that administration of Na_2S led to a conservation of mitochondrial function that was responsible for the reduction of infarct size and the protection of left ventricular function (193).

Later evidence from King *et al.* showed that the protective effects of Na_2S administration on myocardial and hepatic I/R injury were in fact reliant on functional endothelial nitric oxide synthase (eNOS) expression (167). The protective effect of H_2S donor administration was abolished in $eNOS^{-/-}$ mice or $eNOS^{-/-}$ mice expressing a form of eNOS which lacked the Ser1177 residue. Phosphorylation of this residue is stimulatory, leading to increased NO synthesis, and its phosphorylation was found to be induced by Na_2S administration. When mice did not express a form of eNOS that could be phosphorylated in this way, the protective effect of Na_2S was lost (167). These data show that the H_2S and NO signalling pathways have significant and important cross-talk which is important for the beneficial cardiovascular effects of exogenously administered H_2S donors (194). Supporting this idea $Cse^{-/-}$ mice, which suffered worsened responses to myocardial I/R injury, also exhibited decreased NO production and impaired eNOS function, suggesting that cross-talk between the H_2S and NO systems is key in cardiovascular function (167).

1.4.5.3 H₂S and atherosclerosis

$Cse^{-/-}$ mice fed an atherogenic diet for 12 weeks developed fatty streaks within the brachiocephalic branch of the aorta which was not observed in C57BL/6 control mice (187). Treatment with the H_2S donor NaHS significantly reduced the size of the streaks in $Cse^{-/-}$ providing evidence that a lack of H_2S signalling was responsible for the increased development of lesions. However, as in other fields, the concentration of H_2S donor

administered to mice (39 μmol/kg) was far higher than predicted endogenous concentrations in wild type mice. Strikingly, streak development occurred in $Cse^{-/-}$ without requiring breeding with the atherosclerosis susceptible $ApoE^{-/-}$ or $Ldlr^{-/-}$ models. This is unusual within atherosclerotic research as the lipid profile of wild type mice is shifted to HDL and, therefore, is not conducive to formation of atherosclerosis (125). $Cse^{-/-}$ mice exhibited abnormal lipid profiles, including increased cholesterol, and hypertension; both of which are risk factors for atherosclerosis. However, these were normalised using ezetimibe, a cholesterol absorption inhibitor, and hydralazine, an anti-hypertensive, treatment and this did not alter the size of the streaks showing that these risk factors were not responsible for the increased streak volumes. Instead endothelial expression of intercellular adhesion molecule 1 (ICAM-1) was increased in $Cse^{-/-}$ mice and this was suggested as the explanation for increased lesion development (187).

In addition to these findings, $Cse^{-/-}$ mice crossed with a well-established atherosclerosis model; apolipoprotein E knock-out mice ($ApoE^{-/-}$) also exhibited more extensive lesion development than identically treated $ApoE^{-/-}$ mice. Excluding an increase in HDL content in the DKO mice (which would usually be considered protective from atherosclerosis formation), lipid profiles were not altered suggesting that altered lipid metabolism was not the cause of increased atherosclerosis. $ApoE^{-/-}Cse^{-/-}$ double knockout mice treated with NaHS (39μmol/kg) also had decreased lesion formation without any effect on lipid profiles (187). Overall increased H$_2$S is beneficial in the vasculature and can mitigate atherosclerotic lesion development through effects within the vascular endothelium rather than through systemic changes.

1.5 Thiosulfate sulfurtransferase

Thiosulphate sulfurtransferase (EC.2.8.1.1) is a type 1 class detoxification enzyme encoded by the nuclear *Tst* gene and expressed predominantly in the mitochondrial matrix (195). Historically known as 'Rhodanese', it was initially linked to cyanide detoxification through conversion of thiosulfate ($S_2O_3^{2-}$) and cyanide (CN) to thiocyanate (SCN^-), for excretion (196). This reaction illustrates the general mechanism of TST action, which is the acceptance of a sulfur atom from a donor compound (in this case $S_2O_3^{2-}$) leading to formation of a persulfide at the active site cysteine residue. This sulfur is then cleaved from TST and transferred to an acceptor molecule (in this case CN) (196). TST exists within a superfamily of sulfur transferase proteins which contain 'rhodanese' domains (197,198). Many have not been thoroughly investigated however, from initial investigations they do appear to have similar reaction mechanisms to TST (197,198). Whether these enzymes provide physiological roles similar to those of TST is unknown however, from preliminary investigation in our mice 3 other sulfur transferases (TSTD1, D2 and D3) are all minimally expressed in mouse liver (data not shown).

Given the general nature of the sulfur transfer mechanism it is not surprising that TST is promiscuous in its interaction with a variety of sulfur donor and acceptor compounds including H_2S, SO_3^{2-}, $S_2O_3^-$ and persulfides such as glutathione (169). In addition to involvement in the H_2S breakdown pathway (section 1.4.3) TST has also been linked to iron-sulfur cluster regeneration (199,200). . Iron-sulfur clusters are essential components within the active sites of many enzymes including complexes I, II and III of the mitochondrial electron transport chain (201) which are located in close vicinity to TST within the mitochondrial matrix. It has been suggested that TST may play a role in the regeneration of these clusters when they are consumed in enzymatic reactions. In cell free systems TST can incorporate sulfur donated from thiosulfate into succinate dehydrogenase (200) (complex II of the respiratory chain) however, this has not been demonstrated under physiological conditions. Kinetic analysis of TST by Hildebrandt and Grieshaber has shown that the K_m for thiosulfate is far higher than sulfite and persulfides leading them to suggest that its proposed role in H_2S breakdown is its most likely physiological role (169).

1.5.1 Thiosulfate sulfurtransferase and metabolic dysfunction

Work by Morton *et al.* independently led to identification of *Tst* as a potential adipose tissue-specific 'healthy lean gene' (202–204). As discussed in section 1.1.9, there are a large number of genetic factors which may affect a person's propensity for development of obesity and MetS (87). Most studies have investigated genes or polymorphisms which predispose

people to weight gain leading to obesity (205,206). However, the converse approach, i.e. investigating genes which reduce weight gain and promote a lean phenotype, has not been extensively followed (204). Overexpression of *Tst* in the adipose tissue protected mice (Adipoq-*Tst* mice) from weight gain and the negative metabolic consequences of a high fat diet (HFD). Adipoq-*Tst* mice fed HFD had decreased hyperglycaemia, increased insulin sensitivity and decreased mean adipocyte size (Figure 1.6) (204).
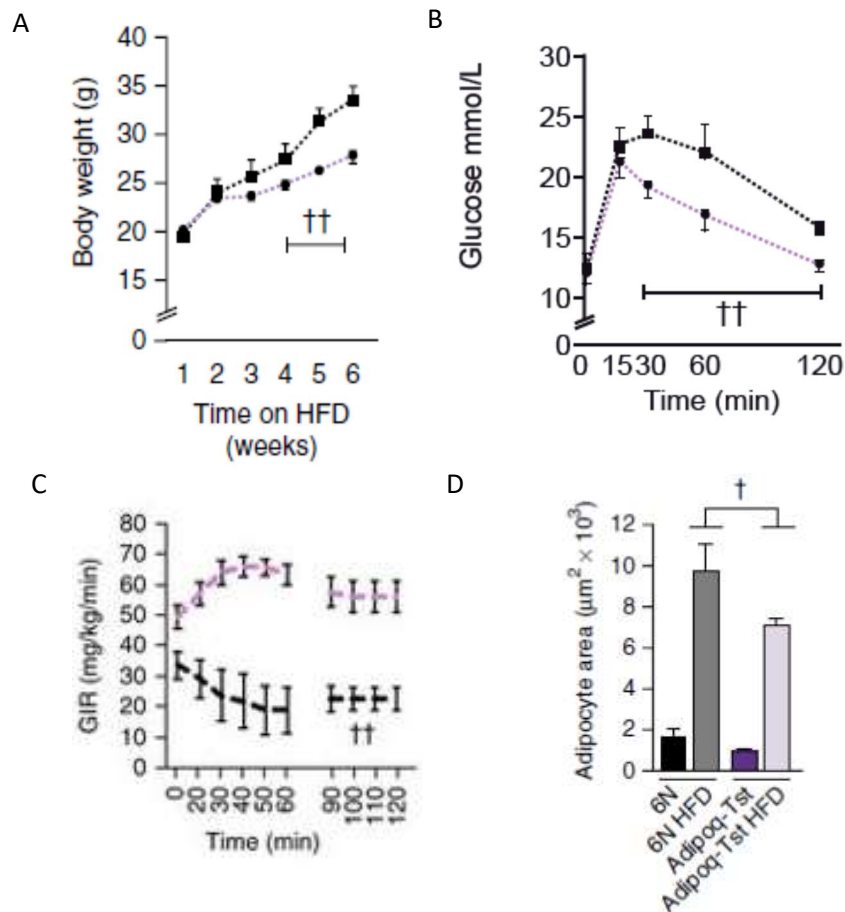
Figure 1.6 The effects of adipose *Tst* overexpression on metabolic function following high fat diet feeding (HFD). C57BL/6N are displayed in black lines, Adipoq-*Tst* in purple. **A)** Body weight measured over 6 weeks of HFD feeding. **B)** A glucose tolerance test performed in mice fed HFD for 6 weeks. **C)** The glucose infusion rate measured in a euglycaemic hyperinsulinaemic clamp performed in C57BL/6N and adipoq-*Tst* mice fed HFD for 2 weeks. **D)** The mean adipocyte area measured in sections of adipose tissue from C57Bl/6N or Adipoq-*Tst* mice fed control chow or HFD for 6 weeks. Reproduced from Morton *et al.* (2016) (204).

In addition to these findings, global deletion of *Tst* (*Tst*^{−/−}) mice was found to be associated with mild hyperglycaemia following HFD and decreased suppression of non-esterified fatty acids (NEFA) although body weight in HFD-fed mice was unchanged compared to C57BL/6N controls (Figure 1.7) (204). Control-fed *Tst*^{−/−} mice also had increased gluconeogenesis following a pyruvate bolus (Figure 1.7) (207). Increased gluconeogenesis is a common phenotype in people with T2DM (section 1.2) and is, therefore, consistent with the hyperglycaemia observed in *Tst*^{−/−} mice fed HFD. Plasma insulin concentrations were unchanged in HFD-fed *Tst*^{−/−} mice, demonstrating that insulin deficiency is not responsible for these effects (204). Instead the finding of increased gluconeogenesis, which occurs only in liver and kidney, suggests that *Tst* deletion within the liver may be mechanistically linked with the whole-body changes in glucose homeostasis. In the mouse *Tst* is also most highly expressed within the liver (208) lending further support to this hypothesis.
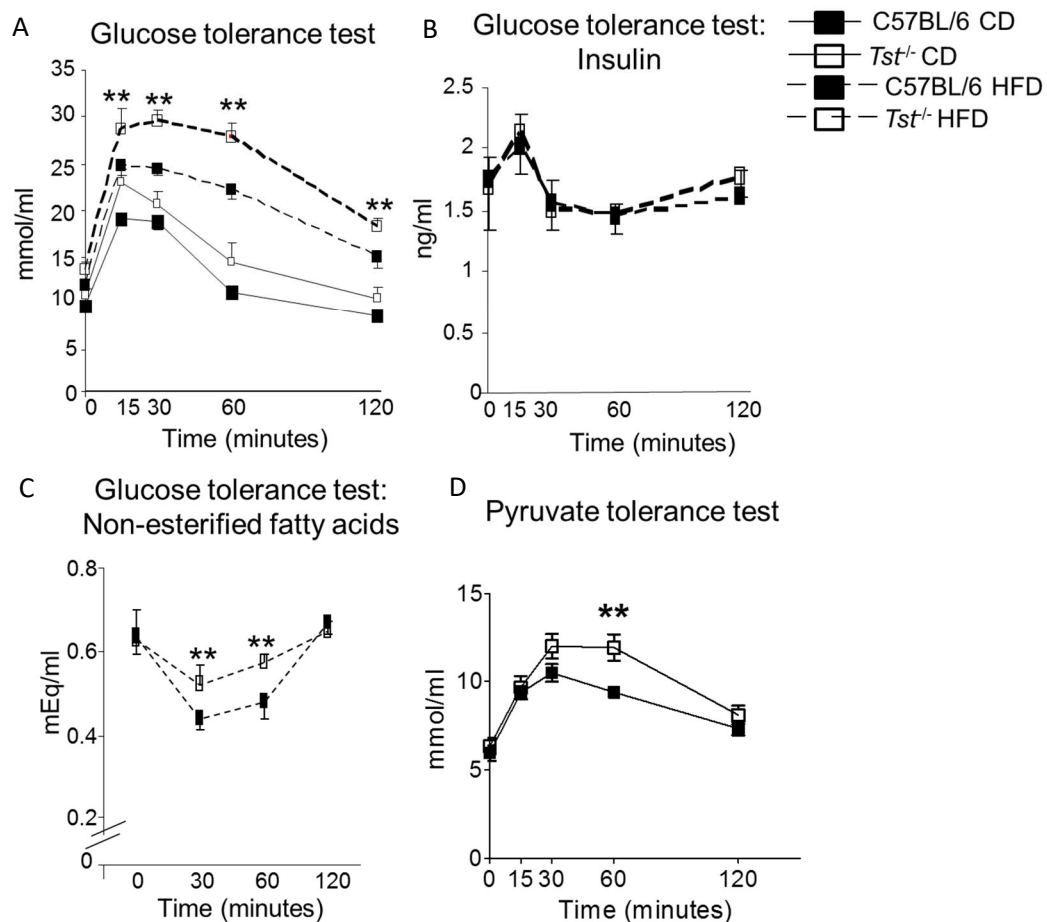
Figure 1.7 Metabolic dysfunction in *Tst*^{−/−} mice. A) A glucose tolerance test in C57BL/6N or *Tst*^{−/−} mice fed control chow (solid lines) or 58% high fat diet (dashed lines) for 6 weeks. Mice were fasted for 4 hours prior to

beginning the test. Following an initial blood glucose measurement (time 0), mice were given a glucose bolus (2 mg/g body weight) and glucose disposal was measured at the indicated time points. **B)** Plasma insulin concentration in C57BL/6N or $Tst^{-/-}$ mice fed HFD for 6 weeks measured over the course of the glucose tolerance test. **C)** Plasma non-esterified fatty acids concentration in C57BL/6N or $Tst^{-/-}$ mice fed HFD for 6 weeks measured over the course of the glucose tolerance test. **D)** A pyruvate tolerance test in C57BL/6N or $Tst^{-/-}$ maintained on control chow diet. **A-C)** reproduced from Morton *et al.* (2016) (204), **D)** Gibbins *et al.* Masters project (207).

Many of the phenotypes observed in Adipoq-*Tst* and $Tst^{-/-}$ mice may be explained by increased or decreased H_2S breakdown, respectively. Increased H_2S has been linked to various symptoms associated with MetS, including worsened glucose tolerance, increased gluconeogenesis and insulin resistance; all of these symptoms have been observed in $Tst^{-/-}$ mice along with reciprocal phenotypes in Adipoq-*Tst* mice. As previously demonstrated in $Ethe1^{-/-}$ mice, deletion of genes within the H_2S breakdown pathway can lead to increased H_2S concentrations. Morton *et al.* recently demonstrated similar findings in $Tst^{-/-}$ mice showing that H_2S and related species, including HS^-, S^{2-} and biologically bound forms of these molecules (such as those associated with human serum albumin and haemoglobin), referred to as 'total sulfide' measured in whole blood by HPLC were significantly increased in $Tst^{-/-}$ compared to C57BL/6 mice (Figure 1.8, 200). Therefore, increased or decreased H_2S signalling represents a plausible mechanistic explanation for the current metabolic phenotypes observed in Adipoq-*Tst* and $Tst^{-/-}$ mice. Investigations directed at the effects of H_2S on lipid homeostasis and cellular metabolism may lead to greater understanding of *Tst* and H_2S.
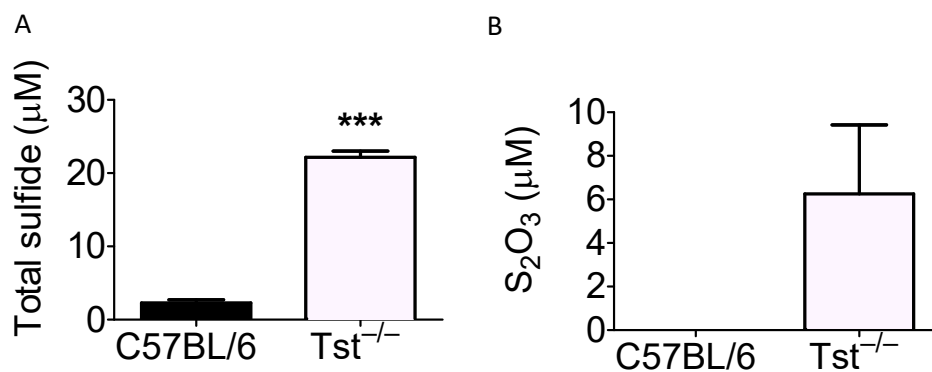
Figure 1.8 Total sulfide and thiosulfate (S$_2$O$_3$) detected in whole blood of C57BL/6 and *Tst*$^{-/-}$ mice. A) Total sulfide detected in whole blood of C57BL/6 and *Tst*$^{-/-}$ mice. B) Thiosulfate detected in whole blood of C57BL/6 and *Tst*$^{-/-}$ mice. Thiosulfate was undetectable in C57BL/6 mice therefore it was not possible to test the data using unpaired t-test. Whole blood reacted with monobromobimane to derivatise -SH containing compounds to sulfide dibimane. Peak identities were assigned using pure chromatography standards. 4 independent biological repeats are shown for each genotype. *** indicates p < 0.0001 unpaired Student's t test. Data was prepared by Martin Barrios-Llorena and provided by Dr Roderick Carter/Prof Nik Morton (personal communication).

1.5.2 Thiosulfate sulfurtransferase in the vasculature

Little work has been reported investigating the effect of *Tst* deletion in the vessels of *Tst*$^{-/-}$ mice, although expression of TST in cardiac vessels has been confirmed by Emerson *et al.* (Figure 1.9, Unpublished observations). As shown by previous work in *Cse*$^{-/-}$ mice, however, decreased H$_2$S signalling within the vasculature can lead to hypertension, a loss of endothelium-mediated vasorelaxation and a worsening of atherosclerosis (187,192). Given the clear findings of elevated H$_2$S in *Tst*$^{-/-}$ mice detected in whole blood (above, 200) the vascular function of *Tst*$^{-/-}$ mice represents a target for further investigation. In addition, the effect of *Tst* deletion on atherosclerotic lesion development in an appropriate model (e.g. *ApoE*$^{-/-}$ mice fed western diet) would be a useful test of the function of *Tst* in chronic vascular disease.
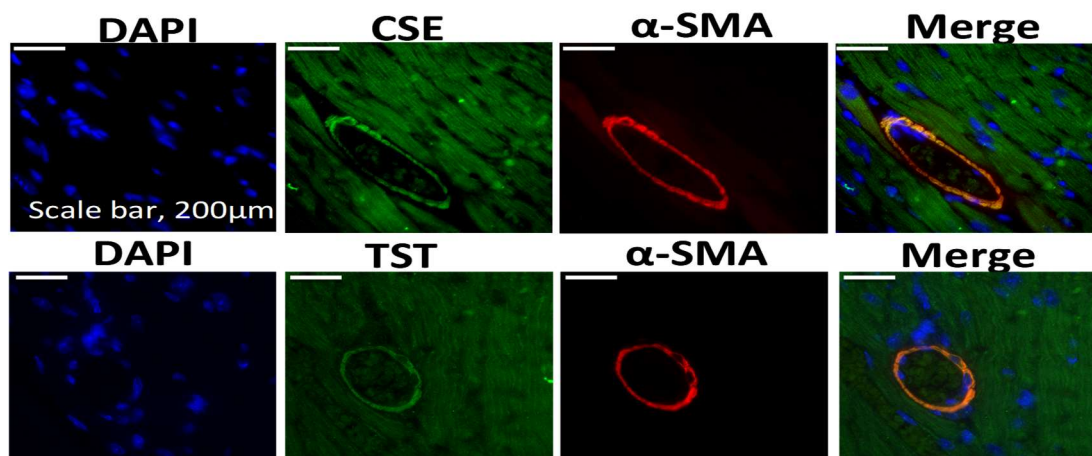
Figure 1.9 TST is expressed in the smooth muscle of cardiac vessels. Fluorescence microscopy of heart sections using a nuclear dye (DAPI; blue), and antibodies against CSE (green, upper panel) and TST (green, lower panel) enzymes co-localised with smooth muscle marker alpha-SMA (red). The far-right panel shows merged images (Emerson *et al*. unpublished data).

1.6 Hypotheses and aims

Based on the evidence described above, 2 major hypotheses were proposed in this Thesis.

1. Deletion of *Tst* engenders hepatic metabolic dysfunction.
2. Deletion of *Tst* results in protection from endothelial dysfunction and atherosclerosis

Aims

To test these hypothesis, the following aims were pursued

1. To undertake extensive metabolic phenotyping of $Tst^{-/-}$ and C57BL/6 mice in control or high fat diet-fed conditions with a focus on aspects of hepatic metabolism, where *Tst* is most highly expressed.
2. To investigate vascular function in control and high fat diet-fed $Tst^{-/-}$ and C57BL/6 mice using isolated arteries to determine whether *Tst* deletion alters contraction or relaxation of the arterial wall.
3. To determine atherosclerotic lesion formation in an inter-cross of $Tst^{-/-}$ with $ApoE^{-/-}$ mice ($ApoE^{-/-}Tst^{-/-}$ double knockout mice) fed an atherosclerosis-accelerating western diet.

2.0 Materials and methods

Unless otherwise stated all reagents were obtained from Sigma-Aldrich, St. Louis, US.

2.1 Experimental Animals

2.1.1 Colony maintenance

Mice were bred, and group housed in a controlled environment at the Biological Research Resources department of the University of Edinburgh. Temperature and humidity were maintained at 21-22°C and 50%, respectively with a 12-hour diurnal light/dark cycle (7am to 7pm). Mice were given ad-libitum access to water and standard mouse CRM 'chow' (Special Diet Services, Essex, UK) except during fasting or high fat feeding experiments (section 2.1.2.) All animal procedures were performed in accordance with the animals (scientific procedures) act 1986 and received local ethical approval.

2.1.2 Alteration of diet

During high fat feeding experiments (details given within results chapters) mice were given ad libitum access to either 'Surwit' 58% fat, high sucrose diet referred to as 'high fat diet' (HFD, Research Diets, New Brunswick, US) or 'Western' 42% fat, 0.15% cholesterol diet (829100, Special Diet Services, Essex, UK). Within HFD experiments standard chow (RM1 diet) was used for control groups. For Western diet fed experiments AIN93M 9.4% fat control diet (Special Diet Services, UK) was used for control groups.

2.1.3 Generation of $ApoE^{-/-}Tst^{-/-}$ double knock-out

Throughout the breeding process genotyping for Tst and $ApoE$ was performed by Transnetyx, Cordova, US. B6.129P2-$Apoe^{tm1Unc/J}$ mice ($ApoE^{-/-}$) were initially purchased from Charles River, Tranent, UK. These mice are on a C57BL/6J background. $Tst^{-/-}$ mice, previously generated (204) as a full Tst deletion ($Tst^{tm1(KOMP)Vlcg}$) by the University of California at Davis knockout mouse project and kindly donated by Prof. Nicholas Morton, were initially on a C57BL/6N background (204). To generate double knock-out and $ApoE^{-/-}$ controls on a uniform C57BL/6J background a speed congenics backcrossing approach was undertaken in collaboration with Prof. Simon Horvat. Initially sex chromosomes were fixed to J by crossing $ApoE^{-/-}$ with $Tst^{-/-}$ and selecting obligate heterozygotic Males (Y(6N), X(6J)) for a second breeding round with $ApoE^{-/-}$ females. Selection of $Tst^{+/-}ApoE^{-/-}$ female offspring then ensured that both sex chromosomes were of J background.
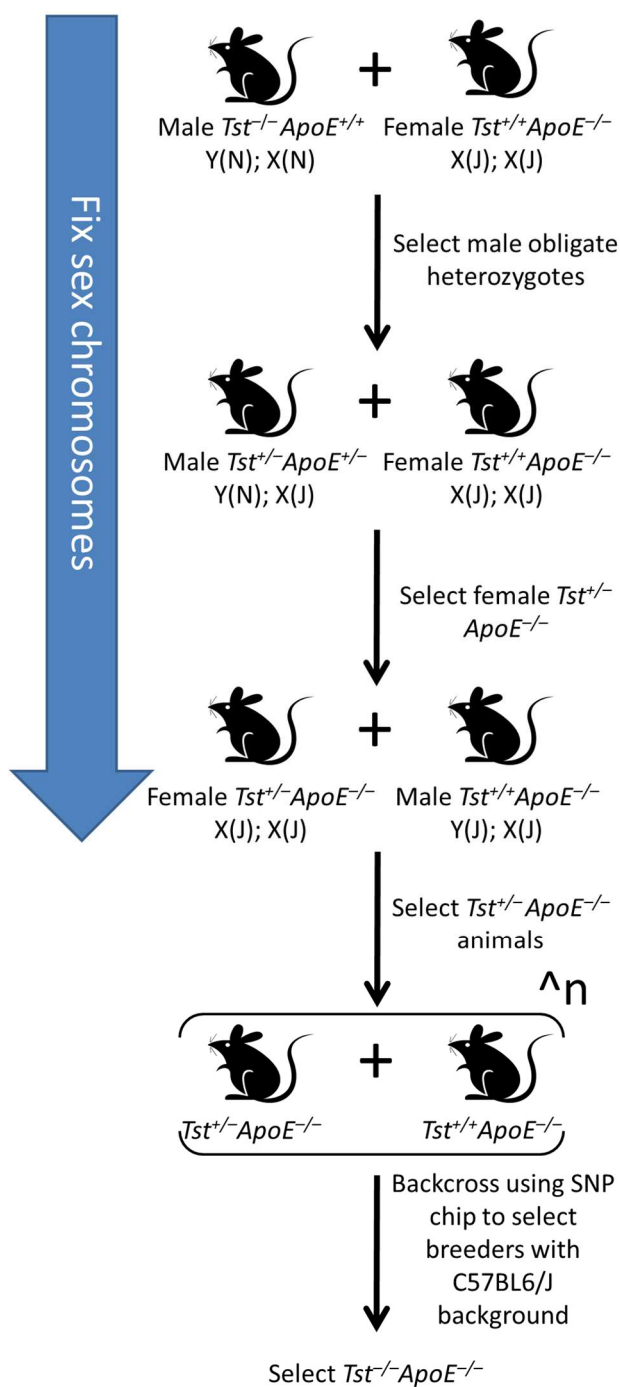
Figure 2.1 Breeding strategy for *ApoE⁻/⁻ Tst⁻/⁻* double knockout breeding. During the initial crosses the sex chromosomes were fixed to J subtype through selection of specific sexes from litters. Following this selection of mice for backcrossing was guided using a speed congenics panel performed by Prof. Simon Horvat designed to identify key differences between N and J subtypes and genotyping for *Tst* and *ApoE* performed by Transnetyx. Once mice were found to be J subtype at all genotyped regions mice were crossed and double knockouts selected.

During the following rounds of breeding a so-called "speed congenics" protocol (209) was used. The starting population was of $ApoE^{-/-}$; $Tst^{+/-}$ genotype on a mixed C57BL/6J/C57BL/6N (N/J) genetic background. Though strains N/J are genetically very closely related, detailed genome sequencing project (210) and especially a comprehensive genomic and phenotypic comparison of the N/J strains (211) identified several SNP and copy number variant differences as well as significant phenotypic differences. In five consecutive backcross generations parents of the next generations were selected based on their proportion of the N/J genome – pairs with the highest proportion of the J genome were chosen for further breeding. Primers (Appendix, table 1) for genotype screening were designed in the Primer 3 software (http://bioinfo.ut.ee/primer3/) based on the information on polymorphisms found between the N/J strains (211). Point mutation loci were screened either by restriction fragment length polymorphism assay in agarose gels or Sanger sequencing, while some structural length variants by resolving PCR products in high resolution 4% agarose gel electrophoresis.

Following completion of the breeding cycles animals were determined as being J substrain at all tested mutation loci. Heterozygous mice were then crossed to generate $ApoE^{-/-}Tst^{+/+}$ and $ApoE^{-/-}Tst^{-/-}$ mice for further testing.

2.2 *In vivo* techniques

2.2.1 Fasting glucose and insulin

Mice were fasted for a short period (4-6 hours) with free access to water. A blood sample was taken from the tail vein to measure glucose using a OneTouch Ultra glucometer (LifeScan, Milpitas, US) and disposable OneTouch testing strips (LifeScan, Milpitas, US). Further blood was taken from the tail using a Sarstedt EGTA blood collection tube and kept on ice. Following manufacturer's guidance these samples were then centrifuged at 20°C at 10000 g for 5 minutes to isolate plasma. Plasma samples were stored at -80°C before insulin was measured following using an Ultra-Sensitive Mouse Insulin ELISA kit (Crystal Chem, Zaandam, Netherlands) following manufacturer's guidance.

2.2.2 Glucose tolerance test

Animals were fasted for 4-6 hours with free access to water. A tail nick was made for blood sampling and an initial baseline blood glucose taken using disposable glucose testing strips and a glucometer. If insulin measurements were being recorded, then a blood sample was also taken into a Sarstedt EGTA blood collection tubes and kept on ice before later centrifugation and collection/storage of blood plasma. This time point was referred to as time 0. Immediately following this 25% glucose dissolved in 0.9% saline (0.9 g NaCl/100 ml 18 Ω H_2O) was administered via intra peritoneal bolus at a dose of 2 mg/g body weight using a 0.3 or 0.5 ml BD Micro-Fine Insulin syringe (BD, Madrid, Spain). The disposal of the glucose bolus was measured by taking blood glucose concentrations at 15, 30, 60 and 120 minutes post injection. Larger samples for plasma collection and insulin measurement were taken as required.

2.2.3 Insulin tolerance test

As above animals were fasted for 4-6 hours with free access to water. A tail nick was made for blood sampling and an initial baseline blood glucose taken using a glucometer and disposable glucose test strips. This sample was referred to as time 0. Immediately following this insulin (Humulin, Eli Lilly, Indianapolis, USA) was administered via intra peritoneal bolus at a dose of 1mU/g body weight. Further blood glucose measurements were performed at 15, 30, 45 and 60 minutes following the bolus to record the effect of insulin administration.

2.2.4 Tail plethysmography

Systolic blood pressure was recorded in conscious mice using a tail cuff system along with automatic recording software (Harvard Apparatus, Cambourne, UK). Briefly, an inflatable

cuff and measurement device capable of detecting the reduction of a luminosity signal caused by blood flow in the tail vein was passed over the tail. Once a blood flow signal was clearly identifiable the measurement program was started. This involved 4 inflation and deflation cycles. As the pressure of the cuff became equal to the systolic pressure of the mouse this was detected as a reduction and finally cessation of the signal oscillation. Deflation was the more accurate measurement (reappearance of the signal was more easily visible) and so the 4 measures of systolic pressure during the deflation cycle were used to calculate the average systolic pressure for the mouse. Details of the number of measurements taken can be found in the results chapter.

2.3 *Ex vivo* techniques

2.3.1 Plasma lipid profiling

Mice were fasted with free access to water for 4 hours prior to cull. During this process, a terminal blood sample was taken by one of two methods. Primarily blood was collected directly into Sarstedt Microvette CB 300 K2E EGTA containing plasma sample tubes (Sarstedt, Nümbrecht, Germany) following cull by decapitation. When other techniques did not allow for this (e.g. perfusion fixation section 2.7.1.1) mice were instead euthanised with an overdose of sodium pentobarbital (Euthatal, Scientific Laboratory Supplies, Wilford, UK) given as an intraperitoneal (i.p.) bolus. Following cessation of respiration, the abdominal cavity was rapidly opened, and blood sampled into a BD Plastipak 1 ml syringe (BD, Madrid, Spain) from the abdominal vena cava. This was then transferred to Sarstedt EGTA containing sample tubes for centrifugation. Blood samples obtained by either method were centrifuged at 20°C and 10000 g for 5 minutes according to manufacturer's guidance to obtain plasma samples.

Plasma samples were analysed for cholesterol and triglyceride content by Prof. Bart Staels and Dr. Anne Muhr-Tailleux as previously described (212). Briefly, samples were subjected to gel filtration chromatography using an integrated Alliance HPLC separations module (e2695, Waters, Milford, US) to separate lipoproteins based on size. Effluent was immediately and continuously mixed with either triglyceride (Infinity Triglyceride, Thermo Scientific, Loughborough, UK) or cholesterol (Infinity Cholesterol, Thermo Scientific, Loughborough, UK) enzymatic colourmetric detection kits at the correct conditions for reaction (as specified in manufacturer's guidance). The optical density was then recorded using a spectrophotometer at the appropriate wavelength and the signal turned into a continuous trace i.e. a lipid profile. By identification of the lipoprotein peaks (based on their time of emergence from the chromatograph) the concentration for each could be calculated.

2.3.2 Myography

2.3.2.1 Vessel isolation and mounting

Mice were euthanised by CO_2 asphyxiation and the descending heart and thoracic aorta were isolated and removed down to the diaphragmatic insertion. The heart and vessel were immediately placed in ice cold physiological salt solution (PSS; 120 mM NaCl, 5 mM KCl, 1.2 mM $MgSO_4.7H_2O$, 25 mM $NaHCO_3$, 1.2 mM KH_2PO_4, 0.034 mM EDTA, 6 mM glucose and 2.5 mM $CaCl_2.2H_2O$) and then transferred to a dissection plate coated with matrigel allowing the vessel to be securely stretched out and pinned down. Using a dissecting

microscope, the adventitial fat was then removed from the aorta using fine forceps and spring scissors (Fine Science Tools, Heidelberg, Germany) and the aorta was detached from the heart. 2 mm long vascular rings for myography were taken from the region of the aorta immediately following the aortic arch. These rings were mounted in the organ baths of a multi myography model 610 M wire myograph (Danish Myo Technology, Aarhus, Denmark). Briefly, vessels were threaded onto 40 μm tungsten wire (Danish Myo Technology, Aarhus, Denmark) and secured between the jaws of the myography supports. A second wire was then passed through the lumen of the vessel and secured to the opposing support.

2.3.2.2 Concentration response measurements

Following mounting the vessels were returned to the myograph which maintained the temperature of the baths at 37°C and continuously perfused with 95%O_2/5%CO_2 (BOC, Guildford, UK). A resting tension of 7.38 mN was applied to aortic vessels for 30 minutes by adjustment of the micrometer. This has been previously determined as the optimal resting force for mouse aorta. Data were recorded by connecting the myography output to a bridge amplifier (AD Instruments Powerlab 8/30, AD Instruments, Oxford, UK) and subsequently into a computer running LabChart 8 software (AD Instruments, Oxford, UK). Following the establishment of a stable resting tension in vessels the myography was zeroed and 3 measurements were recorded following the addition of high K^+ PSS (KPSS; 125 mM KCl, 1.2 mM $MgSO_4.7H_2O$, 25 mM $NaHCO_3$, 1.2 mM KH_2PO_4, 0.034 mM EDTA, 6 mM glucose and 2.5 mM $CaCl_2.2H_2O$, aerated continuously with 95% O2/5% CO_2). Between each stimulation the organ bath was washed with PSS until the vessel had returned to its resting tension. The maximal tension after 2 minutes of constriction with KPSS represented the vessels 'baseline constriction' for normalisation of data.

Following KPSS stimulation vessels were returned to resting tension and then cumulative concentration-response curves to a number of compounds were recorded. If inhibitor compounds such as 10^{-4} M L-NAME and 10^{-5} M indomethacin were used these were incubated for a minimum of 20 minutes before cumulative concentration-response curves were recorded. Vasoconstriction responses to 5-hydroxytryptamine (5-HT) and α1-adrenoreceptor agonist phenylephrine (PE) were recorded in half log steps from 10^{-9} to 10^{-4} M and 10^{-9} to 10^{-5} M, respectively. Vessels were washed with PSS and left to return to resting tension between responses. For vasodilation responses vessels were preconstricted using a concentration of 5-HT to achieve approximately 80% of maximal tension. 5-HT was used for this as opposed to PE because it was found in aorta that 5-HT produced larger more stable constrictions. Following a stable preconstriction of 5-10 minutes a cumulative

concentration-response to vasodilators such as acetylcholine and sodium nitroprusside was recorded in half log steps from 10^{-9} to 10^{-4} M. Exact protocols are recorded in the relevant results section.

2.3.2.3 Normalisation

For vasoconstriction agents, the recorded tension of each vessel in response to administration of the compounds was normalised to the baseline constriction of that vessel and expressed as a percentage. For vasodilation, the response of the vessel was expressed as a percentage of the initial tension of the vessel. These data were plotted using GraphPad Prism 5 software (Graph Pad Software, La Jolla, US) and 3 variable non-linear regression curve fitting performed. From these curves summary data such as E_{Max} (maximal constriction) and EC_{50} (concentration eliciting 50% of E_{Max}, also converted to $-\log(EC_{50})$ i.e. pD_2 or $-\text{Log}(IC_{50})$ for constrictors or dilators, respectively) were calculated automatically. Where responses were recorded with and without L-NAME (10^{-4} M) and indomethacin (10^{-5} M) the difference between the EMax values was calculated (ΔE_{Max}).

2.4 Biochemical assays

2.4.1 Liver triglyceride measurement

Frozen liver samples (approximately 50 mg) were accurately weighed before transfer to a borosilicate glass culture tube (Thermo Scientific, Loughborough, UK). The sample was then homogenised in 10 volumes (W/V) isopropanol (20 volumes W/V was used for 20-week HFD samples) using a mechanical homogeniser (T8.10, IKA Labortechnik, Staufen im Breisgau, Germany). Throughout the remainder of the procedure tubes were covered with Parafilm (Bemis, Neenah, US) to avoid evaporation of samples. Tubes were agitated for 45 minutes on a shaker and vortexed every 10 minutes. Following this samples were centrifuged at 4°C at 835 g for 10 minutes in an Eppendorf 5415 R centrifuge (Eppendorf, Stevenage, UK). The supernatant was removed to a fresh glass sample tube with a stopper to prevent evaporation. Triglyceride content of the samples was detected using Thermo infinity triglyceride reagent (Thermo Scientific, Loughborough, UK). The reaction scheme of this enzymatic reagent is shown below:

1. $Triglycerides + H_2O \xrightarrow{Lipase} Glycerol + Free\ fatty\ acids$

2. $Glycerol + ATP \xrightarrow{Glycerol\ Kinase} Glycerol\ 3\ phosphate + ADP$

3. $Glycerol\ 3\ phosphate + O_2 \xrightarrow{Glycerolphosphate\ oxidase} DAP + 2H_2O_2$

4. $H_2O_2 + 4AAP + 3,5\ DHBS \xrightarrow{Peroxidase} Quinoneimine\ dye + 2H_2O$

Reaction 2.1 Triglyceride assay reaction scheme.

Following manufacturer's instructions 7 glycerol standards between 0.25-8 mmol/L were made up in isopropanol. 2 µl of standard, sample or isopropanol blank was added to a 96 well assay plate (Corning Life Sciences, Amsterdam, The Netherlands) before adding 198 µl of reagent. Samples typically had to be diluted 5-20 times to ensure they were within the standard curve. The reaction was left at 37°C for between 20-40 minutes and then absorbance measured using a plate spectrophotometer (Molecular Devices OPTImax microplate reader and software, Molecular Devices, Wokingham, UK) at 500 nm. All standards, samples or blanks were performed in duplicate. Duplicates were analysed for %CV values and the mean only included in further statistical analysis if <15%. Unknown samples were interpolated from the standard curve and multiplied by their dilution factor giving final units of µmol/g liver.

2.4.2 Liver glycogen measurement

2.4.2.1 Glycogen extraction and breakdown

Frozen liver samples (between 30-90 mg) were accurately weighed and recorded. The sample was added to a 1.5 ml Eppendorf tube (Eppendorf, Stevenage, UK) along with 0.3 ml 30% KOH. Samples were heated to 100°C on a Techne Dri-Block DB-2A (Techne, Stone, UK) for 30 minutes with vigorous shaking at 10-minute intervals to aid dissociation. Following this 0.1 ml 1M Na_2SO_4 and 0.8 ml ethanol were added, and samples were heated for a further 2-3 minutes. Samples were then centrifuged at 4°C at 1011 g in an Eppendorf 5415 R centrifuge for 5 minutes. The supernatant was removed, and the pellet resuspended in distilled H_2O before 0.1 ml 1M Na_2SO_4 and 0.8 ml ethanol were again added, and samples boiled at 100°C for 5 minutes before centrifugation. This was repeated a final time to wash the sample. Following removal of the supernatant after the final wash the pellet was resuspended in a 10 mg/ml (~1200 U/ml) amyloglucosidase enzyme solution dissolved in 0.3 M sodium acetate adjusted to pH 4.8 with HCl. Samples were then incubated at 50°C for 2 hours to allow for glycogen breakdown into glucose. Quantification of samples was then performed using a standard hexokinase-based glucose assay.

2.4.2.2 Hexokinase glucose assay

The assay was performed following manufacturer's instructions. Briefly, 7 glucose standards were made up between 0.25-5 mg/ml in distilled 18 Ω H_2O. Samples were diluted in H_2O to be within the linear range of the assay. All assays were performed in duplicate with the mean taken for further analysis. 2 µl of standard, sample or H_2O blank were added to the wells of a 96 well plate. A non-enzyme control was included for each sample to check for any absorbance caused by the sample itself by replacing the reagent mix with distilled water. 198 µl of glucose reagent or H_2O was added to each sample and left to react for approximately 15 minutes at 20-25°C. Absorbance was then measured using a plate spectrophotometer (Molecular Devices OPTImax microplate reader and software, Molecular Devices, Wokingham, UK). A samples final absorbance was calculated by taking the absorbance of the sample (A_{Sample}) – absorbance of its H_2O control ($A_{Sample\ Blank}$) – absorbance of the 0 mg/ml glucose control (A_{Blank}) (Absorbance = $A_{Sample} - A_{Sample\ Blank} - A_{Blank}$). Unknown samples were interpolated from the standard curve.

2.4.4 Phosphoenol pyruvate carboxykinase (PEPCK) enzyme activity

Cytosol samples were obtained from 100 mg unfrozen fresh liver samples by the following method. All steps were performed on ice or at 4°C. Liver samples were homogenised in 1.2 ml SH buffer (250 mM sucrose, 5 mM HEPES, pH 7.4) using a glass Potter Elvehjem homogeniser and centrifuged for 15 minutes at 4°C at 13362 g in an Eppendorf 5415R centrifuge (Eppendorf, Stevenage, UK). Supernatants were then transferred to a Beckmann polycarbonate ultracentrifuge tube (Beckman Coulter, High Wycombe, UK) and centrifuged at 195028 g for 30 minutes at 4°C in a Beckman Optima TLX ultracentrifuge (Beckman Coulter, High Wycombe, UK). Supernatants were diluted 1:10 and measured for protein concentration using Bio-Rad DC protein reagent (Bio-rad, Watford, UK) and following manufacturer's guidance (described in section 2.9).

For the activity assay reactions were prepared on a 96 well plate. All solutions were kept on ice throughout preparation. The activity of PEPCK was inferred in this assay from the measure of NADH extinction. The reaction scheme is outlined in reaction 2.2. All assays were performed in duplicate with the mean taken for further analysis. Fresh 5 mM NADH, 3 mM dGDP and 5 mM PEP were prepared along with a CO_2 buffer (66 mM $NaHCO_3^-$, 66 mM HEPES, 1.5 mM $MnCl_2$) and a 1:308 dilution of malate dehydrogenase which was diluted in CO_2 buffer. 200 µg protein from the cytosol sample (between 10-20 µl), 10 µl MdeH and 10 µl NADH were added to a variable volume of CO_2 buffer up to a final volume of 182 µl prior to be being placed in a Tecan infinite M1000 spectrophotometer (Script software, Tecan, Reading, UK) which was heated to 37°C. Measurements were set to be taken every 30 seconds at 340 nm for 60 minutes to allow for equilibration of the reaction and establishment of a baseline rate of extinction. The plate was then removed and placed on ice for 30 seconds to slow the reaction before adding 8 µl PEP and 10 µl dGDP and replacing the plate. The reaction was followed using the same settings for a further 60 minutes to record both a linear rate of decrease and the final plateau. For analysis, the rate for each sample was calculated from a linear portion of the curve.

1. $Phosphoenol\ pyruvate + dGDP + CO_2 \xrightarrow{PEPCK} Oxaloacetate + GTP$
2. $Oxaloacetate + NADH \xrightarrow{MDH} Malate + NAD^+$
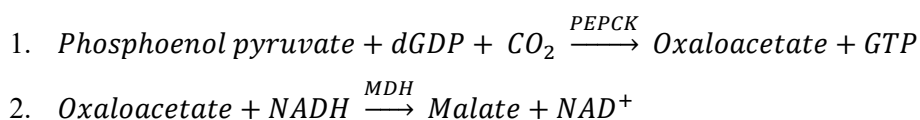
Reaction 2.2 Phosphoenolpyruvate carboxykinase activity assay reactions.

2.4.5 TST activity assay

Reactions were performed in a 96 well plate. 50 µg of protein (collected from tissues as described in 2.9) was used in each reaction and a negative reaction containing no protein was

also prepared. 50 mM KPO_4 and 50 mM NaS_2O_3 were added to the reaction along with a variable volume of 18 Ω H2O to adjust for volume. The reaction (shown below) was started with the addition of 50 mM KCN.

$$\overset{TST}{}$$

1. $S_2O_3^{2-} + CN^- \rightarrow SO_3^{2-} + SCN$
2. $SCN + Fe(NO_3)_3 \rightarrow Fe(SCN)^{2+}$

Reaction 2.3 Reaction scheme for TST activity assay.

All assays were performed in duplicate with the mean taken for further analysis. 7 standards of KSCN were prepared from 0.25-25 mM along with a zero and added to the reaction plate. The reaction was incubated at 30°C for a length of time relative to the tissue expression of TST. Liver protein reactions were left for 30 minutes whereas aortic protein reactions were left for 4 hours. The reaction was stopped with the addition of 10% formalin solution (38% formaldehyde) to all wells. An equal volume of acidified iron nitrate (250 mM Fe(NO3)/26 % nitric acid) was then added to form the iron complex leading to a colour change. Absorbance was then measured at 460 nm using a plate spectrophotometer. The 0 standard was subtracted from all values and a linear standard curve generated. Following further subtraction of the no protein control from the unknown samples the concentrations were interpolated from the standard curve.

2.4.6 Insulin ELISA

Blood samples were collected in Sarstedt Microvette CB 300 K2E EGTA containing plasma sample tubes (Sarstedt, Nümbrecht, Germany) and centrifuged at 20oC at 10000 g for 5 minutes following manufacturer's guidance to collect plasma samples. Insulin concentration was assayed in plasma samples using an Ultra-Sensitive Mouse Insulin ELISA kit (Crystal Chem, Downers Grove, USA) following manufacturer's instructions. All assays were performed in duplicate with the mean taken for further analysis. Briefly, 5 µl of plasma or provided mouse insulin standards was mixed with 95 µl of sample diluent in an antibody coated well of the plate. Plates were then incubated for 2 hours at 4°C before being washed 5 times using provided wash buffer. 100 µl of anti-insulin enzyme conjugate solution was added to wells and left for 30 minutes at 20-25°C to react. Following this; plates were washed 7 times using wash buffer before 100 µl of enzyme substrate was added to wells. Plates were incubated for 40 minutes at 20-25°C avoiding exposure to light before the reaction was stopped through addition of 100 µl of stop solution. Absorbance at 450 and 630 nm was immediately measured using a plate

spectrophotometer. Following manufacturer's instructions A_{630} was subtracted from A_{450} before unknown concentrations were interpolated from the linear standards.

2.5 Molecular Biology

2.5.1 Protein collection

For tissue homogenisation, fresh tissues were collected and stored on ice or at -80ºC for long term storage. The required amount of tissue was transferred to either a PeqLab Precellys 2 ml homogenisation tube (VWR, Lutterworth, UK) or a 2 ml Eppendorf safety lock tube (Eppendorf, Stevenage, UK). Depending on expected protein yield a variable amount of protein lysis buffer (50 mM Tris, 270 mM sucrose, 50 mM NaF, 1 mM EDTA, 1 mM EGTA, 1% Triton-X) with added cOmplete ULTRA protease inhibitor tablets (Roche, Mannheim, Germany) and phosphatase inhibitors (10 mM β-glycerophosphate, 1 mM Na Orthovanadate, 5 mM Na pyrophosphate, 0.1% β-mercaptoethanol, all added fresh on day of use) was used. PeqLab Precellys tubes were used in conjunction with a PeqLab Precellys 24 tissue homogeniser (VWR, Lutterworth, UK). The standard protocol for mechanical homogenisation was 2 x 20 seconds at 6500 RPM.

For homogenisation of samples using Eppendorf tubes a ball bearing was transferred to the tube before placing the tube into a Retch Mixer Mill MM301 tissue homogeniser (Retsch, Haan, Germany) for 30 seconds at 30 Hz. This process was repeated as required until the tissue was completely homogenised. Following either homogenisation technique samples were centrifuged for 10 minutes at 16168 g at 4ºC. The supernatant was then collected as the protein sample. If necessary (due to contamination with lipid content for example) samples were centrifuged again to aid removal.

For cells either 0.1 ml or 3 ml of protein lysis buffer was added to 6 well cell plates (Corning Life Sciences, Amsterdam, The Netherlands) or 75 ml culture flasks (Corning Life Sciences, Amsterdam, The Netherlands), respectively. Cells were then physically lysed by scraping with either pipette tips or a cell scraper (Corning Life Sciences, Amsterdam, The Netherlands). The solution was collected and centrifuged for 10 minutes at 16168 g at 4ºC to remove any crude cell debris.

2.5.2 Protein quantification

Briefly, samples were diluted to ensure absorption was within the linear standard curve (0-1.2 mg/ml, made up using Bovine Serum Albumin). All assays were performed in duplicate with the mean taken for further analysis. 5 μl of standard or sample was added to a 96 well plate (96 well ELISA Microplates, Greiner bio-one). 25 μl of solution A was then added to each sample which were then briefly mixed. 200 μl of solution B was then added to all wells and the plate was incubated for a minimum of 15 minutes at room temperature. Absorption at 750 nm was then measured using a plate spectrophotometer (Molecular

Devices OPTImax microplate reader and software, Molecular Devices, Wokingham, UK). Sample concentrations were interpolated from the standard and adjusted for dilution factors. Following quantification cytosol samples were used immediately in the PEPCK activity assay.

2.5.3 mRNA quantification

2.5.3.1 mRNA isolation

RNA was collected from tissue or cells using Qiazol reagent (Qiagen, Hilden, Germany). All steps were performed on ice or at 4°C unless otherwise stated. For tissues, the sample was placed in 500 µl Qiazol in a PeqLab Precellys homogenisation tube or a 2 ml Eppendorf with a ball bearing. The tissue was then physically homogenised using either a PeqLab Precellys 24 homogeniser (for Precellys tubes) or a Retch Mixer Mill MM301 tissue homogeniser. For cells, a minimal volume of Qiazol was used (approximately 300 µl) to ensure well coverage and cells were physically lysed by scraping. Following this samples from tissue or cells were treated identically.

Samples were centrifuged at 16168 g for 10 minutes at 4°C to remove any crude debris. The supernatant was transferred to a fresh 1.5 ml Eppendorf tube and 1:5 volume of chloroform was added. The sample was thoroughly mixed through inversion and then left for 5 minutes at room temperature to separate. The samples were centrifuged at 16168 g for 5 minutes at 4°C and then the aqueous (top) layer was carefully transferred to a new Eppendorf tube. An equal volume of isopropanol was added and mixed thoroughly with the sample. Samples were then centrifuged to collect the precipitated RNA for 10 minutes at 16168 g at 4°C. The pellet of RNA was washed twice by removing the supernatant and resuspending the pellet in 70% ethanol made with DEPC treated distilled water. Finally, the ethanol was removed, and the pellet allowed to air dry briefly. The pellet was then dissolved in 50 µl DEPC treated distilled water and the solution was quantified for RNA content using a ND-1000 Nanodrop spectrophotometer (Nanodrop, Thermo Scientific, Loughborough, UK).

2.5.3.2 Reverse transcription

RNA samples were used for reverse transcription and quantitative real-time polymerase chain reaction (qRT-PCR) for mRNA quantification. Initial RNA samples were diluted to an appropriate concentration and reverse transcribed using Qiagen QuantiTect Reverse Transcription Kit (Qiagen, Hilden, Germany) following manufacturer's guidance. Briefly, for each sample a known amount of RNA (300 – 1000 ng) was added to a fresh 1.5 ml Eppendorf. A control sample which would not receive the reverse transcription enzyme was also prepared using RNA from a mixture of random samples. The samples were then incubated with genomic DNA Wipeout buffer and a variable volume of RNase free water at

42°C for 2 minutes before being placed on ice. A master mix containing Quantiscript Reverse Transcriptase enzyme, Quantiscript RT Buffer and RT Primer Mix was prepared and the appropriate volume added to each sample. The reaction was then incubated for 30 minutes at 42°C. To terminate the reaction, the temperature was increased to 95°C for 3 minutes at the end of the reaction. Finally, samples were centrifuged briefly (<20 seconds) to collect them. This sample represented the 'neat' cDNA samples. To generate a standard for RT-PCR analysis approximately 4-5 µl was taken from each cDNA sample and added to a pooled standard. This standard was diluted 1:4 for use in RT-PCR. The first standard was assigned the value 256 and then serially diluted 1:2 to generate standards: 256, 128, 64, 32, 16, 8, 4. The remaining cDNA in the samples was diluted 1:10 for use in RT-PCR. All standards and samples were stored at 4°C.

2.5.3.3 Quantitative Real Time Polymerase Chain Reaction (qRT-PCR)
For RT-PCR 2 µl of standard, sample or reverse transcription control was pipetted onto a 384 well RT-PCR compliant wellplate (384 well lightcycler plate, Sarstedt, Nümbrecht, Germany). A no template control (RNAase free water) was also included as a final standard. All reactions were run in triplicate and the mean used for further analysis. *Tst* (Mm01195231_m1), *Tbp* (Mm01277042_m1) and *Gapdh* (Mm99999915_g1) Taqman assay probes were obtained from Applied Biosystems (Thermo Scientific, Loughborough, UK). A master mix for each gene was made up using the Taqman probe, DEPC treated H2O and qRT-PCR master mix (PerfeCTa FastMix, Quantabio, Beverly, USA) per reaction. 8 µl of gene specific master mix was added to each sample. The plate was then sealed using a plastic cover (Sarstedt, Nümbrecht, Germany) and centrifuged using a plate centrifuge (LMC-3000, Grant-Bio, Shepreth, UK) at 560 g for 2 minutes at 20-25°C. The wellplate was added to a Roche Lightcycler (Lightcycler 480, Roche, Mannheim, Germany) RT-PCR machine and a standard FAM hydrolysis protocol run. The quantification segment of the protocol consisted of a repeated amplification cycle where temperature was cycled to 95°C for denaturing (to a single strand), to 60°C for primer annealing, and finally to 72°C for elongation by Taq polymerase. This was repeated for 50 cycles. Based on the standard curve which was recorded and calculated the Roche Lightcycler software the expression value for unknown samples was automatically interpolated. Accuracy of the triplicates Ct values (within 0.2) and efficiency of the amplification (ideally 2.0) was manually checked for acceptability.

2.6 In vitro techniques

2.6.1 Primary hepatocyte isolation and culture

Primary hepatocytes were isolated from mouse liver using a modified protocol from the University of Santa Cruz. Briefly, mice were euthanised using CO_2 before rapid dissection to expose the portal vein and thoracic inferior vena cava. The portal vein was then cut followed immediately by cannulation of the vena cava. Perfusion with Liver Perfusion Media (LPM, 140 mM NaCl, 2.6 mM KCl, 0.28 mM Na_2HPO_4, 5 mM glucose, 10 mM HEPES, 0.5 mM EGTA) was driven by a peristaltic pump (Minipuls 2, Gilson, Dunstable, UK) for 10 minutes. During this time, the liver visibly cleared of blood. Following this the perfusion was switched to Liver Digestion Media (LDM, 140 mM NaCl, 2.6 mM KCl, 0.28 mM Na_2HPO_4, 5 mM glucose, 10 mM HEPES, 5 mM $CaCl_2$) containing 100 U/ml type I collagenase (Worthington Biochemical corporation, Lakewood, US) for between 5-7 minutes depending on the response of the liver to the collagenase. Once the liver was sufficiently digested the perfusion was returned to LPM for 10 minutes to flush the liver of collagenase. The liver was then excised and transferred to DMEM D5546 media containing 10% Hyclone fetal calf serum, 1% Penicillin streptomycin and 8 mM L-glutamine (all Invitrogen, Carlsbad, USA).

Isolation of the cells was then performed in sterile conditions using a BioMAT[2] cell culture flow hood (Contained Air Solutions, Manchester, UK) and aseptic technique. The liver was transferred to a petri dish and physically manipulated with forceps to encourage cells to dissociate into the media. This media was then filtered using a Fischerbrand 100 µm sterile cell strainer filter (Thermo Scientific, Loughborough, UK) to remove any crude tissue and transferred to a clean 50 ml CellStar tubes (Greiner bio-one, Kremsmünster, Austria). Following this, cells were collected by centrifugation at 216 g at 20-25°C in a Heraeus Megafuge 1.0 R (Thermo Scientific, Loughborough, UK) for 5 minutes. The supernatant was removed, and the cells were resuspended in 10 ml DMEM before repeated centrifugation to wash the preparation. Cells were again resuspended in 10 ml DMEM media. A 50% Percoll solution was prepared from 100% commercially available Percoll equalised with DMEM by addition of 11 ml 10x DMEM media and mixed 1:1 with 1x DMEM. 50% Percoll was added underneath the cell containing suspension creating a 2-layered solution. This was centrifuged at 723 g for 15 minutes at 20-25°C. Pelleted cells represented viable primary hepatocytes. The layer of cells contained at the border of the Percoll and DMEM were dead or not hepatocytes and these were removed and disposed of with the rest of the supernatant. Any remaining Percoll was removed by twice washing the cells through centrifugation collection resuspension in DMEM media. The final cell pellet was resuspended in 5 or 10 ml DMEM media depending on size. A sample was taken from the suspension and mixed 1:1 with

Trypan blue stain for dead cells. The number and viability (live cells/total cells x 100) of the preparation was then counted using an Improved NeuBuyer chamber BS.748 (Hawksley, Lancing, Sussex) in preparation for cell seeding. Typical preparations resulted in 20-30 million viable cells with a viable percentage > 85%.

2.6.2 Seahorse extracellular flux analysis

Primary hepatocytes were seeded in Seahorse XFe24 V7 cell culture microplates (SeahorseBio, Copenhagen, Denmark). Optimisation experiments determined the optimal seeding density which was then standardised at 10,000/well. The microplates used for primary hepatocyte experiments were pre-coated with rat tail collagen at a concentration of 10 µg collagen/well diluted from a stock solution with 0.1 M sterile acetic acid. Following coating (a minimum of overnight) any remaining acid was removed by washing with sterile Dulbecco's Phosphate Buffered Saline (DPBS) before the plates were used for cell culture.

Based on manufacturer's guidance cells were seeded initially in 200 µl DMEM media containing 10% FCS, 1% P/S and L-Glutamine. This was then topped up to 500 µl after approximately 4 hours and the plates were then left overnight in a 37°C cell culture incubator. On the day of the experiment Seahorse mitochondrial stress test media (Seahorse assay media, 10 mM glucose, 2 mM Na pyruvate) media was prepared and pH adjusted to 7.35 ± 0.5. Compounds from Seahorse mitochondrial stress test kits (SeahorseBio, Copenhagen, Denmark) were prepared using the appropriate volume of media according to manufacturer's instructions. Cells were washed 3 times with Seahorse media before a final 500 µl of Seahorse media was added to wells. Plates were then incubated for a minimum of 30 minutes at 37°C in a Techne Hybridiser HB-1D oven (Techne, Stone, UK) to allow for CO_2 depletion.

Tests were performed using standard measurement and injection protocols. An initial 12-minute equilibration period was followed by a series of measurement cycles consisting of 3 minutes mixing, 2 minutes waiting and 3 minutes measuring. This measurement cycle was repeated 3 times for basal respiration and then 3 times following the addition of each compound. The mitochondrial stress tests injections were oligomycin, FCCP and antimycin/rotenone. The concentrations used for the compounds are given in results chapters. Raw data responses from each well were normalised to relative protein concentration measured using the sulforhodamine B assay (SRB, described in section 2.6.3) using Wave desktop software. Following this data were collected and averaged (typically 10 wells/genotype) to produce a single value at each measurement time for each biological replicate. This data was used for statistical analysis.
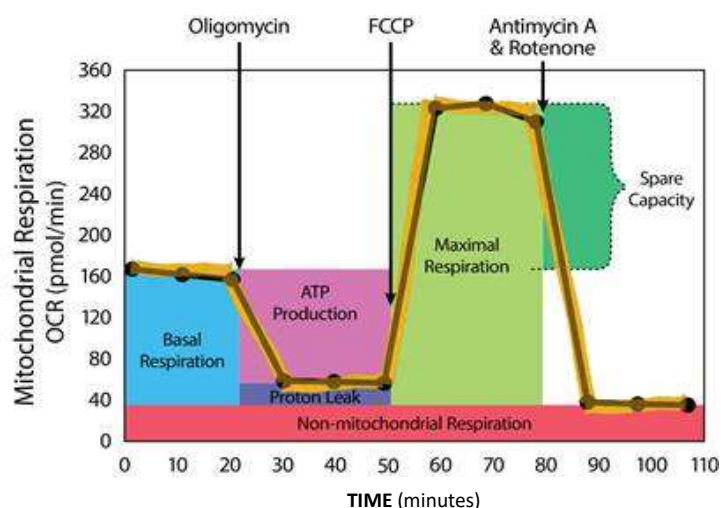
Figure 2.2 Standard Seahorse Mitochondrial stress test with calculated parameters. A standard mitochondrial stress test protocol with example data. The marked columns show the metabolic variables which can be calculated from the test.

Respiration parameter	Description
Basal	Initial mitochondrial respiration. Calculated by subtracting 'non-mitochondrial respiration' from the first measurements.
ATP production	Mitochondrial respiration which is coupled to H+ flow through ATP synthase (complex V). Calculated by subtracting respiration after oligomycin (a complex V inhibitor) addition from basal respiration.
Proton leak	Respiration which is not coupled to ATP synthesis and occurs despite inhibition of complex V and therefore represents 'leak' of protons back across the mitochondrial membrane. Calculated by subtracting non-mitochondrial respiration from respiration occurring following oligomycin addition.
Maximal respiration	The maximal capacity for respiration within the samples wells. Established by allowing unlimited leak of protons across the mitochondrial membrane following FCCP addition. Calculated by subtracting non-mitochondrial respiration from the respiration achieved following FCCP addition.
Spare capacity	The additional respiration above basal that can be achieved through FCCP addition. Calculated by subtraction of basal from maximal respiration
Non-mitochondrial respiration	Consumption of oxygen which is not as a result of mitochondrial respiration. Calculated following the addition of antimycin A (complex III) and rotenone (complex I) inhibitors to completely inhibit mitochondrial electron transport chain activity.

Table 2.1 A description of mitochondrial respiratory parameters determined through Seahorse extracellular flux analysis.

2.6.3 Sulforhodamine B relative protein assay

Following completion of Seahorse tests cells were fixed using 50% trichloroacetic acid (TCA) solution added 1:10 to the remaining Seahorse media. Following incubation for 30

minutes at 4ºC cells were washed 10 times using tap water. Plates were dried in a 37ºC oven. 50 µl of SRB reagent (0.4% SRB dissolved in 1% acetic acid) was then added to bottom of wells and mixed to ensure coverage. Plates were incubated at room temperature for 30 minutes. Plates were then washed 4 times with 1% acetic acid to remove any excess SRB. Finally, bound SRB was released by adding 200 µl 10 mM Tris buffer (pH adjusted to 10.5). Samples were left for a minimum of 30 minutes to allow release of the SRB stain. The solution within the well was mixed using a pipette before a 100 µl sample was taken and transferred to a Costar 96 well assay plate (Corning Life Sciences, Amsterdam, The Netherlands) for measurement. Absorbance readings were measured using a plate spectrophotometer at 540 nm. Absorbance readings were used for a relative normalisation (i.e. no quantification was performed as this was not practical for the experimental design) however, an optimisation experiment showed that absorption at 540 nm was linear between 0-20000 (appendix 1) primary hepatocytes seeded in a Seahorse XFe24 V7 cell culture plate.

2.7 Histology

2.7.1 Optical projection tomography

2.7.1.1 Perfusion fixation and dissection

Mice were euthanised with an overdose of sodium pentobarbital (Euthatal) given as an i.p. bolus. Once toe pinch and corneal reflexes were absent the heart was rapidly exposed, and a cannula placed into the left ventricle. The right atrium was cut, and perfusion begun with PBS containing 20 units Heparin. Perfusion was driven by a peristaltic pump at a rate of 5 ml/min for approximately 2 minutes to clear the vessels and tissues of blood. Once this had been completed the perfusion was switched to 4% formalin solution (38% formaldehyde). Perfusion was continued for approximately 30 seconds after movement was seen in the extremities (a signature of muscle fixation). The aortic arch along with the brachiocephalic, left common carotid and left subclavian artery was cleaned of fat and dissected before being transferred and stored in 4% formalin solution.

2.7.1.2 Embedding and scanning

Arches were embedded in 1.5% agar (Ultrapure LMP agarose, Invitrogen, Carlsbad, UK) for scanning. The agar solution was heated to liquid form and drawn up into 1 ml syringes with the tapered end removed. The aortic arch was then placed into the liquid agar and positioned in the centre. Syringes were chilled for approximately 5 minutes until the agar had become solid. The block of agar was then extruded from the syringe and placed into 50 ml 100% ethanol for dehydration. Following a minimum of 2-days dehydration agar blocks were transferred to benzyl alcohol/benzyl benzoate solution (BABB; 1:2 benzyl alcohol/benzyl benzoate) to increase the tissues transparency. Tissues remained in BABB for several weeks to allow for bubbles within the arches to escape. Once this process had been completed the agar blocks were mounted onto a magnetic stage for placement into a Bioptonics 3001 optical projection tomography scanner (Bioptonics, Edinburgh, UK). Using SkyScan software (Bruker MicroCT, Kontich, Belgium) tissues were positioned within the field of view, focussed and exposure in the GFP channel was adjusted to reduce areas of signal above maximum. A 360° scan was then performed in the GFP channel in increments of 0.9^{o}. 360° TIFF files were reconstructed using NRecon GPU (Bruker MicroCT, Kontich, Belgium) software into 2D slices. CTan software (Bruker MicroCT, Kontich, Belgium) was then used to quantify the 3D volume of atherosclerotic lesions in the brachiocephalic branch between the emergence of the vessel and the bifurcation into the right common carotid and right subclavian arteries. This was performed by defining a region of interest (the slices of the area within the brachiocephalic branch) and then drawing areas of interest around the lumen of the vessel onto these slices. Through adjustment of the signal threshold the

software could detect the lesion within this area. Following assignment of areas of interest along the length of the region of interest the software was then able to calculate the volume of the vessel (total volume of interest) and the volume of the lesion (total object volume) within the vessel wall.

2.8 Statistical analysis

Detailed statistical methods are described in the results chapters. Statistical tests were performed using GraphPad Prism 5 software except for MANOVA analysis (glucose, insulin tolerance tests) which was performed using MiniTab 18 software (Minitab, Coventry, UK). All graphing was performed using GraphPad Prism 5 software.

3.0 The effects of *Tst* deletion on hepatic energy metabolism

3.1 Introduction

Dysfunction of metabolic tissues such as liver, adipose tissue and skeletal muscle is linked to the development of a number of diseases including diabetes, dyslipidaemia and steatosis of the liver (35,213). Many of these disorders occur collectively in what is termed the 'metabolic syndrome' (3). Metabolic syndrome is commonly associated with obesity (2). The rate of obesity is rising in both developed and developing nations (109) and, therefore, research aimed at reducing obesity rates or combatting the metabolic syndrome is of great importance.

3.1.1 Genetic leanness and *Tst*

Recent research undertaken by Morton *et al.* investigated the contrasting phenotype of 'leanness', based upon the idea that some individuals remain intrinsically (genetically) leaner than others despite modern calorie-dense diets (214). Genetic investigations in polygenic lean and fat mice, which were bred over many generations for divergent fat mass, led to the identification of thiosulfate sulfurtransferase (*Tst*) as a candidate adipose tissue-specific 'lean gene'. Adipose *Tst* mRNA and protein levels were inversely correlated with adiposity across a large number of rodent strains and in several human populations (204). Overexpression of *Tst* in the adipose tissue of C57BL/6N mice (Adipoq-*Tst* mice) led to obesity-resistance in the face of high fat diet (HFD) exposure. This was associated with improved glucose homeostasis and insulin sensitisation in adipose tissue and muscle, as well as increased fat oxidation in liver compared to C57BL/6N littermates (204).

3.1.2 The metabolic consequences of *Tst* deletion

In further experiments using mice with global *Tst* deletion (*Tst*$^{-/-}$) Morton *et al.* found that while weight gain on control or HFD appeared to be unchanged *Tst*$^{-/-}$ mice fed HFD for 6 weeks exhibited worsened glucose tolerance and failure to suppress non-esterified fatty acids (NEFA) across the glucose tolerance period, indicative of peripheral insulin resistance (204). This finding was consistent with the idea that TST maintains normal metabolic function in conditions of nutrient excess, such as obesity induced through HFD. However, TST expression is >20-fold higher in liver than in adipose tissues (208) suggesting that hepatic TST also contributes to metabolic homeostasis. Consistent with this, chow-fed *Tst*$^{-/-}$ mice fasted for 16 hours exhibited increased blood glucose concentrations in response to a

pyruvate bolus, suggesting increased hepatic gluconeogenesis in $Tst^{-/-}$ mice (Figure 3.1) (207)).
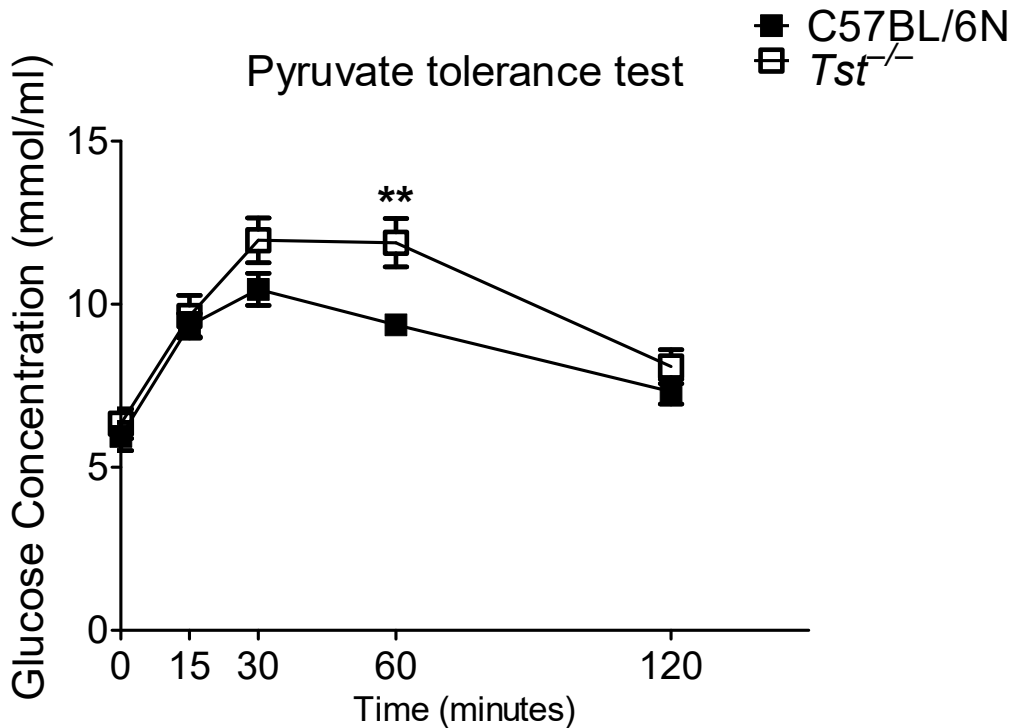
Figure 3.1 Increased gluconeogenesis in control fed $Tst^{-/-}$ mice. A pyruvate tolerance test in C57BL/6N or $Tst^{-/-}$ maintained on control chow diet. Mice were fasted for 16 hours prior to beginning the test. Following an initial blood glucose measurement (time 0) mice were given a pyruvate bolus (1.5 mg/g body weight) and glucose concentration was measured repeatedly at the indicated time points. Data are presented as Mean ± SEM. n = 9 (C57Bl/6N), 8 ($Tst^{-/-}$). Data were tested using Repeated Measures ANOVA with Bonferroni post-hoc testing. ** indicates $p < 0.01$ compared to C57BL/6N mice (207).

3.1.3 $Tst^{-/-}$ mice exhibit elevated blood sulfide levels.

The cause of altered metabolic function in $Tst^{-/-}$ mice is currently unknown. However, TST has recently been linked to the oxidative breakdown of the gasotransmitter hydrogen sulfide (H_2S) (168,169). Consistent with this suggestion initial studies in $Tst^{-/-}$ mice have found that H_2S, detected in whole blood samples by high performance liquid chromatography, is increased in $Tst^{-/-}$ compared to C57BL/6 mice ((204) section 1.5.1). Elevated H_2S signalling within the liver is linked to diabetes and increased gluconeogenesis but, perhaps counterintuitively, reduces liver steatosis through improved lipid metabolism (171,173). Elevated H_2S therefore represents an intriguing possible mechanism for the metabolic alterations in $Tst^{-/-}$ mice.

3.1.4 Hypothesis and Aims

In this chapter, it was <u>hypothesised</u> that: **The diabetogenic phenotype in $Tst^{-/-}$ mice is driven by major defects in hepatic glucose metabolism and lipid metabolism.**

Aims

- To determine whether Tst deletion negatively impacts hepatic glucose metabolism including, gluconeogenesis, glycogen storage and whole-body glucose homeostasis in short (6 week) and long (20 week) term HFD fed $Tst^{-/-}$ and C57BL/6 mice.

- To determine whether Tst deletion induces mitochondrial dysfunction of cellular metabolism in C57BL/6 and $Tst^{-/-}$ hepatocytes.

- To determine whether Tst deletion negatively impacts hepatic lipid metabolism including any effects on lipoprotein secretion in short (6 week) and long (20 week) term HFD fed $Tst^{-/-}$ and C57BL/6 mice.

3.2 Experimental Design

3.2.1 Assessment of metabolic function in $Tst^{-/-}$ mice fed control or high fat diet

Body weight recording, glucose and insulin tolerance tests and blood collection at termination were performed with Prof. Nicholas Morton, Dr Rod Carter and Ms. Clare Mc Fadden. Quantification of plasma cholesterol and triglyceride content was performed by Prof. Bart Staels and Dr Anne Muhr-Tailleux. PEPCK activity quantification, liver glycogen and triglyceride measurement, and all data analysis (including glucose and insulin tolerance test, plasma cholesterol and triglyceride data) was undertaken independently. C57BL/6 or $Tst^{-/-}$ mice maintained in controlled conditions by the Central Biological Services department (section 2.1) of the University of Edinburgh were given *ad libitum* access to either CRM 'chow' diet or 58% fat (kcal) 'Surwit' sucrose diet (HFD) for 6 or 20 weeks (Figure 3.2). The number of biological replicates is reported in results figure legends.
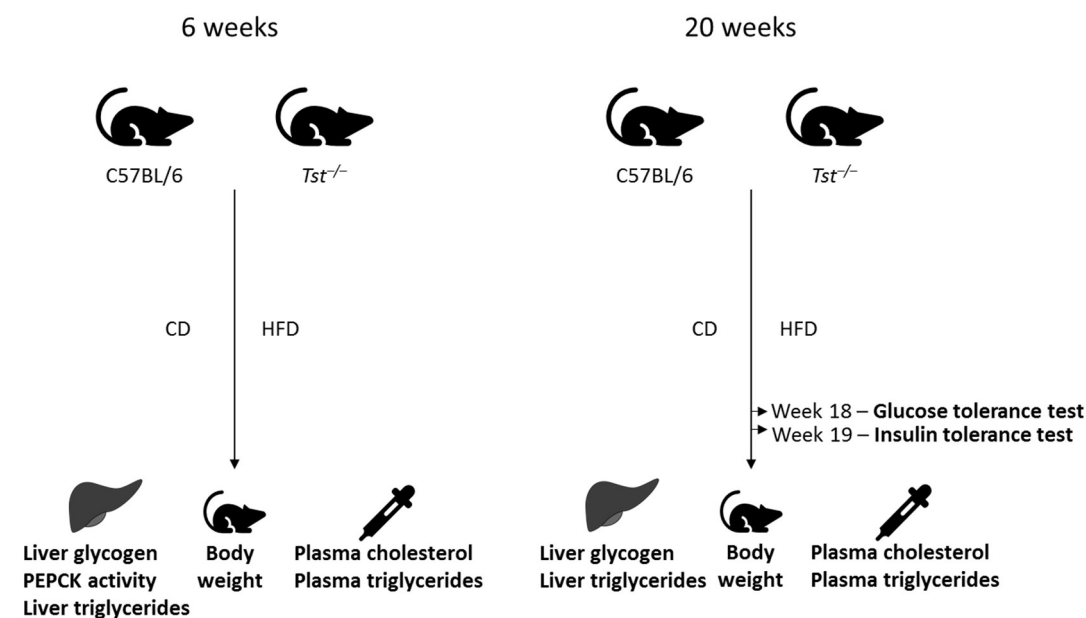
Figure 3.2 Experimental design of investigations into the metabolic consequences of *Tst* deletion in mice fed control and high fat diet. Two independent dietary intervention studies were conducted. Firstly, a 6-week feeding study matched to the previous work performed by Morton *et al.*, was performed to investigate hepatic glucose metabolism in greater detail and examine any changes in lipid metabolism. Secondly, a longer-term 20-week study was performed to test the effects of *Tst* deletion in severe obesity. During both studies mice were given *ad libitum* access to control CRM 'chow' diet or 58% fat (kcal) 'Surwit' sucrose HFD (215). The experimental outcomes are highlighted in bold, details of the methods can be found in section 2. All data except glucose and insulin tolerance tests were tested statistically within study groups (i.e. independently within the 6 and 20-week studies) using 2-way ANOVA with Bonferroni post-hoc testing. Glucose and insulin tolerance test data were tested with a General Linear Model due to the number of factors required for testing (genotype, diet, time). CD; control diet, HFD; high fat diet. Biological replicates (n numbers) are reported in the relevant figure legends within section 3.3.

3.2.2 Assessment of mitochondrial respiration in $Tst^{-/-}$ hepatocytes

Nutrient metabolism is fundamentally regulated by the cellular energy status of the cell. This is comprised of two major components, mitochondrial respiration (largely linked to ATP generation) and glycolysis. These processes are disturbed in diabetes (216,217) and, as such, represent plausible candidates for the diabetogenic phenotype of $Tst^{-/-}$ mice. To assess mitochondrial function in $Tst^{-/-}$ mice compared to C57BL/6 controls, we isolated primary hepatocytes (described in 2.6.1) from control diet fed C57BL/6 and $Tst^{-/-}$ mice and performed a mitochondrial stress test using the Seahorse Extracellular Flux analyser (Figure 3.3). Glycolysis stress tests were not performed, as a pilot study showed that glycolysis was extremely low in the cultured hepatocytes and thus could not be accurately measured (data not shown).
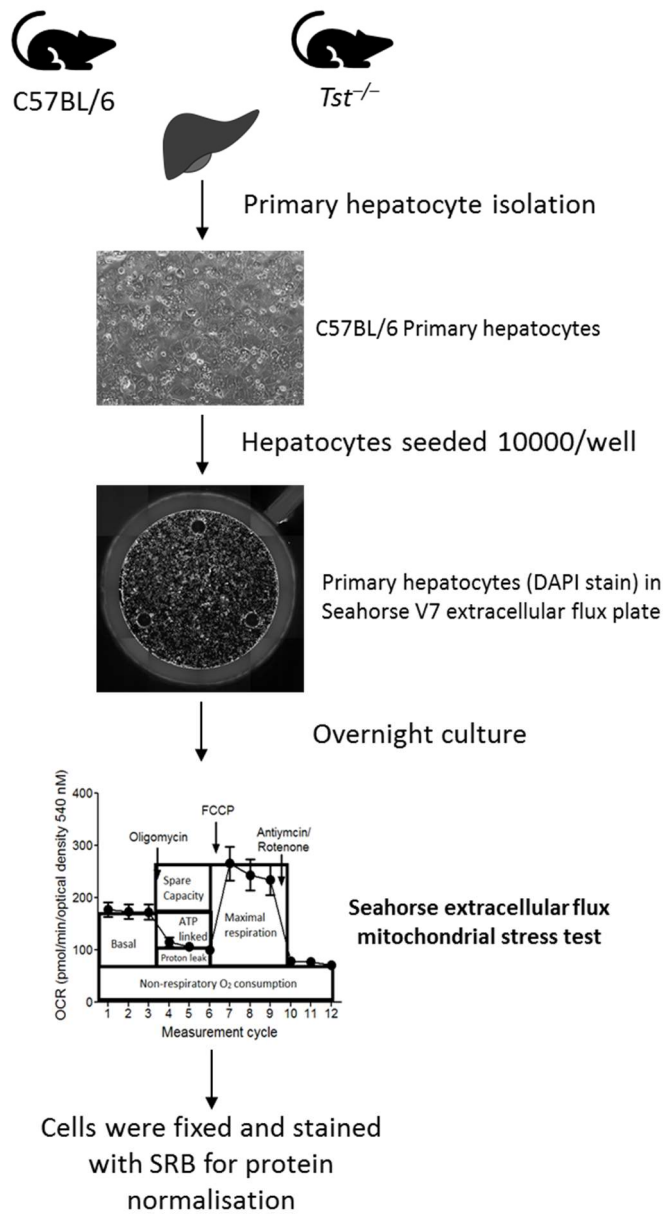
Figure 3.3 Experimental design of investigations into mitochondrial respiration in C57BL/6 and *Tst*$^{-/-}$ primary hepatocytes. The outcome of the experiment was O_2 consumption during the Seahorse extracellular flux mitochondrial stress test. All details of methods can be found in the relevant materials and methods sections (section 2). Experiments were performed in a pairwise fashion i.e. 1 C57BL/6 and 1 *Tst*$^{-/-}$ mouse were processed and analysed together. Following normalisation mitochondrial stress test summary data were calculated as detailed in section 2.6.2 and compared using paired t testing. SRB; sulfrhodamine-B dye.

3.3 Results

3.3.1 *Tst* deletion results in decreased body weight on control diet

Weekly body weight recording revealed that final body weights were lower in 6-week control diet-fed *Tst*$^{-/-}$ mice than in C57BL/6 controls (Figure 3.4A, Bonferroni post-hoc p<0.05). No significant difference was noted in 20-week control diet fed *Tst*$^{-/-}$ mice. 6 or 20-week HFD feeding caused an increase in body weight in C57BL/6 mice. There was no difference in the response of *Tst*$^{-/-}$ mice to HFD at either time point; both genotypes gained similar weight with the HFD intervention (Figure 3.4A&B, 6-week diet).

6 weeks of HFD feeding led to an increase in liver/body weight indicating a larger liver compared to the animal's body weight. *Tst*$^{-/-}$ mice appeared to have greater liver/body weight ratio under control diet-fed conditions, leading to a significant interaction of diet and genotype (Figure 3.4C) however, this increase was not significant by post-hoc testing. No differences due to diet or genotype were found in liver weight at 20 weeks (Figure 3.4D).
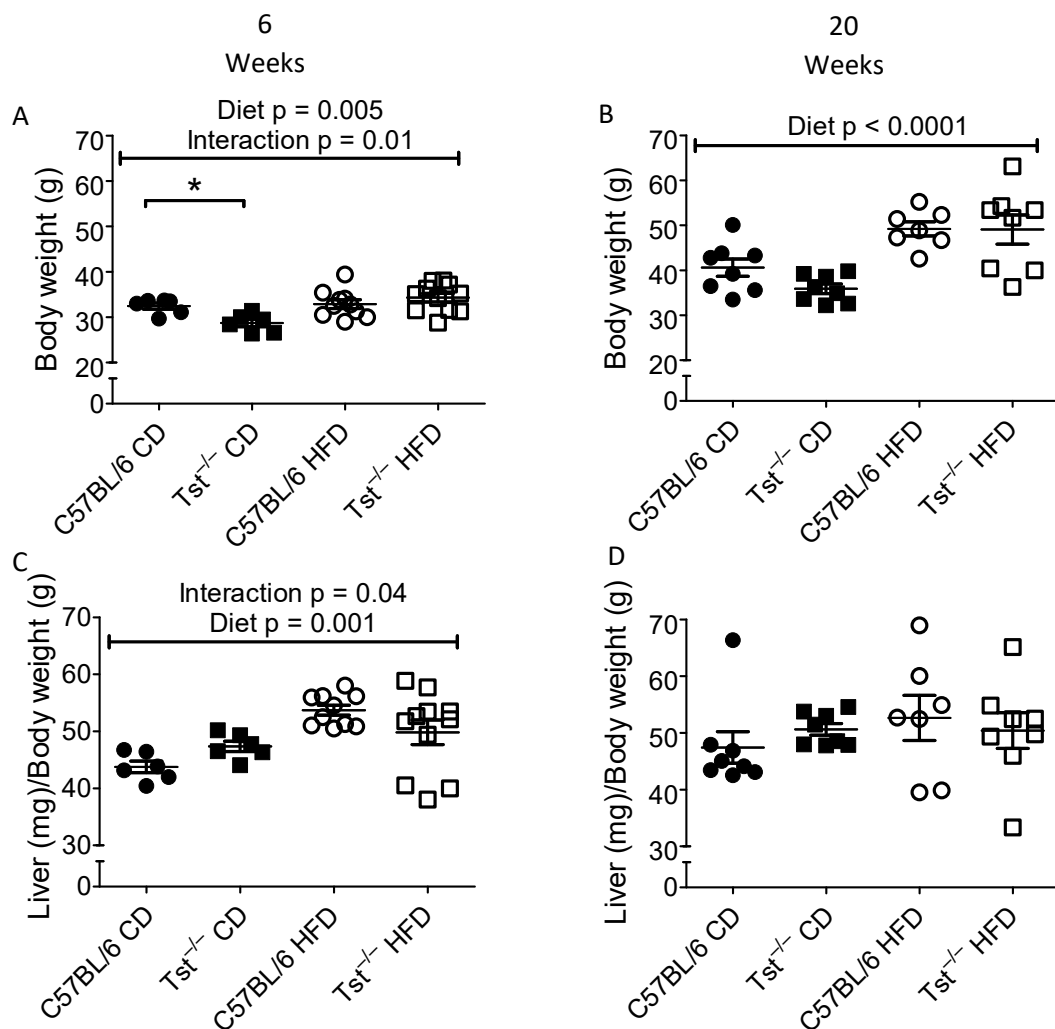
Figure 3.4 Body weight and liver/body weight ratio in C57BL/6 and *Tst*⁻/⁻ mice fed chow or 58% high fat diet (HFD) for 6 or 20 weeks. This work was performed with Dr Roderick Carter and Ms. Clare Mc Fadden. Analysis by MG. **A)** Final body weights for C57BL/6 and *Tst*⁻/⁻ mice fed control or HFD for 6 weeks. **B)** Final body weights for C57BL/6 and *Tst*⁻/⁻ mice fed control or HFD for 20 weeks. **C)** Liver weight normalised to body weight (Liver/body weight) in C57BL/6 and *Tst*⁻/⁻ mice fed control or HFD for 6 weeks. **D)** Liver/body weight in C57BL/6 and *Tst*⁻/⁻ mice fed control or HFD for 20 weeks. Data are presented as Mean ± SEM. n = for 6 (C57BL/6 CD), 6 (*Tst*⁻/⁻ CD), 10 (C57BL/6 HFD), 11 (*Tst*⁻/⁻ HFD) for 6-week data, n = 8 (C57BL/6 CD), 8 (*Tst*⁻/⁻ CD), 7 (C57BL/6 HFD), 8 (*Tst*⁻/⁻ HFD) for 20-week data. Data were compared using 2-way ANOVA and Bonferroni post hoc testing. * indicates $p < 0.05$ by Bonferroni. CD; Control diet, HFD; High fat diet.

3.3.2 *Tst* deletion exacerbates the effect of long term HFD feeding on glucose intolerance

To test for changes in glucose homeostasis in $Tst^{-/-}$ mice, a glucose tolerance test (GTT) was performed near the end of long term dietary exposure to HFD (18 weeks of feeding). No difference was found in glucose tolerance between control diet fed C57BL/6 and $Tst^{-/-}$ mice (Figure 3.5A). HFD feeding led to worsened glucose tolerance (blood glucose concentrations reached higher peaks and took longer to normalise) in both C57BL/6 and $Tst^{-/-}$ mice (Figure 3.5A). However, it was also noted that *Tst* deletion exacerbated this effect overall i.e. the worsening of glucose tolerance was greater in $Tst^{-/-}$ mice than in C57BL/6 controls as demonstrated by the significant interaction of genotype and diet (p=0.04) although no specific time point was different by post-hoc testing (Figure 3.5A).

Blood insulin concentrations were also measured in samples taken over the time course of the glucose tolerance test to give insight into the endogenous insulin secretory response (early phase 0-15 minutes) and insulin clearance/resistance (15-120 minutes) in HFD-induced metabolic dysfunction. HFD feeding led to an increase in blood insulin concentrations over the entire time course of the GTT in both C57BL/6 and $Tst^{-/-}$ mice. However, on both chow diet and HFD $Tst^{-/-}$ mice demonstrated an overall reduction in blood insulin concentration (General linear model ANOVA genotype p < 0.0001) although no specific time points was different by post-hoc testing (Figure 3.5B).
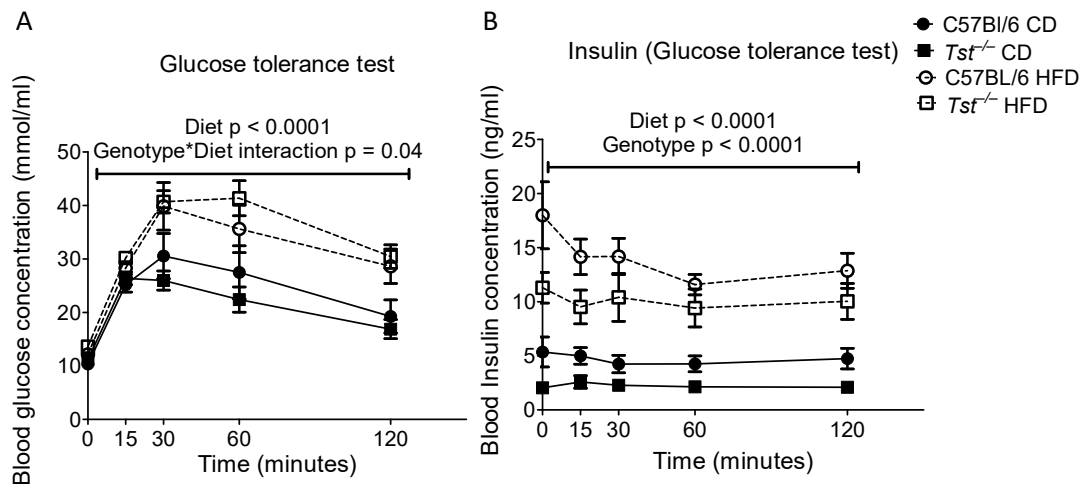
Figure 3.5 Glucose tolerance test along with blood insulin concentrations in C57BL/6 and $Tst^{-/-}$ mice fed control or HFD for 20 weeks. This work was performed with Prof. Nicholas Morton, Dr. Roderick Carter, Ms. Rhona Aird and Ms. Clare Mc Fadden. Intraperitoneal injection was performed by NM, blood sampling was performed equally by MG, RC and CM. Insulin ELISA was performed by RA. Analysis by MG. **A)** A glucose

tolerance test (GTT) performed in C57BL/6 and $Tst^{-/-}$ mice fed control or HFD for 18 weeks. Mice were fasted (with free access to water) for 6 hours prior to the test. Following an initial blood glucose measurement mice were given a glucose bolus (2 mg/g body weight) at time 0 and glucose disposal was monitored through repeated blood glucose measurement at times 15, 30, 60 and 120 minutes. **B)** Blood insulin concentrations measured over the time course of the GTT. Data are presented as Mean ± SEM. n = 6 (C57BL/6 CD), 8 ($Tst^{-/-}$ CD), 6 (C57BL/6 HFD), 8 ($Tst^{-/-}$ HFD). Data were tested using General Linear Model ANOVA (diet, mouse number, genotype and time factors). CD; Control diet, GTT; Glucose tolerance test, HFD; High fat diet.

3.3.3 *Tst* deletion accentuates the blood glucose decrement in response to insulin bolus

To assess the effect of *Tst* deletion on changes to whole body insulin sensitivity, an insulin tolerance test (ITT) was performed following 19 weeks of feeding with control or HFD. No differences were found in the response of control fed C57Bl/6 and *Tst*$^{-/-}$ to the insulin bolus. Consistent with the changes observed in the glucose tolerance test, HFD feeding led to an increase in blood glucose concentrations over the time course of the ITT in C57BL/6 mice (Figure 3.6). This effect was exacerbated by *Tst* deletion over the time course of the ITT; i.e. the increase in blood glucose concentrations was greater in *Tst*$^{-/-}$ mice fed HFD compared to C57BL/6 mice as shown by the significant interaction of genotype and diet (General linear model ANOVA genotype diet interaction p =0.001). However, no specific time point was different between HFD fed C57BL/6 and *Tst*$^{-/-}$ mice by post-hoc testing (Figure 3.6).

Further to this, the decrease in blood glucose (decrement) induced by the insulin bolus was calculated at 15 and 30 minutes (concentrations mostly plateaued after this time) to assess the response to insulin (Table 3.1). In both C57BL/6 and *Tst*$^{-/-}$ mice, HFD feeding resulted in an attenuated decrement at 15-minutes compared to control diet-fed mice. There were no differences between the genotypes in the response at the 15-minute point (Table 3.1).

HFD feeding did not result in an altered 30-minute blood glucose decrement in either C57BL/6 or *Tst*$^{-/-}$ mice. However, overall in *Tst*$^{-/-}$ mice the blood glucose decrement at 30 minutes was found be greater compared to C57BL/6 mice (2-way ANOVA genotype p = 0.01) although neither diet group was individually different from C57BL/6 mice by post-hoc testing (Table 3.1).
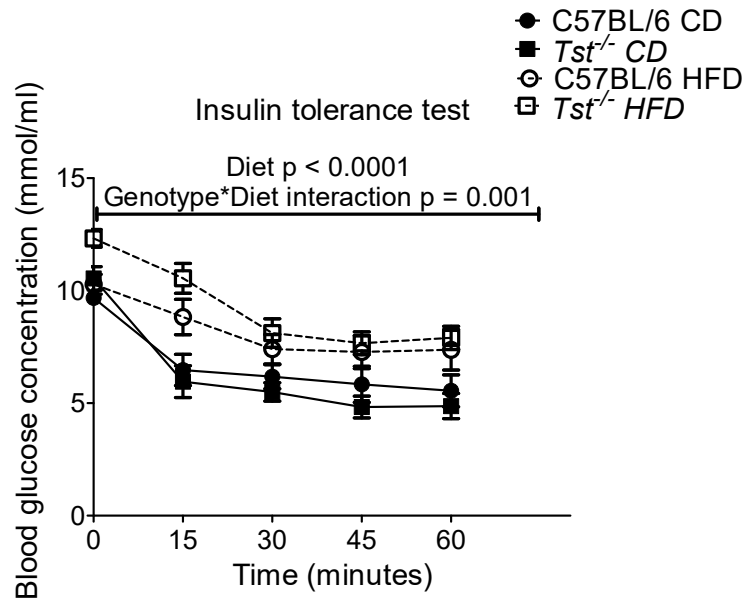
Figure 3.6 An insulin tolerance test performed in C57BL/6 and *Tst*$^{-/-}$ mice fed control or HFD for 19 weeks. This work was performed with Prof. Nicholas Morton, Dr. Roderick Carter and Ms. Clare Mc Fadden. Intraperitoneal injection was performed by NM, blood sampling was performed equally by MG, RC and CM. All analysis was done by MG. Mice were fasted (with free access to water) for 6 hours prior to the test. Following an initial blood glucose measurement, mice were given an insulin bolus (1 mU/g body weight) at time 0 and the suppression of blood glucose monitored through repeated blood glucose measurement at times 15, 30, 45 and 60 minutes. n = 8 (C57BL/6 CD), 7 (*Tst*$^{-/-}$ CD), 7 (C57BL/6 HFD), 8 (*Tst*$^{-/-}$ HFD). Data were tested using General Linear Model ANOVA (diet, mouse number, genotype and time factors). CD; Control diet, HFD; High fat diet.

| Time (minutes) | Blood glucose decrement (-Δmmol/ml) | | | | 2-way ANOVA (Diet, Genotype, Interaction) |
	C57Bl/6 CD	*Tst*$^{-/-}$ CD	C57Bl/6 HFD	*Tst*$^{-/-}$ HFD	
15	3.20 ± 0.6	4.59 ± 0.7	1.46 ± 0.8	1.78 ± 0.8	**0.004**, 0.25, 0.47
30	3.50 ± 0.4	5.04 ± 0.4	2.89 ± 0.5	4.21 ± 0.7	0.18, **0.01**, 0.84

Table 3.1 Blood glucose decrements during an insulin tolerance test in C57BL/6 and *Tst*$^{-/-}$ mice fed control or HFD for 19 weeks. This work was performed with Prof. Nicholas Morton, Dr. Roderick Carter, Ms. Rhona Aird and Ms. Clare Mc Fadden. Intraperitoneal injection was performed by NM, blood sampling was performed equally by MG, RC and CM. All analysis was done by MG. Blood glucose decrements at the indicated times were calculated by subtraction of blood glucose concentration at that time-point from the Time 0 concentration. n = 8 (C57BL/6 CD), 7 (*Tst*$^{-/-}$ CD), 7 (C57BL/6 HFD), 8 (*Tst*$^{-/-}$ HFD). Data were tested using 2-way ANOVA with Bonferroni post-hoc testing. CD; Control diet, HFD; High fat diet.

3.3.4 *Tst* deletion increases liver phosphoenolpyruvate carboxykinase activity in control diet-fed mice

To test whether phosphoenolpyruvate carboxykinase (PEPCK), a key regulatory enzyme of gluconeogenesis, was affected by *Tst* deletion, activity was measured in 6-week control and HFD fed mice (Figure 3.7A). There was no overall effect of HFD feeding on PEPCK activity in C57BL/6 or $Tst^{-/-}$ mice. However, overall $Tst^{-/-}$ mice exhibited significantly increased PEPCK activity compared to C57BL/6 controls (genotype p = 0.01) although no specific differences were found between groups using post-hoc testing (Figure 3.7B).
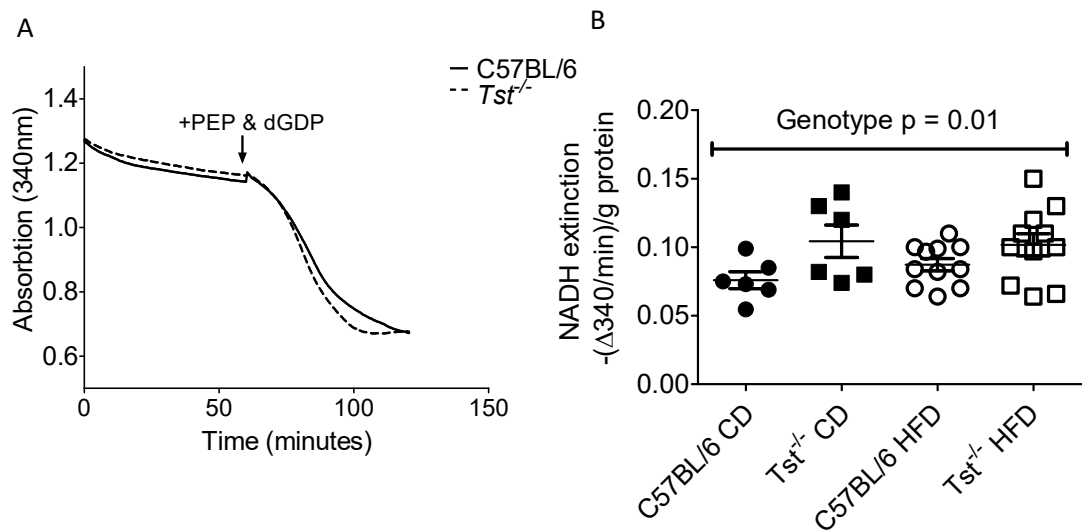
Figure 3.7 Liver phosphoenolpyruvate carboxykinase (PEPCK) activity in C57BL/6 and $Tst^{-/-}$ mice fed control or HFD for 6 weeks. A) An example trace of PEPCK activity measured in C57BL/6 and $Tst^{-/-}$ mice fed control diet for 6 weeks. The addition of PEP and dGDP to the reaction mixture is indicated by the arrow. **B)** Quantification of PEPCK activity in 6-week control and HFD fed C57BL/6 and $Tst^{-/-}$ mice. NADH extinction was calculated from the linear portion of the reaction curve following PEP and dGDP addition. Data are presented as Mean (figure A) or Mean ± SEM (figure B). n = 6 (C57BL/6 CD), 6 ($Tst^{-/-}$ CD), 11 (C57BL/6 HFD), 11 ($Tst^{-/-}$ HFD). Data were tested using 2-way ANOVA and Bonferroni post hoc testing. CD; Control diet, dGDP; Deoxyguanosine diphosphate, HFD; High fat diet, NADH; nicotinamide adenine dinucleotide, PEP; phosphoenol pyruvate.

3.3.5 *Tst* deletion does not alter liver glycogen content in chow- and high fat diet-fed mice

To test whether glycogen storage, a process sensitive to insulin signalling, was altered in $Tst^{-/-}$ mice, glycogen content of the liver ((mg/ml)/mg of liver tissue) was analysed in 6 and 20-week HFD fed mice. No change in liver glycogen content was found in mice fed chow or HFD for 6 weeks (Figure 3.8A). There were also no changes in liver glycogen content between C57BL/6 and $Tst^{-/-}$ mice fed either diet for 6 weeks. Following 20 weeks of diet mice fed HFD did exhibit decreased liver glycogen content overall compared to chow fed mice (2-way ANOVA $p < 0.01$) (Figure 3.8B). However, there were no differences between C57BL/6 and $Tst^{-/-}$ mice.
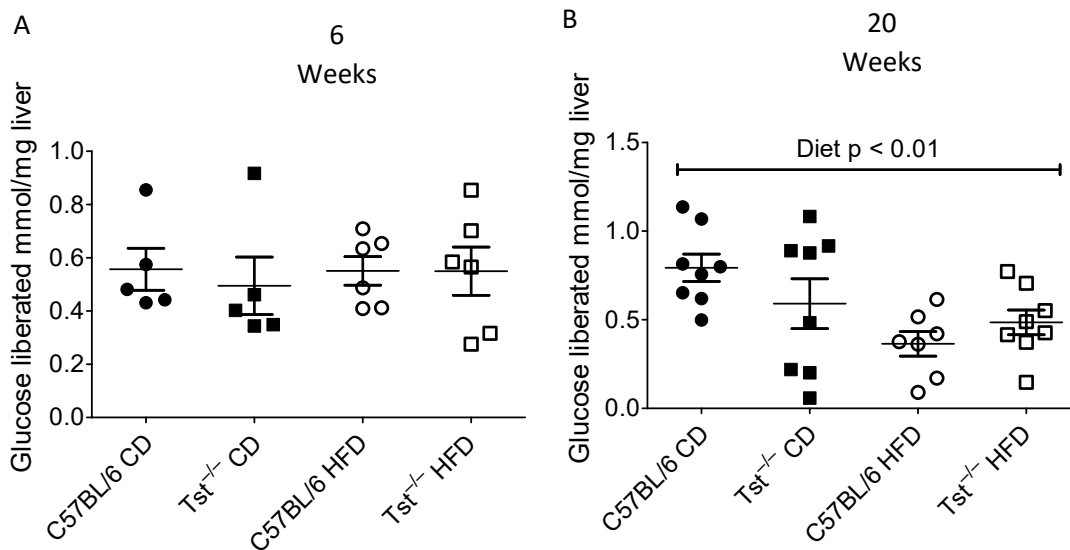
Figure 3.8 Liver glycogen content in C57BL/6 and $Tst^{-/-}$ mice fed control or HFD for 6 or 20 weeks. A) Liver glycogen content following 6 weeks of control or HFD feeding. **B)** Liver glycogen content following 20 weeks of control or HFD feeding. Data are presented as Mean ± SEM. n = 5 (C57BL/6 CD), 5 ($Tst^{-/-}$ CD), 6 (C57BL/6 HFD), 6 ($Tst^{-/-}$ HFD) for 6-week data, n = 8/8/7/8 for 8 (C57BL/6 CD), 8 ($Tst^{-/-}$ CD), 7 (C57BL/6 HFD), 8 ($Tst^{-/-}$ HFD) for 20-week data. Data were tested using 2-way ANOVA and Bonferroni post hoc testing. CD; Control diet, HFD; High fat diet.

3.3.6 *Tst* deletion in Hepatocytes increases ATP-linked and leak mitochondrial respiration

Evaluation of mitochondrial metabolism was performed on C57BL/6 and *Tst*$^{-/-}$ primary hepatocytes isolated from control diet fed mice at 12-14 weeks of age. An initial observation from these experiments showed that wells seeded with *Tst*$^{-/-}$ hepatocytes contained more protein than wells containing hepatocytes from C57BL/6 liver, despite seeding at the same cell density (Figure 3.9C). Mitochondrial stress test results showed that *Tst*$^{-/-}$ hepatocytes displayed increased basal respiration (Figure 3.10A). Examination of the components of basal metabolism (ATP-linked and leak respiration) showed that both parameters were increased in *Tst*$^{-/-}$ hepatocytes compared to C57BL/6 (Figure 3.10B). No changes were observed in non-mitochondrial O_2 consumption, maximum respiration or spare capacity between the genotypes.

A
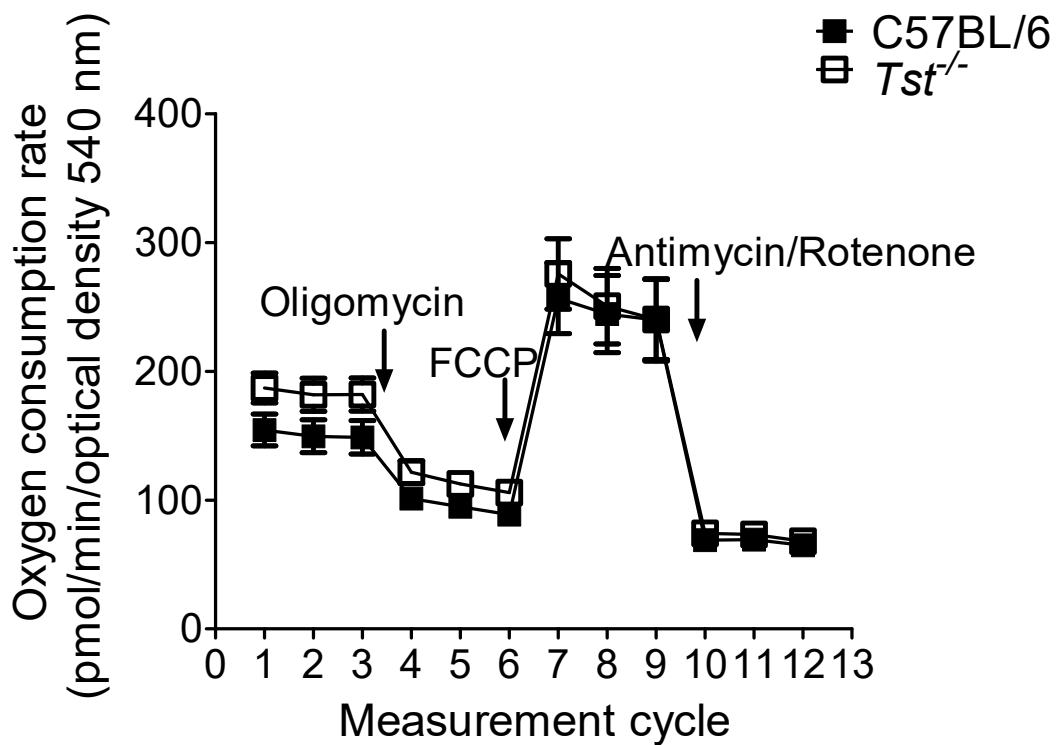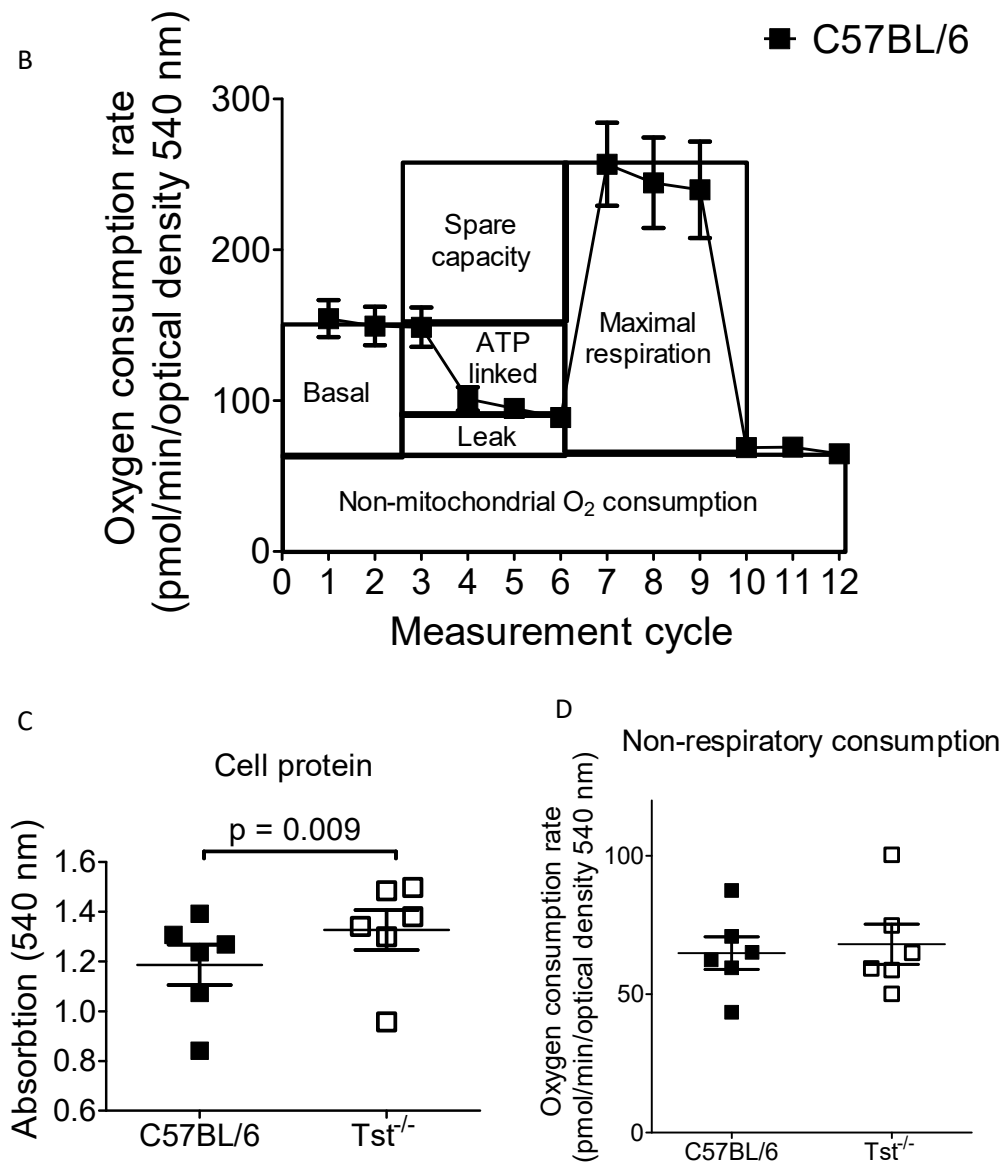
Figure 3.9 Mitochondrial respiration in C57BL/6 and *Tst*^{-/-} primary hepatocytes from control diet fed mice.
A) A summary trace showing a standard mitochondrial stress test protocol on C57BL/6 and *Tst*^{-/-} primary hepatocytes. The time of addition for each compound is marked with arrows. The measurement cycles used for further calculations are highlighted in the dashed boxes i.e. 3, 6, 7 and 12. For the method of summary statistic calculations refer to section 2.6.2 **B)** The C57BL/6 trace is used as an example to show the quantifiable characteristics of the mitochondria based on the compounds added. **C)** Sulfrhodamine B absorption was used as a measure of protein content in wells. **D)** Non-mitochondrial respiration. Data are presented as Mean ± SEM. Biological n = 6 for both genotypes with 10 technical replicates per plate. Experiments were performed in a pairwise fashion and data were tested using paired t tests.
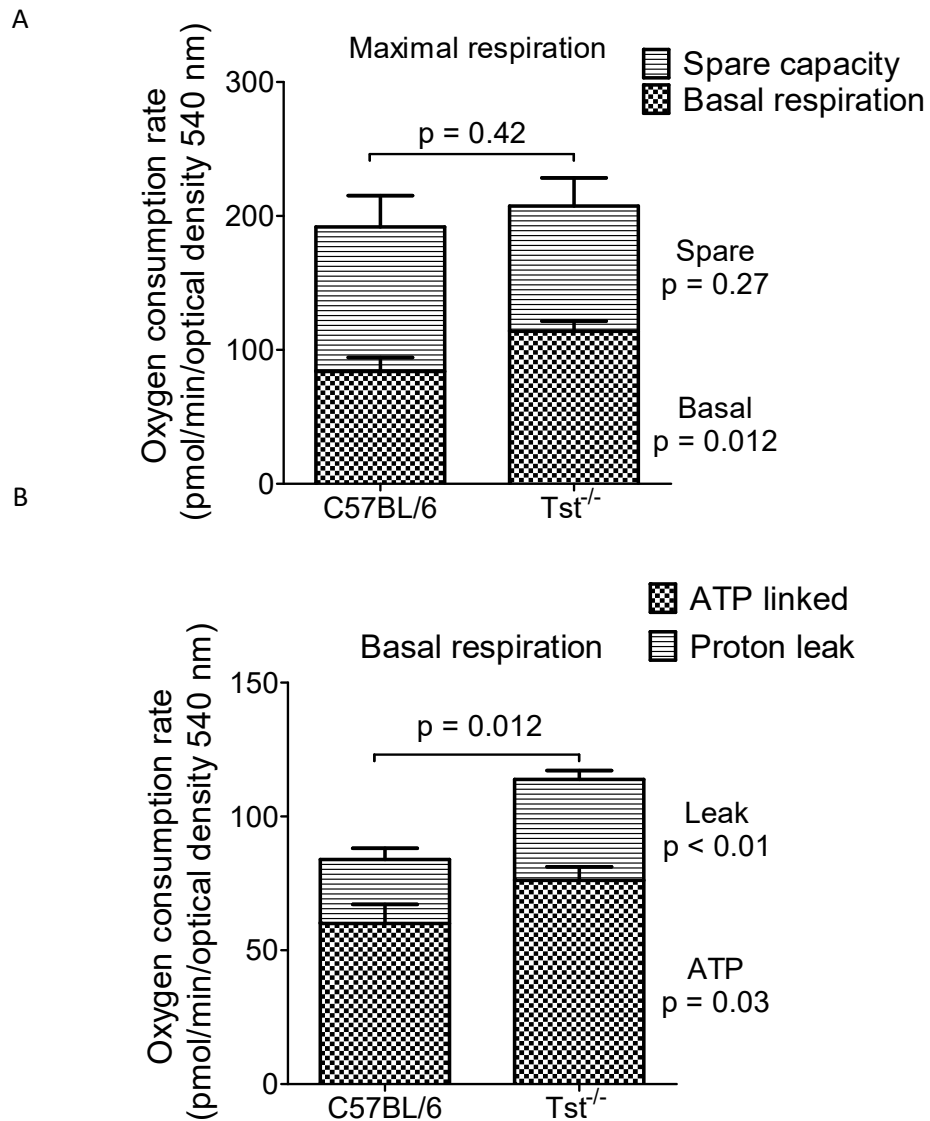
Figure 3.10 Quantification of mitochondrial respiration parameters in primary hepatocytes from control fed C57BL/6 and *Tst*^{-/-} mice. A) Maximal respiration separated into basal respiration and spare respiratory capacity components. **B)** Basal respiration separated into ATP linked respiration and proton leak components. Data are presented as Mean ± SEM. Biological n = 6 for both genotypes with 10 technical replicates per plate. Experiments were performed in a pairwise fashion and data were tested using paired t tests.

3.3.7 *Tst* deletion increases plasma triglycerides in control diet-fed mice

To determine whether *Tst* deletion altered lipid metabolism, HPLC analysis of the triglyceride and cholesterol carrying lipoprotein fractions in plasma was performed (example profiles shown in Figure 3.11). The analysis allowed for VLDL, LDL, HDL and total cholesterol and triglyceride content to be quantified as well as total glycerol (Table 3.2).

All plasma cholesterol fractions (VLDL, LDL, HDL and total) were significantly increased following HFD feeding for 6 weeks. A similar pattern was seen following 20 weeks of HFD feeding although VLDL cholesterol was unaffected in this group. No differences were found in cholesterol content between C57BL/6 mice and $Tst^{-/-}$ fed either diet.

In 6-week fed mice HFD feeding led to increased triglyceride content of the LDL fraction compared to chow fed controls only. $Tst^{-/-}$ mice fed control diet exhibited increased VLDL triglyceride content compared with C57BL/6 controls as detected by post-hoc testing ($p < 0.05$). This effect was not seen following HFD feeding for 6 weeks (post-hoc test $p > 0.05$) in which C57BL/6 VLDL triglyceride content increased to similar levels as $Tst^{-/-}$ mice (Table 3.2) demonstrating an interaction of genotype and diet (2-way ANOVA interaction $p = 0.01$).

In 20-week fed mice both LDL and HDL triglyceride content were increased with HFD feeding compared to chow fed controls. However, no differences were noted between genotypes in 20-week fed mice.

Both 6 and 20-weeks of HFD feeding led to significantly increased glycerol but no differences in genotype were observed.

A
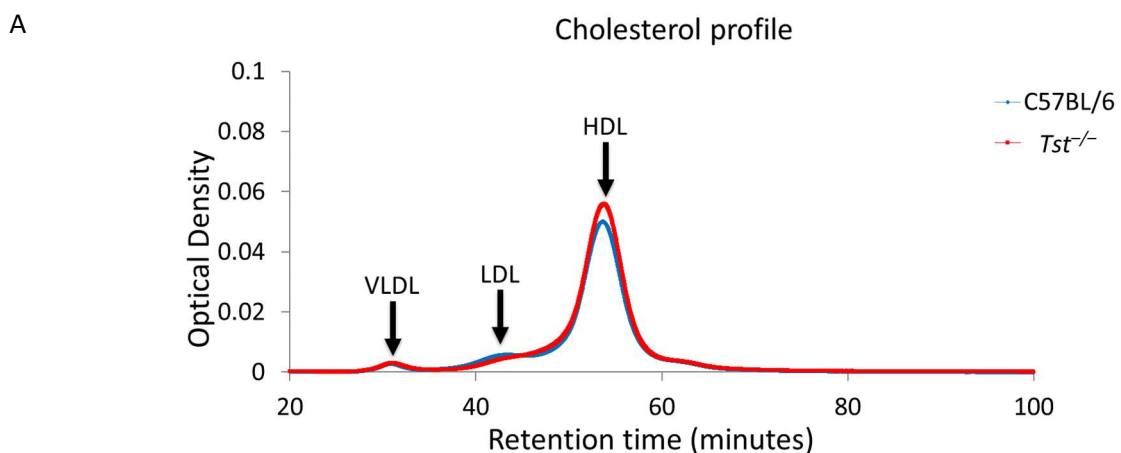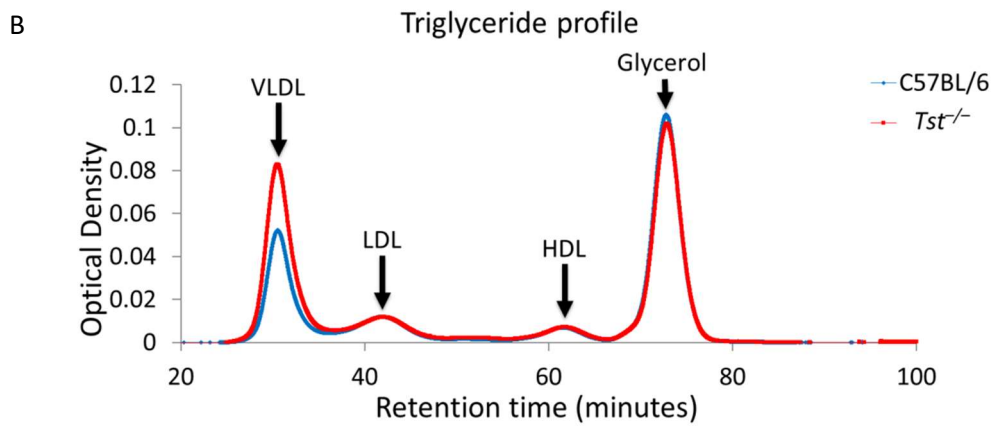
Figure 3.11 Example plasma cholesterol and triglyceride profiles from C57BL/6 and *Tst*$^{-/-}$ mice fed control diet for 6 weeks. A) Plasma cholesterol content with VLDL, LDL and HDL fraction peaks indicated. **B)** Plasma triglyceride content with VLDL, LDL, HDL and glycerol fraction peaks indicated. n = 6 for C57BL/6 and *Tst*$^{-/-}$ traces. HDL; high density lipoprotein, LDL; low density lipoprotein, VLDL; very low-density lipoprotein.

6 Week Diet (mg/dL ± SEM)				
Cholesterol	C57BL/6 CD	*Tst*⁻/⁻ CD	C57BL/6 HFD	*Tst*⁻/⁻ HFD	2-way ANOVA (genotype, diet, interaction)
Total	106 ± 5	114 ± 8	224 ± 7	218 ± 13	0.88, **<0.0001**, 0.51
VLDL	3.0 ± 0.4	3.4 ± 0.3	6.6 ± 1	6.9 ± 0.4	0.66, **0.0001**, 0.94
LDL	12 ± 2	11 ± 1	52.6 ± 3.6	59 ± 8	0.74, **<0.0001**, 0.52
HDL	90 ± 4	100 ± 7	165 ± 5	153 ± 8	0.90, **<0.0001**, 0.12
Triglycerides					
Total	45 ± 5	**68 ± 8***	63 ± 3	57 ± 4	0.13, 0.53, **0.007**
VLDL	26 ± 5	**46 ± 7***	36 ± 3	33 ± 4	0.06, 0.77, **0.01**
LDL	12 ± 1	14 ± 1	16 ± 1	14 ± 1	0.99, **0.01**, 0.07
HDL	7.3 ± 2	8.9 ± 1	12 ± 2	9.0 ± 1	0.73, 0.10, 0.12
Glycerol	56 ± 3	57 ± 3	80 ± 6	77 ± 3	0.86, **<0.0001**, 0.61
20 Week Diet (mg/dL ± SEM)				
Cholesterol					
Total	118 ± 6	117 ± 9	249 ± 9	214 ± 21	0.15, **<0.0001**, 0.17
VLDL	1.8 ± 0.2	2.8 ± 0.5	2.7 ± 0.2	3.1 ± 0.4	0.06, 0.09, 0.48
LDL	15 ± 2	13 ± 2	80 ± 5	63 ± 12	0.17, **<0.0001**, 0.25
HDL	101 ± 5	101 ± 6	167 ± 4	148 ± 9	0.14, **<0.0001**, 0.15
Triglycerides					
Total	32 ± 3	36 ± 6	42 ± 2	39 ± 5	0.29, **0.0003**, 0.87
VLDL	17 ± 2	21 ± 4	18 ± 2	19 ± 5	0.41, 0.87, 0.64
LDL	9.9 ± 1	9.8 ± 1	16 ± 1	14 ± 1	0.28, **<0.0001**, 0.32
HDL	5.6 ± 0.6	5.4 ± 1	8.3 ± 1	6.4 ± 0.4	0.09, **0.007**, 0.20
Glycerol	61 ± 5	49 ± 4	83 ± 3	76 ± 6	0.07, **<0.0001**, 0.61

Table 3.2. Plasma cholesterol and triglyceride concentrations in 6 or 20-week control and high fat diet fed C57BL/6 and *Tst*⁻/⁻ mice. Data are presented as mg/dL ± SEM. Data were tested within groups using 2-way ANOVA and p values are given in the final column. * indicates p < 0.05 by Bonferroni post-hoc testing (between genotypes). CD; Control diet, HDL; high density lipoprotein, HFD; High fat diet, LDL; low density lipoprotein, VLDL; very low-density lipoprotein. n = 6 (C57Bl/6 CD), 6 (*Tst*⁻/⁻ CD), 11 (C57BL/6 HFD), 11 (*Tst*⁻/⁻ HFD) for 6-week data, n = 8 (C57BL/6 CD), 8 (*Tst*⁻/⁻ CD), 7 (C57BL/6 HFD), 7 (*Tst*⁻/⁻ HFD) for 20-week data.

3.3.8 *Tst* deletion does not affect liver triglyceride accumulation on control or HFD

To determine whether deletion of *Tst* altered the regulation of lipid metabolism specifically within liver tissue, the triglyceride content of the liver was analysed in 6- and 20-week HFD fed mice. No change in liver triglyceride content was found in mice fed control or HFD for 6 weeks. There were also no effects of genotype on liver triglyceride content between C57BL/6 and *Tst*$^{-/-}$ mice fed control of HFD for 6 weeks (Figure 3.12A).

Following 20 weeks of feeding, mice fed HFD exhibited increased liver triglyceride content overall (2-way ANOVA diet $p < 0.0001$) compared to chow fed controls (Figure 3.12B). However, there were no differences found between C57BL/6 and *Tst*$^{-/-}$ mice.
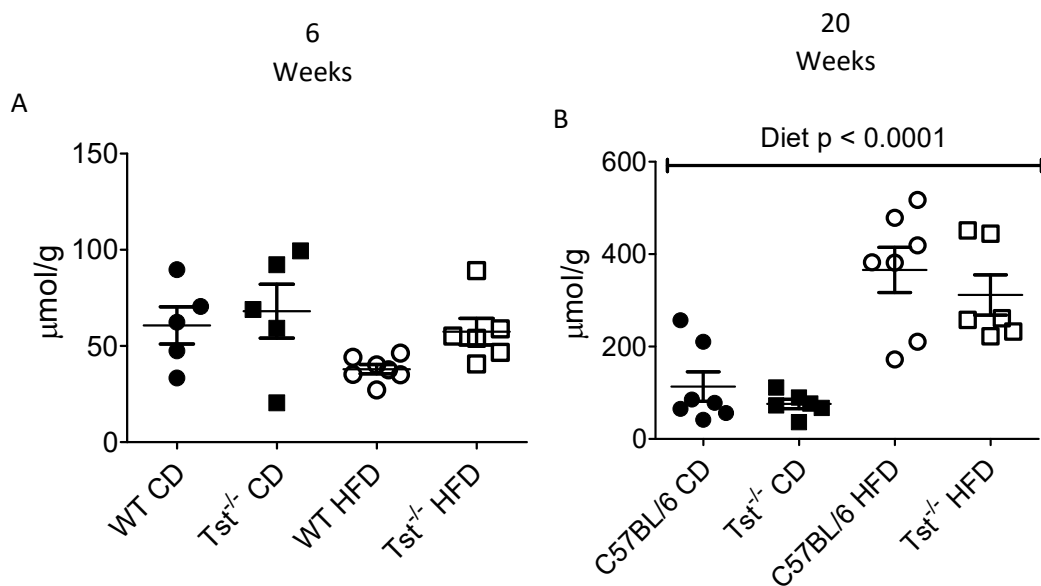

Figure 3.12 Liver triglyceride content in C57BL/6 and *Tst*$^{-/-}$ mice fed control or HFD for 6 or 20 weeks. A) Liver triglyceride content following 6 weeks of control or HFD feeding. **B)** Liver triglyceride content following 20 weeks of control or HFD feeding. Data are presented as Mean ± SEM. n = 5 (C57BL/6 CD), 5 (*Tst*$^{-/-}$ CD), 7 (C57BL/6 HFD), 6 (*Tst*$^{-/-}$ HFD) for 6-week data, n = 7 (C57BL/6 CD), 6 (*Tst*$^{-/-}$ CD), 7 (C57BL/6 HFD), 6 (*Tst*$^{-/-}$ HFD) for 20-week data. Data were tested using 2-way ANOVA and Bonferroni post hoc testing. CD; Control diet, HFD; High fat diet.

3.4 Discussion

This work aimed to further investigate the metabolic consequences of *Tst* deletion in mice, with the hypothesis that **the diabetogenic phenotype in *Tst*$^{-/-}$ mice is driven by major defects in hepatic glucose metabolism and lipid metabolism**. Previous work from Morton *et al.* (204) established *Tst* as an adipose-tissue associated 'lean gene' and showed that *Tst* gene deletion led to a worsening of glucose tolerance in mice fed HFD for 6 weeks. Within a Masters project (207) it was also found that control diet-fed *Tst*$^{-/-}$ mice exhibited increased gluconeogenesis in response to a pyruvate bolus (section 3.1.2). Gluconeogenesis can occur within the liver and kidney (218).

Investigation of glucose metabolism has shown that the worsening of glucose tolerance due to *Tst* deletion during 6 weeks of HFD feeding also occurs following 20 weeks of HFD feeding, although the size of the effect is reduced compared to previous data at 6 weeks. Interestingly, novel data showing that insulin sensitivity is relatively preserved in *Tst*$^{-/-}$ mice compared to C57BL/6N mice fed HFD for 20 weeks is presented, which adds complexity to the biology of the *Tst* knockout phenotype. *Tst*$^{-/-}$ mice released less insulin over the time-course of the GTT when fed either control or HFD and an ITT demonstrated increased sensitivity (30-minute decrement) of *Tst*$^{-/-}$ mice to insulin on either diet. This indicates that *Tst*$^{-/-}$ mice likely have suppressed endogenous insulin release, a novel observation that could be followed with analysis of their pancreatic β-cell function. Increased sensitivity to insulin (greater glucose decrement in response to an insulin bolus) is more challenging to place within the context of a mouse that exhibits increased gluconeogenesis.

Greater insulin sensitivity would predict that gluconeogenesis is suppressed, as this is a process that is exquisitely sensitive to the suppressing effects of insulin. However, consistent with the previous finding of increased gluconeogenesis in a pyruvate tolerance test (207), increased PEPCK activity was observed in 6-week control or HFD fed *Tst*$^{-/-}$ mice. One explanation for this discrepancy is that insulin sensitivity is maintained in the muscle, and perhaps even to some extent in the liver of *Tst*$^{-/-}$ mice, and that an insulin-independent mechanism drives increased hepatic gluconeogenesis and impaired glucose tolerance in *Tst*$^{-/-}$ mice.

Investigations of hepatic metabolic function *in vitro* demonstrated that basal mitochondrial respiration was increased in *Tst*$^{-/-}$ hepatocytes. One potential explanation for this finding is that *Tst*$^{-/-}$ mice have increased energy demand because of increased synthetic metabolism. Synthetic (anabolic) metabolism includes gluconeogenesis and triglyceride secretion which require energy and have been shown to be increased in *Tst*$^{-/-}$ mice. This increase in energy

demand may therefore be supplied by increased basal mitochondrial respiration. Increased H_2S signalling provides a second mechanism which may explain increased mitochondrial respiration in $Tst^{-/-}$ mice. Evidence in the literature has frequently linked a moderately (non-toxic) increased H_2S signal to increased mitochondrial respiration (219–221). As $Tst^{-/-}$ mice exhibit increased H_2S in the blood (204) this may explain the changes in mitochondrial metabolism.

Finally, investigations into hepatic lipid and lipoprotein metabolism also found that plasma triglyceride concentrations were increased in control diet fed $Tst^{-/-}$ mice. A similar increase in VLDL triglycerides has previously been observed in diabetic patients (48) and insulin-resistant mouse models (47,86,222) and, therefore, this effect is consistent with the 'diabetic-like' phenotype of $Tst^{-/-}$ mice. In combination, these findings suggest that multiple organ-specific effects (suppression of islet insulin secretion, enhanced peripheral – likely muscle - insulin sensitivity, and an increase in insulin-independent hepatic glucose production and triglyceride export) conspire to engender a "diabetogenic" phenotype in $Tst^{-/-}$ mice.

3.4.1 *Tst* deletion reduces body weight in control- and high fat diet-fed mice

Initial observations of body weight on control and HFD showed that $Tst^{-/-}$ mice had reduced body weight when fed control diet for 6 weeks. A similar trend was seen in mice fed control diet for 20 weeks. The cause of this reduction in body weight following 6 weeks of feeding is unclear. It does not appear to be related to poor health or failure to thrive as mice are grossly healthy and reproduce as expected. Interestingly in 6-week chow-fed mice the liver was larger in size compared to the animal's body weight, resulting in a higher liver/body weight ratio than in C57BL/6 mice. This effect was not seen in mice fed chow diet for 20 weeks. Hepatomegaly (an enlargement of the liver) can be a response to several diseases including non-alcoholic fatty liver disease (46) and glycogen storage disease (223), which result in increased storage of triglycerides or glycogen in hepatocytes, respectively . However, triglyceride and glycogen content of the liver were not increased in 6-week control diet fed $Tst^{-/-}$ mice compared to C57BL/6. The cause of hepatomegaly in $Tst^{-/-}$ mice is also extremely unlikely to be infection (224) or tumour related as no gross changes in liver morphology were observed in $Tst^{-/-}$ mice (Emerson *et al.* unpublished observations). Therefore, at this stage the increase in liver mass in $Tst^{-/-}$ is unexplained.

20 weeks of feeding with chow diet also increased the body weight of the animals compared to 6 weeks of control diet feeding. While this may simply represent increased aging and maturation of mice to higher body weights (225) it could also indicate that the control diet used does not merely maintain body weight, but is calorific enough to induce excessive

weight gain over this chronic time period. As expected, HFD feeding with Surwit diet for 6 or 20 weeks led to an increase in body weight in both C57BL/6 and $Tst^{-/-}$ mice (215,226), with 20 weeks' feeding leading to greater weight gain than 6 weeks. HFD feeding equalised body weights in $Tst^{-/-}$ mice compared with C57BL/6, eliminating the difference observed on control diet where $Tst^{-/-}$ mice had lower body weight. In 6-week fed mice this led to a significant interaction of diet and genotype suggesting that $Tst^{-/-}$ mice gained more weight when fed HFD than C57Bl/6 controls.

HFD feeding led to an increase in liver/body weight ratios in 6-week fed mice but not in 20-week fed mice. This discrepancy is most likely explained by the longer experimental length in 20-week fed mice. This extended feeding time allows for body weight to increase and normalise the liver/body weight ratio. However, this explanation suggests that in the early stages of HFD feeding the liver tends to increase in mass before body weight although, as this investigation has shown, this is not due to increased triglyceride or glycogen storage in the liver as these were not increased following 6 weeks of diet. The reason for this increase in liver weight is not clear from this study and little exists in the literature to explain the finding. One potential avenue for further investigation would be immune cell infiltration of the liver following HFD feeding which is known to occur as triglyceride content of the liver begins to increase and leads to lesion formation in the liver and steatohepatitis (213).

3.4.2 *Tst* deletion worsens glucose tolerance through liver and pancreatic actions

Consistent with previous glucose tolerance tests performed by Morton *et al.* (204) on C57BL/6 and $Tst^{-/-}$ fed control or HFD for 6 weeks it was found that *Tst* deletion did not alter glucose tolerance in 20-week control fed mice. However, it was noted that, compared to mice fed control diet for 6 weeks, 20-week control diet-fed mice had higher fasting glucose measurements (measured at time 0) and showed mild glucose intolerance (a slower rate of disposal over the 2-hour period). This worsening of glucose tolerance in mice fed chow for a longer period is similar to the effect seen in body weights where chow feeding for 20-weeks led to increased body weight compared to 6-week fed mice (discussed above). This indicates that either mouse age (225) or the constituents of the rodent chow diet are inducing mild metabolic dysfunction in mice. More closely matched control diets are available for experiments using 'Surwit' HFD and, therefore, using these in the future may help to elucidate any effect of long term CRM 'rodent chow' feeding on metabolic function.

As expected, and previously shown, HFD feeding induced substantial glucose and insulin intolerance in C57BL/6 mice (215,226). It was noted that the difference in glucose tolerance between control and HFD groups was less clear at 20 weeks than previously seen at 6 weeks

(204) due to increased blood glucose concentrations in chow-fed mice. When comparing the genotypes in isolation $Tst^{-/-}$ mice fed HFD for 20 weeks are not more glucose intolerant than C57BL/6. fed HFD. This is not what has been seen in previous experiments (204), where $Tst^{-/-}$ mice fed HFD for 6 weeks had noticeably impaired glucose tolerance compared to C57BL/6 fed HFD. However, in this present study it was noticed that when comparing to the chow fed mice high fat feeding for 20 weeks induced greater glucose intolerance in $Tst^{-/-}$ mice than C57BL/6. This significant interaction of genotype and diet (a worsened response to HFD feeding in $Tst^{-/-}$ mice) is consistent with the previous data in these mice following 6 weeks of HFD feeding (204). This difference may have occurred because, following 20 weeks of HFD, C57BL/6 mice were beginning to converge in phenotype with $Tst^{-/-}$ mice as their own metabolic dysfunction became more pronounced and was equal to the glucose intolerance in $Tst^{-/-}$ mice fed HFD. Overall these data suggest that any future work focussed on glucose tolerance in HFD fed conditions should be conducted at the 6-week time point.

The exact cause of worsened glucose tolerance in $Tst^{-/-}$ is currently unknown. Notably, increased H_2S signalling has been linked with diabetes and hepatic dysfunction (171,227,228). Exogenous NaHS administration resulted in disturbed glucose homeostasis and the development of insulin resistance in HepG2 and primary hepatocytes (173). Primary hepatocytes isolated from $Cse^{-/-}$ mice appeared to be more insulin sensitive and to favour insulin driven processes, such as glycogen storage and a decrease in gluconeogenesis (173). However, very interestingly, H_2S has been found to suppress insulin release from the pancreatic β cells, as a result of increased K_{ATP} channel opening following persulfidation by H_2S (32,163,179,229,230). Given the findings presented here on insulin signalling within $Tst^{-/-}$ mice (see below) this also presents the new hypothesis that abnormal β-cell function contributes to worsened glucose tolerance in $Tst^{-/-}$ mice.

3.4.3 Tst deletion reduces insulin concentrations leading to increased insulin sensitivity

Insulin concentrations measured during the GTT performed in 18-week control or HFD C57BL/6 and $Tst^{-/-}$ mice showed clearly that $Tst^{-/-}$ mice have lower blood insulin concentrations over the entire time course. It should be noted that these concentrations were measured under fasted conditions (at time 0, and following glucose bolus after this) and, therefore, it cannot be ruled out that under normal *ad libitum* feeding conditions no deficit of insulin would be found. However, the fact that the blood insulin concentration maintains a distinct deficit over the entire time course of the GTT suggests that $Tst^{-/-}$ mice likely have lower blood concentrations generally.

A reduction in blood insulin concentration during a GTT was not found in the previous work performed by Morton *et al.* (204) following 6 weeks of HFD feeding and was not measured in the 6-week fed mice within this work. One explanation for the contradiction in insulin findings between Morton *et al.* and this study may be a difference in the mouse background between studies. Work by Morton *et al.* was performed on a defined C57BL/6N background with control animals also on this background whereas this study was performed on mice which were had a mixed C57BL/6N and C57BL/6J background as the work was set against the background of a backcrossing program to harmonise the *Tst*$^{-/-}$ allele onto the 6J strain. Previous studies suggested that genetic differences between the C57BL/6 N and J substrains in the nicotinamide nucleotide transhydrogenase (NNT) gene can have effects on insulin secretion in mice (211,231–233) although this has recently been disputed (234). As mice in this study were not genotyped for their J/N SNP background it is possible that the C57BL/6 and *Tst*$^{-/-}$ mice used may also differed at the NNT gene; and this could explain the finding of reduced insulin in *Tst*$^{-/-}$ mice. However, this is unlikely as C57BL/6 and *Tst*$^{-/-}$ mice came from the same breeding colony which has presumably been equally diluted by J substrain breeding. Later data (chapter 5) also provide an argument that a difference in NNT substrain is unlikely to explain the findings here.

Assuming that the *Tst*$^{-/-}$ mice used did not differ at NNT one mechanistic explanation for this deficit in insulin signalling may be that increased H_2S concentrations in *Tst*$^{-/-}$ mice (as suggested by the independent whole blood measurements (204)) are indicative of increased H_2S signalling within pancreatic β cells (179,229,230). According to general transcriptional data from BioGPS *Tst* mRNA expression has been found in the pancreas (208). However, Pullen *et al.* actually identified *Tst* as one of the genes which is selectively disallowed within pancreatic β-cells to ensure normal function (235). Therefore, deletion within pancreatic β-cells is unlikely to lead to specific elevation of H_2S on a cellular level. Instead high circulating H_2S concentrations (as demonstrated by the high H_2S levels detected in whole blood of *Tst*$^{-/-}$ mice) may lead to modifications which affect β-cell function. H_2S has been shown to reduce insulin release due to activation of K_{ATP} channels (163) and suppression of β cell actions potentials which cause insulin release (32). This effect could explain why insulin is continuously suppressed in *Tst*$^{-/-}$ mice. Intriguingly the reduction in insulin does not result in glucose intolerance on control fed conditions possibly due to increased insulin sensitivity (discussed below). However, H_2S inhibition of insulin release may explain why *Tst* deletion exacerbates glucose intolerance induced by HFD. As seen from C57BL/6 mice in this study during HFD feeding there is a clear need to increase insulin production. This is also observed in type 2 diabetic patients (33,77) and in rodent models of diet induced obesity

(236). However, $Tst^{-/-}$ mice are unable to sufficiently increase in insulin production due to the inhibition of the β cells by H_2S resulting in increased hyperglycaemia. This could further explain why $Tst^{-/-}$ mice develop worsened glucose intolerance than C57BL/6 mice.

Further to the assessment of insulin release over the GTT time course an insulin tolerance test was also performed for the first time on $Tst^{-/-}$ mice and allowed some conclusions to be drawn on insulin sensitivity. The raw blood glucose measurements themselves confirmed the findings of the GTT that Tst deletion exacerbated the glucose intolerance (i.e. mice had higher blood glucose concentrations) induced by HFD. However, the calculated decreases in blood glucose are more useful as measures of insulin sensitivity. From these it was observed that in both genotypes HFD feeding led to a change in profile of the response to insulin. In control fed mice insulin produced a larger drop in glucose at 15 minutes than in HFD fed mice. By 30 minutes there was no detectable difference in the decrement between diet groups although this appears to be due in part to high variation in the data. This observed reduction in response to insulin is consistent with previous studies in which insulin tolerance tests have been performed on HFD fed mice (237–239).

No difference in glucose decrement was observed between the genotypes on either diet at the 15-minute time point (representing the initial fast response to insulin). However, at 30 minutes $Tst^{-/-}$ mice fed either diet demonstrated a clear accentuation of blood glucose decrement compared to C57BL/6 mice, indicating an increased sensitivity to insulin or increased ability to take up glucose during this phase of insulin response. Insulin receptors undergo desensitisation when exposed to higher insulin concentrations, either by a reduction in membrane receptors (37) or an uncoupling of receptor binding to downstream effects (36). It has also been shown that reducing insulin concentrations in the *ob/ob* experimental model of diabetes, through prolonged fasting, led to increased insulin binding and action on muscle tissue (240); consistent with the general theory that reducing hormone concentrations leads to sensitisation of tissues (35). Therefore, the reduction in insulin concentrations observed in $Tst^{-/-}$ mice may explain the increased sensitivity in $Tst^{-/-}$ mice which is able to compensate, at least in control fed conditions, and maintain normal glucose homeostasis. However, the findings in $Tst^{-/-}$ mice fed HFD suggest that, in conditions of dietary stress, this increase in sensitisation is no longer able to compensate for the reduced insulin concentrations observed in $Tst^{-/-}$ mice; therefore, glucose tolerance is worsened compared to C57BL/6 mice.

3.4.4 *Tst* deletion enhances gluconeogenesis

It has previously been shown (207)that glucose production from a pyruvate bolus is increased in $Tst^{-/-}$ mice fed control diet compared to C57BL/6 mice (section 3.1.2). This

pyruvate tolerance test was a simple measure of gluconeogenesis; a process which generates glucose from pyruvate molecules during fasting conditions in order to supply tissues such as the brain with a useable energy source (85). Gluconeogenesis occurs primarily within the liver and to some extent in the kidney (218). In this present work, it was found that PEPCK activity was increased in livers from $Tst^{-/-}$ mice. This was found to a greater extent in chow-fed mice reflecting the original finding of increased glucose production during the PTT which was performed in chow-fed mice. Following HFD feeding for 6 weeks, PEPCK activity in C57BL/6 mice increased and was approximately the same as that in $Tst^{-/-}$ mice.

Here, PEPCK activity was investigated particularly because of its role as the first committed step of gluconeogenesis (201). It is also highly regulated at the expression level through inhibition by insulin or stimulation by glucagon secretion (85). Insulin is considered to be the dominant factor however, due to its inhibition, via Akt-mediated phosphorylation, of many pro-gluconeogenic transcription factors (85). Therefore, it is possible that increased PEPCK activity in $Tst^{-/-}$ mice is simply the result of the reduction in insulin concentrations observed in these mice, leading to increased PEPCK expression. However, although it was not possible to measure PEPCK expression in the livers used to measure activity, previous work performed on 6-week HFD C57BL/6N or $Tst^{-/-}$ liver samples demonstrated that PEPCK expression was unchanged (207).

Another possible explanation for the increase in gluconeogenesis in $Tst^{-/-}$ mice may be increased H_2S signalling within the liver. Unfortunately, H_2S concentrations were not measured within this study, however Morton et al. have previously demonstrated that H_2S is elevated in whole blood samples from $Tst^{-/-}$ mice. In HepG2 cells and primary hepatocytes, exogenous H_2S stimulates an increase in gluconeogenesis (173). Furthermore, reduced gluconeogenesis was found in primary hepatocytes from $Cse^{-/-}$ mice which have lower H_2S levels than C57BL/6 mice in liver tissue (171,173). Further work has suggested that the increase in gluconeogenesis observed with H_2S administration is the result of a specific persulfidation of pyruvate carboxylase (PC) leading to increased activity and production of oxaloacetate: the substrate for PEPCK (166). PC has previously been considered an anaplerotic enzyme without a regulatory role in gluconeogenesis (174). However, some work has suggested that this is a simplification and increased PC expression or activity is associated with increased gluconeogenesis in fasting and diabetic conditions (174,175,218). An increase in PC activity could be partly responsible for the increase in activity observed in our biochemical method of assessing PEPCK activity, as this method relies on the

production of oxaloacetate to measure activity. Therefore, future investigation of PC activity in $Tst^{-/-}$ mice is certainly warranted.

3.4.5 Mitochondrial respiration in $Tst^{-/-}$ mice

Mitochondrial function is central to the metabolic processes of the cell (241). Mitochondrial activity is altered in some tissues in conditions, such as diabetes, in which nutrient homeostasis is impaired. For example, mitochondrial activity is reduced, compared to normal patients, in the skeletal muscle of diabetic patients who are insulin resistant (without other comorbidities) (216). This finding was also expanded by work showing that elderly patients who exhibited age-related insulin resistance compared to body weight-matched young adult controls also had reduced mitochondrial respiration in muscle (217).

In this work, we found that basal mitochondrial activity in primary hepatocytes from control fed mice was higher in $Tst^{-/-}$ than in C57BL/6 mice. Maximal activity (revealed by the addition of the uncoupling compound FCCP) was not increased in $Tst^{-/-}$ mice suggesting that there are not simply more mitochondria in $Tst^{-/-}$ hepatocytes leading to a higher O_2 consumption. The increase in basal respiration appears to be split evenly between ATP (i.e. useful energy producing)-linked respiration and leak respiration (non-energy producing respiration resulting from H^+ 'leak' across the mitochondrial membrane without ATP production). This distinction means that the increase is unlikely to be the result of increased expression of proteins that regulate mitochondrial leak, such as the UCP protein family (242).

The cause of this greater basal respiration is not clear. One explanation may be that $Tst^{-/-}$ hepatocytes require a greater amount of ATP than C57BL/6. This presents a clear explanation as ATP production is strictly controlled by the cell so that it is not wastefully overproduced. Following the classical theory of respiratory control, the activity of ATP synthase is solely regulated by the intra-mitochondrial concentration of its substrate ADP (243). Therefore, an increase in the ADP:ATP ratio, as would occur in the case of an increase in demand as ATP is being used up more rapidly, would result in increased mitochondrial respiration to meet this demand. Within this work, an increase in energy demand in $Tst^{-/-}$ mice can be hypothesised due to the increased synthetic processes which are occurring. Both gluconeogenesis and VLDL particle synthesis are energy demanding pathways which have been identified as increased in control fed $Tst^{-/-}$ mice *in vivo*. *In vitro* it was also found that $Tst^{-/-}$ hepatocytes exhibited higher protein concentrations than hepatocytes from C57BL/6 controls. Whether this represents increased protein synthesis *in vivo* is currently unknown, but this would increase energy demand in cells.

Two other potential explanations are suggested by research on H_2S stimulation of mitochondrial respiration. Many groups have shown that increased H_2S signalling, either as a result of exogenously applied H_2S from mitochondrially targeted donors such as AP123 and AP39 (219,244,245) or overexpression of the H_2S producing CBS protein (246), results in increased basal mitochondrial respiration. Szabo *et al.* have suggested several methods by which this can occur, including persulfidation of ATP synthase (220), and activation of a protein kinase signalling system within mitochondria (personal communication, 4th International Conference on the Biology of Hydrogen Sulfide 2016). This work suggests that the increased basal mitochondrial respiration in $Tst^{-/-}$ hepatocytes may be explained by an increase in H_2S concentrations.

However, much of this previous literature ignores the principle that ATP is not synthesised unless required when ADP concentrations increase in conditions of increased energy demand. In many of these experiments there is not a clear need for increased energy production and researchers do not suggest any precise mechanisms by which increased H_2S allows increased respiration to occur without an increase in energy demand. Therefore, it is possible that the observed increases in respiration with increased H_2S concentrations are artefactual. Bouillaud *et al.* have shown that the breakdown of H_2S by the SOU within the mitochondria leads to electron donation to the mitochondrial electron transport chain and then consumption of O_2; i.e. respiration in mammalian cells (247). In addition to this process, however, (which would generate ATP or leak as conventionally understood) the further breakdown of H_2S by SDO leads to an additional consumption of O_2 (Figure 3.13; 53). This additional consumption could contribute to the increase in O_2 consumption seen during Seahorse experiments. It has been demonstrated that inhibition of complex III of the mitochondrial transport chain by antimycin prevents this breakdown as the electron can no longer be donated to the transport chain (248–250). The resulting drop in O_2 consumption (which is used in the Seahorse method to calculate respiration) would be indistinguishable from conventional respiration occurring using organic fuels. Therefore, additional H_2S burden in the mitochondria could appear to increase in respiration but in fact be the result of the mitochondrial breakdown of H_2S. The increase in respiration of $Tst^{-/-}$ hepatocytes could be attributed to either described mechanism but awaits definite measurement of H_2S concentration within the liver or hepatocytes of $Tst^{-/-}$ mice before further investigations could be considered.
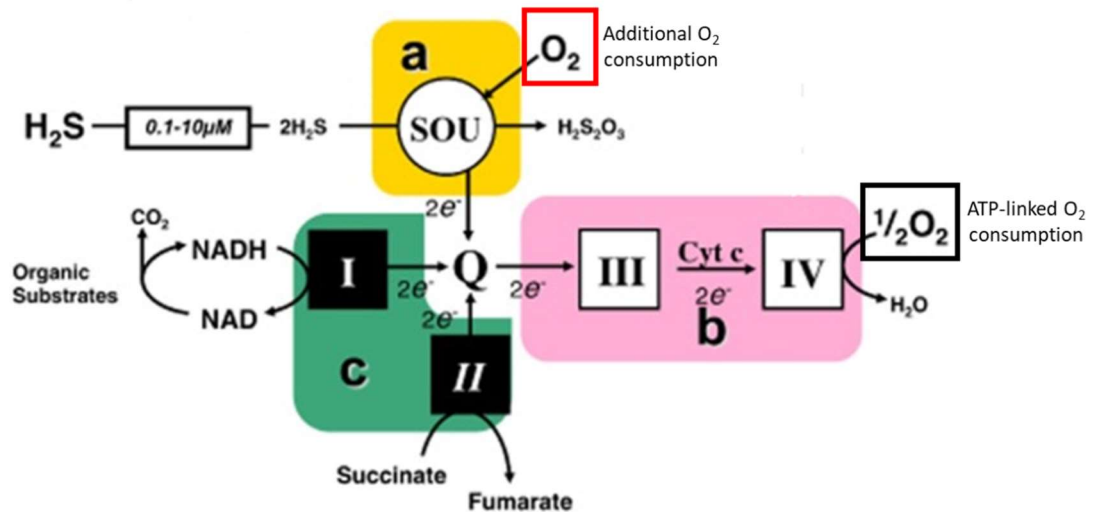
Figure 3.13 Mitochondrial O₂ consumption during H₂S metabolism. At non-toxic concentrations, H_2S (0.1-10 µM) has been demonstrated to act as an inorganic substrate for mitochondrial metabolism. Donation of electrons from H_2S to the mitochondrial transport train occurs through the SQR protein in the sulfide oxidising unit (SOU) (**a**). These electrons are transported to complexes III and IV to generate the proton motive force (which generates ATP through complex V) before being accepted by a molecule of oxygen leading to O_2 consumption and production of water (**b**). This process is identical to the donation of electrons by NADH (produced by the KREBS cycle) at complex I or through succinate conversion to fumarate at complex II (**c**). However, in addition to the O_2 consumed at complex IV the further steps of H_2S metabolism result in the additional consumption (highlighted in the red box) of a molecule of O_2 compared to organic substrates. Cyt c; cytochrome c, SOU; sulfide oxidising unit. Reproduced from Szabo *et al.* (2014) (221).

3.4.6 *Tst* deletion increases plasma VLDL triglyceride content

Another key role of the liver is to maintain homeostasis of plasma lipid concentrations. The liver is central to this process as it both synthesises and releases VLDL particles from the free fatty acids (FFA) it receives, and it is also involved in the processing and clearance of remnant particles from the blood (85,117). It was found that total and VLDL triglyceride content were increased in $Tst^{-/-}$ mice fed chow diet for 6 weeks. This increase was not seen in 20-week chow-fed diet mice. This discrepancy may be due to the general decrease in plasma triglyceride levels observed in chow-fed 20-week fed mice compared to 6-week chow-fed mice. One explanation for the reduction in plasma triglyceride concentrations in 20-week fed mice may be that plasma triglyceride concentrations decrease with increased age. Lower plasma triglyceride concentrations have been described in chow-fed aged mice compared with young adult mice, indicating that the regulation of triglyceride may change with age (225). However, it should be noted that Houtkooper *et al.* used mice that were over

22 months old compared to only 26-30 weeks in this present work casting doubt on whether the reduction at this age would be enough to explain the findings in this current work.

It was also noted that 20-week chow fed mice developed greater hepatic steatosis (triglyceride deposition in the liver) than 6-week control fed mice. This is an unusual finding as steatosis of the liver should not occur under control conditions (213). This may be linked with the other noted findings of increased body weight and worsened glucose tolerance in 20-week chow-fed mice and again indicates that mice fed chow for 20 weeks have mild metabolic dysfunction compared 6-week control diet fed mice. This evidence again suggests that 6-week investigations should be the focus for future studies on metabolic dysfunction in $Tst^{-/-}$ mice to ensure that mice are compared with a metabolically healthy control.

An increase in total or VLDL triglycerides specifically, as observed in 6-week control diet fed $Tst^{-/-}$ mice, has previously been associated with insulin resistance with or without hyperglycaemia (47,48). There are many suggested mechanisms by which a reduction in insulin signalling may cause increased VLDL triglyceride concentrations. One explanation which has been suggested is that in conditions of insulin resistance there is a lack of suppression of lipolysis in adipose tissue depots resulting in increased FFA delivery to the liver (47). The synthesis of VLDL particles is highly dependent upon substrate availability and, therefore, this increase in availability results in increased synthesis. Blood insulin concentrations were not measured in these 6-week fed mice and, so it is not clear whether they also have an insulin deficit as seen in 20-week fed mice. However, if this was present then it may provide an explanation for increased hepatic production of VLDL via increased FFA delivery from adipose tissue and, therefore, would be interesting to test in this model.

Interestingly increased H_2S concentrations, as seen in by Morton et $al.$ in $Tst^{-/-}$ mice (204), have also been linked with increased VLDL secretion in mice. Mani et $al.$ have shown that $Cse^{-/-}$ mice exhibit lower total triglyceride than C57BL/6 controls when fed control or atherogenic diet, and that this was normalised in atherogenic diet-fed mice by the administration of NaHS, a H_2S donor compound (171,187). One study has shown that the administration of garlic oil, which contains natural H_2S donor compounds, ameliorated hepatic steatosis through modulation of the transcription factor sterol regulatory element binding protein 1c (SREBP-1c) (251). SREBP-1c regulates the expression of a large cohort of genes associated with de $novo$ lipid synthesis within the liver (47). Increased SREBP-1c activation resulting in increased hepatic de $novo$ lipogenesis is a suggested mechanism for the increase in VLDL production observed in conditions of insulin resistance (47,48,86). Therefore, SREBP-1c and its downstream targets such as acetyl CoA carboxylase (ACC) and

fatty acid synthase (FAS) also represent intriguing potential mechanisms for investigation in chow-fed $Tst^{-/-}$ mice once increased H_2S within $Tst^{-/-}$ liver has been confirmed. This could initially be done by measuring mRNA expression levels of the genes of interest.

No differences were noted in plasma triglyceride concentrations in mice fed with HFD for 6 or 20 weeks. Within the 6-week HFD-fed mice following HFD feeding total and VLDL triglyceride content in C57BL/6 mice reaches similar levels to those in $Tst^{-/-}$ mice (which exhibit a slight drop in concentration compared to chow-fed mice). Therefore, following HFD C57BL/6 mice appear to be converging in phenotype with $Tst^{-/-}$ mice; reducing the differences between the genotypes as was seen in PEPCK activity measurements.

Examination of hepatic triglyceride levels showed that there were no differences between C57BL/6 and $Tst^{-/-}$ mice fed control or HFD for 6 or 20 weeks. Increased H_2S concentrations have previously been suggested to reduce hepatic steatosis in mice (171,186,252) (as a result of the same SREBP-1c activation which promotes VLDL production) and, therefore, this finding challenges the presumption within this work that $Tst^{-/-}$ mice have increased H_2S concentrations. However, most of the evidence for the effects of H_2S on hepatic steatosis come from genetic models of reduced H_2S production ($Cse^{-/-}$ and $Cbs^{-/-}$) both of which also exhibit hyperhomocystinaemia as a result of their effects on the trans-sulfuration pathway (186,253). Increased homocysteine has been linked with hepatic steatosis (188,254) and, therefore, the effects of Cse and Cbs deletion on hepatic steatosis may not be solely linked to reduced H_2S.

3.4.7 Conclusions

This work has confirmed the hypothesis that altered liver function affecting both carbohydrate and lipid homeostasis in $Tst^{-/-}$ mice is a major driver of the metabolic dysfunction observed in these mice. However, it has also raised the hypothesis that reduced insulin secretion by the pancreas in $Tst^{-/-}$ mice could be a contributing factor for many of these phenotypes. It is intriguing that many of the phenotypes observed in this work may be partly explained by a reduction in insulin concentrations. Therefore, investigation of pancreatic function and, especially, whether increased H_2S signalling plays a role in supressing insulin release must be of the highest priority in future investigations.

Many of the findings in this work (such as the increase in gluconeogenesis, the reduction in blood insulin concentrations, the increase hepatic mitochondrial respiration and the increase in VLDL triglyceride content) are also consistent with effects described for increased H_2S concentrations in either the liver or pancreas. Therefore, a second mechanism for the

phenotypes observed in this work is that TST contributes to H_2S breakdown and that deletion or inhibition of the protein can result in elevated H_2S concentrations, which explain the phenotypes observed in the mice. Future investigations will need to specifically measure H_2S concentrations in the tissues of interest as well as examining the effects of increased H_2S using molecular biology techniques such as detection of persulfidated proteins (163,255). Overall the evidence here suggests that *Tst* deletion engenders a 'diabetogenic' phenotype in mice and that HFD feeding leads to exacerbation of these defects and therefore a worsened response to the diet resulting in overt metabolic disease. The aim of the current work is now to examine how this metabolic dysfunction, which has been linked to vascular injury, and elevated H_2S, which has been linked to vascular protection, may influence the vascular function of $Tst^{-/-}$ mice fed control or HFD.

4.0 The effects of *Tst* deletion on vascular function

4.1 Introduction

4.1.1 H$_2$S in vasculature

Many studies on H$_2$S have focussed on its role within the cardiovascular system, where the enzymes known to synthesise H$_2$S are highly expressed and where it has shown functional effects (167,193,253,256). Gasotransmitters, such as nitric oxide (NO), are important in the vascular system where they can act as second messenger molecules stimulated by activation of G-protein coupled receptors (257). There is also evidence that endothelial dysfunction, which is commonly associated with reduced production of NO, is a symptom of, or even a precursor to, vascular diseases such as atherosclerosis (114,258). Studies on H$_2$S have shown that similar to NO exogenously administered H$_2$S, usually given in high doses of µmol concentration, is protective in a number of mouse models of vascular dysfunction (reviewed in 16). Conversely models of reduced H$_2$S generation, such as *Cse*$^{-/-}$ mice, exhibit inhibited vasodilator responses to acetylcholine and develop cardiovascular diseases such as hypertension (253). In addition *Cse*$^{-/-}$ mice fed western diet were also found to have exacerbated atherosclerosis compared to control mice (187).

In a study of atherosclerosis *Cse*$^{-/-}$ mice were found to have increased atherosclerotic plaque volume compared to control mice and this was associated with increased intercellular adhesion molecule 1 (ICAM1) expression on aortic endothelial cells (187). The authors therefore suggested that a lack of H$_2$S production and signalling was affecting endothelial cell function, although the mechanism responsible for this effect was not identified. Finally, an *in vitro* investigation using endothelial cells found that exogenous H$_2$S donor NaHS protected against mitochondrial dysfunction induced by reactive oxygen species (ROS) overproduction in response to high glucose concentrations (260). The modulation of endothelial function by NaHS has, therefore, emerged as a promising target for the use of H$_2$S donor compounds in common vascular pathologies.

4.1.2 Potential mechanisms of H$_2$S actions in the vasculature

The mechanisms underlying the actions of H$_2$S in the vasculature are not clearly defined. One potential mechanism is the direct effect of H$_2$S is to elicit vascular relaxation (180). This is mediated, at least in part, through persulfidation-mediated activation of the smooth-muscle K$_{ATP}$ channel (181). However, recent studies have also identified TRPA1 channels located within vascular nerve endings as potential targets for H$_2$S vasodilator signalling through a combined mechanism involving production of HNO- molecules in a reaction of H$_2$S and NO (261). Activation of these channels may then lead to the release of vasodilator signals such as ACh from nerve endings resulting in a secondary vasodilation. Activation of K$^+$ channels,

leading to hyperpolarisation of vascular smooth-muscle cells, has been suggested as a component of endothelium-derived hyperpolarising factor (EDHF)-induced relaxation (190,191).

It should be noted that the concentrations of H_2S donor compounds used to elicit direct vasodilation are usually 10-1000 times the maximal predicted endogenous concentrations casting doubt on the role of H_2S as an independent vasodilator.

Instead H_2S may act in concert with NO to mediate vasodilation. H_2S signalling modulates phosphorylation of endothelial nitric oxide synthase (eNOS) (4,5) at the activating serine 1177 residue, thereby increasing synthesis of NO. Further to this, H_2S can decrease breakdown of cGMP, a downstream effector of NO signalling, through inhibition of phosphodiesterase 5 (PDE5) (263). Taken together, these effects support the idea that H_2S exhibits cross-talk with NO signalling and acts to augment NO signalling in the cardiovascular system. Because a lack of NO production has previously been linked with vascular diseases (114,258) the protective effect of exogenously administered H_2S observed in some of these models may in fact represent a secondary effect on NO signalling. A recent study investigated this idea and found that the protective effect of exogenous Na_2S in a model of cardiac ischaemia-reperfusion was reliant on functional *eNOS* expression and this protection was lost in mutant model expressing a non-phosphorylatable eNOS (S1179A) on an otherwise *eNOS*$^{-/-}$ background (167).

4.1.3 H_2S in *Tst*$^{-/-}$ mice

As discussed (above), the majority of investigations addressing the vascular effects of H_2S have focussed either on manipulation of H_2S production via cystathionine-gamma lyase (CSE), or on pharmacological stimulation using sulfide donors (173,187,219,264). An alternative and under-explored approach is the elevation of endogenous H_2S levels through inhibition of clearance pathways. Genetic deletion of proteins in the sulfide oxidising unit (SOU)(168) represents one potential method by which endogenous H_2S levels can be increased. The only previous studies of SOU protein deletion were in mice with genetic deletion of sulfur dioxygenase (SDO, *Ethe1*). *Ethe1* deletion resulted in rapid post-natal death from sulfide toxicity (170). Recently published work confirmed that genetic deletion of *Tst* (*Tst*$^{-/-}$), a modulatory protein of the SOU, results in marked elevation of blood 'sulfides' detected using monobromobimane (MBB) (204). Despite this, *Tst*$^{-/-}$ mice remain grossly viable and healthy, albeit with impaired glucose homeostasis (204); unlike mice with genetic deletion of SDO.

4.1.4 Hypothesis and aims

In this chapter, it was <u>hypothesised</u> that: **$Tst^{-/-}$ mice would have to altered baseline vascular function in response to vasoconstrictor and dilator compounds and be protected from vascular dysfunction induced by high fat diet feeding.**

Aims

- To determine whether *Tst* deletion alters aortic vascular constriction and relaxation responses.
- To examine the extent of vascular dysfunction (in both constriction and relaxation responses) induced by short (7-week) and long (20-week) HFD feeding in mice.
- To determine whether *Tst* deletion protected mice from the adverse vascular effects of HFD feeding.

4.2 Materials and methods

4.2.1 mRNA collection, reverse transcription and quantification

To generate data on the expression of *Tst,* C56BL/6 mice were culled, and the thoracic aorta and liver removed. The mRNA was then extracted from these tissues and reverse transcribed. *Tst* (Mm01195231_m1), *Tbp* (Mm01277042_m1) and *Gapdh* (Mm99999915_g1) Taqman assay probes were obtained from Applied Biosystems (Thermo Scientific, Loughborough, UK) and expression was quantified using real time polymerase chain reaction (section 2.5.3). NormFinder software (University Hospital, Aarhus, Denmark) was used to analyse *Tbp* and *Gapdh* housekeeping genes. The software compared the 'Stability value' of each gene separately and as an average. An average of *Tbp* and *Gapdh* was found to have the highest 'Stability value' and was therefore used to normalise *Tst* expression.

4.2.2 Myography

C57BL/6 and $Tst^{-/-}$ mice were given *ad libitum* access to control 'rodent chow' (CRM diet, Special Diet Services, UK) or 'Surwit' 58% high fat diet (HFD, Research Diets, New Brunswick, US) for 7 or 20 weeks to induce weight gain and metabolic dysfunction, including hyperglycaemia (Figure 4.1).
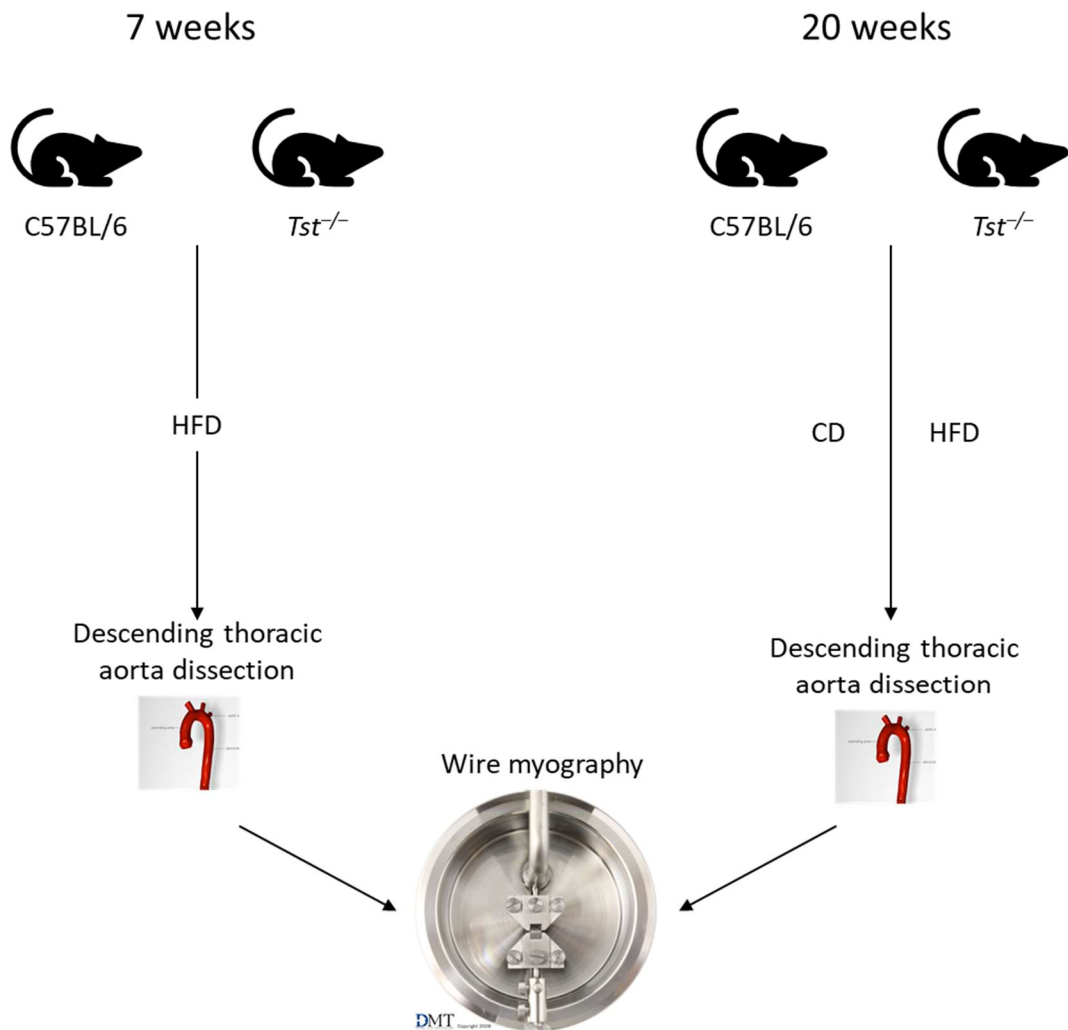
Figure 4.1 Experimental design of investigations into the effect of *Tst* deletion on vascular function in control and HFD fed mice. Two studies were conducted using age matched C57BL/6 and *Tst*$^{-/-}$ mice. Note that at the 7-week time point no chow diet was used so only HFD fed groups were included. Wire myography was performed on the descending thoracic aorta (section 2.3.2). Investigations with L-NAME (an inhibitor of endothelial nitric oxide synthase) and Indomethacin (an inhibitor of cyclooxygenase) were performed by mounting 2 consecutive sections of aorta in separate myograph tissue baths and exposing one to L-NAME (10^{-4} M) and indomethacin (10^{-5} M) for a minimum of 20 minutes prior to beginning concentration-response curves. Concentration-response curves were performed in response to vasoconstrictors; 5-HT and phenylephrine (10^{-9} – $10^{-4.5}$ M), and vasodilators ACh (10^{-9} – $10^{-5.5}$ M) and sodium nitroprusside (SNP; 10^{-9} – $10^{-4.5}$ M). Preconstriction (for vasodilator responses) was elicited using a concentration of 5-HT to reach approximately 80% of maximal 5-HT constriction.
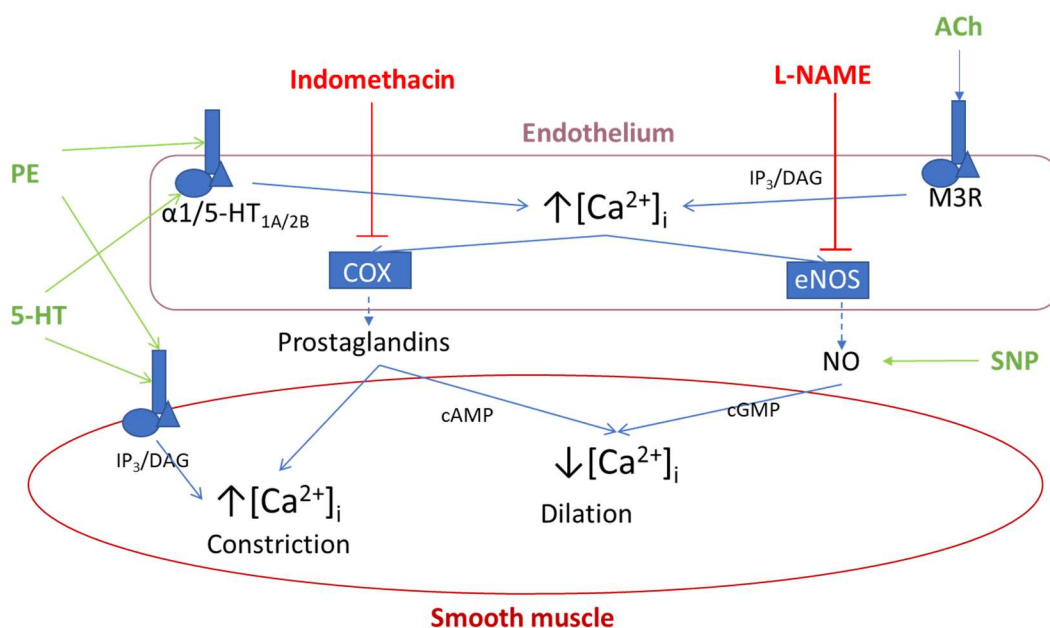
Figure 4.2 Signalling pathways investigated using myography. The key components of the signalling pathways mediating vasodilation and vasoconstriction which were investigated. Stimulator compounds (vasoconstrictors PE and 5-HT and vasodilator ACh and SNP) are shown in green with the eNOS and COX inhibitors L-NAME and indomethacin, respectively are shown in red. 5-HT; 5-hydroxytryptamine, 5-HT1A/2B; 5-hydroxytryptamine receptor 1A/2B, α1; α1 adrenoreceptor, ACh; acetylcholine, cAMP; cyclic adenosine monophosphate, cGMP; cyclic guanosine monophosphate, COX; cyclooxygenase, DAG; diacylglycerol, eNOS; endothelial nitric oxide synthase, IP3; triphosphoinositol, L-NAME; Nω-nitro-L-arginine methyl ester, M3R;l muscarinic receptor type 3, PE; phenylephrine, SNP; sodium nitroprusside.

4.2.3 Myography statistical analysis

Vasoconstrictor responses were normalised as a percentage to the maximal constriction recorded with KPSS (section 2.3.2). Vasodilation responses were first normalised to a percentage of the preconstriction tension elicited with 5-HT (section 2.3.2) before being converted to 'Relaxation' values by subtracting responses from 100. Summary statistics for maximal constriction/dilation (E_{Max}) and sensitivity, measured as the concentration required for 50% E_{Max}, (EC_{50} or IC50 where vessels relaxed) were generated using linear regression of curves. EC_{50} values were converted to either pD_2 for contraction responses or $-Log(IC_{50})$ for relaxation responses using the formula $= -Log(EC/IC_{50})$. The change in maximal constriction/relaxation caused by L-NAME/Indomethacin addition was also calculated (ΔE_{Max}). For the 20-week groups (C57BL/6 CD, $Tst^{-/-}$ CD, C57BL/6 HFD and $Tst^{-/-}$ HFD) statistical comparisons were made using the generated summary statistics (E_{Max}, pD_2/-$Log(IC_{50})$, ΔE_{Max}) on the effect of diet and genotype using two-way ANOVA with

Bonferroni post hoc tests made between genotypes. The two 7-week groups (C57BL/6 HFD and $Tst^{-/-}$ HFD) were compared using Student's unpaired t test.

4.3 Results

4.3.1 $Tst^{-/-}$ mice have similar body weights to C57BL/6 controls

C57BL/6 and $Tst^{-/-}$ mice fed chow diet for 20 weeks had comparable body weights at the time of cull (Figure 4.3B). In mice fed HFD for 7-weeks, final body weights were similar to those in 20-week control fed mice (37-39 g) but there was no difference in body weight between C57BL/6 and $Tst^{-/-}$ mice. HFD feeding for 20 weeks induced glucose intolerance (shown in section 3.3.2) and increased body weight in both genotypes compared to control diet (2-way ANOVA $p < 0.0001$, Figure 4.3B) fed but there was no difference in body weights of C57BL/6 and $Tst^{-/-}$ mice at the time of cull (Figure 4.3B).
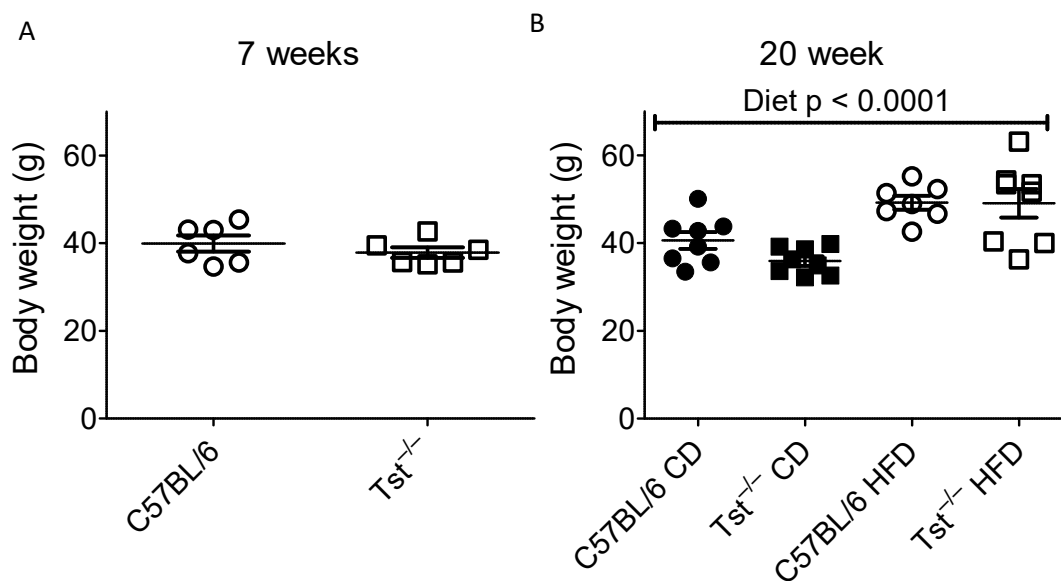
Figure 4.3 Body weights in C57BL/6 and $Tst^{-/-}$ mice fed chow or high fat diet for 7 or 20 weeks. A) Final body weights from mice fed HFD only for 7 weeks. **B)** Final body weights from mice control or HFD for 20 weeks. Data are presented as Mean ± SEM. n = 6 for both 7-week groups; for 20-week data n = 8 (C57BL/6 CD), 8 ($Tst^{-/-}$ CD), 7 (C57BL/6 HFD), and 8 ($Tst^{-/-}$ HFD). 7-week data were compared using Student's unpaired t test, 20-week data were compared using 2-way ANOVA with Bonferroni post hoc test. CD; control diet, HFD; High fat diet.

4.3.2 *Tst* mRNA is expressed in aorta

Tst mRNA expression was confirmed in mouse aorta using quantitative RT-PCR (Figure 4.4).
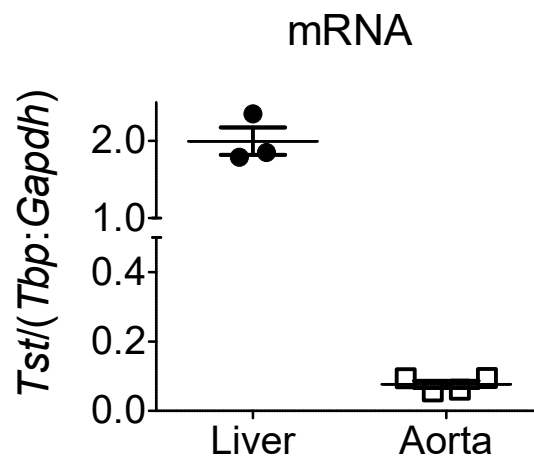
Figure 4.4. *Tst* mRNA is present in aortic tissue. Quantitative real time reverse transcriptase PCR was performed on aorta and liver samples taken from C57BL/6 mice. Analysis using a mixed standard curve showed a low but detectable level of *Tst* mRNA in aortic samples. n = 3 liver, 4 aortae. Tbp; TATA binding protein, Gapdh; Glyceraldehyde-3-phsophate dehydrogenase.

4.3.3 *Tst* deletion reveals a NOS- and COX-independent component of ACh-mediated relaxation in aortae from HFD-fed mice

ACh produced a concentration-dependent relaxation in isolated aorta and these responses were similar in C57BL/6 and *Tst$^{-/-}$* mice fed chow diet (Figure 4.5A) for 20 weeks. The combination of L-NAME (10^{-4} M) and indomethacin (10^{-5} M) reduced ACh-mediated relaxation to 1/3 of its standard response in 20-week control diet-fed C57BL/6 mice (C57BL/6 E$_{Max}$ Standard 75.1 ± 2.3%, +L-NAME/Indomethacin 19.2 ± 4.8%, Figure 4.5A, Table 4.1).

ACh-mediated relaxation was not impaired in either genotype by 7 or 20 weeks of HFD feeding (Figure 4.5B, C & Table 4.1). The addition of L-NAME and indomethacin reduced relaxation in aortas from C57BL/6 HFD mice to a similar degree to that seen in chow-fed mice (C57BL/6 CD E$_{Max}$ + L-NAME/Indomethacin 19.2 ± 4.8%, C57BL/6 HFD 21.4 ± 4.8%, Table 4.1). However, in *Tst$^{-/-}$* mice fed HFD for 7 or 20 weeks L-NAME and indomethacin addition was less effective at reducing relaxation than in C57BL/6 HFD groups (Figure 4.5B, C, Table 4.1) resulting in a significant residual relaxation compared to C57BL/6 mice.

Comparison of ΔE$_{Max}$ values (Table 4.1) showed that the efficacy of L-NAME/Indomethacin in reducing ACh-mediated relaxation was unaffected by diet (C57BL/6 ΔE$_{Max}$ chow 55.9%, HFD 52.3%). However, *Tst$^{-/-}$* mice fed either chow or HFD had a trend towards smaller ΔE$_{Max}$ values compared to C57BL/6 mice (Table 4.1, genotype p = 0.06). ΔE$_{Max}$ also showed a trend towards being reduced in *Tst$^{-/-}$* mice fed HFD for 7 weeks when compared to C57BL/6 fed HFD (ΔE$_{Max}$ C57BL/6 53.7 ± 5.8%, *Tst$^{-/-}$* 36.9 ± 4.9%, p = 0.07, Table 4.1).

Endothelium independent relaxation was investigated in 7-week HFD mice using the NO donor compound SNP. Relaxation of vessels in response to SNP was similar in C57BL/6 and *Tst$^{-/-}$* mice (Figure 4.6). The addition of L-NAME and indomethacin did not affect the maximal relaxation to SNP.

20 weeks
Chow Diet

7 weeks
High Fat Diet

20 weeks
High Fat Diet
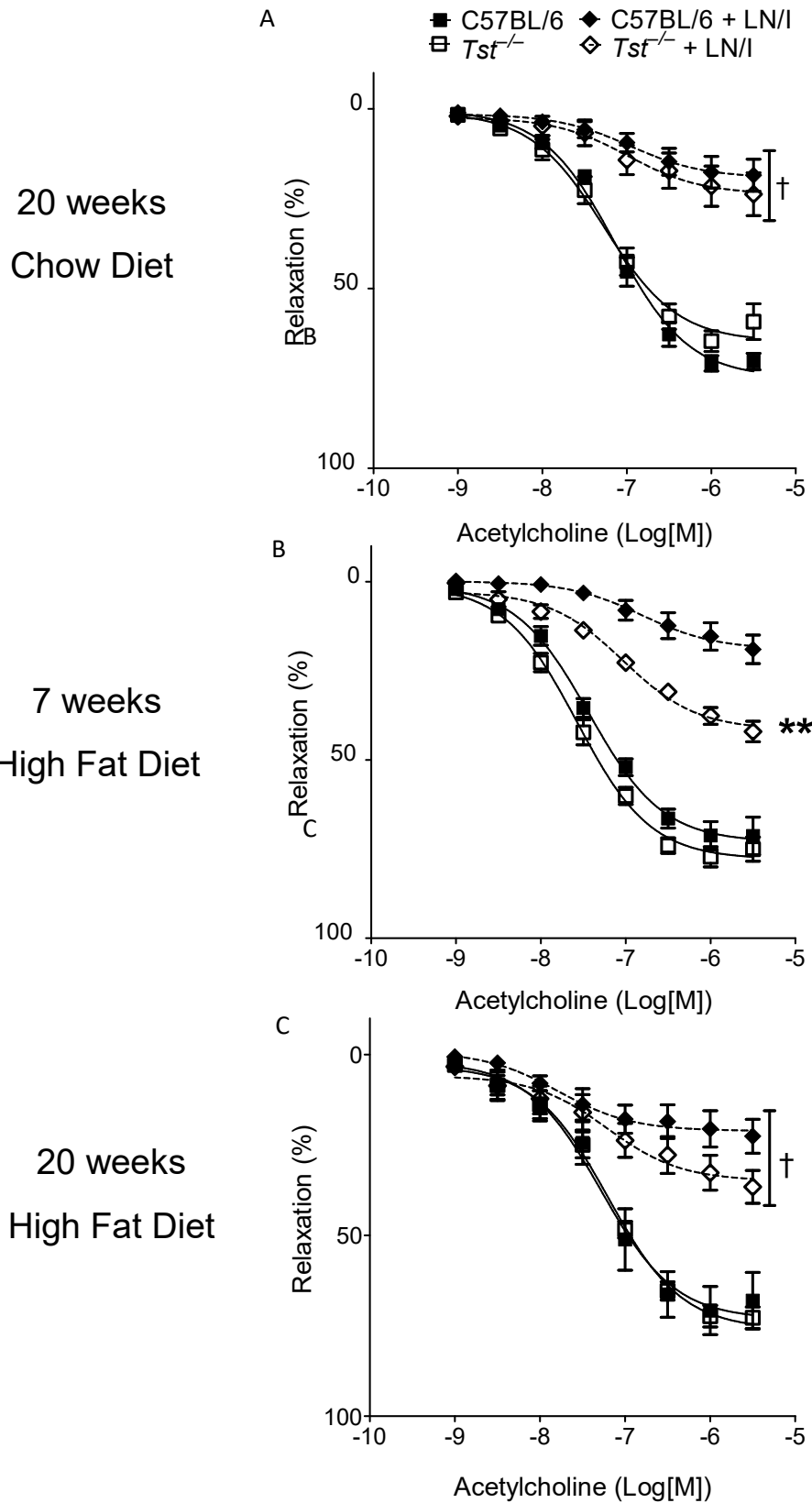
Figure 4.5 Acetylcholine-mediated vasodilation in C57BL/6 and *Tst*^{-/-} mice fed chow or HFD for 7 or 20 weeks. A) Acetylcholine-mediated relaxation of aortae from C57BL/6 and *Tst*^{-/-} mice fed chow diet. Pharmacological inhibitors L-NAME (10^{-4} M) and indomethacin (10^{-5} M) were used and responses + L-NAME/Indomethacin are shown with dashed lines. **B)** The impact of 7 weeks of high fat diet (HFD) feeding on acetylcholine-mediated relaxation of aortae from C57BL/6 and *Tst*^{-/-} mice. **C)** Acetylcholine-mediated relaxation following 20 weeks of HFD feeding. Data are Mean ± SEM. 20-week chow and HFD summary statistics were compared using 2-way ANOVA and Bonferroni post hoc testing. 7-week summary statistics were tested using Student's t test. Data were compared between genotypes and diet groups and not between standard and +L-NAME/Indomethacin responses. For 20-week data n = 8 (C57BL/6 CD), 7 (*Tst*^{-/-} CD), 6 (C57BL/6 HFD), and 8 (*Tst*^{-/-} HFD); for 7-week groups n = 4 for both genotypes. † indicates genotype p<0.05 in 2-way ANOVA, ** indicates p < 0.01 by Student's t test.
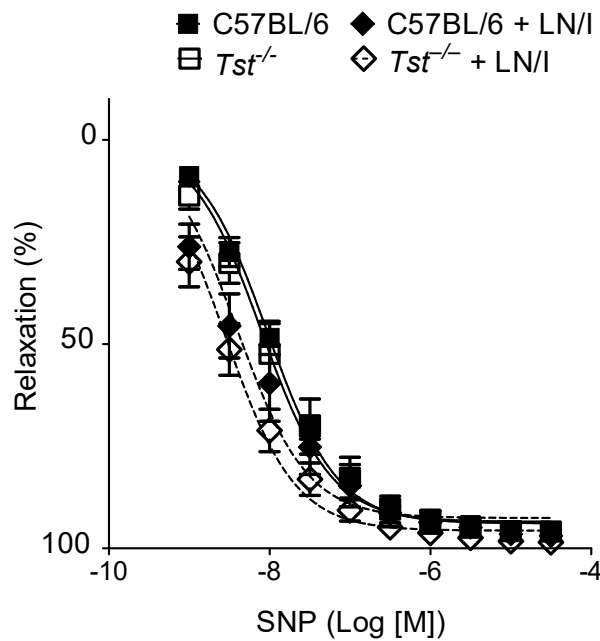
Figure 4.6 Sodium nitroprusside (SNP)-mediated relaxation of aortae from C57BL/6 and *Tst*^{-/-} mice fed HFD for 7 weeks. The effects of L-NAME (10^{-4} M) and indomethacin (10^{-5} M) on SNP-induced vessel relaxation are shown using dashed lines. Data are Mean ± SEM. Summary statistics for C57Bl/6 and *Tst*^{-/-} responses were tested using Student's unpaired t test. n = 6 for both groups. SNP; sodium nitroprusside.

	L-NAME/ Indo	Parameter	Group averages % ± SEM				Statistical tests
			C57BL/ 6 CD	$Tst^{-/-}$ CD	C57BL/6 HFD	$Tst^{-/-}$ HFD	
			7 weeks				Student's t test
ACh	-	Relaxation			73.1 ± 4.3	78.2 ± 3.0	0.37
	-	-Log(IC$_{50}$)			7.4 ± 0.04	7.6 ± 0.1	0.28
	+	Relaxation			19.5 ± 3.8	**41.3 ± 3.8****	**0.007**
	+	-Log(IC$_{50}$)			6.7 ± 0.2	7.1 ± 0.2	0.18
	+/-	ΔE_{Max}			53.7 ± 5.8	36.9 ± 4.9	0.07
SNP	-	Relaxation			94.2 ± 0.3	94.6 ± 2.0	0.84
	-	-Log(IC$_{50}$)			8.0 ± 0.1	8.1 ± 0.1	0.78
	+	Relaxation			94.9 ± 1.7	96.7 ± 1.5	0.43
	+	-Log(IC$_{50}$)			8.4 ± 0.2	8.6 ± 0.1	0.47
	+/-	ΔE_{Max}			0.3 ± 1.6	-1.9 ± 0.8	0.26
			20 weeks				2-way ANOVA p values (genotype, diet, interaction)
ACh	-	Relaxation	75.1 ± 2.3	65.9 ± 3.4	73.7 ± 7.1	75.9 ± 3.1	0.39, 0.29, 0.17
	-	-Log(IC$_{50}$)	7.1 ± 0.04	7.3 ± 0.1	7.3 ± 0.1	7.2 ± 0.1	0.51, 0.44, 0.30
	+	Relaxation	19.2 ± 4.8	24.0 ± 5.8	21.4 ± 4.8	37.0 ± 3.5	**0.05**, 0.13, 0.28
	+	-Log(IC$_{50}$)	7.1 ± 0.2	7.2 ± 0.3	7.7 ± 0.2	7.2 ± 0.3	0.38, 0.16, 0.24
	+/-	ΔE_{Max}	55.9 ± 6.0	41.9 ± 7.6	52.3 ± 8.0	39.4 ± 6.3	0.06, 0.66, 0.93

Table 4.1 Summary statistics of vasodilator responses in C57BL/6 and $Tst^{-/-}$ mice fed control diet for 20 weeks or high fat diet for 7 or 20 weeks. Data are presented as Mean ± SEM. 7-week data were tested using Student's unpaired t test, 20-week data were tested using 2-way ANOVA with Bonferroni post-hoc testing. ** indicates $p < 0.01$ by Student's t test. For 7-week ACh data n = 4 for both genotypes; for 7-week SNP data n = 6 for both genotypes; for 20-week data n = 8 (C57BL/6 CD), 7 ($Tst^{-/-}$ CD), 6 (C57BL/6 HFD), and 8 ($Tst^{-/-}$ HFD). ACh; acetylcholine, CD; control diet, HFD; high fat diet, SNP; sodium nitroprusside.

4.3.4 Long term HFD feeding reduces L-NAME/Indomethacin-induced enhancement of agonist mediated contraction in aortas from C57BL/6 but not from $Tst^{-/-}$ mice

PhE and 5-HT induced concentration–dependent contractions in aortae from chow-fed C57BL/6 mice. These responses were not altered by in $Tst^{-/-}$ mice (Figures 4.7 A&B). Addition of L-NAME/Indomethacin led to an increase (>2 fold) in PhE-mediated contraction (C57BL/6 E_{Max} Control 111.8 ± 12.9%, +L-NAME/Indomethacin 240.8 ± 8.1%, Figure 4.7A, Table 4.2). An increase with L-NAME/Indomethacin addition was also seen when 5-HT was used to elicit contraction (C57BL/6 E_{Max} Control 175 ± 11.3%, +L-NAME/Indomethacin 247.9 ± 9.9%, Figure 4.7B, Table 4.2). Maximum contraction was similarly increased by the addition of L-NAME/Indomethacin to aortas from chow-fed $Tst^{-/-}$ mice (Figure 4.7A&B, Table 4.2).

7-week HFD feeding did not alter contractile responses to PhE or 5-HT in C57BL/6 or $Tst^{-/-}$ mice in the absence of inhibitors (Figure 4.7C, D; Table 4.2). Consistent with previous results addition of the combination of L-NAME/Indomethacin led to an increase in PhE-mediated contraction (C57BL/6 E_{Max} Control 143.5 ± 8%, +L-NAME/Indomethacin 235.4 ± 10.7%, Figure 4.7C, Table 4.2). However, in 7-week HFD fed mice the increase in contraction caused by L-NAME/Indomethacin was not as pronounced when 5-HT was used to elicit contraction (C57BL/6 E_{Max} Control 242.1 ± 12.7%, +L-NAME/Indomethacin 264.7 ± 21.3%, Figure 4.7D, Table 4.2). Similar increases in maximum contraction caused by L-NAME/Indomethacin addition were also observed in aortae from $Tst^{-/-}$ mice (Figure 4.7C, D, Table 4.2). Calculation of ΔE_{Max} values for PhE and 5-HT-mediated constriction with L-NAME/Indomethacin addition confirmed the identical response of aortae from C57BL/6 and $Tst^{-/-}$ mice to L-NAME and indomethacin (Table 4.2).

20-week HFD feeding did not alter contractile responses to PhE or 5-HT in either genotype in the absence of inhibitors (Figure 4.7E, F; Table 4.2). However, in the presence of L-NAME/Indomethacin PhE- and 5-HT-mediated contraction was lower in C57BL/6 than in $Tst^{-/-}$ mice (5-HT genotype p = 0.03, PhE genotype p = 0.004, Figure 4.7E, F; Table 4.2). Calculation of ΔE_{Max} values showed that the enhancement of agonist-induced constriction by L-NAME and indomethacin was lower in aortae from HFD-fed C57BL/6 mice than those from $Tst^{-/-}$ mice for both 5-HT (ΔE_{Max} C57BL/6 20W HFD 30.9 ± 5.5%, $Tst^{-/-}$ 82.3 ± 15.3%, p <0.05 Bonferroni post hoc test, Table 4.2) and PhE (ΔE_{Max} C57BL/6 20W HFD 96.2 ± 28.4%, $Tst^{-/-}$ 172.9 ± 18.5%, p <0.05 Bonferroni post hoc test, Table 4.2).
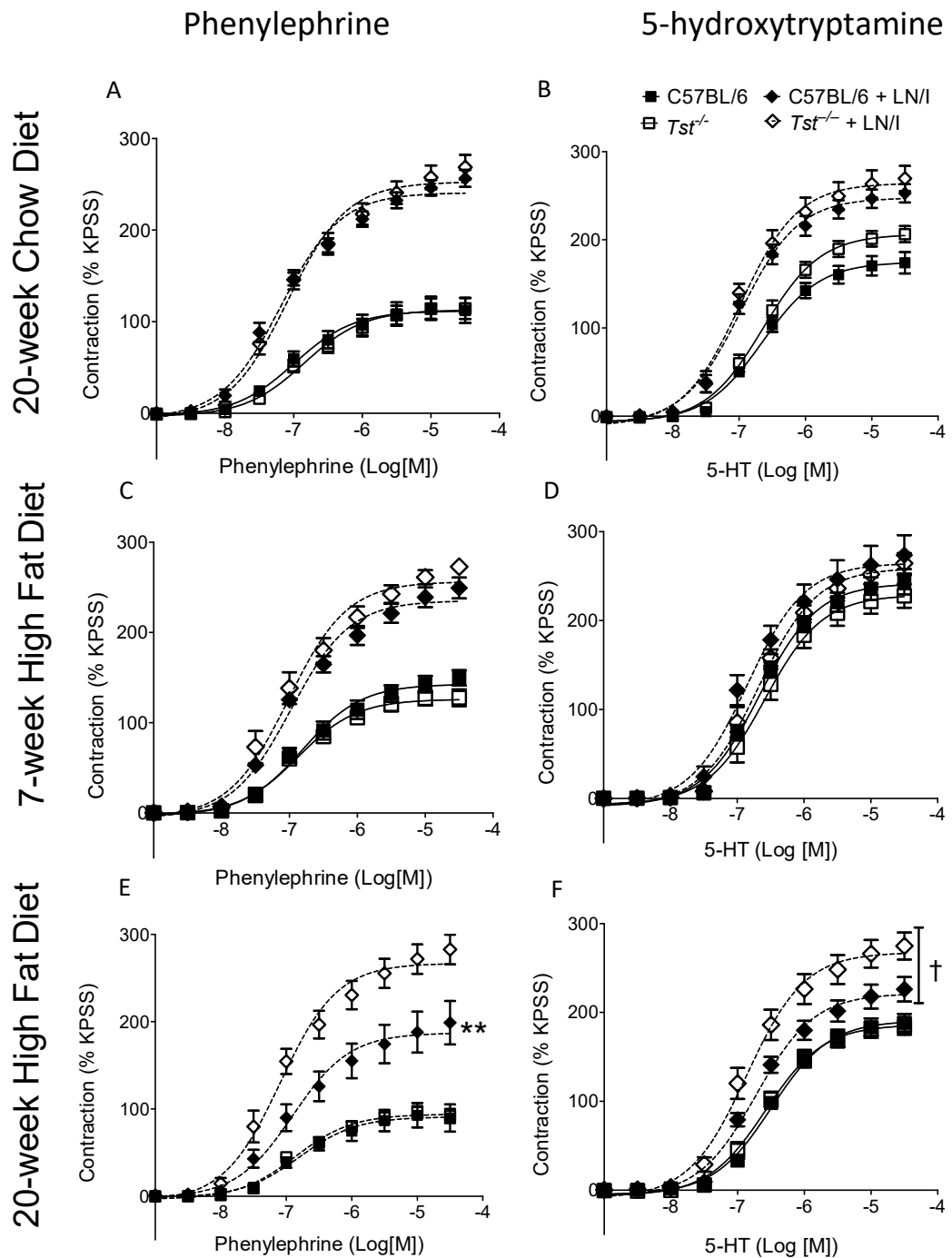
Figure 4.7 Phenylephrine and 5-hydroxytryptamine vasoconstriction responses in C57BL/6 and *Tst*$^{-/-}$ mice fed control diet for 20 weeks or high fat diet for 7 and 20 weeks. Responses are presented as normalised percentages to the vessels maximal constriction with KPSS. Dashed lines are responses + L-NAME and indomethacin (indicated by '+LN/I' in figure legend). **A)** and **B)** Phenylephrine or 5-HT-mediated vasoconstriction in 20-week chow fed mice. **C)** and **D)** Phenylephrine or 5-HT-mediated vasoconstriction following 7 weeks of HFD. **E)** and **F)** Phenylephrine or 5-HT-mediated vasoconstriction following 20 weeks of HFD. Data are Mean ± SEM. 20-week chow and HFD data were tested with 2-way ANOVA and Bonferroni post hoc testing. Data were compared between genotypes and diet groups and not between standard and +L-

NAME/Indomethacin responses. 7-week data were tested using Student's unpaired t test. For 20-week data n = 8 (C57BL/6 CD), 7 (*Tst*$^{-/-}$ CD), 6 (C57BL/6 HFD), and 8 (*Tst*$^{-/-}$ HFD); for both 7-week groups n = 4-6. † indicates genotype $p<0.05$ in 2-way ANOVA, ** indicates $p < 0.01$ by Bonferroni post-hoc test.

	L-NAME/Indo	Parameter	C57BL/6 CD	$Tst^{-/-}$ CD	C57BL/6 HFD	$Tst^{-/-}$ HFD	Statistical tests
			Group averages % ± SEM				
					7 weeks		Student's t test
KPSS	-	Maximum contraction (mN)			4.5 ± 0.4	4.2 ± 0.3	0.58
5-HT	-	E_{Max}			242 ± 13	229 ± 13	0.50
	-	pD_2			6.7 ± 0.04	6.6 ± 0.1	0.36
	+	E_{Max}			265 ± 21	260 ± 12	0.85
	+	pD_2			6.9 ± 0.1	6.7 ± 0.1	0.23
	+/-	ΔE_{Max}			23 ± 18	42 ± 11	0.40
PhE	-	E_{Max}			143.5 ± 8.0	126.5 ± 8.1	0.17
	-	pD_2			6.8 ± 0.1	6.9 ± 0.1	0.49
	+	E_{Max}			235.4 ± 10.7	257.4 ± 5.2	0.12
	+	pD_2			7.0 ± 0.04	7.0 ± 0.1	0.89
	+/-	ΔE_{Max}			91.8 ± 16.8	128.4 ± 7.3	0.09
			20 weeks				2-way ANOVA p values (genotype, diet, interaction)
KPSS	-	Maximum contraction (mN)	5.4 ± 0.3	5.1 ± 0.3	5.2 ± 0.4	4.6 ± 0.3	0.19, 0.26, 0.73
5-HT	-	E_{Max}	175 ± 11	207 ± 9	191 ± 10	186 ± 9	0.18, 0.81, 0.07
	-	pD_2	6.6 ± 0.03	6.6 ± 0.1	6.5 ± 0.04	6.6 ± 0.04	0.52, **0.05**, 0.36
	+	E_{Max}	248 ± 10	264 ± 16	222 ± 14	269 ± 15	**0.03**, 0.44, 0.29
	+	pD_2	7.0 ± 0.1	7.0 ± 0.03	6.7 ± 0.04	6.8 ± 0.1	0.27, **0.004**, 0.38
	+/-	ΔE_{Max}	73 ± 13	57 ± 12	31 ± 6	**82 ± 15***	0.18, 0.52, **0.02**
PhE	-	E_{Max}	112 ± 13	113 ± 11	91 ± 14	94 ± 7.3	0.84, 0.10, 0.93
	-	pD_2	7.0 ± 0.04	6.8 ± 0.1	6.8 ± 0.1	6.9 ± 0.1	0.31, 0.24, 0.09
	+	E_{Max}	241 ± 8	253 ± 12	187 ± 23	**267 ± 16*** *	**0.004**, 0.20, **0.03**
	+	pD_2	7.2 ± 0.1	7.1 ± 0.1	6.9 ± 0.1	7.1 ± 0.1	0.45, **0.03**, **0.02**
	+/-	ΔE_{Max}	129 ± 20	136 ± 19	96 ± 28	**173 ± 19***	0.06, 0.93, 0.11

Table 4.2 Summary statistics of vasoconstrictor responses in C57BL/6 and $Tst^{-/-}$ mice fed control diet for 20 weeks or high fat diet for 7 or 20 weeks. Data are Mean ± SEM. Contraction data were normalised as a percentage to the maximal response of the vessel to KPSS; E_{Max} and pEC_{50} values were determined using linear regression of responses. The change in response because of L-NAME and indomethacin addition was calculated as ΔE_{Max} = +L-NAME/Indomethacin E_{Max} – Control E_{Max}. 7-week data were tested using Student's unpaired t

test, 20-week data were tested using 2-way ANOVA with Bonferroni post-hoc testing. * or ** indicates p < 0.05 or <0.01, respectively by Bonferroni post-hoc test. For 20-week data n = 8 (C57BL/6 CD), 7 *(Tst⁻/⁻ CD)*, 6 (C57BL/6 HFD), and 8 *(Tst⁻/⁻ HFD)*; for both 7-week groups n = 4-6. 5-HT; 5-hydroxytryptamine, CD; control diet, HFD; high fat diet, KPSS; high potassium physiological salt solution, PhE; phenylephrine.

4.4 Discussion

The work shown in this chapter describes the attempt to assess the effects of deletion of an enzyme of the sulfide oxidising unit (SQR, ETHE1 and TST) (168) on vascular function. The work addressed the hypothesis that impaired clearance of H_2S would protect against endothelial cell dysfunction induced by high fat feeding. It was hypothesised that this protection would occur despite a potential for worsened hyperglycaemia, a predisposing factor for endothelial dysfunction (61), in $Tst^{-/-}$ mice fed HFD as previously observed (section 3.3.2).

In chow-fed C57BL/6 mice ACh-induced relaxation was significantly reduced, and agonist-induced contraction was enhanced, by inhibition of endothelium-derived vasodilator (NO, prostaglandins) production, consistent with published work (265–267). Contractile responses were largely unchanged in $Tst^{-/-}$ mice compared to C57BL/6. However, $Tst^{-/-}$ mice did demonstrate a small but significant residual vasodilator response in the presence of L-NAME and indomethacin which was not seen in C57BL/6 mice. This residual response was exaggerated in HFD fed $Tst^{-/-}$ mice following both 7 and 20 weeks of HFD feeding. HFD in C57BL/6 mice, perhaps unexpectedly, did not impair ACh-mediated relaxation. However, 20 weeks HFD feeding reduced the enhancement of contractile response caused by L-NAME/Indomethacin addition in C57BL/6 mice. In contrast, aortae from $Tst^{-/-}$ mice fed HFD for 20 weeks did not exhibit the reduced contractile response when exposed to inhibitors and instead maintained similar contraction responses to those of control diet fed mice.

4.4.1 *Tst* expression in the aorta

BioGPS data (208) suggest that *Tst* is abundantly expressed in many tissues including liver, stomach, intestine, brain, lung, kidney, heart, adipose and muscle but expression in the vasculature has not been previously determined. The highest expression levels of *Tst* are observed in liver and intestine (208), consistent with a role for *Tst* in detoxification. Data have previously shown that high *Tst* expression in tissues such as liver is correlated with high levels of *Tst* activity (Carter *et al.* Unpublished observations).

Results reported in this chapter showed that *Tst* was expressed at a low level in aortic tissue compared to liver but was readily detectable and, therefore, may have a role in clearance of H_2S within this vessel. This represents the first confirmation that *Tst*, a protein of the Sulfide Oxidising Unit (SOU) (168), is expressed within the aorta. The expression of sulfide:quinone reductase (SQR) and sulfide dioxygenase (SDO, historically ETHE1) which along with TST comprise the SOU in the mitochondria (169) has not yet been confirmed. However, the

expression of CSE in the aorta (253) and the reported levels of free sulfide (256) within aortic tissue suggest that it is likely that cells will express the proteins responsible for breakdown given the high toxicity of H_2S.

4.4.2 The effects of *Tst* deletion on vasodilator responses

This chapter addressed the hypothesis that deletion of *Tst* would influence arterial function, particularly in the presence of the metabolic stress (e.g. hyperglycaemia) induced by high fat feeding. Surprisingly, HFD did not impair ACh-mediated relaxation in either C57BL/6 or $Tst^{-/-}$ mice. This was unexpected given previous findings of reduced reactivity to ACh in aortas from HFD fed mice (15, 39) and due to the suggested role of hyperglycaemia in causing endothelial dysfunction in humans and mouse models (12, 27, 32). However, the published literature on the influence of high fat diet on vascular function is somewhat contradictory. Groups have previously reported that C57BL/6 mice do not develop aortic endothelial dysfunction following exposure to high fat diet (268). For example, d'Uscio *et al.* demonstrated that aortae from 30-week-old C57BL/6 mice fed a "western diet" for 26 weeks did not develop endothelial dysfunction with ACh inducing >85% relaxation in preconstricted vessels (9). HFD-induced endothelial dysfunction is also contentious in atherosclerosis-prone $ApoE^{-/-}$ mice (23). Jiang *et al.* reported that aortic endothelial cell dysfunction in $ApoE^{-/-}$ mice developed only in the abdominal aorta and no changes were observed in the thoracic aorta (14). Furthermore, Gervias *et al.* also demonstrated that 20-week western diet feeding had no effect on aortic endothelial cell function in $ApoE^{-/-}$ mice compared with C57BL/6 controls (11). Studies in humans using brachial flow-mediated dilation measurements to assess endothelial function have revealed contradictory results where short-term high fat diets either induced dysfunction (25) or had no effect (29). These data suggest that endothelial dysfunction because of HFD feeding remains controversial and further studies are needed.

The marked reduction of ACh-mediated relaxation by the combination of L-NAME and Indomethacin is consistent with previous observations from $eNOS^{-/-}$ mice (265) that ACh-mediated relaxation of the aorta is predominantly mediated by the release of endothelium-derived NO. In aortas from $Tst^{-/-}$ mice the L-NAME/Indomethacin-induced inhibition of ACh-mediated relaxation was decreased compared to C57BL/6 controls. In the 20-week cohort this effect was more pronounced in HFD-fed mice. After 7-weeks of HFD the reduced effectiveness of L-NAME/Indomethacin-induced inhibition of ACh-mediated vasodilation in $Tst^{-/-}$ mice compared to C57BL/6 is striking. The residual relaxation response in aortae from $Tst^{-/-}$ mice (particularly those fed HFD) in the presence of L-NAME/Indomethacin suggests a role for additional endothelium-derived relaxing factors (EDRFs), of which several have

been identified in other arteries (269). Previous investigations have shown that alterations in the balance of EDRFs can occur. In patients with Normal Pressure Glaucoma (NPG) it was noted that endothelium-derived hyperpolarising factor (EDHF) made a greater contribution to resistance artery relaxation than observed in non-diseased controls, suggesting endothelial cells from NPG patients had an altered balance of EDRFs. This supports the idea that similar alterations to the balance of EDRFs could occur in $Tst^{-/-}$ mice. Given the suspected effects of Tst deletion on H_2S signalling (inferred from the findings of Morton et al. of increased whole blood H_2S concentrations), a primary candidate for the additional relaxant response observed in the presence of L-NAME and indomethacin is H_2S. Persulfidation and activation of smooth muscle K_{ATP} as well as involvement of Intermediate potassium (IK_{Ca}) and small potassium (SK_{Ca}) calcium sensitive channels leading to hyperpolarisation of the smooth muscle have established H_2S as an EDHF (181). However, confirmation that H_2S mediated EDHF was responsible for the observed effects in this chapter would require a detailed, systematic study using exposure to the relevant inhibitors of K_{ATP} (glibencamide), IK_{Ca} (charybdotoxin) and SK_{Ca} (apamin) to investigate their contribution to the additional vasodilation response (270,271).

4.4.3 The effects of Tst deletion on vasoconstrictor responses

Functional analysis in aortae from chow fed mice demonstrated that deletion of Tst had no effect on PhE, 5-HT or K^+-mediated contraction in endothelium-intact blood vessels. These data suggest that Tst deletion does not induce a change in aortic constrictor function in chow fed mice. Addition of L-NAME/indomethacin promoted contraction in aortae from chow fed animals, consistent with previous evidence that endothelium-derived relaxant factors modify the vascular response to constrictors (266,267). This was not different in chow fed $Tst^{-/-}$ mice. Consistent with the investigations of vasodilator function, it appears that Tst deletion has no modulatory effect on vasoconstriction in mice fed a chow diet.

20-week HFD feeding reduced the ability of L-NAME/Indomethacin to increase agonist-induced contraction in aortae of C57BL/6 mice. Strikingly, this reduction did not occur in the aortae from $Tst^{-/-}$ mice. The reduction of L-NAME/Indomethacin's ability to enhance contraction only occurred in the 20-week HFD fed C57BL/6 mice and not in 7-week fed mice. These data suggest that the reduction in L-NAME/Indomethacin enhancement of contraction only occurs with longer periods of HFD feeding or increased age of mice. The reduction of L-NAME/Indomethacin enhancement of contraction in 20-week HFD fed C57BL/6 mice is likely the result of reduced release of EDRFs by the endothelium in response to vasoconstrictors. This is supported by the finding that KPSS-induced contraction of vessels from HFD-fed mice was unchanged compared to chow fed mice, showing that

vessels do not simply have a decreased ability to contract in response to increased intracellular calcium. Instead the data suggest that HFD affects agonist-mediated receptor signalling in the endothelium and that deletion of *Tst* is protective against this effect. The mechanism of this protection is currently unknown however, a hypothesised mechanism is that H_2S-induced activating phosphorylation of eNOS protein (167) or antioxidant effects of elevated sulfide lead to a reduction of oxidative stress in endothelial cells (260). Previous studies have not investigated this process as an aspect of aortic function in HFD fed mice and, therefore, these findings represent a first insight into the effects of HFD on the ability of the endothelium to modulate contractile responses.

4.4.4 Conclusions

Overall these data suggest that *Tst* deletion has little effect on baseline vasodilator or vasoconstrictor function in chow or HFD fed mice. In addition, only mild detrimental effects of HFD on vascular function were observed. HFD for 7 or 20 weeks did not reduce ACh-mediated vasodilation or increase constrictor-mediated contraction, meaning it is hard to evaluate the effect of *Tst* on overt vascular dysfunction (i.e. a reduction in NO production) as this was not evident. However, investigations with L-NAME and indomethacin did reveal some latent changes in aortic responses in $Tst^{-/-}$ mice; these retained residual relaxation to ACh whereas this response in aortas from C57BL/6 were nearly completed inhibited. Finally, it was also observed that 20-week HFD did in fact reduce L-NAME/Indomethacin-induced enhancement of constrictor-mediated contraction in C57BL/6 mice.

5.0 The effects of *Tst* gene deletion on atherosclerosis development in *ApoE*$^{-/-}$ mice

5.1 Introduction

5.1.1 Atherosclerosis

Cardiovascular disease (CVD) is the leading cause of death worldwide and research from the WHO has shown it is highly prevalent in both developed and developing nations (109). Atherosclerosis, the formation of fatty plaques within blood vessels, is a frequent cause of CVD as plaque development within vessels creates a risk of rupture and thrombosis leading to vascular occlusion. This is the most common cause of stroke and myocardial infarction: two serious CVD events (45,112).

Previous research has identified a number of modifiable risk factors associated with the development of atherosclerosis, including: increased plasma LDL cholesterol content, hyperglycaemia, high blood pressure and endothelial dysfunction (45). Therapies which can counter these risk factors, such as the reduction in blood cholesterol concentration using statins, have proven useful in reducing the occurrence of severe CVD events associated with atherosclerotic disease (140,272). Small scale studies in atherosclerotic patients have also suggested that short term intensive statin therapy may be able to reduce the lipid content and size of atherosclerotic lesions directly (273). However, statins are not universally tolerated and studies have shown that they may increase patients risk of developing diabetes by 9% (140). Therefore, they do not eliminate the need for other therapies. Moreover, there is some evidence that statins may increase the risk of T2DM, in part by increasing weight gain (274). Therefore, given the increasing rate of CVD worldwide there is extensive need for new treatments which can reduce atherosclerotic lesion development through alternative mechanisms of action.

5.1.2 H$_2$S and atherosclerosis

Recent work by Mani *et al.* established a link between the availability of H$_2$S and the development of atherosclerosis (187,275). They demonstrated that *Cse*$^{-/-}$ mice, which have low H$_2$S levels, develop atherosclerotic lesions when fed a high fat (42% kcal) high cholesterol 'western diet'. This occurred even in mice which did not have *ApoE* gene deletion: an unusual finding as atherogenesis in mice commonly requires severe alteration of the plasma cholesterol profile through *ApoE* or *Ldlr* gene deletion (44,125). Further to this, deletion of the *Cse* gene on an *ApoE*$^{-/-}$ background (*ApoE*$^{-/-}$*Cse*$^{-/-}$ mice) led to a worsening of lesion development compared to *ApoE*$^{-/-}$ controls (187). The authors identified a number

of potential causes for the increase in lesion development, including: increased plasma LDL cholesterol, increased systolic blood pressure (SBP), and increased oxidative stress and endothelial cell expression of the macrophage adhesion molecule intercellular adhesion molecule 1 (ICAM-1); a feature of endothelial dysfunction (276). Hydralazine and ezetimibe were used to reduce SBP and plasma cholesterol, respectively in mice with *Cse* deletion, but this did not reduce lesion area. The authors therefore concluded that increased endothelial ICAM-1 expression because of decreased H_2S signalling which led to increased endothelial ROS and ICAM-1 expression. Therefore, it appears that with regards to atherosclerotic lesion development the availability of H_2S within the vascular endothelium is more important than modulation of risk factors such as cholesterol and SBP.

Strikingly, in $Cse^{-/-}$ and $ApoE^{-/-}Cse^{-/-}$ mice, administration of intravenous NaHS reduced lesion volume and in $Cse^{-/-}$ only also reduced SBP and plasma cholesterol. In combination, these findings presented clear evidence that exogenous H_2S donor protects against atherosclerosis and should be investigated as a therapy for the reduction of atherosclerotic lesion volume.

Mani *et al.* and many other researchers in related fields have used exogenous H_2S administration or reduced endogenous production to investigate the effects of H_2S. However, no group to date has investigated whether decreased H_2S elimination through endogenous breakdown pathways could elicit similar effects in models of CVD disease. As previously discussed (sections; 1.5, 3.0 and 4.0) $Tst^{-/-}$ mice represent a model in which a protein of the mitochondrial H_2S breakdown pathway is absent logically suggesting that H_2S breakdown will be compromised. Pilot data has shown that circulating H_2S concentrations are increased in $Tst^{-/-}$ mice compared to C576BL/6 controls (section 1.5.1) and in addition the glucose intolerance observed in $Tst^{-/-}$ mice is also consistent with the literature findings of increased H_2S concentrations (section 3.0). $Tst^{-/-}$ mice therefore represent a useful model for the investigation of whether endogenously elevated H_2S concentrations can affect atherosclerotic lesion size.

5.1.3 Hypothesis and aims

In this chapter, it was hypothesised that: **vascular protective actions in $Tst^{-/-}$ mice predominate over the detrimental metabolic changes and result in decreased atherosclerotic lesion formation.**

Aims

- To generate an $ApoE^{-/-}Tst^{-/-}$ double knockout mouse for use in atherosclerotic investigations and confirm *Tst* deletion.
- To determine whether *Tst* gene deletion on the $ApoE^{-/-}$ genetic background induces metabolic dysfunction by examining glucose homeostasis (glucose tolerance test)
- To determine whether *Tst* gene deletion reduces atherosclerotic lesion formation induced by 12 weeks of western diet feeding in $ApoE^{-/-}$ mice using optical projection tomography.
- To investigate the consequences of *Tst* gene deletion on key risk factors for atherosclerosis on the $ApoE^{-/-}$ genetic background by examining SBP (tail cuff plethysmography) and plasma lipid concentrations in western diet fed $ApoE^{-/-}$ and $ApoE^{-/-}Tst^{-/-}$ mice.

5.2 Materials and methods

5.2.1 TST activity

Liver and aortic protein samples were isolated from chow diet-fed $ApoE^{-/-}$ and $ApoE^{-/-}Tst^{-/-}$ mice (section 2.5.1). Protein concentration was assayed (section 2.5.2) and 50 µg of protein were used to prepare TST activity reactions (section 2.4.5). A negative (no enzyme) control was run in parallel with samples and its absorbance subtracted from samples before further analysis. Unknown SCN^- concentrations (a measure of TST activity) from experimental samples were then interpolated from a linear SCN^- standard curve prepared on the same 96 well plate as samples.

5.2.2 Atherosclerotic lesion quantification and metabolic phenotyping in $ApoE^{-/-}$ and $ApoE^{-/-}Tst^{-/-}$ mice fed western diet

$ApoE^{-/-}$ and $ApoE^{-/-}Tst^{-/-}$ mice (bred as described in section 2.1.3) were maintained in a 12-hour light/dark cycle and humidity-controlled environment (section 2.1). During experiments mice were given *ad-libitum* access to 42% fat (kcal) and 0.15% (w/w) cholesterol – the so called 'western Diet' (829100, Special Diet Services, Witham, UK) for 12 weeks to induce lesion formation in line with previous literature (8, Figure 5.1). The operator was blinded to mouse genotype at the beginning of feeding and mice were selected for experimental days using a random number generator (Random.org, Dublin, Ireland).
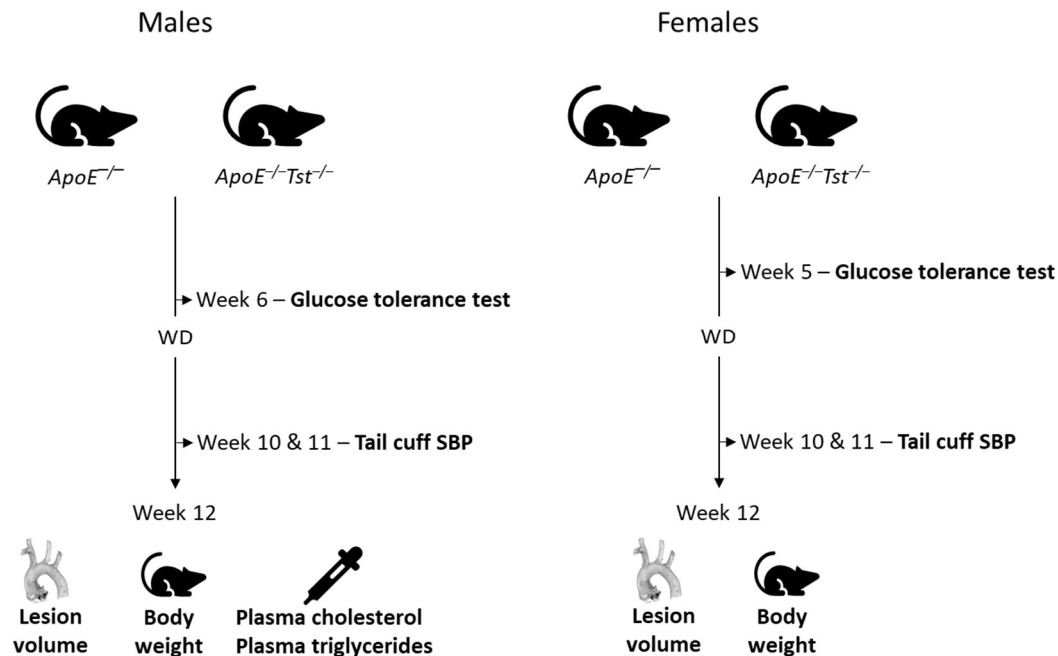
Figure 5.1 Experimental design of investigations into the effect of *Tst* gene deletion on atherosclerosis.
$ApoE^{-/-}$ or $ApoE^{-/-}Tst^{-/-}$ mice were fed for 12 weeks with 42% (kcal) fat and 0.15% (w/w) cholesterol 'western

diet' to induce lesion formation. During feeding a glucose tolerance test (section 2.2.2) was performed on mice following 5 or 6 weeks of western diet feeding for female or male mice, respectively. Systolic blood pressure was measured during weeks 10 &11 using a tail cuff measurement system (section 2.2.4). Mice were measured twice/week over 2 weeks to reduce the stress response to the procedure and the final day measurements were used for analysis. Following completion of the diet, final body weights were recorded and the aortic arch including the brachiocephalic, left common carotid and left brachiocephalic arteries was dissected following perfusion fixation (section 2.7.1). In male mice, a terminal blood sample was also collected for measurement of plasma cholesterol and triglyceride content (section 2.3.1). Lesion volume quantification in the right brachiocephalic branch was measured using optical projection tomography (OPT, section 2.7.1). Scanning and analysis of aortic arches from female mice was performed by Ms. Charlotte Hickman. Male body weight data from western diet fed mice was combined with age matched animals from a subsequent study including control diet fed mice and tested using 2-way ANOVA. All other data were tested using Student's t test. Glucose tolerance test data was analysed using General Linear Model ANOVA due to the number of relevant factors for testing (time, genotype, diet). Abbreviations: systolic blood pressure; SBP, western diet; WD.

5.3 Results

5.3.1 Confirmation of *Tst* deletion in *ApoE*$^{-/-}$*Tst*$^{-/-}$ mice liver and aorta

Genotyping of mice for *Tst* and *ApoE* was performed by Transnetyx (Cordova, US). For confirmation, a TST activity assay was performed using protein isolated from *ApoE*$^{-/-}$ and *ApoE*$^{-/-}$*Tst*$^{-/-}$ control fed mice (Figure 5.2). Equal protein concentrations were added for each tissue (50 µg). TST activity in *ApoE*$^{-/-}$ mice liver was 20x higher in liver tissue than in aorta. This was especially notable as liver samples were incubated for only 30 minutes compared with 4 hours in aorta. Despite this there was still a clear loss of activity in both tissues from *ApoE*$^{-/-}$*Tst*$^{-/-}$ mice (liver p < 0.0001, aorta p = 0.003) confirming successful breeding of the double knock-out (Figure 5.2).
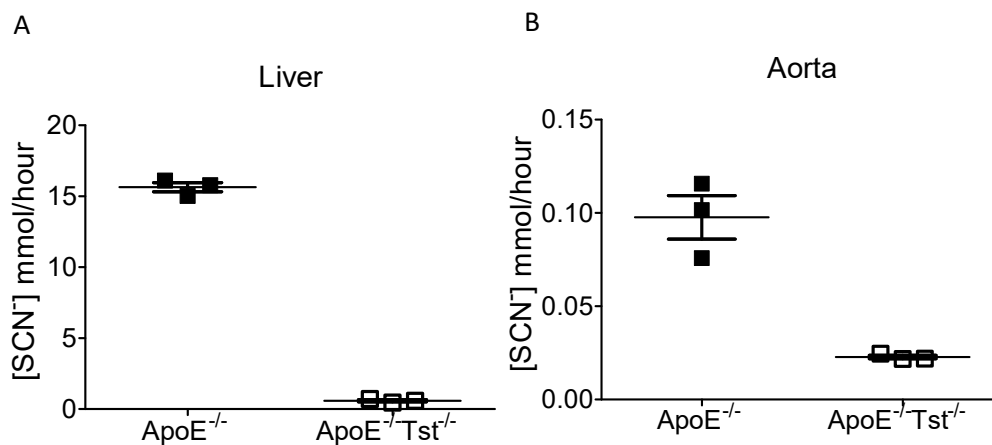
Figure 5.2 TST activity measured in liver and aortic protein samples from *ApoE*$^{-/-}$ and *ApoE*$^{-/-}$*Tst*$^{-/-}$ control fed mice. A) TST activity (measured as SCN$^-$ production from S$_2$O$_3$$^{2-}$ and KCN) in 50 µg of liver protein. Samples were incubated for 30 minutes. **B)** TST activity in 50 µg of protein isolated from aorta, note the difference in y-axis scale between graphs. Samples were incubated for 4 hours. Data are presented as Mean ± SEM. n = 3 for all groups and were compared using Student's unpaired t test. ** and *** indicate p < 0.01 and 0.001, respectively.

5.3.2 *Tst* deletion reduces final body weight in *ApoE$^{-/-}$* fed western diet

Male *ApoE$^{-/-}$* and *ApoE$^{-/-}$Tst$^{-/-}$* mice were fed control AIN93M diet or western diet for 12 weeks. Weekly body weights showed that WD feeding led to increased body weight in both genotypes. Body weights at week 12 were not taken as mice were fasted. *ApoE$^{-/-}$Tst$^{-/-}$* mice did not appear to gain as much weight and this was particularly noticeable at later weeks. Analysis of the body weights at week 11 confirmed that diet significantly increased body weight (2-way ANOVA diet p < 0.0001) but that *ApoE$^{-/-}$Tst$^{-/-}$* fed WD had lower body weight than *ApoE$^{-/-}$* controls (Bonferroni post-hoc test p < 0.05).

A cohort of Female *ApoE$^{-/-}$* and *ApoE$^{-/-}$Tst$^{-/-}$* were also fed WD for 12 weeks. As seen in male mice, WD feeding led to weight gain in female mice (Figure 5.3C). However, there was no difference in body weight between *ApoE$^{-/-}$* and *ApoE$^{-/-}$Tst$^{-/-}$* mice when this was compared at the final week (Figure 5.3D).
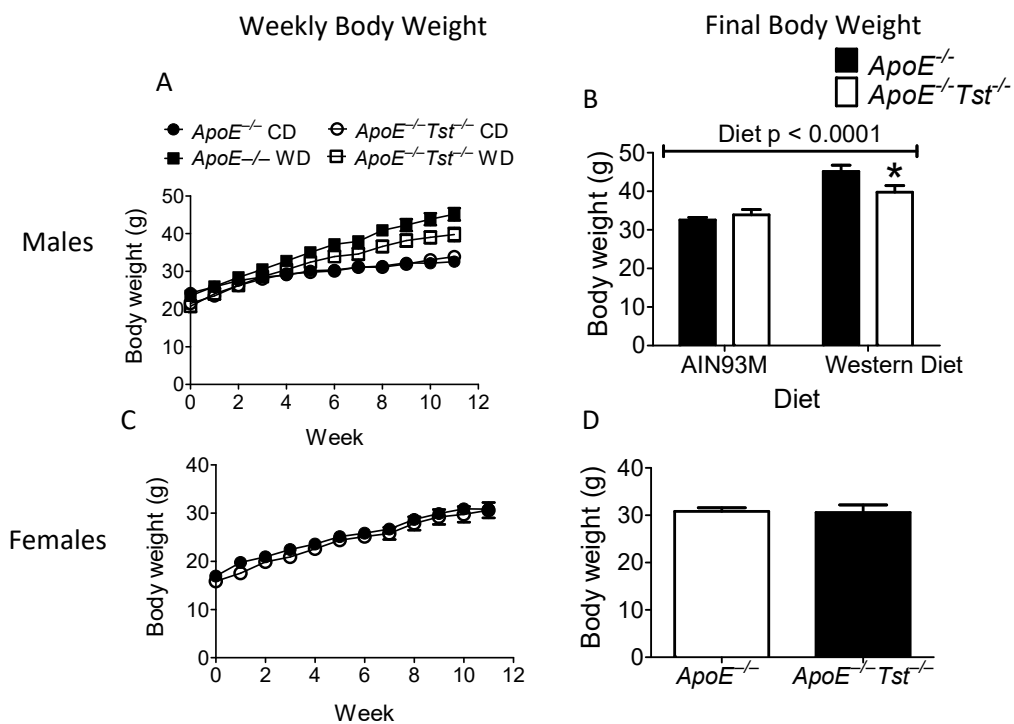
Figure 5.3 Body weight measurements in male or female *ApoE$^{-/-}$* and *ApoE$^{-/-}$Tst$^{-/-}$* mice fed AIN93M control or 'western' diet. A) Body weights were taken weekly over an 11-week period in male *ApoE$^{-/-}$* and *ApoE$^{-/-}$Tst$^{-/-}$* mice fed AIN93M or western diet. **B)** Final body weights in male mice. **C)** Body weights were taken weekly over an 11-week period in female *ApoE$^{-/-}$* and *ApoE$^{-/-}$Tst$^{-/-}$* mice fed AIN93M or western diet. Week 12 data are not shown as these measurements were taken after a fasting period. **D)** Final body weights (unaffected by fast) in female mice. Data are presented as Mean ± SEM. n = 8 (*ApoE$^{-/-}$* CD), 5 (*ApoE$^{-/-}$Tst$^{-/-}$* CD), 16 (*ApoE$^{-/-}$* WD) and 14 (*ApoE$^{-/-}$Tst$^{-/-}$* WD) for male mice and 7 (*ApoE$^{-/-}$* WD) and 11 (*ApoE$^{-/-}$Tst$^{-/-}$* WD) for female mice. Data from male mice were tested using 2-way ANOVA and Bonferroni post-hoc tests. Data

from female mice were tested using Student unpaired t test. * indicates p < 0.05 by Bonferroni test. CD; control diet, WD; western diet.

5.3.3 *Tst* deletion worsens glucose tolerance in male *ApoE*$^{-/-}$ mice fed western diet

Glucose tolerance tests were performed in female and male mice following 5 or 6 weeks of western diet feeding, respectively. In male mice, the degree of glucose intolerance was more severe than female mice (Figure 5.4B). Male *ApoE*$^{-/-}$*Tst*$^{-/-}$ mice also presented with more glucose intolerance compared with *ApoE*$^{-/-}$ controls (General Linear Model; genotype p = 0.006). No differences were observed between female *ApoE*$^{-/-}$ and *ApoE*$^{-/-}$*Tst*$^{-/-}$ genotypes (General Linear Model; genotype p = 0.28).

Blood insulin concentrations were measured over the time course of the GTT for male mice. These data (Figure 5.5) showed a clear deficit of insulin production in *ApoE*$^{-/-}$*Tst*$^{-/-}$ mice compared to *ApoE*$^{-/-}$ (General Linear Model; genotype p < 0.0001).
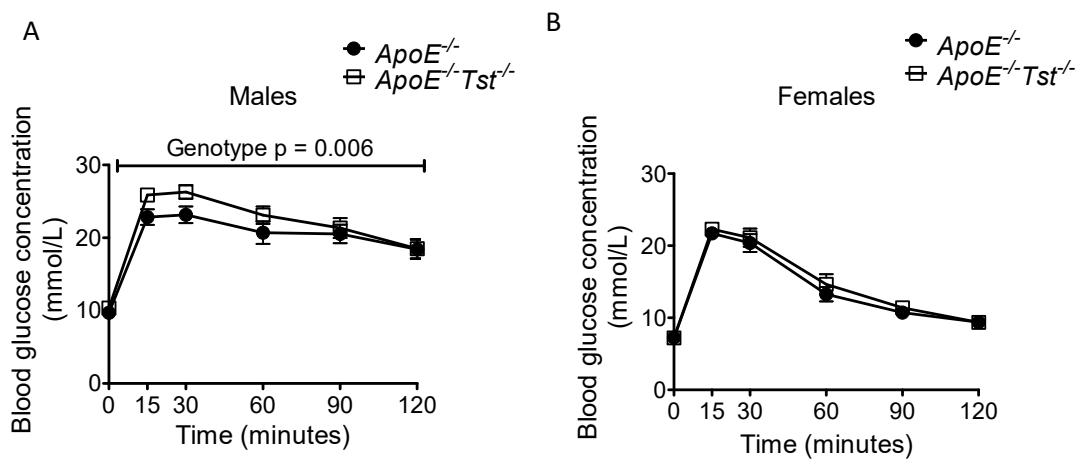
Figure 5.4 Glucose tolerance tests (GTT) in male and female *ApoE*$^{-/-}$ or *ApoE*$^{-/-}$*Tst*$^{-/-}$ mice fed western diet. A) Glucose tolerance tests on male *ApoE*$^{-/-}$ and *ApoE*$^{-/-}$*Tst*$^{-/-}$ mice fed Western diet for 6 weeks. **B)** Glucose tolerance tests on female *ApoE*$^{-/-}$ and *ApoE*$^{-/-}$*Tst*$^{-/-}$ mice fed Western diet for 5 weeks. Data are presented as Mean ± SEM. n = 9 for both Male groups. n = 7 *ApoE*$^{-/-}$/11 *ApoE*$^{-/-}$*Tst*$^{-/-}$ for Female groups. Data were tested using General Linear Model ANOVA (genotype, mouse number, time factors).
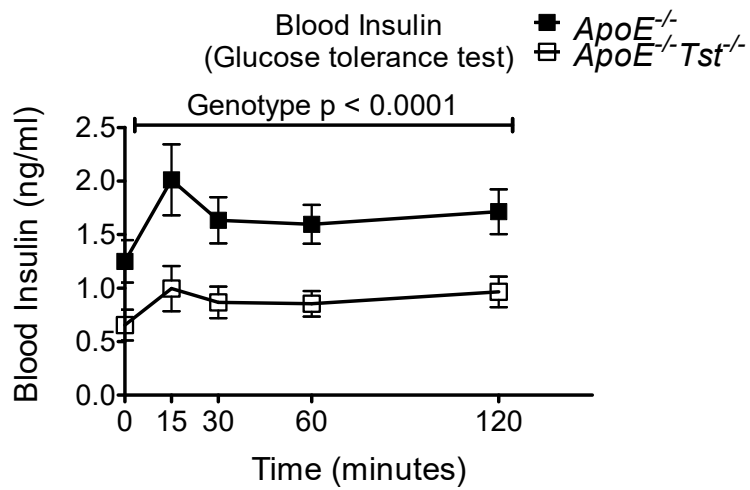
Figure 5.5 Blood insulin concentration across the glucose tolerance test in male *ApoE*^{-/-} and *ApoE*^{-/-}*Tst*^{-/-} mice fed western diet for 6 weeks. Blood insulin concentration was recorded over the time course of a glucose tolerance test in male *ApoE*^{-/-} and *ApoE*^{-/-}*Tst*^{-/-} mice fed Western diet for 6 weeks. Data are presented as Mean ± SEM. n = 9 for both groups. Data were tested using General Linear Model ANOVA (genotype, mouse number, time factors).

5.3.4 *Tst* deletion reduces lesion volume in *ApoE*^{−/−} mice fed western diet

Volumetric and mean cross sectional area measurements of atherosclerotic lesion size were assessed in male and female *ApoE*^{−/−} and *ApoE*^{−/−}*Tst*^{−/−} mice following 12 weeks of western diet feeding using OPT. CTan analysis software generated summary statistics for assessment including: volume of the vessel lumen (lumen volume); volume of the lesion (lesion volume); percentage lesion volume (lesion volume/lumen volume); mean lumen area (average 2D lumen area) and mean lesion area (mean 2D area of lesion). Additional information collected included maximal lesion area and maximal narrowing % (maximal: lesion area/region of interest). All statistics are detailed in Table 5.1.

Overall male *ApoE*^{−/−}*Tst*^{−/−} mice had significantly reduced lumen volume, lesion volume, mean lumen area, mean lesion area and maximal lesion area compared to *ApoE*^{−/−} mice. Percentage lesion volume and maximal narrowing were unchanged (Table 5.1). Lesion quantification in female mice was performed by Ms Charlotte Hickman. In these female mice, the *ApoE*^{−/−}*Tst*^{−/−} group exhibited a similar pattern in most parameters, i.e. decreased lumen and lesion volume/area compared to *ApoE*^{−/−}, although this failed to reach significance (Table 5.1). Trends towards reduced lumen and lesion volume were noted (Total VOI p = 0.098, object volume p = 0.077) as well as a trend for reduced maximal lesion area (p = 0.088, Table 5.1).

A
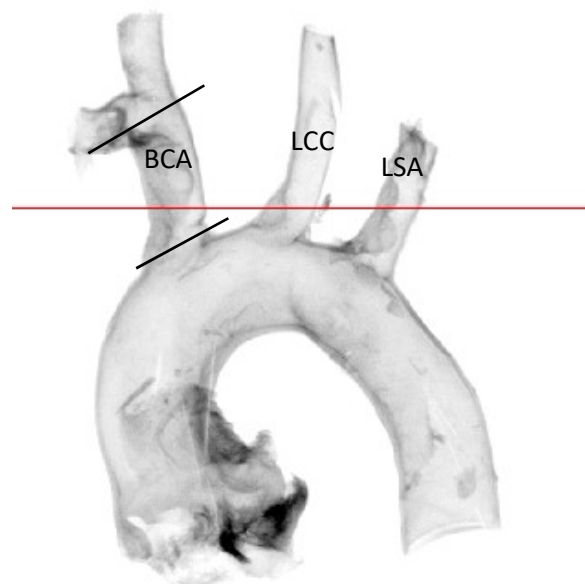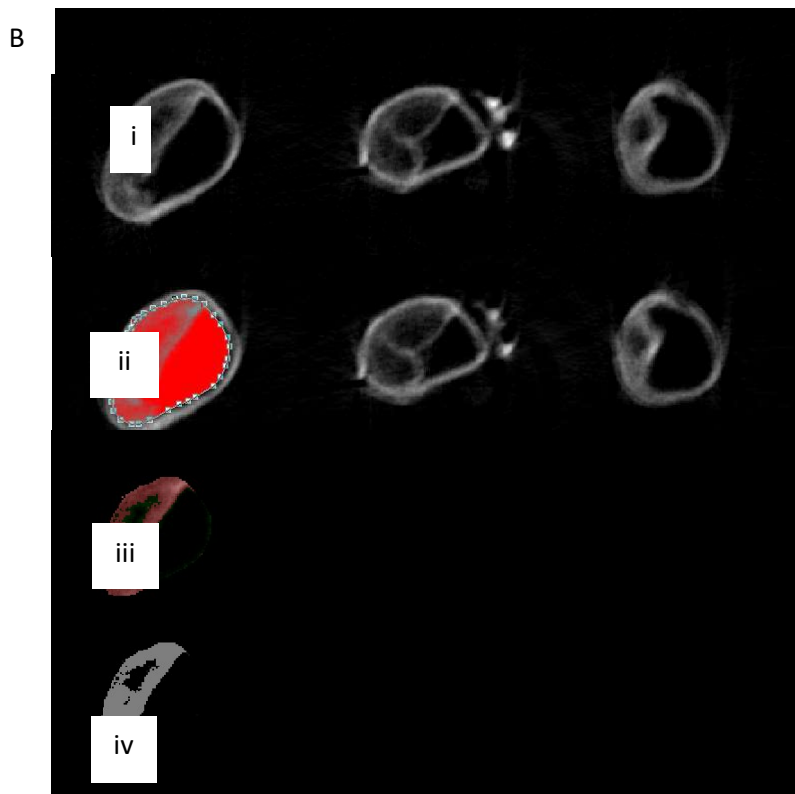
Figure 5.6 Atherosclerotic lesion volume measurement by Optical Projection Tomography (OPT). A) An example image generated during 360º scanning. Signal was recorded from the tissues auto-fluorescence in the GFP channel. The black lines indicate the volume of interest where lesion volume was measured; between the emergence of the brachiocephalic trunk from the aortic arch and the bifurcation into the right subclavian and common carotid arteries. The red line indicates the transverse slice show in image B. **B)** Examples showing the different steps of analysis for lesion quantification from transverse reconstructed slices (i). A region of interested is manually drawn around the lumen of the vessel (ii), thresholds for signal detection are adjusted (iii) and finally the program models and measures the identified object (iv). BCA; brachiocephalic artery, LCC; left common carotid artery, LSA; left subclavian artery.

Males			
Measurement	$ApoE^{-/-}$	$ApoE^{-/-}Tst^{-/-}$	P
Lumen volume (x10^6 μM^3)	260.1 ± 14.2	220.0 ± 12.1	**0.046**
Lesion volume (x10^6 μM^3)	121.6 ± 11.4	81.2 ± 15.1	**0.048**
Percentage lesion volume (%)	46.0 ± 2.6	35.9 ± 6.0	0.14
Mean lumen area (x10^3 μM^2)	218.2 ± 11.0	176.9 ± 10.4	**0.02**
Mean lesion area (x10^3 μM^2)	101.6 ± 9.2	66.5 ± 12.8	**0.04**
Maximal lesion area (x10^3 μM^2)	166.0 ± 9.2	115.8 ± 14.5	**0.01**
Maximal lumen narrowing (%)	67.3 ± 3.1	59.2 ± 6.4	0.27
Females			
Lumen volume (x10^6 μM^3)	221.4 ± 23.5	181.4 ± 10.6	0.10
Lesion volume (x10^6 μM^3)	108.1 ± 28.2	57.7 ± 11.9	0.08
Percentage lesion volume (%)	44.3 ± 10.3	30.7 ± 5.7	0.23
Mean lumen area (x10^3 μM^2)	185.3 ± 17.0	163.6 ± 10.0	0.25
Mean lesion area (x10^3 μM^2)	90.3 ± 22.4	53.6 ± 12.4	0.14
Maximal lesion area (x10^3 μM^2)	166.9 ± 40.1	98.9 ± 16.0	0.09
Maximal lumen narrowing (%)	63.1 ± 11.2	49.4 ± 5.6	0.24

Table 5.1 Atherosclerotic lesion quantification in male and female $ApoE^{-/-}$ and $ApoE^{-/-}Tst^{-/-}$ mice fed western diet for 12 weeks. Data are presented as Mean ± SEM. n = 9 for both Male groups. n = 7 $ApoE^{-/-}$/11 $ApoE^{-/-}Tst^{-/-}$ for Female groups. Data were tested using Student's unpaired t test.

5.3.5 *Tst* deletion induces a trend towards decreased systolic blood pressure in male *ApoE*$^{-/-}$ mice fed western diet

SBP was recorded in *ApoE*$^{-/-}$ and *ApoE*$^{-/-}$*Tst*$^{-/-}$ mice fed western diet for 11 weeks. No difference in genotype was noted in female mice (Figure 5.7B); however, a trend towards reduced SBP in *ApoE*$^{-/-}$*Tst*$^{-/-}$ compared to *ApoE*$^{-/-}$ mice was noted in male animals (Figure 5.7A, p = 0.09).
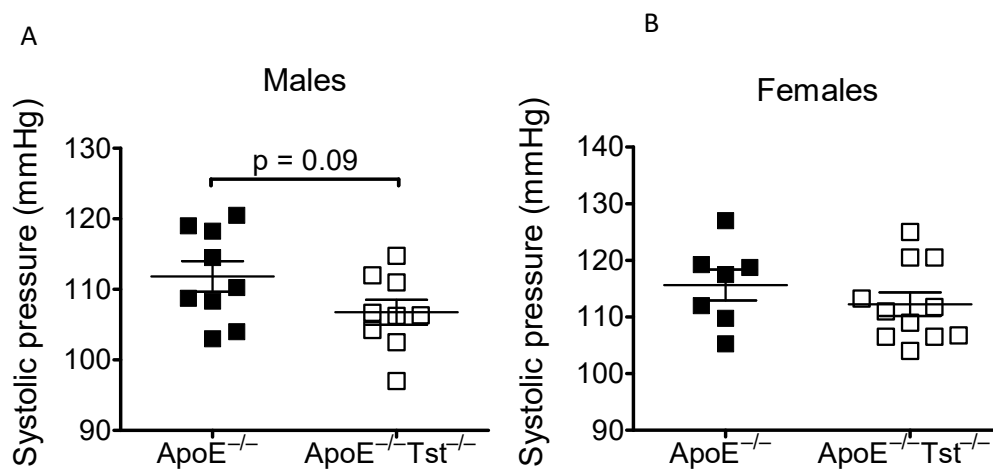
Figure 5.7 Systolic blood pressure in male and female *ApoE*$^{-/-}$ and *ApoE*$^{-/-}$*Tst*$^{-/-}$ mice fed western diet for 11 weeks. A) SBP in male *ApoE*$^{-/-}$ and *ApoE*$^{-/-}$*Tst*$^{-/-}$ mice fed western diet for 11 weeks. **B)** SBP in female *ApoE*$^{-/-}$ and *ApoE*$^{-/-}$*Tst*$^{-/-}$ mice fed western diet for 11 weeks. Data are presented as Mean ± SEM. n = 9 for both Male groups. n = 7 (*ApoE*$^{-/-}$) and 11 (*ApoE*$^{-/-}$*Tst*$^{-/-}$) for Female groups. Data were tested using Student's unpaired t test.

5.3.6 *Tst* deletion reduces plasma cholesterol content in male *ApoE*$^{-/-}$ mice

Plasma cholesterol quantification was performed by Dr Anne Muhr-Tailleux in collaboration with Prof. Bart Staels (Figure 5.8). This showed that total cholesterol was lower in *ApoE*$^{-/-}$ *Tst*$^{-/-}$ mice than in *ApoE*$^{-/-}$ controls. This was the result of a significant reduction in VLDL cholesterol content and a trend towards reduction in LDL cholesterol (Table 5.2).
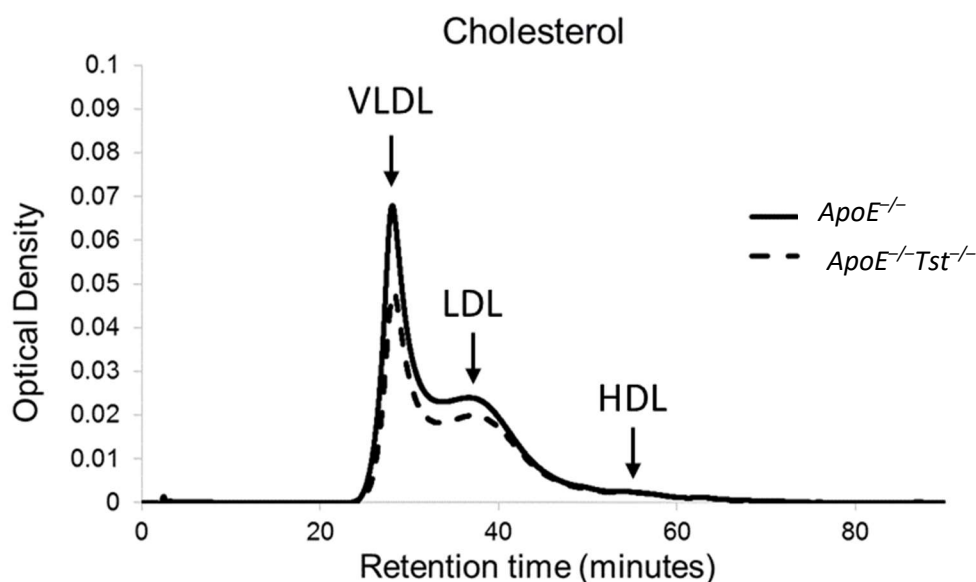
Figure 5.8 Plasma cholesterol gel filtration chromatography profile in Male *ApoE*$^{-/-}$ and *ApoE*$^{-/-}$*Tst*$^{-/-}$ mice fed western diet for 12 weeks. Cholesterol concentrations in the major lipoprotein fractions are detected by filtration of the sample through a gel column. As the sample is eluted it reacts with a cholesterol detection agent (section 2.3.1). Data are presented as Mean. n = 8 (*ApoE*$^{-/-}$), 9 (*ApoE*$^{-/-}$*Tst*$^{-/-}$). HDL; high density lipoprotein, LDL; low density lipoprotein, VLDL; very-low density lipoprotein.

Measurement (mg/dL)	*ApoE*$^{-/-}$	*ApoE*$^{-/-}$*Tst*$^{-/-}$	P
Total Cholesterol	1203 ± 85.2	983.2 ± 47.5	**0.03**
VLDL Cholesterol	540.9 ± 53.5	396.3 ± 23.8	**0.02**
LDL Cholesterol	552.2 ± 34.2	473.0 ± 28.0	0.09
HDL Cholesterol	110.1 ± 7.56	113.8 ± 6.73	0.71

Table 5.2 Plasma cholesterol quantification in male *ApoE*$^{-/-}$ and *ApoE*$^{-/-}$*Tst*$^{-/-}$ mice fed western diet for 12 weeks. Data are Mean ± SEM. n = 8 *ApoE*$^{-/-}$/9 *ApoE*$^{-/-}$*Tst*$^{-/-}$. Data were tested using Student's unpaired t test.

5.4 Discussion

This chapter tested the hypothesis that *Tst* gene deletion was protective in a model (*ApoE*$^{-/-}$ mice fed western diet) of atherosclerosis. Specifically, it was hypothesised that protection, in this case defined as a reduction in lesion volume, would occur in *ApoE*$^{-/-}$*Tst*$^{-/-}$ mice despite any metabolic dysfunction induced by *Tst* deletion (as shown in previous chapters).

The data presented broadly support this hypothesis. Male *ApoE*$^{-/-}$*Tst*$^{-/-}$ mice demonstrated a reduction in various parameters used to assess lesion size compared to *ApoE*$^{-/-}$ mice. This reduction occurred despite worsened glucose tolerance in *ApoE*$^{-/-}$*Tst*$^{-/-}$ mice; a known risk factor for atherosclerosis, and a finding consistent with previous investigations in *Tst*$^{-/-}$ mice (204).

Most likely due to a lack of statistical power only a trend towards reduced lesion volume was also observed in female *ApoE*$^{-/-}$*Tst*$^{-/-}$ mice. No difference in glucose tolerance was noted in female mice. The lack of a metabolic phenotype in both *ApoE*$^{-/-}$ and *ApoE*$^{-/-}$*Tst*$^{-/-}$ female mice is not surprising as it is known that female mice are resistant to a number of cardiovascular and metabolic diseases due to the protective actions of oestrogen (238,277). However, the finding that *Tst* deletion does not induce metabolic dysfunction in female mice is novel.

Potential mechanisms were identified that may explain the reduction in lesion volume in male mice. Most prominently *ApoE*$^{-/-}$*Tst*$^{-/-}$ mice had reduced plasma cholesterol compared to *ApoE*$^{-/-}$ mice. A trend towards reduced systemic blood pressure in *ApoE*$^{-/-}$*Tst*$^{-/-}$ mice was also noted.

5.4.1 *Tst* deletion reduces body weight in male *ApoE*$^{-/-}$ mice

As expected, and previously shown, WD feeding induced substantial weight gain above that of the low-fat control diet (278,279) (in this case AIN93M). *ApoE*$^{-/-}$*Tst*$^{-/-}$ mice had reduced body weight following 12 weeks of WD feeding but not when fed the AIN93M control diet. The cause of lower body weight in *ApoE*$^{-/-}$*Tst*$^{-/-}$ mice is not clear from this study although interestingly data from chapter 3 also identified lower body weight in *Tst*$^{-/-}$ mice fed chow diet. Whether a common mechanism could be found to explain these findings is a topic for future investigation.

Consistent with the normal parameters of the background strain (JAX C57BL/6 strain body weight information) female mice were found to have lower body weights than male mice even when fed WD. No difference in body weight was noticed in female mice between *ApoE*$^{-/-}$ and *ApoE*$^{-/-}$*Tst*$^{-/-}$. The findings of a lower body weight in female than male mice was

expected as less weight gain on high fat diet has been observed and is attributed to the actions of oestrogen through the oestrogen receptor α promoting the use of lipids as an energy source and decreasing storage (238,277). The lack of body weight gain in female mice fed WD means that it is difficult to detect whether $ApoE^{-/-}Tst^{-/-}$ mice fed WD have lower body weight than $ApoE^{-/-}$ as was found in male mice.

5.4.2 Tst deletion worsens glucose tolerance and decreases insulin concentrations in male $ApoE^{-/-}$ mice

In male mice both $ApoE^{-/-}$ and $ApoE^{-/-}Tst^{-/-}$ genotypes exhibited substantial glucose intolerance at week 6 of western diet feeding. No control diet mice were tested for glucose tolerance within this study however, by comparing the glucose tolerance in WD fed mice to control diet fed mice from other studies or those tested in chapter 3 it is clear that 6-week WD fed male mice have severe glucose intolerance. Whether the glucose intolerance is a result of western diet feeding or just $ApoE$ deletion cannot be assessed in this study. However, previous studies have shown that $ApoE^{-/-}$ mice fed a control diet of similar total fat content (11% kcal compared to 9.4% in this study) for 12 weeks exhibit normal glucose tolerance (280). Therefore, it is likely that the poor glucose tolerance seen in both genotypes is a result of western diet feeding which has been shown to cause glucose intolerance in $ApoE^{-/-}$ and C57BL/6 mice (281,282). Female mice did not develop glucose intolerance when fed WD. This is not surprising as it is well known that oestrogen has a protective effect on glucose intolerance by increasing insulin sensitivity (283). For example it has previously been shown that female C57BL/6 mice fed 60% kcal fat HFD for 14 or 20 weeks are protected from glucose intolerance compared to male C57BL/6 mice (238,284).

Tst deletion in male $ApoE^{-/-}$ mice led to a worsening of glucose tolerance. This effect is consistent with the previously published findings on C57BL/6N and $Tst^{-/-}$ mice fed 'Surwit' HFD for 6 weeks (204) and also with the evidence from chapter 3 that Tst deletion led to a worsening of glucose tolerance. Previously a difference in the genetic background at the NNT gene of the mice was suggested as a possible explanation for the difference in glucose tolerance of $Tst^{-/-}$ mice. C57BL/6N and 6J mice differ at the NNT gene and this has been found to worsen glucose tolerance in C57BL/6J mice (211,231,232). This was unlikely as mice were of a mixed N/J background, but it could not be ruled out as a cause of the altered glucose tolerance. In this study however, mice were bred, using a speed congenics backcrossing technique, to the C57Bl/6J background of $ApoE^{-/-}$ mice. During this backcrossing SNP genotyping at key 6N/J differences was performed to select the best animals for further breeding until animals were found to be of C57BL/6J background at all

SNPs. Therefore, it is now extremely unlikely that $ApoE^{-/-}$ and $ApoE^{-/-}Tst^{-/-}$ could differ at the NNT gene. Instead the worsened glucose tolerance in $ApoE^{-/-}Tst^{-/-}$ mice must be the result of Tst deletion.

Glucose tolerance in female mice fed WD was unchanged by Tst deletion and both genotypes exhibited comparable glucose tolerance results to those observed in control diet fed mice in chapter 3. Similar to the lack of phenotype observed in body weight in female mice, it is possible that the protection of female mice from metabolic disease through the actions of oestrogen (238) means that a difference between $ApoE^{-/-}$ and $ApoE^{-/-}Tst^{-/-}$ cannot be tested.

The most likely explanation for glucose intolerance in male mice is the reduction in insulin found over the time course of the glucose tolerance test. This was also observed in 20-week 'Surwit' HFD fed $Tst^{-/-}$ mice. A failure of the pancreas to meet the insulin requirements of insulin resistant patients or mice has been suggested as a formative feature of type II diabetes (33,35,77). As insulin is solely produced and secreted by the β-cells within the pancreatic islets (31) the mechanism by which Tst deletion affects blood insulin concentrations is likely to lie in this tissue. A potential mechanism for this reduction could be increased H_2S signalling with the pancreatic cells.

Pullen *et al.* have previously shown that transcription of Tst is supressed within the pancreas (235) which rules out a direct action of the enzyme within the β-cells of the pancreas. However, high circulating H_2S levels, which have been reported in a separate cohort of $Tst^{-/-}$ mice (204), could potentially still act upon channels within the pancreatic β-cell to decrease insulin release. *In vitro* evidence from using an insulin expressing cell line has demonstrated that exogenously applied H_2S led to a decrease in insulin release through a K_{ATP} channel dependent mechanism (179). H_2S has previously been shown to result in persulfide modification of K_{ATP} channels, leading to an increase in function and hyperpolarisation of vascular smooth muscle (181) and insulin expressing cell lines (179). Hyperpolarisation of pancreatic β cells would lead to prevention of the action potentials associated with insulin release (32). Consistent with this hypothesis L-cysteine, which serves as a substrate for H_2S generation, inhibited insulin release from isolated pancreatic islets (172). In addition to this mechanism, it has also been shown that exogenous H_2S can reduce insulin secretion through inhibition of L-type Ca^{2+} channels in pancreatic β-cells (178). Increased H_2S signalling within pancreatic β-cells may explain the insulin reduction observed in male $Tst^{-/-}$ HFD fed and $ApoE^{-/-}Tst^{-/-}$ western diet-fed mice and the worsening of glucose tolerance in both

models. Therefore, electrophysiology studies should be used to investigate the functioning of pancreatic β-cells with *Tst* deletion.

5.4.3 *Tst* deletion reduces atherosclerotic lesion formation in *ApoE*$^{-/-}$ mice

The main aim of this study was to investigate whether *Tst* deletion was protective against atherosclerotic lesion formation. It was found that *Tst* deletion in male mice reduced both final lesion and vessel lumen volumes following 12 weeks of western diet feeding. The smaller lesion volume clearly demonstrates the protective effect of *Tst* deletion against atherosclerotic lesion formation in *ApoE*$^{-/-}$ mice. Both volume and mean area of lesion were smaller by approximately 33%. The magnitude of this effect is similar to that found in other *ApoE*$^{-/-}$ double knockout studies (such as *ApoE*$^{-/-}$ interleukin 18, 11β-HSD1, and PPARα double knockouts) investigating protective actions in *ApoE*$^{-/-}$ mice fed western diet (281,285–287).

In female mice, a trend towards smaller lesion volumes was also observed although this failed to reach significance. The most likely explanation for this is a lack of statistical power to detect the reduction due to the low biological group size and high variation of the *ApoE*$^{-/-}$ group. Power calculations (DSS Research, Statistical Power Calculator, Average, 2-sample) showed that the current data have only 42.6% power to detect a difference in lesion volume. Using the power calculator along with the standard deviation figures for the data shows that increasing the number of animals to 15 for each group would increase the statistical power to detect a difference in lesion volume to 80%.

Male *ApoE*$^{-/-}$*Tst*$^{-/-}$ mice also had smaller lumen volumes than *ApoE*$^{-/-}$ controls. This finding is likely to be influenced by expansive vascular remodelling during atherosclerotic lesion development. Expansive remodelling or 'compensatory enlargement' has been demonstrated to occur in the aorta of *ApoE*$^{-/-}$ mice (189,288–291). As lesion volume increases, there is a compensatory increase in vessel volume either due to unavoidable changes in the pressure and flow of vessels or as a compensatory mechanism to attempt to reduce the burden of the lesion on the vessel. Therefore, the fact that total vessel volume was reduced in *ApoE*$^{-/-}$*Tst*$^{-/-}$ mice may also be explained by the protective phenotype in these mice resulting in smaller lesions and less need for vessel expansion. Again, the same trend was observed in female mice although the lack of statistical power prevents this from being detected. To examine this further it would be useful to measure vessel volume in control fed *ApoE*$^{-/-}$ and *ApoE*$^{-/-}$ *Tst*$^{-/-}$ to confirm that it is development of atherosclerotic lesions which leads to vessel expansion and not a feature of *Tst* deletion generally. The adaptation of the vessel and

expansion during lesion formation also potentially explains why the calculated 'percentage measurements' (percentage lesion volume, maximal narrowing) are not significant.

Although OPT analysis has allowed detailed examination of lesion size in 3D it cannot accurately define the cause of smaller lesion size in $ApoE^{-/-}Tst^{-/-}$ mice. To further investigate the atherosclerotic lesions in $ApoE^{-/-}Tst^{-/-}$ mice 2D histology would allow for staining and quantification of lesion components (292). This could be used to assess if there is a specific action to reduce one constituent of atherosclerotic lesions or a general reduction in all constituents (292). Therefore, 2D histological staining of lesions from $ApoE^{-/-}$ and $ApoE^{-/-}Tst^{-/-}$ mice to quantify lipid, collagen, immune cell and α smooth muscle actin (αSMA) content of lesions will be a vital component of future investigations to further understand the mechanism responsible for the reduction in lesion volume demonstrated here.

5.4.4 Potential mechanisms of reduced lesion volume in $ApoE^{-/-}$ mice with Tst deletion

5.4.4.1 Tst deletion reduces systolic blood pressure

SBP was measured in this study using a tail cuff method. Data from male mice showed a trend towards reduced SBP in mice with Tst deletion. Increased blood pressure has been repeatedly linked to increased risk of atherosclerosis and to development of lesions in both humans and mice (293). The cause for this is hypothesised to be linked to increased vascular shear stress, increased oxidative stress in the vascular wall and endothelial cell damage (128,294); processes which are linked to the initiation of atherosclerosis. Although the trend for reduction in blood pressure demonstrated in this chapter appears numerically small at 5 mmHg, even slight reductions in SBP have been linked to improved cardiovascular health (295) and reduced atherosclerotic lesion formation in $ApoE^{-/-}$ mice (293,296,297). Therefore, if this trend towards lower SBP is confirmed this finding could provide an explanation for reduced lesion development in $ApoE^{-/-}Tst^{-/-}$ mice.

Although circulating H_2S concentrations were not measured in this work a reduction in SBP is consistent with the previous finding by Morton *et al.* that circulating H_2S concentrations are increased in $Tst^{-/-}$ mice (204). H_2S is a known physiological vasodilator and H_2S administration in vivo has been demonstrated to reduce SBP in wild type and $Cse^{-/-}$ mice (253). In $Cse^{-/-}$ mice, which exhibit low H_2S concentrations, an increase of approximately 20 mmHg SBP has been demonstrated in several studies (181,187,253), again suggesting that global knockout of enzymes which regulate H_2S signalling can alter blood pressure.

It should be noted that the reduction in SBP in $ApoE^{-/-}Tst^{-/-}$ mice was only observed in males. Female $ApoE^{-/-}Tst^{-/-}$ mice appeared to have identical SBP to $ApoE^{-/-}$ controls. Because lesion volume was also reduced in female mice this argues that a reduction in blood pressure is not be linked to the protective phenotype. However, as SBP is a known risk factor for atherosclerosis it is certainly worth further investigation in males. This should be performed using the more accurate arterial cannulation telemetry method to confirm the reduction and assess blood pressure in mice under unstressed conditions, and to observe any potential circadian alterations in the normal SBP rhythm. Further to this the contribution of any reduction in SBP to the reduced lesion volume in $ApoE^{-/-}Tst^{-/-}$ mice could be examined by using antihypertensive agents, such as hydralazine, to reduce the SBP of $ApoE^{-/-}$ mice to levels of $ApoE^{-/-}Tst^{-/-}$ mice. If the reduction in lesion volume was attenuated in this type of investigation it would provide evidence that the reduction in SBP is a causal factor of the protective phenotype in $ApoE^{-/-}Tst^{-/-}$ mice.

5.4.4.2 Tst deletion reduces plasma cholesterol content

In this study $ApoE^{-/-}Tst^{-/-}$ mice demonstrated a clear reduction in total and VLDL plasma cholesterol concentrations. There was also a trend towards reduction in the LDL fraction but no change in HDL content. Increased plasma cholesterol content in the VLDL and LDL fractions is a well-known risk factor for atherosclerosis (45,272). Human population studies have shown that reducing LDL cholesterol, using pharmacological compounds such as statins which inhibit cholesterol production, is one of the few therapeutic options for reducing rates of cardiovascular disease (142). Lowering plasma cholesterol using statins or inhibitors of cholesterol absorption from the gastrointestinal tract (e.g. ezetimibe) has also been shown to reduce atherosclerotic lesion size in the $ApoE^{-/-}$ mouse model of atherosclerosis (125,298).

The mechanism by which *Tst* deletion reduces circulating cholesterol levels is unknown but the reduction is consistent with the hypothesised effects of H_2S on cholesterol production (171). Wang *et al*. showed that total and LDL cholesterol content were increased in $Cse^{-/-}$ mice fed western diet for 12 weeks compared to C57Bl/6 controls (187). Studies in rat adipose and liver tissues have also shown that the administration of certain statins, such as atorvastatin, leads to an increase in H_2S concentrations and inhibition of H_2S breakdown (299,300). These studies suggest that increases in H_2S signalling within these tissues may be partly responsible for the effectiveness of statins in normalising blood cholesterol concentrations and decreasing atherosclerosis risk. In addition to these studies, more recent evidence has demonstrated that atorvastatin can also increase *Cse* mRNA expression in a

macrophage cell line leading to increased H_2S production (301). Although H_2S concentrations were not measured directly in this work Morton et al. have shown that H_2S concentrations are increased in whole blood samples of $Tst^{-/-}$ mice.

Cholesterol content was not measured in female mice, so it cannot be concluded whether, as in male mice, they exhibit a reduction in total and VLDL cholesterol which could explain the reduction in lesion volume. Therefore, examining cholesterol concentrations in female mice would be a useful future experiment to provide further evidence of whether the reduction in circulating cholesterol is an important mechanism or not. Further to this, the importance of cholesterol could be assessed by reducing the total and VLDL cholesterol concentrations of $ApoE^{-/-}$ mice to $ApoE^{-/-}Tst^{-/-}$ levels using a pharmacological agent such as ezetimibe to lower absorption of cholesterol. Ezetimibe treatment of $ApoE^{-/-}$ mice has previously been performed and resulted in reduced lesion development compared to control $ApoE^{-/-}$ mice (298). Similar to manipulation of SBP, this type of study should be able to demonstrate whether the reduction in cholesterol in $ApoE^{-/-}Tst^{-/-}$ is a causal mechanism for the reduction in lesion volume.

5.4.5 Conclusions

This study has confirmed the overall hypothesis that Tst deletion is protective in a model of atherosclerosis despite worsened metabolic function. Interestingly it has also suggested several mechanisms by which Tst deletion may lead to this protection, including: reduced SBP, reduced plasma cholesterol and potential improvement of vascular endothelial function. A common mechanism which has emerged from both this and previous chapters is increased H_2S signalling within tissues. This is consistent with the hypothesised role of TST in breaking down H_2S and therefore should be pursued in mechanistic investigations to explain the phenotypes observed.

6.0 Discussion

This project aimed to investigate the metabolic and vascular consequences of *Tst* gene deletion in mice. Previous work had demonstrated that when fed HFD for 6 weeks *Tst*$^{-/-}$ mice developed more severe glucose intolerance than C57BL/6N controls (204). Given the high level of *Tst* expression in the liver (208), it was hypothesised that this organ played a key role in mediating the metabolic effects of TST. Thus, the liver was a logical target for investigation regarding metabolic phenotypes. A number of phenotypes associated with altered glucose metabolism were identified, including increased activity of the gluconeogenic enzyme PEPCK, consistent with the previous work showing impaired glucose tolerance (204), and a decrease in insulin concentrations, which remain unexplained. At the cellular level, hepatocytes from *Tst*$^{-/-}$ mice exhibited increased mitochondrial respiration. Finally, studies of lipid metabolism showed increased triglyceride secretion from the livers of control diet-fed *Tst*$^{-/-}$ mice, a finding which is consistent with "diabetic-like" liver function.

Investigations into vascular function were stimulated by initial data showing that *Tst* deletion led to increased H$_2$S (or sulfides/sulfide species) detected in whole blood (204). H$_2$S is a known vasodilator (181,253) and increased H$_2$S concentrations are linked to protection from atherosclerosis in an *ApoE*$^{-/-}$ model (187). Therefore, in this study, vascular function was investigated in aortae from C57BL/6 and *Tst*$^{-/-}$ mice, either under control diet-fed 'baseline' conditions or when mice were fed a high fat diet (HFD) to induce vascular dysfunction, as has previously been performed by others (302,303). Unfortunately, in this work HFD failed to induce overt endothelial dysfunction in this study. However, there were clear indications of altered vasodilator function of *Tst*$^{-/-}$ aorta and a protective phenotype resulting from *Tst* gene deficiency in conditions of HFD feeding.

Finally, atherogenesis was investigated through the generation of a unique atherosclerosis-susceptible *ApoE*$^{-/-}$*Tst*$^{-/-}$ double knockout mouse. As hypothesised, *Tst* deletion on an *ApoE*$^{-/-}$ background led to a reduction in atherosclerotic lesion development, despite impaired glucose intolerance in the mice. Several potential mechanisms to explain this effect were identified, including a reduction of plasma cholesterol and trend for reduced SBP.

Overall this project has confirmed the central hypothesis that *Tst* deletion engenders vascular protection despite worsening of metabolic function. It has also satisfied the primary aims of investigating the phenotypes associated with *Tst* deletion and has identified several avenues

for future investigation which will aim to study in detail the mechanistic changes responsible for the phenotypes described.

6.1 *Tst* deletion and metabolic dysfunction

6.1.1 Glucose metabolism

Glucose metabolism appears to be the key metabolic process affected by *Tst* deletion. In this work it was shown that, consistent with the previous results at 6 weeks (204), $Tst^{-/-}$ mice exhibited worsened glucose tolerance when fed HFD for 20 weeks compared to C57BL/6 control mice (section 3.3.2). Investigations into the molecular basis of increased gluconeogenesis (higher glucose production in response to pyruvate challenge) observed in $Tst^{-/-}$ mice found that the activity of PEPCK, the key regulatory enzyme of gluconeogenesis (175), was increased in $Tst^{-/-}$ mice fed control or HFD for 6 weeks (section 3.3.4). Further, a worsening of glucose tolerance was also observed in $ApoE^{-/-}Tst^{-/-}$ mice compared to $ApoE^{-/-}$ controls fed 6 weeks of western diet (section 5.3.3). The findings in $ApoE^{-/-}Tst^{-/-}$ mice lend support to the idea that the alterations in glucose metabolism in $Tst^{-/-}$ mice represent a true biological effect and are not specific to only one model. Glucose intolerance and increased gluconeogenesis are two common features of type II diabetes (77). Therefore, these data suggest that deletion or inhibition of *Tst*/TST may be associated with the development of diabetes. This is especially interesting as $Tst^{-/-}$ mice in these studies had either no difference in gross body weight or under certain conditions (chow for 6 weeks or when fed western diet) were significantly lighter. The latter is a new observation that could be related to the isogeneity of the background genetic strain achieved in these more recent studies compared to the mixed 6N/6J background used in the original body mass studies (204). Therefore, it appears that the effect of *Tst* on glucose metabolism is not related to a worsening of obesity and, instead, may help to delineate actions of specific organs, particularly the liver, which contribute to diabetes.

The full causal relationship for the diabetogenic phenotype observed in $Tst^{-/-}$ mice cannot be concluded from this work, but the data generated suggest that insulin production or secretion may also be involved. Blood insulin concentrations were measured over the time course of the glucose tolerance tests performed in 20-week chow or HFD fed C57BL/6 and $Tst^{-/-}$ mice (section 3.3.3) and 6-week western diet fed $ApoE^{-/-}$ and $ApoE^{-/-}Tst^{-/-}$ mice (section 5.3.3). In both experiments (during which mice with *Tst* deletion exhibited worsened glucose tolerance) blood insulin concentrations were reduced in mice with *Tst* deletion. As insulin concentration is not increasing to levels seen in the control mice despite the worsening of glucose tolerance this implies that the insulin concentrations may be insufficient and that the

production or release of insulin by the pancreatic β-cells may be defective. It has been suggested by previous work that H$_2$S signalling within pancreatic β-cells could inhibit their normal depolarisation in response to increasing glucose which results in insulin secretion (32,172,178,179). However, to the author's knowledge this has not been tested in mouse models of decreased or increased H$_2$S concentrations.

Investigations of mitochondrial respiration in hepatocytes from $Tst^{-/-}$ mice were proposed based on the hypothesis that the impaired glucose tolerance and inferred insulin resistance may be associated with decreased respiration, as observed in the muscle of insulin resistant humans (216,217). In fact, it was found that mitochondrial respiration was increased in $Tst^{-/-}$ hepatocytes (section 3.3.6). The cause of this increase is unknown; however, it is intriguing that both glucose and lipid data suggest that synthetic pathways may be increased in $Tst^{-/-}$ hepatocytes. As these pathways are highly energy demanding this may be a compensatory increase (85). Further to this, an increase in mitochondrial respiration has been frequently associated with increased H$_2$S concentrations in mitochondria (219,221,260) despite the known toxic inhibitory effects of H$_2$S at very high concentrations (170). Therefore, the increase in mitochondrial respiration seen in $Tst^{-/-}$ hepatocytes could also be the result of exposure to increased H$_2$S *in vivo*.

Overall this work has augmented the previous work by Morton *et al.*, confirming the effects of Tst deletion on glucose metabolism without effects on weight gain (204). However, a key difference between this work and that of Morton *et al.* is the finding of decreased blood insulin concentrations in $Tst^{-/-}$ mice. Contrary to this Morton *et al.* found that insulin concentrations measured over the time course of a glucose tolerance test was identical between HFD fed C57BL/6N and $Tst^{-/-}$ mice. This difference may again be associated with genetic differences in the substrain background of mice. Within this work however, decreased insulin release could explain several phenotypes identified including increased gluconeogenesis and worsened glucose tolerance and therefore it is an essential topic for further investigation. Further to these findings the data are also strikingly consistent with the proposed effects of increased H$_2$S on glucose metabolism, insulin release, and mitochondrial respiration. Therefore, they also lend weight to the suggestion that increased H$_2$S in $Tst^{-/-}$ mice is a major cause of the observed phenotypes.

6.1.2 Lipid metabolism

The effect of Tst deletion on lipid metabolism in the liver had not been previously investigated but it was hypothesised that triglyceride content would be increased and cholesterol content decreased due to increased H$_2$S concentrations in $Tst^{-/-}$ mice. Previous

work linked increased H_2S signalling to increased VLDL triglyceride secretion (171), decreased cholesterol secretion (187), and protection from hepatic steatosis (accumulation of lipids within hepatocytes) (251). Although H_2S was not measured directly in this work based on previous work by Morton *et al.* $Tst^{-/-}$ mice are presumed to have increased circulating H_2S. In $Tst^{-/-}$ mice fed with chow diet for 6 weeks, an increase in plasma VLDL triglyceride content was observed compared to C57BL/6 mice (section 3.3.7), consistent with the hypothesised effect of increased H_2S (171,187) in these mice. However, this increase in VLDL triglycerides was not found under any other conditions including in 20-week control diet-fed mice. The cause of this discrepancy is unknown. One possible explanation may be that triglyceride concentrations are reduced in older mice resulting in a loss of this phenotype. Comparison of triglyceride concentrations between 6 and 20-week chow fed mice does suggest that plasma triglyceride concentrations were generally reduced in older 20-week chow fed mice. A reduction in plasma triglyceride has also previously been shown to occur in a study of the metabolic effects of aging in mice (225).

Plasma cholesterol content was unchanged in $Tst^{-/-}$ mice fed either chow or HFD (section 3.3.7). However, in $ApoE^{-/-}Tst^{-/-}$ mice fed western diet total and VLDL cholesterol concentrations were significantly lower than in $ApoE^{-/-}$ controls (section 5.3.6). The lack of effect in mice without $ApoE$ deletion may be explained by the differences in plasma lipid profiles between $ApoE^{-/-}$ and C57BL/6 mice. While C57BL/6 mice carry cholesterol almost exclusively in the HDL lipoprotein fraction the deletion of $ApoE$ disturbs normal homeostasis and instead shifts cholesterol predominantly into the VLDL and LDL fractions (125). This difference may mean that Tst deletion exerts a greater effect on cholesterol content in $ApoE^{-/-}$ mice as VLDL, and to an extent LDL, content and secretion is determined by liver-mediated processes where Tst is highly expressed (48,117,208). It is also worth noting that the initial suggestion that H_2S could reduce circulating cholesterol content was implied from the finding that $Cse^{-/-}$ mice, which have lower H_2S concentrations, exhibited increased circulating cholesterol (187). However, this was only found in mice fed an 'atherogenic' (i.e. high cholesterol) diet which also raised VLDL and LDL cholesterol concentrations in control mice. Therefore, it may be that H_2S can influence circulating cholesterol concentrations (but only in conditions where VLDL and LDL cholesterol content is increased initially. This would explain the lack of effect of Tst deletion in $ApoE^{+/+}$ models.

No effect of Tst gene deletion was found on hepatic accumulation of triglyceride (steatosis) when mice were fed control or HFD (section 3.3.8). This finding is seemingly at odds with the notion that $Tst^{-/-}$ mice have elevated circulating H_2S concentrations as H_2S has been

148

suggested to inhibit hepatic steatosis and maintain healthy lipid metabolism by the liver (171,186,251). However, it should be noted that the evidence for protection from steatosis of the liver is again proposed from results in $Cse^{-/-}$ and $Cbs^{-/-}$ mice (models of low H_2S concentrations where triglyceride accumulation in the liver was found to be enhanced (171,186,254)) and is, therefore, indirect. There is no direct evidence that increased H_2S can prevent hepatic steatosis in mice fed HFD. $Cse^{-/-}$ and $Cbs^{-/-}$ mice exhibit increased levels of homocysteine due to inhibition of the trans-sulfuration pathway (171,254). Homocysteine is linked to the development of hepatic steatosis (188) and, although they challenge the notion that increased homocysteine can cause hepatic steatosis alone, the authors of this paper also do not provide evidence that it is not the cause of steatosis in their mice. Therefore, the lack of effect of Tst deletion on hepatic steatosis does not necessarily provide a strong argument against increased H_2S levels in $Tst^{-/-}$ mice.

Overall investigations into lipid metabolism have shown that the effects of Tst deletion are less dramatic when compared to the effects of this deletion on glucose metabolism and may depend on the nature of the model being investigated. However, the fact that the changes in lipid were exclusively observed in the VLDL lipoprotein fraction is consistent with TST having key metabolic roles in the liver. Both findings may also be linked to increased H_2S in the liver based on the available information from the literature. This would lend weight to the hypothesis that altered H_2S signalling is a primary mechanism for the effects of Tst deletion.

6.2 *Tst* deletion and vascular function

H_2S is a known vasodilator via its action as an endothelium-derived hyperpolarising factor (EDHF) (181,253,258) and is also hypothesised to interact with, and enhance, NO signalling (167,304). As increased whole blood H_2S levels have previously been found in mice with Tst deletion (204), it was hypothesised that vasodilation would be increased in mice with Tst deletion. Interestingly no changes were noted in vascular relaxation or contraction of aortae from $Tst^{-/-}$ mice fed control or HFD (section 4.3.3&4). The lack of effect of Tst deletion on normal vascular function is surprising and was unexpected given the inhibition of vasorelaxation previously observed in $Cse^{-/-}$ mice (253). As this study focussed only on aortic function it is possible that further investigations of vascular function in other vessels which have a greater EDHF component (such as mesenteric arteries) (258,305) may be able to reveal an influence of Tst deletion on vascular function.

Another hypothesised action of increased H_2S signalling at vascular endothelial cells is the protection of vessels in conditions of vascular stress, such as hyperglycaemia (260) from

endothelial dysfunction (259). This work aimed to investigate this process in $Tst^{-/-}$ mice by inducing endothelial dysfunction through HFD feeding in C57BL/6 and $Tst^{-/-}$ mice (section 4.3.3). Unfortunately, HFD feeding failed to cause overt endothelial dysfunction (defined as a reduction in ACh-mediated relaxation (114,306)) so this could not be tested. However, HFD feeding in C57BL/6 for 20 weeks did reduce the ability of L-NAME and indomethacin to increase maximal contraction in response to PhE or 5-HT (section 4.3.4). L-NAME and indomethacin inhibit endothelial cell production of NO and prostaglandins, respectively, and, therefore, the impact of HFD on the effectiveness of these compounds reflects a reduction in endothelial production of NO and/or prostaglandins. Interestingly $Tst^{-/-}$ mice did not exhibit the same reduction when fed HFD and maintained maximal contractions similar to those seen in control diet-fed mice, suggesting a protective role for Tst.

Within this work it has not been possible to test the effect of Tst deletion in conditions of overt endothelial dysfunction because HFD did not affect endothelial mediated relaxation in either genotype. However, these data do suggest that deletion of Tst confers some protection to the endothelium which can be observed indirectly when compounds inhibiting the NO and prostaglandin systems are used. Protection of the endothelium would be consistent with previous evidence that H_2S can protect endothelial cells from dysfunction under conditions of vascular stress. Based on the findings in this work it would be interesting to investigate whether in models of decreased H_2S (such as $Cse^{-/-}$ mice) the ability of L-NAME and indomethacin to inhibit relaxation or augment contraction is increased or reduced, respectively.

6.3 *Tst* deletion and atherosclerosis

Investigations into the effect of Tst deletion on atherosclerosis have clearly shown that it reduces atherosclerotic lesion size in $ApoE^{-/-}$ mice (section 5.3.4). This confirms the original hypothesis that, despite worsened metabolic function (which was observed in $ApoE^{-/-}Tst^{-/-}$ in the form of worsened glucose tolerance), Tst deletion protects against atherosclerosis. Based on the data presented in this work however, the exact mechanism behind this protection cannot be defined. A trend towards reduced SBP (section 5.3.5) and a clear reduction in total and VLDL plasma cholesterol concentrations (section 5.3.6) were identified in $ApoE^{-/-}\,Tst^{-/-}$ mice and, if the reduction in SBP is confirmed, are two possible mechanisms responsible for the protection. Both increased plasma cholesterol and increased SBP are recognised risk factors for atherosclerosis (307–310) and, therefore, lower values in $ApoE^{-/-}\,Tst^{-/-}$ mice could explain the decreased size of lesions. The reduction in plasma cholesterol levels is more likely to be the result of changes within metabolic tissues, such as the liver, and,

therefore, the protection afforded by *Tst* deletion may not be exclusively linked to vascular actions. Further investigations into lesion composition, for example using 2D histology, may reveal information such as the lipid content. This data could help to refine the hypothesis as to which specific mechanism(s) underlie the phenotype in $ApoE^{-/-}Tst^{-/-}$ mice that ultimately account for the reduced lesion size in $ApoE^{-/-} Tst^{-/-}$ mice.

Strikingly, in this study all of the findings in $ApoE^{-/-}Tst^{-/-}$ mice (including worsened glucose tolerance (171,173), reduced blood insulin concentrations (172,178,179), a trend for reduced SBP (180,253,311), reduced plasma cholesterol (171,187), improved endothelial function (in control diet fed mice (187,259,260)) and reduced atherosclerotic lesion development (187)), are consistent with the published literature on the effects of increased H_2S concentrations. Therefore, this work lends substantial support to the hypothesis that increased H_2S concentrations as a result of *Tst* deletion are responsible for the phenotypes observed in $Tst^{-/-}$ and $ApoE^{-/-}Tst^{-/-}$ mice and that H_2S availability can plays a role in atherosclerosis disease progression.

6.4 Future investigations

6.4.1 Metabolic dysfunction in $Tst^{-/-}$ mice

The key findings from the work presented here have confirmed that deletion of *Tst* results in worsened glucose tolerance (section 3.3.2 & section 5.3.3) when mice are fed HFD. However, limited information is available regarding the mechanism behind this. Therefore, this should be the key concern for future work. From the data here, potential mechanisms can be identified, including biochemical alterations in the gluconeogenic pathway and reduced blood insulin concentrations.

6.4.1.1 What is the cause of increased gluconeogenesis in Tst$^{-/-}$ mice and what is its contribution to worsened glucose tolerance?

Increased PEPCK activity was observed in $Tst^{-/-}$ mice (section 3.3.4). This finding supports the previous finding of increased gluconeogenesis measured using a pyruvate tolerance test found in control diet fed $Tst^{-/-}$ mice (207). Increased gluconeogenesis has also been observed in diabetic patients (31,175). Therefore, inappropriately increased PEPCK activity in $Tst^{-/-}$ mice may contribute to their increased gluconeogenesis and lead to the worsened glucose tolerance seen in $Tst^{-/-}$ mice fed HFD (204). PEPCK protein expression was previously investigated and found to be unchanged in $Tst^{-/-}$ mice fed HFD for 6 weeks (207) and, therefore, this was not pursued here. However, it would be important to measure PEPCK

protein expression in livers from control diet fed mice to determine whether increased PEPCK expression could account for the increased PEPCK activity in these mice.

Intriguingly, however, increased gluconeogenesis has been linked to increased H_2S signalling (173) in the liver and specifically to persulfidation of pyruvate carboxylase (PC), leading to increased activity of this enzyme (166). PC catalyses the reaction in gluconeogenesis that precedes the reaction catalysed by PEPCK; the conversion of pyruvate to oxaloacetate (174,312). Increased PC activity may have resulted in our finding of increased PEPCK activity through contribution to oxaloacetate production which was the biochemical method for assaying PEPCK activity. Recent papers have also assigned PC a more substantial role in gluconeogenesis than previously thought (174) and, therefore, increased activity could contribute to the increased gluconeogenesis observed in $Tst^{-/-}$ mice. Therefore, PC represents an interesting target for further investigation to find the cause of increased gluconeogenesis in $Tst^{-/-}$ mice and assess its contribution to worsened glucose tolerance.

Initial investigations should focus on assessing PC activity in control diet fed $Tst^{-/-}$ mice. If this were found to be increased, further work to accurately measure H_2S levels in the liver of these mice would provide support for the hypothesis that H_2S was responsible for this increase. Molecular biology techniques could then confirm the presence of increased PC persulfidation of the enzyme using a 'biotin-switch' assay to pull down, and then measure, the percentage of persulfidated protein. Finally, site-specific mutation of the enzyme to remove this modification site and expression of the modified PC form in $Tst^{-/-}$ mice would provide evidence of whether increased PC activity is linked to increased gluconeogenesis in $Tst^{-/-}$. This would allow assessment of whether this increase is responsible for worsened glucose tolerance when mice are fed HFD.

6.4.1.2 What is the cause of decreased blood insulin concentrations in Tst⁻/⁻ mice and what is its contribution to worsened glucose tolerance?

Decreased plasma insulin concentrations were observed in 20-week control or HFD fed $Tst^{-/-}$ mice (section 3.3.2) and in male $ApoE^{-/-}Tst^{-/-}$ mice fed western diet for 6 weeks (section 5.3.3). This reduction was not found in the original work of Morton *et al.* (204) and this may be explained by differences in the genetic background of the mice used in the current and in the original studies. Within this current work, however, the reduction is clear and the insufficient increase in insulin concentrations in response to high fat diets could explain the worsened glucose tolerance in mice with *Tst* deletion. A decrease in the release of insulin from pancreatic β-cells could also be linked to increased H_2S signalling within the pancreatic

islets (172,178). Given the previous evidence of increased H_2S in $Tst^{-/-}$ mice, investigation into insulin secretion is clearly warranted in $Tst^{-/-}$ mice.

Pancreatic islet number should be assessed in mice fed control and HFD initially to confirm that Tst deletion does not lead to a simple reduction in the number of islets within the pancreas. Islet health could then also be investigated *in vitro* to assess whether islets from $Tst^{-/-}$ mice are at greater risk of death or have impaired function. This could potentially be achieved using Seahorse extracellular flux analysis to detect any metabolic abnormalities in glycolytic function between genotypes. Insulin concentrations within islets and released into the *in vitro* cell media, both at rest and following glucose stimulation, could then be measured to address the question of whether synthesis or release of insulin is impaired in $Tst^{-/-}$ mice.

Assuming release of insulin was found to be impaired, the next steps would require patch clamp investigation of pancreatic β-cell membrane potential to confirm a reduction in action potentials. K_{ATP} channel blockers (sulfonylureas e.g. glibencamide (178)) could then determine the involvement of these channels in suppression of glucose-stimulated action potentials. To link increased K_{ATP} activity with increased H_2S concentrations in $Tst^{-/-}$ mice accurate measurement of H_2S in the pancreas would be essential; followed potentially by patch clamp experiments in the presence of H_2S inhibitor propylargylglycine (PAG (313)) or a suitable absorber compound such as bismuth subnitrate (314). Finally, intervention (e.g. using glibencamide) treatment in $Tst^{-/-}$ mice could confirm whether insulin concentrations returned to normal and whether this in turn returned glucose intolerance on HFD to levels similar to C57BL/6 mice. Additionally, exogenous treatment of control mice with H_2S donor compounds could be performed to compare the diabetic phenotype with that of $Tst^{-/-}$ mice potentially providing evidence that increased H_2S signalling is behind the effects of Tst deletion.

6.4.2 Vascular function and protection in $Tst^{-/-}$ mice

The central findings in this work showed that deletion of Tst engendered some protection of endothelial NO production in conditions of vascular stress (section 4.3.4). The mechanism of this protection is currently unclear and, therefore, would be worth further investigation. In addition, the work suffered from an inability to test the effect of Tst deletion on severe endothelial dysfunction and, so it could not be concluded whether $Tst^{-/-}$ mice are protected from endothelial dysfunction. Therefore, a study which induced clear endothelial dysfunction and robust controls would be useful. This may be achieved through the use of other high fat diets or feeding regimes as several studies have observed aortic endothelial

dysfunction induced by high fat diet feeding (302,303,315). In addition, hyperhomocystinaemia has been consistently linked to endothelial dysfunction (316). Therefore, inducing hyperhomocystinaemia in mice by feeding a methionine rich and folate deficient diet should lead to the development of endothelial dysfunction (317). This would allow the effects of *Tst* deletion to be assessed in a clear model of endothelial dysfunction.

6.4.2.1 How does deletion of Tst protect the endothelium's ability to modulate constriction in conditions of vascular stress?

All the studies in this work were performed in the aorta. As it is known that NO is the main vasodilator in the mouse aorta (305) it is, therefore, likely that the findings of increased maximal constriction in response to L-NAME and indomethacin are the result of increased NO production. Activating phosphorylation of eNOS protein has previously been linked with increased H_2S signalling (167,304) and so this regulatory mechanism should be of particular interest. A small study has shown that phosphorylation of eNOS at the activating S1177 site is increased in control diet-fed $Tst^{-/-}$ mice (Emerson *et al.* Unpublished observations). Therefore, an obvious next step would be to repeat this measurement in 20-week HFD fed C57BL/6 and $Tst^{-/-}$ mice to confirm whether phosphorylation was also increased following HFD feeding. It would also be key to compare the effect of HFD on C57BL/6 mice to $Tst^{-/-}$ mice. If HFD induced a loss of eNOS phosphorylation in C57BL/6 mice which was not seen in $Tst^{-/-}$ mice, this may explain the protection observed.

To link this finding with increased H_2S it would also be important to perform accurate measurements of circulating and, if possible, aortic H_2S concentrations in control and HFD fed C57BL/6 mice. A reduction in H_2S with HFD in C57BL/6 could be implicated in the worsened vascular function and (as above) if this was restored in $Tst^{-/-}$ mice it would provide a clear mechanism for the protection of vascular function in these mice. Finally, an experiment in which C57BL/6 mice fed with HFD were supplemented with exogenous H_2S, using NaHS given intravenously as has previously been performed (187), should provide evidence of whether the increase in H_2S signalling can lead to protection of vascular function.

6.4.2.2 Can Tst deletion protect ACh-mediated relaxation in a model of endothelial cell dysfunction?

The initial hypothesis of the vascular investigations in this work was that *Tst* deletion would protect mice from endothelial dysfunction; classically defined as a reduced response to ACh due to reduced NO production. In this work, some evidence was found of improved NO production and, hence, endothelial function (section 4.3.4). However, it was not possible to

evaluate the effect of *Tst* deletion in a model of overt endothelial dysfunction as HFD failed to reduce ACh-mediated relaxation (section 4.3.3). To answer this question further studies are needed in which endothelial dysfunction is clearly induced by the treatment and not observed in control mice. The effect of *Tst* on this development could then be assessed. As discussed above a different model of diet induced dysfunction (302,303,315) or the use of hyperhomocystinaemia inducing diets (316,317) may be useful to induce clear endothelial dysfunction for testing.

6.4.3 Atherosclerosis in $Tst^{-/-}$ mice

This work has clearly shown that deletion of *Tst* in $ApoE^{-/-}$ mice reduces the size of atherosclerotic lesions induced by 12 weeks of western diet feeding (section 5.3.4). The initial hypothesis proposed that this would be due to vascular specific actions of *Tst* deletion since *Tst* deletion was also expected to induce metabolic dysfunction. Whilst the latter was true for glucose homeostasis, which was worsened in $ApoE^{-/-}Tst^{-/-}$ mice, plasma cholesterol concentrations were actually reduced in these animals (section 5.3.6). Therefore, the question remains as to what mechanism is important for protection in $ApoE^{-/-}Tst^{-/-}$ mice. To investigate the reduction in lesion formation initial studies should focus on further assessing the changes in the lesions from $ApoE^{-/-}Tst^{-/-}$ mice. Follow on experiments using either pharmacological manipulation of risk factors or tissue-specific *Tst* knockouts could then assess the contribution of individual phenotypes to the overall protection.

6.4.3.1 Is atherosclerotic lesion composition altered by Tst deletion?

While the investigations in this work have been able to conclude that lesion volume is reduced in $ApoE^{-/-}Tst^{-/-}$ mice they do not give any insight into the cause of this reduction. Traditional 2D histology of lesion area should allow for staining of the major lesion components including lipid, immune cells, collagen and αSMA to provide data on whether there is a specific reduction in one or more components within $ApoE^{-/-}Tst^{-/-}$ lesions (292). These data could also provide information on the mechanisms leading to lesion reduction within $ApoE^{-/-}Tst^{-/-}$ mice. For example, if lipid was the main component that was reduced in lesions from $ApoE^{-/-}Tst^{-/-}$ mice (compared to $ApoE^{-/-}$ controls) it would strongly implicate alterations in lipid transport/accumulation in lesions as the mechanism for reduced lesion size in $ApoE^{-/-}Tst^{-/-}$ mice.

2D histology should also allow for investigation of endothelial adhesion molecule expression in $ApoE^{-/-}$ and $ApoE^{-/-}Tst^{-/-}$ mice. This should be investigated as an increase in ICAM1 expression was previously observed in $Cse^{-/-}$ mice and was defined as the cause of increased atherosclerotic lesion volume in these mice (187). Further to this, exogenous H_2S treatment

appeared to reduce ICAM1 expression. The decrease in ICAM1 expression was indirectly attributed to a reduction in endothelial ROS mediated by increased H$_2$S signalling leading to an improvement of endothelial cell function.

6.4.3.2 What is the cause of reduced atherosclerotic lesion volume in ApoE$^{-/-}$Tst$^{-/-}$ mice?

This work has identified several potential mechanisms which could explain the reduced lesion volume observed in *ApoE$^{-/-}$Tst$^{-/-}$* mice. These include a reduction in plasma cholesterol concentrations (section 5.3.6) and a trend for reduced SBP (section 5.3.5). Further investigation of the SBP phenotype should be performed using the more accurate intra-arterial catheter telemetry monitors to record blood pressure under unstressed conditions and to confirm or reject the trend seen with tail cuff measurements. Further investigation of the effect of *Tst* deletion on endothelial cell function should also be performed using myography or *in vivo* measurements such as invasive blood pressure recording in response to vasodilator and constrictor compounds. 2D histology, as previously discussed, should also be used as evidence of decreased ICAM1, or similar adhesion molecules, expression would certainly increase the interest in this phenotype.

Two approaches could be taken to identify the mechanism(s) responsible for reduced lesion volume in *ApoE$^{-/-}$Tst$^{-/-}$* mice. The first is to normalise plasma cholesterol or SBP of *ApoE$^{-/-}$* mice to those of *ApoE$^{-/-}$Tst$^{-/-}$* using pharmacological treatment. Previous work has used this approach and demonstrated that ezetimibe treatment can reduce plasma cholesterol levels and hydralazine can reduce SBP in mice (187). By giving the relevant compound to normalise cholesterol or SBP during western diet feeding and lesion development to the levels seen in *ApoE$^{-/-}$Tst$^{-/-}$* mice the effect of that risk factor on lesion size could be assessed. These experiments would help to determine whether the decrease in cholesterol or trend towards decreased SBP contribute to the smaller lesion size observed in *ApoE$^{-/-}$Tst$^{-/-}$* mice.

A second approach would be the use of the newly developed *Tst loxP* mouse which would enable tissue specific knockout of *Tst*. By breeding the *Tst loxP* mouse first onto an *ApoE$^{-/-}$* background and then with tissue-specific CRE expressing lines, deletion of *Tst* could be limited to one tissue of interest to investigate its effects. Deletion of *Tst* in the liver (albumin-cre expression) or the endothelium (V cadherin–cre expression) or smooth muscle (SM22-CRE expression) of the blood vessels would allow testing of the specific roles of *Tst* in these tissues. This primarily should answer the question of whether *Tst* deletion in the vessel is exclusively responsible for reduced atherosclerotic lesions in mice with global *Tst* deletion. In addition, tissue-specific knockouts could provide evidence of which tissues are linked to which phenotypes. For example, *Tst* deletion in the liver would test the role of hepatic TST

in regulating plasma cholesterol levels. Deletion of *Tst* in the smooth muscle or endothelial cells of the vessels may test which cellular location is responsible for the observed trend towards reduction in SBP (if this is confirmed using the techniques described above) and whether deletion of *Tst* in the endothelial cells results in improved vascular function. The effect of *Tst* on immune cell function has also not been considered in this work (2D histology may provide evidence of involvement in the future) but previous studies have shown that changes in immune cells can affect lesion development (287). Therefore, tissue specific knockout of *Tst* in immune cells could also be used to investigate this if warranted by future data.

In conjunction with all of the experiments detailed above it would be valuable to include groups of control mice treated with exogenous H_2S donor compounds such as NaHS or AP123. While previous data have already established that exogenous NaHS administration can decrease atherosclerotic lesion formation this has not been performed in these models using OPT for lesion and artery volume calculation. Comparison of H_2S treated control mice with mice lacking *Tst* would test whether similar effects are observed. In combination with direct measurements of H_2S concentration the addition of this group could provide strong evidence that the effects of *Tst* deletion are mediated through increased H_2S concentrations and hence signalling.

6.5 Conclusions

Overall this work has confirmed its original hypothesis by clearly demonstrating that *Tst* is protective against the formation of atherosclerosis despite induction of metabolic dysfunction; specifically, glucose intolerance. Future work should focus on refining these findings using tissue-specific *Tst* knockout models to focus on the exact mechanisms behind these phenotypes. Based on the consistent alignment of findings in this work with the published effects of increased H_2S signalling, a central hypothesis for this future work should be that increased H_2S signalling is responsible for the phenotypes described. In a wider context, these studies provide further evidence for the involvement of H_2S in cardiometabolic diseases including diabetes and atherosclerosis. Further to this the work has shown that inhibition of TST can be used for investigation of the effects of raised endogenous H_2S in disease conditions. Future work could aim to develop compounds for TST inhibition and test them as novel compounds for the treatment of atherosclerosis (by aiming to inhibit development or progression of lesions), a major cause of cardiovascular disease and death worldwide. However, this is with the caveat that glucose homeostasis may be detrimentally affected, and so future work will need to evaluate the benefit and risk of any

inhibition. The ability to target TST inhibition to specific organs, e.g. endothelial cells and not liver may allow therapeutic benefits without detrimental metabolic side effects.

7.0 Bibliography

1.   Kaur J. A comprehensive review on metabolic syndrome. Cardiol Res Pract. 2014;2014:1–21.

2.   Eckel RH, Alberti K, Grundy SM, Zimmet PZ. The metabolic syndrome. Lancet. 2010;375(9710):181–3.

3.   Alberti KGMM, Zimmet P, Shaw J. The metabolic syndrome - A new worldwide definition. Lancet. 2005;366(9491):1059–62.

4.   Vague J. A determinant factor of the forms of obesity. Obes Res. 1996;4(2):201–3.

5.   Reaven GR. Role of insulin resistance in human disease. Diabetes. 1988;37(12):1595–607.

6.   Kaplan NM. The deadly quartet. Arch Intern Med. 1989;149(7):1514.

7.   Alberti KGMM, Zimmet PZ. Definition, diagnosis and classification of diabetes mellitus and its complications. Part 1: diagnosis and classification of diabetes mellitus. Provisional report of a WHO consultation. Diabet Med. 1998;15(7):539–53.

8.   Balkau B, Charles MA. Comment on the provisional report from the WHO consultation. Diabet Med. 1999;16(5):442–3.

9.   Expert Panel on Detection, Evaluation and Treatment of HBC in Adults. Executive summary of the third report of the national cholesterol education program (NCEP) expert panel on detection, evaluation, and treatment of high blood cholesterol in adults (adult treatment panel III). JAMA. 2001;285(19):2486–97.

10.   Einhorn, D. American College of Endocrinology Position Statement on the Insulin Resistance Syndrome. Endocr Pract. 2003;9(Supplement 2):5–21.

11.   Alberti KGMM, Zimmet P, Shaw J. Metabolic syndrome-a new world-wide definition. A consensus statement from the international diabetes federation. Diabet Med. 2006;23(5):469–80.

12.   Desroches S, Lamarche B. The evolving definitions and increasing prevalence of the metabolic syndrome. Appl Physiol Nutr Metab. 2007;32(1):23–32.

13.   Cameron AJ, Shaw JE, Zimmet PZ. The metabolic syndrome: prevalence in worldwide populations. Endocrinol Metab Clin North Am. 2004;33(2):351–75.

14. Kolovou GD, Anagnostopoulou KK, Salpea KD, Mikhailidis DP. The prevalence of metabolic syndrome in various populations. Am J Med Sci. 2007;333(6):362–71.

15. Park Y-W, Zhu S, Palaniappan L, Heshka S, Carnethon MR, Heymsfield SB. The metabolic syndrome: prevalence and associated risk factor findings in the US population from the third national health and nutrition examination survey, 1988-1994. Arch Intern Med. 2003;163(4):427–36.

16. Ford ES, Giles WH, Dietz WH. Prevalence of the metabolic syndrome among US adults. JAMA. 2002;287(3):356.

17. Ponholzer A, Temml C, Rauchenwald M, Marszalek M, Madersbacher S. Is the metabolic syndrome a risk factor for female sexual dysfunction in sexually active women? Int J Impot Res. 2008;20(1):100–4.

18. Reilly MP. The metabolic syndrome: more than the sum of its parts? Circulation. 2003;108(13):1546–51.

19. Andreadis E, Tsourous G, Tzavara C, Georgiopoulos D, Katsanou P, Marakomichelakis G, et al. Metabolic syndrome and incident cardiovascular morbidity and mortality in a mediterranean hypertensive population. Am J Hypertens. 2007;20(5):558–64.

20. Westphal SA. Obesity, Abdominal obesity, and insulin resistance. Clin Cornerstone. 2008;9(1):23–31.

21. Lemieux S, Prud'homme D, Bouchard C, Tremblay A, Després JP. Sex differences in the relation of visceral adipose tissue accumulation to total body fatness. Am J Clin Nutr. 1993;58(4):463–7.

22. Cameron AJ, Zimmet PZ. Expanding evidence for the multiple dangers of epidemic abdominal obesity. Circulation. 2008;117(13):1624–6.

23. Schäffler A, Schölmerich J, Büchler C. Mechanisms of disease: adipocytokines and visceral adipose tissue—emerging role in nonalcoholic fatty liver disease. Nat Clin Pract Gastroenterol Hepatol. 2005;2(6):273–80.

24. Hosogai N, Fukuhara A, Oshima K, Miyata Y, Tanaka S, Segawa K, et al. Adipose tissue hypoxia in obesity and its impact on adipocytokine dysregulation. Diabetes. 2007;56(4):901–11.

25. Fontana L, Eagon JC, Trujillo ME, Scherer PE, Klein S. Visceral fat adipokines

secretion is associated with systemic inflammation in obese humans. Diabetes. 2007;56(April):1010–3.

26. Pérusse L, Després JP, Lemieux S, Rice T, Rao DC, Bouchard C. Familial aggregation of abdominal visceral fat level: Results from the Quebec family study. Metabolism. 1996;45(3):378–82.

27. Bouchard C, Després JP, Mauriège P. Genetic and nongenetic determinants of regional fat distribution. Endocr Rev. 1993;14(1):72–93.

28. Frayn KN. Visceral fat and insulin resistance — causative or correlative? Br J Nutr. 2000;83(S1).

29. Martini FH, Nath JL. Fundamentals of anatomy & physiology. 8th ed. 2009.

30. Saltiel AR, Kahn CR. Insulin signalling and the regulation of glucose and lipid metabolism. Nature. 2001;414(6865):799–806.

31. Wilcox G. Insulin and insulin resistance. Clin Biochem Rev. 2005;26(2):19–39.

32. Rorsman P, Eliasson L, Kanno T, Zhang Q, Gopel S. Electrophysiology of pancreatic ß-cells in intact mouse islets of Langerhans. Vol. 107, Progress in Biophysics and Molecular Biology. 2011. p. 224–35.

33. Kahn SE. The relative contributions of insulin resistance and beta-cell dysfunction to the pathophysiology of type 2 diabetes. Diabetologia. 2003;46:3–19.

34. Reaven GM. Role of insulin resistance in human disease (syndrome X): An expanded definition. Annu Rev Med. 1993;44(1):121–31.

35. Shanik MH, Xu Y, Skrha J, Dankner R, Zick Y, Roth J. Insulin resistance and hyperinsulinemia: is hyperinsulinemia the cart or the horse? Diabetes Care. 2008;31 Suppl 2.

36. Zick Y. Role of Ser/Thr kinases in the uncoupling of insulin signaling. Int J Obes Relat Metab Disord. 2003;27 Suppl 3:S56-60.

37. Gavin JR, Roth J, Neville DM, de Meyts P, Buell DN. Insulin-dependent regulation of insulin receptor concentrations: a direct demonstration in cell culture. Proc Natl Acad Sci USA. 1974;71(1):84–8.

38. Pessin JE, Saltiel AR. Signaling pathways in insulin action : molecular targets of insulin resistance. J Clin Invest. 2000;106(2):165–9.

39. Hwang IS, Ho H, Hoffman BB, Reaven GM. Fructose-induced insulin resistance and hypertension in rats. Hypertension. 1987;10(5):512–6.

40. Basciano H, Federico L, Adeli K. Fructose, insulin resistance, and metabolic dyslipidemia. Nutr Metab. 2005;2(1):5.

41. Segal KR, Landt M, Klein S. Relationship between insulin sensitivity and plasma leptin concentration in lean and obese men. Diabetes. 1996;45(7):988–91.

42. Hotta K, Funahashi T, Bodkin NL, Ortmeyer HK, Arita Y, Hansen BC, et al. Circulating concentrations of the adipocyte protein adponectin are decreased in parallel with reduced insulin sensitivity during the progression to type 2 diabetes in Rhesys Monkeys. Diabetes. 2001;50(May):1126–33.

43. DeFronzo RA, Ferrannini E. Insulin resistance. A multifaceted syndrome responsible for NIDDM, obesity, hypertension, dyslipidemia, and atherosclerotic cardiovascular disease. Diabetes Care. 1991;14(3):173–94.

44. Wouters K, Shiri-Sverdlov R, van Gorp PJ, van Bilsen M, Hofker MH. Understanding hyperlipidemia and atherosclerosis: lessons from genetically modified *apoe* and *ldlr* mice. Clin Chem Lab Med. 2005;43(5):470–9.

45. Weber C, Noels H. Atherosclerosis: current pathogenesis and therapeutic options. Nat Med. 2011;17(11):1410–22.

46. Loomba R, Sanyal AJ. The global NAFLD epidemic. Nat Rev Gastroenterol Hepatol. 2013;10(11):686–90.

47. Choi SH, Ginsberg HN. Increased very low density lipoprotein (VLDL) secretion, hepatic steatosis, and insulin resistance. Trends Endocrinol Metab. 2011;22(9):353–63.

48. Howard B V. Lipoprotein metabolism in diabetes mellitus. J Lipid Res. 1987;28(6):613–28.

49. Ginsberg HN, Zhang Y-L, Hernandez-Ono A. Regulation of plasma triglycerides in insulin resistance and diabetes. Arch Med Res. 2005;36(3):232–40.

50. James PA, Oparil S, Carter BL, Cushman WC, Dennison-Himmelfarb C, Handler J, et al. 2014 Evidence-based guideline for the management of high blood pressure in adults. JAMA. 2014;311(5):507.

51.   Kannel WB. Blood pressure as a cardiovascular risk factor. JAMA. 1996;275(20):1571.

52.   Kannel WB, Neaton JD, Wentworth D, Thomas HE, Stamler J, Hulley SB, et al. Overall and coronary heart disease mortality rates in relation to major risk factors in 325,348 men screened for the MRFIT. Am Heart J. 1986;112(4):825–36.

53.   Morse SA, Zhang R, Thakur V, Reisin E. Hypertension and the metabolic syndrome. Am J Med Sci. 2005;330(6):303–10.

54.   Malhotra A, Kang BPS, Cheung S, Opawumi D, Meggs LG. Angiotensin II promotes glucose-induced activation of cardiac protein kinase C isozymes and phosphorylation of troponin I. Diabetes. 2001;50(8):1918–26.

55.   Bravo PE, Morse S, Borne DM, Aguilar EA, Reisin E. Leptin and hypertension in obesity. Vasc Health Risk Manag. 2006;2(2):163–9.

56.   Belin de Chantemèle EJ, Mintz JD, Rainey WE, Stepp DW. Impact of leptin-mediated sympatho-activation on cardiovascular function in obese mice. Hypertension. 2011;58(2):271–9.

57.   Rahmouni K. Leptin-induced sympathetic nerve activation: Signaling mechanisms and cardiovascular consequences in obesity. Curr Hypertens Rev. 2010;6(2):104–209.

58.   Kraemer-Aguiar LG, Laflor CM, Bouskela E, Vries G de, Stehouwer CDA, Belch JJ. Skin microcirculatory dysfunction is already present in normoglycemic subjects with metabolic syndrome. Metabolism. 2008;57(12):1740–6.

59.   Jiang F, Gibson AP, Dusting GJ. Endothelial dysfunction induced by oxidized low-density lipoproteins in isolated mouse aorta: a comparison with apolipoprotein-E deficient mice. Eur J Pharmacol. 2001;424(2):141–9.

60.   Davis N, Katz S, Wylie-Rosett J. The effect of diet on endothelial function. Cardiol Rev. 2007;15(2):62–6.

61.   Hadi H a R, Suwaidi J Al. Endothelial dysfunction in diabetes mellitus. Vasc Health Risk Manag. 2007;3(6):853–76.

62.   Harrison DG. Cellular and molecular mechanisms of endothelial cell dysfunction. J Clin Invest. 1997;100(9):2153–7.

63. Particone F, Ceravolo R, Pujia A, Ventura G, Iacopino S, Scozzafava A, et al. Prognostic significance of endothelial dysfunction in hypertensive patients. Circulation. 2001;104(2):191–6.

64. Festa A, D'Agostino R, Howard G, Mykkänen L, Tracy RP, Haffner SM. Chronic subclinical inflammation as part of the insulin resistance syndrome: the insulin resistance atherosclerosis study (IRAS). Circulation. 2000;102(1):42–7.

65. Ridker PM. C-reactive protein, the metabolic syndrome, and risk of incident cardiovascular events: An 8-year follow-up of 14 719 initially healthy American women. Circulation. 2003;107(3):391–7.

66. Eckel RH, Grundy SM, Zimmet PZ. The metabolic syndrome. Lancet. 2005;365(9468):1415–28.

67. Ordovas JM. Genetic links between diabetes mellitus and coronary atherosclerosis. Curr Atheroscler Rep. 2007;9(3):204–10.

68. Locke AE, Kahali B, Berndt SI, Justice AE, Pers TH, Day FR, et al. Genetic studies of body mass index yield new insights for obesity biology. Nature. 2015;518(7538):197–206.

69. Shungin D, Winkler TW, Croteau-Chonka DC, Ferreira T, Locke AE, Mägi R, et al. New genetic loci link adipose and insulin biology to body fat distribution. Nature. 2015;518(7538):187–96.

70. Abate N, Chandalia M, Snell PG, Grundy SM. Adipose tissue metabolites and insulin resistance in nondiabetic Asian Indian men. J Clin Endocrinol Metab. 2004;89(6):2750–5.

71. Blundell J, Stubbs R, Golding C, Croden F, Alam R, Whybrow S, et al. Resistance and susceptibility to weight gain: Individual variability in response to a high-fat diet. Physiol Behav. 2005;86(5):614–22.

72. Maes HHM, Neale MC, Eaves LJ. Genetic and environmental factors in relative body weight and human adiposity. Behav Genet. 1997;27(4):325–51.

73. Laakso M. Gene variants, insulin resistance, and dyslipidaemia. Curr Opin Lipidol. 2004;15(2):115–20.

74. Poulsen P, Levin K, Petersen I, Christensen K, Beck-Nielsen H, Vaag A. Heritability of insulin secretion, peripheral and hepatic insulin action, and intracellular glucose

partitioning in young and old Danish twins. Diabetes. 2005;54(1):275–83.

75.   Hales CN, Barker DJP. Type 2 (non-insulin-dependent) diabetes mellitus: the thrifty phenotype hypothesis. Diabetologia. 1992;35(7):595–601.

76.   Hales CN, Desai M, Ozanne SE. The thrifty phenotype hypothesis: how does it look after 5 years? Diabet Med. 1997;14(3):189–95.

77.   Kahn BB. Type 2 diabetes: When insulin secretion fails to compensate for insulin resistance. Cell. 1998;92(5):593–6.

78.   Grundy SM, Benjamin IJ, Burke GL, Chait A, Eckel RH, Howard B V., et al. Diabetes and cardiovascular disease: a statement for healthcare professionals from the American Heart Association. Circulation. 1999;100(10):1134–46.

79.   World Health Organization. Global report on diabetes. World Health Organisation. 2016. 1-88 p.

80.   Danaei G, Finucane MM, Lu Y, Singh GM, Cowan MJ, Paciorek CJ, et al. National, regional, and global trends in fasting plasma glucose and diabetes prevalence since 1980: systematic analysis of health examination surveys and epidemiological studies with 370 country-years and 2·7 million participants. Lancet. 2011;378(9785):31–40.

81.   Shaw JE, Sicree RA, Zimmet PZ. Global estimates of the prevalence of diabetes for 2010 and 2030. Diabetes Res Clin Pract. 2010;87(1):4–14.

82.   Magnusson I, Rothman DL, Katz LD, Shulman RG, Shulman GI. Increased rate of gluconeogenesis in type II diabetes mellitus. A 13C nuclear magnetic resonance study. J Clin Invest. 1992;90(4):1323–7.

83.   Puigserver P, Rhee J, Donovan J, Walkey CJ, Yoon JC, Oriente F, et al. Insulin-regulated hepatic gluconeogenesis through FOXO1–PGC-1α interaction. Nature. 2003;423(6939):550–5.

84.   Quinn PG, Yeagley D. Insulin regulation of PEPCK gene expression: a model for rapid and reversible modulation. Curr Drug Targets - Immune, Endocr Metab Disord. 2005;5(4):423–37.

85.   Rui L. Energy metabolism in the liver. In: Comprehensive Physiology. 2014. p. 177–97.

86.   Biddinger SB, Hernandez-Ono A, Rask-Madsen C, Haas JT, Alemán JO, Suzuki R, et

al. Hepatic insulin resistance is sufficient to produce dyslipidemia and susceptibility to atherosclerosis. Cell Metab. 2008;7(2):125–34.

87. Diabetes genetics initiative of Broad Institute of Harvard and MIT, Lund University and NI of BR, Saxena R, Voight BF, Lyssenko V, Burtt NP, de Bakker PIW, et al. Genome-wide association analysis identifies loci for type 2 diabetes and triglyceride levels. Science. 2007;316(5829):1331–6.

88. Krishnamurthy J, Ramsey MR, Ligon KL, Torrice C, Koh A, Bonner-Weir S, et al. p16INK4a induces an age-dependent decline in islet regenerative potential. Nature. 2006;443(7110):453–7.

89. Kondo H, Shimomura I, Matsukawa Y, Kumada M, Takahashi M, Matsuda M, et al. Association of adiponectin mutation with type 2 diabetes. Diabetes. 2002;51(7):2325–8.

90. Giugliano D, Ceriello A, Paolisso G. Oxidative stress and diabetic vascular complications. Diabetes Care. 1996;19(3):257–67.

91. Watkins PJ. Retinopathy. BMJ. 2003;326(7395):924–6.

92. Gross JL, de Azevedo MJ, Silveiro SP, Canani LH, Caramori ML, Zelmanovitz T. Diabetic nephropathy: diagnosis, prevention, and treatment. Diabetes Care. 2005;28(1):164–76.

93. Pecoraro RE, Reiber GE, Burgess EM. Pathways to diabetic limb amputation: basis for prevention. Diabetes Care. 1990;13(5):513–21.

94. Duby JJ, Campbell RK, Setter MS, White JR, Rasmussen AK. Diabetic neuropahty: an intensive review. Am J Heal Pharm. 2004;61(2):160–75.

95. Zanuso S, Jimenez A, Pugliese G, Corigliano G, Balducci S. Exercise for the management of type 2 diabetes: a review of the evidence. Acta Diabetol. 2010;47(1):15–22.

96. Davis N, Forbes B, Wylie-Rosett J. Nutritional strategies in type 2 diabetes mellitus. Mt Sinai J Med A J Transl Pers Med. 2009;76(3):257–68.

97. Palmer SC, Mavridis D, Nicolucci A, Johnson DW, Tonelli M, Craig JC, et al. Comparison of clinical outcomes and adverse events associated with glucose-lowering drugs in patients with type 2 diabetes. JAMA. 2016;316(3):313.

98.   Kirpichnikov D, McFarlane SI, Sowers JR. Metformin: an update. Ann Intern Med. 2002;137(1):25.

99.   World Health Organization. Model list of essential medicines. 2011.

100.   Zhou G, Myers R, Li Y, Chen Y, Shen X, Fenyk-Melody J, et al. Role of AMP-activated protein kinase in mechanism of metformin action. J Clin Invest. 2001;108(8):1167–74.

101.   Musi N, Hirshman MF, Nygren J, Svanfeldt M, Bavenholm P, Rooyackers O, et al. Metformin increases AMP-activated protein kinase activity in skeletal muscle of subjects with type 2 diabetes. Diabetes. 2002;51(7):2074–81.

102.   Rena G, Pearson ER, Sakamoto K. Molecular mechanism of action of metformin: old or new insights? Diabetologia. 2013;56(9):1898–906.

103.   Fantus IG, Brosseau R. Mechanism of action of metformin: insulin receptor and postreceptor effects in vitro and in vivo. J Clin Endocrinol Metab. 1986;63(4):898–905.

104.   Seino S. Cell signalling in insulin secretion: the molecular targets of ATP, cAMP and sulfonylurea. Diabetologia. 2012;55(8):2096–108.

105.   Saltiel AR, Olefsky JM. Thiazolidinediones in the treatment of insulin resistance and type II diabetes. Diabetes. 1996;45(12):1661–9.

106.   Hauner H. The mode of action of thiazolidinediones. Diabetes Metab Res Rev. 2002;18(S2):S10–5.

107.   Graham DJ, Ouellet-Hellstrom R, MaCurdy TE, Ali F, Sholley C, Worrall C, et al. Risk of acute myocardial infarction, stroke, heart failure, and death in elderly medicare patients treated with rosiglitazone or pioglitazone. JAMA. 2010;304(4):411.

108.   Ripsin CM, Kang H, Urban RJ. Management of blood glucose in type 2 diabetes mellitus. Am Fam Physician. 2009;79(1):29–36.

109.   World Health Organization. Global status report on noncommunicable diseases 2014. World Health Organization. 2014. 1-273 p.

110.   Stary HC, Chandler AB, Glagov S, Guyton JR, Insull W, Rosenfeld ME, et al. A definition of initial, fatty streak, and intermediate lesions of atherosclerosis. A report from the committee on vascular lesions of the council on arteriosclerosis, American

heart association. Circulation. 1994;89(5):2462–78.

111. Enos WF. Coronary disease among United States soldiers killed in action in Korea. J Am Med Assoc. 1953;152(12):1090.

112. Libby P, Ridker PM, Hansson GK. Progress and challenges in translating the biology of atherosclerosis. Nature. 2011;473(7347):317–25.

113. Lusis AJ. Atherosclerosis. Nature. 2000;407(6801):233–41.

114. Davignon J, Ganz P. Role of endothelial dysfunction in atherosclerosis. Circulation. 2004;109(23 Suppl 1):III27-32.

115. Alexander RW. Hypertension and the pathogenesis of atherosclerosis. Hypertension. 1995;25(2):155–61.

116. Doherty TM, Asotra K, Fitzpatrick LA, Qiao J-H, Wilkin DJ, Detrano RC, et al. Calcification in atherosclerosis: bone biology and chronic inflammation at the arterial crossroads. Proc Natl Acad Sci USA. 2003;100(20):11201–6.

117. Gibbons GF, Wiggins D, Brown a-M, Hebbachi a-M. Synthesis and function of hepatic very-low-density lipoprotein. Biochem Soc Trans. 2004;32(Pt 1):59–64.

118. Eisenberg S. High density lipoprotein metabolism. J Lipid Res. 1984;25(10):1017–58.

119. Gofman JW, Jones HB, Lindgren FT, Lyon TP, Elliott HA, Strisower B. Blood lipids and human atherosclerosis. Circulation. 1950;2(2):161–78.

120. Kwiterovich PO. The metabolic pathways of high-density lipoprotein, low-density lipoprotein, and triglycerides: a current review. Am J Cardiol. 2000;86(12):5–10.

121. Yu KC, Cooper AD. Postprandial lipoproteins and atherosclerosis. Front Biosci. 2001;6:D332-54.

122. Goldstein LJ, Brown SM. The low-density lipoprotein pathway and its relation to atherosclerosis. Annu Rev Biochem. 1977;46(1):897–930.

123. Véniant MM, Zlot CH, Walzem RL, Pierotti V, Driscoll R, Dichek D, et al. Lipoprotein clearance mechanisms in LDL receptor-deficient "Apo-B48-only" and "Apo-B100-only" mice. J Clin Invest. 1998;102(8):1559–68.

124. Kannel WB. Cholesterol in the prediction of atherosclerotic disease. Ann Intern Med.

1979;90(1):85.

125. Zadelaar S, Kleemann R, Verschuren L, De Vries-Van Der Weij J, Van Der Hoorn J, Princen HM, et al. Mouse models for atherosclerosis and pharmaceutical modifiers. Arterioscler Thromb Vasc Biol. 2007;27(8):1706–21.

126. Austin MA, Hutter CM, Zimmern RL, Humphries SE. Genetic causes of monogenic heterozygous familial hypercholesterolemia: a HuGE prevalence review. Am J Epidemiol. 2004;160(5):407–20.

127. Bonetti PO. Endothelial dysfunction: a marker of atherosclerotic risk. Arterioscler Thromb Vasc Biol. 2003;23(2):168–75.

128. Alexander RW. Hypertension and the pathogenesis of atherosclerosis. Hypertension. 1995;25(2):155-161.

129. Cai H, Harrison DG. Endothelial dysfunction in cardiovascular diseases: the role of oxidant stress. Circ Res. 2000;87(10):840–4.

130. Malek AM. Hemodynamic shear stress and its role in atherosclerosis. JAMA. 1999;282(21):2035.

131. Davies PF. Hemodynamic shear stress and the endothelium in cardiovascular pathophysiology. Nat Clin Pract Cardiovasc Med. 2009;6(1):16–26.

132. Giacco F. Oxidative stress and diabetic complications. Circ Res. 2011;107(9):1058–70.

133. Steinberg HO, Chaker H, Leaming R, Johnson A, Brechtel G, Baron AD. Obesity/insulin resistance is associated with endothelial dysfunction. Implications for the syndrome of insulin resistance. J Clin Invest. 1996;97(11):2601–10.

134. Kim J, Montagnani M, Koh KK, Quon MJ. Reciprocal relationships between insulin resistance and endothelial dysfunction: molecular and pathophysiological mechanisms. Circulation. 2006;113(15):1888–904.

135. Hansson GK. Inflammation, atherosclerosis, and coronary artery disease. N Engl J Med. 2005;352(16):1685–95.

136. Tedgui A, Mallat Z. Cytokines in atherosclerosis: pathogenic and regulatory pathways. Physiol Rev. 2006;86(2):515–81.

137. Rosendorff C, Lackland DT, Allison M, Aronow WS, Black HR, Blumenthal RS, et

al. Treatment of hypertension in patients with coronary artery disease. Hypertension. 2015;65(6):1372–407.

138. Antithrombotic trialists' collaboration. Collaborative meta-analysis of randomised trials of antiplatelet therapy for prevention of death, myocardial infarction, and stroke in high risk patients. BMJ. 2002;324(7329):71–86.

139. Corti R, Fayad Z a, Fuster V, Worthley SG, Helft G, Chesebro J, et al. Effects of lipid-lowering by simvastatin on human atherosclerotic lesions: a longitudinal study by high-resolution, noninvasive magnetic resonance imaging. Circulation. 2001;104(3):249–52.

140. Taylor F, Huffman MD, Macedo AF, Moore TH, Burke M, Davey Smith G, et al. Statins for the primary prevention of cardiovascular disease (Review). Huffman MD, editor. Cochrane Database Syst Rev. 2014;(1):1–97.

141. Baigent C, Keech A, Kearney PM, Blackwell L, Buck G, Pollicino C, et al. Efficacy and safety of cholesterol-lowering treatment: prospective meta-analysis of data from 90,056 participants in 14 randomised trials of statins. Lancet. 2005 8;366(9493):1267–78.

142. Taylor F, Huffman MD, Macedo AF, Moore TH, Burke M, Davey Smith G, et al. Statins for the primary prevention of cardiovascular disease. In: Huffman MD, editor. Cochrane Database of Systematic Reviews. 2013. p. 1–97.

143. James PA, Oparil S, Carter BL, Cushman WC, Dennison-Himmelfarb C, Handler J, et al. Evidence-based guideline for the management of high blood pressure in adults. JAMA. 2013;1097(5):1–14.

144. Roush GC, Kaur R, Ernst ME. Diuretics. J Cardiovasc Pharmacol Ther. 2014;19(1):5–13.

145. Mehta PK, Griendling KK. Angiotensin II cell signaling: physiological and pathological effects in the cardiovascular system Am J Physiol Cell Physiol. 2007;292(1):82–97.

146. Schmieder RE, Hilgers KF, Schlaich MP, Schmidt BM. Renin-angiotensin system and cardiovascular risk. Lancet. 2007;369(9568):1208–19.

147. Hansson L, Lindholm LH, Niskanen L, Lanke J, Hedner T, Niklason A, et al. Effect of angiotensin-converting-enzyme inhibition compared with conventional therapy on

cardiovascular morbidity and mortality in hypertension: the captopril prevention project (CAPPP) randomised trial. Lancet. 1999;353(9153):611–6.

148. Burnier M, Brunner H. Angiotensin II receptor antagonists. Lancet. 2000;355(9204):637–45.

149. Elliott WJ, Ram CVS. Calcium channel blockers. J Clin Hypertens. 2011;13(9):687–9.

150. Law M, Wald N, Morris J. Lowering blood pressure to prevent myocardial infarction and stroke: a new preventive strategy. Health Technol Assess. 2003;7(31):1–94.

151. Smith S, Blair S, Bonow R, Brass L, Cerqueira M, Dracup K, et al. AHA/ACC guidelines for preventing heart attack and death in patients with atherosclerotic cardiovascular disease: 2001 update. J Am Coll Cardiol. 2001;38(13):1581–3.

152. Ramsay LE, Williams B, Johnston GD, MacGregor GA, Poston L, Potter JF, et al. British hypertension society guidelines for hypertension management 1999: summary. BMJ. 1999;319(7210):630–5.

153. Andreotti F, Testa L, Biondi-Zoccai GGL, Crea F. Aspirin plus warfarin compared to aspirin alone after acute coronary syndromes: an updated and comprehensive meta-analysis of 25 307 patients. Eur Heart J. 2006;27(5):519–26.

154. Catella-Lawson F, Reilly MP, Kapoor SC, Cucchiara AJ, DeMarco S, Tournier B, et al. Cyclooxygenase inhibitors and the antiplatelet effects of aspirin. N Engl J Med. 2001;345(25):1809–17.

155. Hirsh J, Dalen JE, Anderson DR, Poller L, Bussey H, Ansell J, et al. Oral anticoagulants: mechanism of action, clinical effectiveness, and optimal therapeutic range. Chest. 1998;114(5 Suppl):445S–469S.

156. Streeter E, Ng HH, Hart JL. Hydrogen sulfide as a vasculoprotective factor. Med Gas Res. 2013;3(1):9.

157. Cooper CE, Brown GC. The inhibition of mitochondrial cytochrome oxidase by the gases carbon monoxide, nitric oxide, hydrogen cyanide and hydrogen sulfide: chemical mechanism and physiological significance. J Bioenerg Biomembr. 2008;40(5):533–9.

158. Abe K, Kimura H. The possible role of hydrogen sulfide as an endogenous neuromodulator. J Neurosci. 1996;16(3):1066–71.

159.　Wang R. Two's company, three's a crowd: can H_2S be the third endogenous gaseous transmitter? FASEB J. 2002;16(13):1792–8.

160.　Kamoun P. Endogenous production of hydrogen sulfide in mammals. Amino Acids. 2004;26(3):243–54.

161.　Stein A, Bailey SM. Redox biology of hydrogen sulfide: implications for physiology, pathophysiology, and pharmacology. Redox Biol. 2013;1(1):32–9.

162.　Shen X, Peter E a., Bir S, Wang R, Kevil CG. Analytical measurement of discrete hydrogen sulfide pools in biological specimens. Free Radic Biol Med. 2012;52(11–12):2276–83.

163.　Mustafa AK, Gadalla MM, Sen N, Kim S, Mu W, Gazi SK, et al. H_2S signals through protein S-sulfhydration. Sci Signal. 2009;2(96):ra72.

164.　Lu C, Kavalier A, Lukyanov E, Gross SS. S-sulfhydration/desulfhydration and S-nitrosylation/denitrosylation: a common paradigm for gasotransmitter signaling by H_2S and NO. Methods. 2013;62(2):177–81.

165.　Filipovic MR. Persulfidation (S-sulfhydration) and H_2S. In: Moore P, Whiteman M, editors. Chemistry, Biochemistry and Pharmacology of Hydrogen Sulfide. 2015. p. 29–59.

166.　Ju Y, Untereine A, Wu L, Yang G. H_2S-induced S-sulfhydration of pyruvate carboxylase contributes to gluconeogenesis in liver cells. Biochim Biophys Acta - Gen Subj. 2015;1850(11):2293–303.

167.　King AL, Polhemus DJ, Bhushan S, Otsuka H, Kondo K, Nicholson CK, et al. Hydrogen sulfide cytoprotective signaling is endothelial nitric oxide synthase-nitric oxide dependent. Proc Natl Acad Sci USA. 2014;111(8):3182–7.

168.　Libiad M, Yadav PK, Vitvitsky V, Martinov M, Banerjee R. Organization of the human mitochondrial hydrogen sulfide oxidation pathway. J Biol Chem. 2014;289(45):30901–10.

169.　Hildebrandt TM, Grieshaber MK. Three enzymatic activities catalyze the oxidation of sulfide to thiosulfate in mammalian and invertebrate mitochondria. FEBS J. 2008;275(13):3352–61.

170.　Tiranti V, Viscomi C, Hildebrandt T, Di Meo I, Mineri R, Tiveron C, et al. Loss of ETHE1, a mitochondrial dioxygenase, causes fatal sulfide toxicity in ethylmalonic

encephalopathy. Nat Med. 2009;15(2):200–5.

171.   Mani S, Cao W, Wu L, Wang R. Hydrogen sulfide and the liver. Nitric Oxide. 2014;41(March):62–71.

172.   Kaneko Y, Kimura Y, Kimura H, Niki I. L-cysteine inhibits insulin release from the pancreatic ß-cell: possible involvement of metabolic production of hydrogen sulfide, a novel gasotransmitter. Diabetes. 2006;55(5):1391–7.

173.   Zhang L, Yang G, Untereiner A, Ju Y, Wu L, Wang R. Hydrogen sulfide impairs glucose utilization and increases gluconeogenesis in hepatocytes. Endocrinology. 2013;154(1):114–26.

174.   Jitrapakdee S, St Maurice M, Rayment I, Cleland WW, Wallace JC, Attwood P V. Structure, mechanism and regulation of pyruvate carboxylase. Biochem J. 2008;413(3):369–87.

175.   Andrikopoulos S, Proietto J. The biochemical basis of increased hepatic glucose production in a mouse model of type 2 (non-insulin-dependent) diabetes mellitus. Diabetologia. 1995;1389–96.

176.   Yang G, Tang G, Zhang L, Wu L, Wang R. The pathogenic role of cystathionine γ-lyase/hydrogen sulfide in streptozotocin-induced diabetes in mice. Am J Pathol. 2011;179(2):869–79.

177.   Ratnam S, Maclean KN, Jacobs RL, Brosnan ME, Kraus JP, Brosnan JT. Hormonal regulation of cystathionine beta-synthase expression in liver. J Biol Chem. 2002;277(45):42912–8.

178.   Tang G, Zhang L, Yang G, Wu L, Wang R. Hydrogen sulfide-induced inhibition of L-type Ca^{2+} channels and insulin secretion in mouse pancreatic beta cells. Diabetologia. 2013;56(3):533–41.

179.   Ali MY, Whiteman M, Low CM, Moore PK. Hydrogen sulphide reduces insulin secretion from HIT-T15 cells by a K_{ATP} channel-dependent pathway. J Endocrinol. 2007;195(1):105–12.

180.   Zhao W, Zhang J, Lu Y, Wang R. The vasorelaxant effect of H_2S as a novel endogenous gaseous K_{ATP} channel opener. Eur Mol Biol Organ J. 2001;20:6008–16.

181.   Mustafa AK, Sikka G, Gazi SK, Steppan J, Jung SM, Bhunia AK, et al. Hydrogen sulfide as endothelium-derived hyperpolarizing factor sulfhydrates potassium

channels. Circ Res. 2011;109(11):1259–68.

182. Yang G, Yang W, Wu L, Wang R. H_2S, endoplasmic reticulum stress, and apoptosis of insulin-secreting beta cells. J Biol Chem. 2007;282(22):16567–76.

183. Kaneko Y, Kimura T, Taniguchi S, Souma M, Kojima Y, Kimura Y, et al. Glucose-induced production of hydrogen sulfide may protect the pancreatic beta-cells from apoptotic cell death by high glucose. FEBS Lett. 2009;583(2):377–82.

184. Okamoto M, Ishizaki T, Kimura T. Protective effect of hydrogen sulfide on pancreatic beta-cells. Nitric Oxide. 2015;46:32–6.

185. Jain SK, Micinski D, Lieblong BJ, Stapleton T. Relationship between hydrogen sulfide levels and HDL-cholesterol, adiponectin, and potassium levels in the blood of healthy subjects. Atherosclerosis. 2012;225(1):242–5.

186. Namekata K, Enokido Y, Ishii I, Nagai Y, Harada T, Kimura H. Abnormal lipid metabolism in cystathionine beta-synthase-deficient mice, an animal model for hyperhomocysteinemia. J Biol Chem. 2004;279(51):52961–9.

187. Mani S, Li H, Untereiner A, Wu L, Yang G, Austin RC, et al. Decreased endogenous production of hydrogen sulfide accelerates atherosclerosis. Circulation. 2013;127(25):2523–34.

188. Gulsen M, Yesilova Z, Bagci S, Uygun A, Ozcan A, Ercin CN, et al. Elevated plasma homocysteine concentrations as a predictor of steatohepatitis in patients with non-alcoholic fatty liver disease. J Gastroenterol Hepatol. 2005;20(9):1448–55.

189. Bonthu S, Heistad DD, Chappell DA, Lamping KG, Faraci FM. Atherosclerosis, vascular remodeling, and impairment of endothelium-dependent relaxation in genetically altered hyperlipidemic mice. Arterioscler Thromb Vasc Biol. 1997;17(11):2333–40.

190. Weston AH, Edwards G, Dora KA, Gardener MJ, Garland CJ. K^+ is an endothelium-dreived hyperpolarizing factor in rat arteries. Nature. 1998;396(6708):269–72.

191. Edwards G, Gardener MJ, Feletou M, Brady G, Vanhoutte PM, Weston a H. Further investigation of endothelium-derived hyperpolarizing factor (EDHF) in rat hepatic artery: studies using 1-EBIO and ouabain. Br J Pharmacol. 1999;128(5):1064–70.

192. Yang G, Wu L, Jiang B, Yang W, Qi J, Cao K, et al. H_2S as a physiologic vasorelaxant: hypertension in mice with deletion of cystathionine -lyase. Science.

2008;322(5901):587–90.

193. Elrod JW, Calvert JW, Morrison J, Doeller JE, Kraus DW, Tao L, et al. Hydrogen sulfide attenuates myocardial ischemia-reperfusion injury by preservation of mitochondrial function. Proc Natl Acad Sci USA. 2007;104(39):15560–5.

194. Yong Q-C, Cheong JL, Hua F, Deng L-W, Khoo YM, Lee H-S, et al. Regulation of heart function by endogenous gaseous mediators—crosstalk between nitric oxide and hydrogen sulfide. Antioxid Redox Signal. 2011;14(11):2081–91.

195. Drawbaugh RB, Marrs TC. Interspecies differences in rhodanese (thiosulfate sulfurtransferase, EC 2.8.1.1) activity in liver, kidney and plasma. Comp Biochem Physiol Part B Comp Biochem. 1987;86(2):307–10.

196. Frankenberg L. Enzyme therapy in cyanide poisoning: effect of rhodanese and sulfur compounds. Arch Toxicol. 1980;45(4):315–23.

197. Libiad M, Motl N, Akey DL, Sakamoto N, Fearon ER, Smith JL, et al. Thiosulfate sulfurtransferase-like domain-containing 1 protein interacts with thioredoxin. J Biol Chem. 2018;293(8):2675–86.

198. Melideo SLS, Jackson MMR, Jorns MMS. Biosynthesis of a central intermediate in hydrogen sulfide metabolism by a novel human sulfurtransferase and its yeast ortholog. Biochemistry. 2014;53:4739–53.

199. Lill R. Function and biogenesis of iron-sulphur proteins. Nature. 2009;460(7257):831–8.

200. Bonomi F, Pagani S, Cerletti P, Cannella C. Rhodanese-mediated sulfur transfer to succinate dehydrogenase. Eur J Biochem. 1977;72(1):17–24.

201. Horton, R. H., Moran, L. A., Scrimgeour, K. G., Perry, M. D. & Rawn JD. Principles of biochemistry. 4th ed. 2006.

202. Horvat S, Bünger L, Falconer VM, Mackay P, Law a, Bulfield G, et al. Mapping of obesity QTLs in a cross between mouse lines divergently selected on fat content. Mamm Genome. 2000;11(1):2–7.

203. Morton NM, Nelson YB, Michailidou Z, Di Rollo EM, Ramage L, Hadoke PWF, et al. A stratified transcriptomics analysis of polygenic fat and lean mouse adipose tissues identifies novel candidate obesity genes. PLoS One. 2011;6(9):e23944.

204. Morton NM, Beltram J, Carter RN, Michailidou Z, Gorjanc G, McFadden C, et al. Genetic identification of thiosulfate sulfurtransferase as an adipocyte-expressed antidiabetic target in mice selected for leanness. Nat Med. 2016;22(7):771–9.

205. Frayling TM, Timpson NJ, Weedon MN, Zeggini E, Freathy RM, Lindgren CM, et al. A common variant in the FTO gene is associated with body mass index and predisposes to childhood and adult obesity. Science. 2007;316(5826):889–94.

206. Nguyen DM, El-Serag HB. The epidemiology of obesity. Gastroenterol Clin North Am. 2010;39(1):1–7.

207. Gibbins MTG. The impact of detoxifying enzyme *Tst* gene knockout on liver metabolism in the mouse [Masters dissertation]. Edinburgh, UK. University of Edinburgh. 2013.

208. Wu C, Jin X, Tsueng G, Afrasiabi C, Su AI. BioGPS: Building your own mash-up of gene annotations and expression profiles. Nucleic Acids Res. 2016;44(D1):D313–6.

209. Markel P, Shu P, Ebeling C, Carlson GA, Nagle DL, Smutko JS, et al. Theoretical and empirical issues for marker-assisted breeding of congenic mouse strains. Nat Genet. 1997;17(3):280–4.

210. Keane TM, Goodstadt L, Danecek P, White M a, Wong K, Yalcin B, et al. Mouse genomic variation and its effect on phenotypes and gene regulation. Nature. 2011;477(7364):289–94.

211. Simon MM, Greenaway S, White JK, Fuchs H, Gailus-Durner V, Wells S, et al. A comparative phenotypic and genomic analysis of C57BL/6J and C57BL/6N mouse strains. Genome Biol. 2013;14(7):R82.

212. Peters JM, Hennuyer N, Staels B, Fruchart JC, Fievet C, Gonzalez FJ, et al. Alterations in lipoprotein metabolism in peroxisome proliferator-activated receptor alpha-deficient mice. J Biol Chem. 1997;272(43):27307–12.

213. Hebbard L, George J. Animal models of nonalcoholic fatty liver disease. World J Gastroenterol. 2011;8(1):35–44.

214. Simoncic M, Horvat S, Stevenson PL, Bünger L, Holmes MC, Kenyon CJ, et al. Divergent physical activity and novel alternative responses to high fat feeding in polygenic fat and lean mice. Behav Genet. 2008;38(3):292–300.

215. Surwit RS, Feinglos MN, Rodin J, Sutherland A, Petro AE, Opara EC, et al.

Differential effects of fat and sucrose on body composition in C57BL/6 and A/J mice. Metabolism. 1998;47(11):1354–9.

216.   Petersen KF, Dufour S, Befroy D, Garcia R, Shulman GI. Impaired mitochondrial activity in the insulin-resistant offspring of patients with type 2 diabetes. N Engl J Med. 2004;350(7):664–71.

217.   Petersen KF. Mitochondrial dysfunction in the elderly: possible role in insulin resistance. Science. 2003;300(5622):1140–2.

218.   Salto R, Sola M, Oliver FJ, Vargas AM. Effects of starvation, diabetes and carbon tetrachloride intoxication on rat kidney cortex and liver pyruvate carboxylase levels. Arch Physiol Biochem. 1996;104(7):845–50.

219.   Gerö D, Torregrossa R, Perry A, Waters A, Trionnaire S Le, Whatmore JL, et al. The novel mitochondria-targeted hydrogen sulfide (H_2S) donors AP123 and AP39 protect against hyperglycemic injury in microvascular endothelial in vitro. Pharmacol Res. 2016;113:186–98.

220.   Módis K, Ju Y, Ahmad A, Untereiner AA, Altaany Z, Wu L, et al. S- sulfhydration of ATP synthase by hydrogen sulfide stimulates mitochondrial bioenergetics. Pharmacol Res. 2016;113:116–24.

221.   Szabo C, Ransy C, Módis K, Andriamihaja M, Murghes B, Coletta C, et al. Regulation of mitochondrial bioenergetic function by hydrogen sulfide. Part I. Biochemical and physiological mechanisms. Br J Pharmacol. 2014;171(8):2099–122.

222.   Han S, Liang CP, Westerterp M, Senokuchi T, Welch CL, Wang Q, et al. Hepatic insulin signaling regulates VLDL secretion and atherogenesis in mice. J Clin Invest. 2009;119(4):1029–41.

223.   Julián MT. Hepatic glycogenosis: an underdiagnosed complication of diabetes mellitus? World J Diabetes. 2015;6(2):321.

224.   Talwani R, Gilliam BL, Howell C. Infectious diseases and the liver. Clin Liver Dis. 2011;15(1):111–30.

225.   Houtkooper RH, Argmann C, Houten SM, Cantó C, Jeninga EH, Andreux P a., et al. The metabolic footprint of aging in mice. Sci Rep. 2011;1(1):134.

226.   Petro AE, Cotter J, Cooper DA, Peters JC, Surwit SJ, Surwit RS. Fat, carbohydrate, and calories in the development of diabetes and obesity in the C57BL/6J mouse.

Metabolism. 2004;53(4):454–7.

227. Szabo C. Roles of hydrogen sulfide in the pathogenesis of diabetes mellitus and its complications. Antioxid Redox Signal. 2012;17(1):68–80.

228. Wallace JL, Wang R. Hydrogen sulfide-based therapeutics: exploiting a unique but ubiquitous gasotransmitter. Nat Rev Drug Discov. 2015;14(5):329–45.

229. Tang G, Wu L, Wang R. Interaction of hydrogen sulfide with ion channels: frontiers in research review: The pathophysiological significance of sulphur-containing gases. Clin Exp Pharmacol Physiol. 2010;37(7):753–63.

230. Yang W, Yang G, Jia X, Wu L, Wang R, Wang R. Activation of K_{ATP} channels by H_2S in rat insulin-secreting cells and the underlying mechanisms. J Physiol. 2005;5692:519–31.

231. Toye AA, Lippiat JD, Proks P, Shimomura K, Bentley L, Hugill A, et al. A genetic and physiological study of impaired glucose homeostasis control in C57BL/6J mice. Diabetologia. 2005;48(4):675–86.

232. Freeman H, Shimomura K, Horner E, Cox RD, Ashcroft FM. Nicotinamide nucleotide transhydrogenase: a key role in insulin secretion. Cell Metab. 2006;3(1):35–45.

233. Mekada K, Abe K, Murakami A, Nakamura S, Nakata H, Moriwaki K, et al. Genetic differences among C57BL/6 substrains. Exp Anim. 2009;58(2):141–9.

234. Wong N, Blair AR, Morahan G, Andrikopoulos S. The deletion variant of nicotinamide nucleotide transhydrogenase (Nnt) does not affect insulin secretion or glucose tolerance. Endocrinology. 2010;151(1):96–102.

235. Pullen TJ, Khan AM, Barton G, Butcher SA, Sun G, Rutter GA. Identification of genes selectively disallowed in the pancreatic islet. Islets. 2010;2(2):89–95.

236. Reuter TY. Diet-induced models for obesity and type 2 diabetes. Drug Discov Today Dis Model. 2007;4(1):3–8.

237. Darkhal P, Gao M, Ma Y, Liu D. Blocking high-fat diet-induced obesity, insulin resistance and fatty liver by overexpression of Il-13 gene in mice. Int J Obes. 2015;39(8):1292–9.

238. Pettersson US, Waldén TB, Carlsson P-O, Jansson L, Phillipson M. Female mice are

protected against high-fat diet induced metabolic syndrome and increase the regulatory T cell population in adipose tissue. PLoS One. 2012;7(9):e46057.

239. Fraulob JC, Ogg-Diamantino R, Fernandes-Santos C, Aguila MB, Mandarim-de-Lacerda C. A mouse model of metabolic syndrome: insulin resistance, fatty liver and non-alcoholic fatty pancreas disease (NAFPD) in C57BL/6 mice fed a high fat diet. J Clin Biochem Nutr. 2010;46(3):212–23.

240. Le Marchand Y, Loten EG, Assimacopoulos-Jeannet F, Forgue ME, Freychet P, Jeanrenaud B. Effect of fasting and streptozotocin in the obese hyperglycemic (ob/ob) mouse. Apparent lack of a direct relationship between insulin binding and insulin effects. Diabetes. 1977;26(6):582–90.

241. Kwak SH, Park KS, Lee KU, Lee HK. Mitochondrial metabolism and diabetes. J Diabetes Investig. 2010;1(5):161–9.

242. Echtay KS, Roussel D, St-Pierre J, Jekabsons MB, Cadenas S, Stuart J a, et al. Superoxide activates mitochondrial uncoupling proteins. Nature. 2002;415(6867):96–9.

243. Das AM. Regulation of the mitochondrial ATP-synthase in health and disease. Mol Genet Metab. 2003;79(2):71–82.

244. Módis K, Coletta C, Erdélyi K, Papapetropoulos A, Szabo C. Intramitochondrial hydrogen sulfide production by 3-mercaptopyruvate sulfurtransferase maintains mitochondrial electron flow and supports cellular bioenergetics. FASEB J. 2013;27(2):601–11.

245. Reily C, Mitchell T, Chacko BK, Benavides GA, Murphy MP, Darley-Usmar VM. Mitochondrially targeted compounds and their impact on cellular bioenergetics. Redox Biol. 2013;1(1):86–93.

246. Szabo C, Coletta C, Chao C, Modis K, Szczesny B, Papapetropoulos A, et al. Tumor-derived hydrogen sulfide, produced by cystathionine-β-synthase, stimulates bioenergetics, cell proliferation, and angiogenesis in colon cancer. Proc Natl Acad Sci USA. 2013;110(30):12474–9.

247. Lagoutte E, Mimoun S, Andriamihaja M, Chaumontet C, Blachier F, Bouillaud F. Oxidation of hydrogen sulfide remains a priority in mammalian cells and causes reverse electron transfer in colonocytes. Biochim Biophys Acta - Bioenerg.

2010;1797(8):1500–11.

248. Goubern M, Andriamihaja M, Nubel T, Blachier F, Bouillaud F. Sulfide, the first inorganic substrate for human cells. FASEB J. 2007;21(8):1699–706.

249. Yong R, Searcy DG. Sulfide oxidation coupled to ATP synthesis in chicken liver mitochondria. Comp Biochem Physiol Part B Biochem Mol Biol. 2001;129(1):129–37.

250. Völkel S, Grieshaber MK. Mitochondrial sulfide oxidation in Arenicola marina. Evidence for alternative electron pathways. Eur J Biochem. 1996;235(1–2):231–7.

251. Zeng T, Zhang C-L, Song F-Y, Zhao X-L, Xie K-Q. Garlic oil alleviated ethanol-induced fat accumulation via modulation of SREBP-1, PPAR-α, and CYP2E1. Food Chem Toxicol. 2012;50(3–4):485–91.

252. Robert K, Nehmé J, Bourdon E, Pivert G, Friguet B, Delcayre C, et al. Cystathionine β synthase deficiency promotes oxidative stress, fibrosis, and steatosis in mice liver. Gastroenterology. 2005;128(5):1405–15.

253. Yang G, Wu L, Jiang B, Yang W, Qi J, Cao K, et al. H_2S as a physiologic vasorelaxant : hypertension in mice with deletion of cystathionine gamma-lyase. Science. 2008;322:587–90.

254. Hamelet J, Demuth K, Paul JL, Delabar JM, Janel N. Hyperhomocysteinemia due to cystathionine beta synthase deficiency induces dysregulation of genes involved in hepatic lipid homeostasis in mice. J Hepatol. 2007;46(1):151–9.

255. Gao X, Krokowski D, Guan B, Bederman I, Majumder M, Parisien M, et al. Quantitative H_2S-mediated protein sulfhydration reveals metabolic reprogramming during the integrated stress response. Elife. 2015;4:1–21.

256. Levitt MD, Abdel-Rehim MS, Furne J. Free and acid-labile hydrogen sulfide concentrations in mouse tissues: anomalously high free hydrogen sulfide in aortic tissue. Antioxid Redox Signal. 2011;15(2):373–8.

257. Ignarro LJ, Buga GM, Wood KS, Byrns RE, Chaudhurit G, Sawyer CH. Endothelium-derived relaxing factor produced and released from artery and vein is nitric oxide (endothelium-dependent relaxation/vascular smooth muscle/cyclic GMP). Med Sci. 1987;84(December):9265–9.

258. Luksha L, Agewall S, Kublickiene K. Endothelium-derived hyperpolarizing factor in

vascular physiology and cardiovascular disease. Atherosclerosis. 2009;202(2):330–44.

259. Wang R, Szabo C, Ichinose F, Ahmed A, Whiteman M, Papapetropoulos A. The role of H$_2$S bioavailability in endothelial dysfunction. Trends Pharmacol Sci. 2015;1–11.

260. Suzuki K, Olah G, Modis K, Coletta C, Kulp G, Gero D, et al. Hydrogen sulfide replacement therapy protects the vascular endothelium in hyperglycemia by preserving mitochondrial function. Proc Natl Acad Sci USA. 2011;108(33):13829–34.

261. Eberhardt M, Dux M, Namer B, Miljkovic J, Cordasic N, Will C, et al. H$_2$S and NO cooperatively regulate vascular tone by activating a neuroendocrine HNO-TRPA1-CGRP signalling pathway. Nat Commun. 2014;5:4381.

262. Altaany Z, Ju Y, Yang G, Wang R. The coordination of S-sulfhydration, S-nitrosylation, and phosphorylation of endothelial nitric oxide synthase by hydrogen sulfide. Sci Signal. 2014;7(342):ra87.

263. Bibli S-I, Yang G, Zhou Z, Wang R, Topouzis S, Papapetropoulos A. Role of cGMP in hydrogen sulfide signaling. Nitric Oxide. 2015;46:7–13.

264. Meng G, Zhu J, Xiao Y, Huang Z, Zhang Y, Tang X, et al. Hydrogen sulfide donor GYY4137 protects against myocardial fibrosis. Oxid Med Cell Longev. 2015;2015:1–14.

265. Chataigneau T, Félétou M, Huang PL, Fishman MC, Duhault J, Vanhoutte PM. Acetylcholine-induced relaxation in blood vessels from endothelial nitric oxide synthase knockout mice. Br J Pharmacol. 1999;126(1):219–26.

266. Bullock GR, Taylor SG, Weston AH. Influence of the vascular endothelium on agonist-induced contractions and relaxations in rat aorta. Br J Pharmacol. 1986;89(4):819–30.

267. Martin W, Furchgott RF, Villani GM, Jothianandan D. Depression of contractile responses in rat aorta by spontaneously released endothelium-derived relaxing factor. J Pharmacol Exp Ther. 1986;237(2):529–38.

268. Heinonen I, Rinne P, Ruohonen ST, Ruohonen S, Ahotupa M, Savontaus E. The effects of equal caloric high fat and western diet on metabolic syndrome, oxidative stress and vascular endothelial function in mice. Acta Physiol. 2014;211(3):515–27.

269. Brandes RP, Schmitz-Winnenthal FH, Félétou M, Gödecke a, Huang PL, Vanhoutte PM, et al. An endothelium-derived hyperpolarizing factor distinct from NO and prostacyclin is a major endothelium-dependent vasodilator in resistance vessels of wild-type and endothelial NO synthase knockout mice. Proc Natl Acad Sci USA. 2000;97(17):9747–52.

270. Cleary C, Buckley CH, Henry E, McLoughlin P, O'Brien C, Hadoke PWF. Enhanced endothelium derived hyperpolarising factor activity in resistance arteries from normal pressure glaucoma patients: implications for vascular function in the eye. Br J Ophthalmol. 2005;89(2):223–8.

271. McIntyre CA, Buckley CH, Jones GC, Sandeep TC, Andrews RC, Elliott AI, et al. Endothelium-derived hyperpolarizing factor and potassium use different mechanisms to induce relaxation of human subcutaneous resistance arteries. Br J Pharmacol. 2001;133(6):902–8.

272. Stone NJ, Robinson JG, Lichtenstein AH, Bairey Merz CN, Blum CB, Eckel RH, et al. 2013 ACC/AHA guideline on the treatment of blood cholesterol to reduce atherosclerotic cardiovascular risk in adults. Circulation. 2014;129(25 suppl 2):S1–45.

273. Kini AS, Baber U, Kovacic JC, Limaye A, Ali Z a., Sweeny J, et al. Changes in plaque lipid content after short-term intensive versus standard statin therapy: The YELLOW trial (reduction in Yellow Plaque by Aggressive Lipid-Lowering Therapy). J Am Coll Cardiol. 2013;62(1):21–9.

274. Swerdlow DI, Preiss D, Kuchenbaecker KB, Holmes M V, Engmann JEL, Shah T, et al. HMG-coenzyme A reductase inhibition, type 2 diabetes, and bodyweight: evidence from genetic analysis and randomised trials. Lancet. 2015;385(9965):351–61.

275. Xu S, Liu Z, Liu P. Targeting hydrogen sulfide as a promising therapeutic strategy for atherosclerosis. Int J Cardiol. 2014;172(2):313–7.

276. Endemann DH, Schiffrin EL. Endothelial dysfunction. J Am Soc Nephrol. 2004;15(8):1983–92.

277. Couse JF, Korach KS. Estrogen receptor null mice: what have we learned and where will they lead us? Endocr Rev. 1999;20(3):358–417.

278. Hammond CL, Wheeler SG, Ballatori N, Hinkle PM. *Ost*$^{-/-}$ mice are not protected from western diet-induced weight gain. Physiol Rep. 2015;3(1):e12263–e12263.

279. Schierwagen R, Maybüchen L, Zimmer S, Hittatiya K, Bäck C, Klein S, et al. Seven weeks of western diet in apolipoprotein-E-deficient mice induce metabolic syndrome and non-alcoholic steatohepatitis with liver fibrosis. Sci Rep. 2015;5(1):12931.

280. Hofmann SM, Perez-Tilve D, Greer TM, Coburn BA, Grant E, Basford JE, et al. Defective lipid delivery modulates glucose tolerance and metabolic response to diet in apolipoprotein E deficient mice. Diabetes. 2008;57(1):5–12.

281. Tordjman K, Bernal-Mizrachi C, Zemany L, Weng S, Feng C, Zhang F, et al. PPARα deficiency reduces insulin resistance and atherosclerosis in *apoE*-null mice. J Clin Invest. 2001;107(8):1025–34.

282. Newberry EP, Xie Y, Kennedy SM, Luo J, Davidson NO. Protection against western diet-induced obesity and hepatic steatosis in liver fatty acid-binding protein knockout mice. Hepatology. 2006;44(5):1191–205.

283. Lizcano F, Guzmán G. Estrogen deficiency and the origin of obesity during menopause. Biomed Res Int. 2014;2014:757461.

284. Gallou-Kabani C, Vigé A, Gross M, Rabès J-P, Boileau C, Larue-Achagiotis C, et al. C57BL/6J and A/J mice fed a high-fat diet delineate components of metabolic syndrome. Obesity. 2007;15(8):1996–2005.

285. Elhage R. Reduced atherosclerosis in interleukin-18 deficient apolipoprotein E-knockout mice. Cardiovasc Res. 2003;59(1):234–40.

286. Smith E, Prasad KMR, Butcher M, Dobrian A, Kolls JK, Ley K, et al. Blockade of interleukin-17A results in reduced atherosclerosis in apolipoprotein E-deficient mice. Circulation. 2010;121(15):1746–55.

287. Kipari T, Hadoke PWF, Iqbal J, Man T-Y, Miller E, Coutinho AE, et al. 11B-hydroxysteroid dehydrogenase type 1 deficiency in bone marrow-derived cells reduces atherosclerosis. FASEB J. 2013;27:1519–31.

288. Lutgens E, de Muinck ED, Heeneman S, Daemen MJ. Compensatory enlargement and stenosis develop in *apoE*(-/-) and *apoE**3-Leiden transgenic mice. Arterioscler Thromb Vasc Biol. 2001;21:1359–65.

289. Moghadasian MH, McManus BM, Godin D V, Rodrigues B, Frohlich JJ.

Proatherogenic and antiatherogenic effects of probucol and phytosterols in apolipoprotein E–deficient mice. Circulation. 1999;99(13):1733 LP-1739.

290. Seo HS, Lombardi DM, Polinsky P, Powell-Braxton L, Bunting S, Schwartz SM, et al. Peripheral vascular stenosis in apolipoprotein E-deficient mice. Arterioscler Thromb Vasc Biol. 1997;17(12):3593-3601.

291. Bentzon JF, Pasterkamp G, Falk E. Expansive remodeling is a response of the plaque-related vessel wall in aortic roots of *apoE*-deficient mice: An experiment of nature. Arterioscler Thromb Vasc Biol. 2003;23(2):257–62.

292. Wadsworth MP, Sobel BE, Schneider DJ, Tra W, van Hirtum H, Taatjes DJ. Quantitative analysis of atherosclerotic lesion composition in mice. In: Taatjes DJ, Mossman BT, editors. Cell imaging techniques: methods and protocols. 2006. p. 137–52.

293. Lu H, Cassis LA, Daugherty A. Atherosclerosis and arterial blood pressure in mice. Curr Drug Targets. 2007;8(11):1181–9.

294. Stocker R, Keaney JF. Role of oxidative modifications in atherosclerosis. Physiol Rev. 2004;84(4):1381–478.

295. Staessen JA, Li Y, Thijs L, Wang J-G. Blood pressure reduction and cardiovascular prevention: an update including the 2003-2004 secondary prevention trials. Hypertens Res. 2005;28(5):385–407.

296. Watson AMD, Li J, Schumacher C, De Gasparo M, Feng B, Thomas MC, et al. The endothelin receptor antagonist avosentan ameliorates nephropathy and atherosclerosis in diabetic apolipoprotein e knockout mice. Diabetologia. 2010;53(1):192–203.

297. Keidar S, Attias J, Coleman R, Wirth K, Scholkens B, Hayek T. Attenuation of atherosclerosis in apolipoprotein E-deficient mice by ramipril is dissociated from its antihypertensive effect and from potentiation of bradykinin. J Cardiovasc Pharmacol. 2000;35(1):64–72.

298. Davis HR, Compton DS, Hoos L, Tetzloff G. Ezetimibe, a potent cholesterol absorption inhibitor, inhibits the development of atherosclerosis in *ApoE* knockout mice. Arterioscler Thromb Vasc Biol. 2001;21(12):2032–8.

299. Wójcicka G, Jamroz-Wiśniewska A, Atanasova P, Chaldakov GN, Chylińska-Kula B, Bełtowski J. Differential effects of statins on endogenous H_2S formation in

perivascular adipose tissue. Pharmacol Res. 2011;63(1):68–76.

300. Bełtowski J, Jamroz-Wiśniewska A. Modulation of H_2S metabolism by statins: a new aspect of cardiovascular pharmacology. Antioxid Redox Signal. 2012;17(1):81–94.

301. Xu Y, Du H-P, Li J, Xu R, Wang Y-L, You S-J, et al. Statins upregulate cystathionine γ-lyase transcription and H_2S generation via activating Akt signaling in macrophage. Pharmacol Res. 2014;87:18–25.

302. Ketonen J, Pilvi T, Mervaala E. Caloric restriction reverses high-fat diet-induced endothelial dysfunction and vascular superoxide production in C57Bl/6 mice. Heart Vessels. 2010;25(3):254–62.

303. Xu X, Ying Z, Cai M, Xu Z, Li Y, Jiang SY, et al. Exercise ameliorates high-fat diet-induced metabolic and vascular dysfunction, and increases adipocyte progenitor cell population in brown adipose tissue. AJP Regul Integr Comp Physiol. 2011;300(5):R1115–25.

304. Coletta C, Papapetropoulos A., Erdelyi K, Olah G, Modis K, Panopoulos P, et al. Hydrogen sulfide and nitric oxide are mutually dependent in the regulation of angiogenesis and endothelium-dependent vasorelaxation. Proc Natl Acad Sci USA. 2012;109(23):9161–6.

305. Pohl U, De Wit C, Gloe T. Large arterioles in the control of blood flow: Role of endothelium-dependent dilation. Acta Physiol Scand. 2000;168(4):505–10.

306. d'Uscio L V., Baker T a., Mantilla CB, Smith L, Weiler D, Sieck GC, et al. Mechanism of endothelial dysfunction in apolipoprotein E-deficient mice. Arterioscler Thromb Vasc Biol. 2001;21(6):1017–22.

307. Van Haperen R, De Waard M, Van Deel E, Mees B, Kutryk M, Van Aken T, et al. Reduction of blood pressure, plasma cholesterol, and atherosclerosis by elevated endothelial nitric oxide. J Biol Chem. 2002;277(50):48803–7.

308. Kinosian B, Glick H, Garland G. Cholesterol and coronary heart disease: predicting risks by levels and ratios. Ann Intern Med. 1994;121(9):641–7.

309. Stone NJ, Robinson JG, Lichtenstein AH, Bairey Merz CN, Blum CB, Eckel RH, et al. 2013 ACC/AHA guideline on the treatment of blood cholesterol to reduce atherosclerotic cardiovascular risk in adults. Circulation. 2014;129(25 suppl 2):S1–45.

310.   Davis HR, Compton DS, Hoos L, Tetzloff G. Ezetimibe, a potent cholesterol absorption inhibitor, inhibits the development of atherosclerosis in *ApoE* knockout mice. Arterioscler Thromb Vasc Biol. 2001;21(12):2032–8.

311.   Eberhardt M. H₂S and NO cooperatively regulate vascular tone by activating a neuroendocrine HNO–TRPA1–CGRP signalling pathway. Nat Commun. 2014;5(4381);1–17.

312.   Crabtree B, Higgins S, Newsholme E. The activities of pyruvate carboxylase, phosphoenolpyruvate carboxylase and fructose diphosphatase in muscles from vertebrates and invertebrates. Biochem J. 1972;391–6.

313.   Asimakopoulou A, Panopoulos P, Chasapis CT, Coletta C, Zhou Z, Cirino G, et al. Selectivity of commonly used pharmacological inhibitors for cystathionine β synthase (CBS) and cystathionine γ lyase (CSE). Br J Pharmacol. 2013;169:922–32.

314.   Levitt MD, Springfield J, Furne J, Koenig T, Suarez FL. Physiology of sulfide in the rat colon: use of bismuth to assess colonic sulfide production. J Appl Physiol. 2002;92(4):1655–60.

315.   Molnar J, Yu S, Mzhavia N, Pau C, Chereshnev I, Dansky HM. Diabetes induces endothelial dysfunction but does not increase neointimal formation in high-fat diet fed C57BL/6J mice. Circ Res. 2005;96(11):1178–84.

316.   Balakumar P, Jindal S, Shah DI, Singh M. Experimental models for vascular endothelial dysfunction. Trends Med Res. 2007;2(1):12–20.

317.   Lentz SR, Rodionov RN, Dayal S. Hyperhomocysteinemia, endothelial dysfunction, and cardiovascular risk: the potential role of ADMA. Atheroscler Suppl. 2003;4(4):61–5.

8.0 Appendix

Chromosome	Primer name	Primer sequence
1	1-141133664 L1	AAGACAGCTACAGTTCTTATCGaTGT
1	1-59847112 L	CGTCTGGCTCATTCTGTGAC
1	1-59847271 R	TTCTTCATGCTGGATCTTTCAA
2	2-70619835 L	CCCTTTAATCCCAGCACTCA
2	2-70619835 R	ATAGGCACAGCTGCGAACTT
3	3-95,734,715 L	CAACCTGACTTCTGCGAACA
3	3-95,734,962 R	GCTGTGGAAGGGACAGAGAC
3	3-18484710 L	GAAAAGCAGCATGGAAATGG
3	3-18484710 R	CTCTGCAGGCAAGCTCTCTT
4	4-101954274 L	GGGGAAGCTCCTGGAAATAG
4	4-101954274 R	TCAGTGCCTAAGCCTGACAA
4	4-116051393 L	AACCAAGGACTTGCCTCAGA
4	4-116051393 R	GGCCAGGAAACCACATCTAA
4	4-137777588 L1	CATCCTAAGGCATgCCCA
4	4-140354038 L	GCTGGAGGTGTGGAGGATAA
4	4-140354038 R	CTCCATGAGCTGAGGCTAGG
5	5-90356490 L	GCCAGAGAACCTCAGTCCAC
5	5-90356490 R	AATCCTCATGCACCATGACA
5	5-96758095 L	CGAGAATGGCATGAGTCCTT
5	5-96758323 R	GCACATTGGGATCCTTCTTG
6	6-86478779 L	CTCAGTTGCTTGTGGATGGA
6	6-86478779 R	GATCTGATGCCCTCTTCTGG
7	7-120135075 L	TCGGGATGACGATTTTCAAT
7	7-120135261 R	AAGGTCTTGAGCAGGAACGA
7	7-3222538 L	TATCCTGGTCGGCTTCATTC
7	7-3222538 R	TGCAAGAGCAGAAGCATACG
7	7-63386662 L	GATGGTGGCTTCTGGACTGT
7	7-63386662 R	TTGTGAAGCCAGAACCAAAG
9	9-25674550 L	AGGAGGAAGTCAAGGGGAAA
9	9-25674550 R	GCTTAGGTGCTCAGGTCTGG
9	9-65127938 L1	GCCGGCGTGGAAGCATGcGC
9	9-65127938 R1	CGTGGGGGCCCTGTGGCAATCA
10	10-66700922 L1	CCATAAGCATCTGATGtCGAC
11	11-104906390 L	CCAGCTGATCGTGAGTTTACC
11	11-104906390 R	ACGTGAGCTTTCTTGGCTTC
13	13-73465884 L1	CCGGCGGAAGGTCAGtACCG
13	13-73465884 R1	GCCGCAGCTCCGCATCCTAT
15	15-31106173 L	GTGAGTGGGAGGTGTCCAGT
15	15-31106173 R	TAAAAGGCAACTCCCTGCAC
15	15-11266138 L1	AACTGAAGATCAAGACCAGaTCCT
16	16-35291630 L1	CTGCTGGCCTGCTCCGgGTT
16	16-35291630 R1	CCACACGTGCCACCCTGGAT
16	16-35291477 L	TGACATGGCCCTCTCTCTCT

16	16-35291709 R	CCGCTACAGGGAGCAAATAA
17	17-60286367 L	TGCTCAAATGAACACCCTGT
17	17-60286367 R	TCCTTCCTGGAACAGTTTGTG
17	17-47537359 L1	GACTTGCCCTCCATGATcTT
17	17-47400378	CTCAGCTCTTCCACGGACTT
17	17-47400608	CTCCGGCATCTCTAGTTTGG
X	X-15697909 L	GCAGAGTCTCCATTCACAAGC
X	X-15697909 R	GAAACAGGGCCTCATTGTGT
X	X-134692902 L	ACTGTAGACCAGGCCAATGC
X	X-134693152 R	CCCAAGACCCTTCATCACTG

Appendix table 1. Primer sequences for C57BL/6 N and J substrain genotyping. A complete list of the primers used for genotyping mice during backcrossing to the 6J genetic background. This genotyping was performed by Prof. Simon Horvat.